Glial Response to Oligodendrocytic Connexin Knockout Within the Murine Central Nervous System

BY

SAMANTHA KEIL

B.A. Augustana College, 2012

THESIS

Submitted as partial fulfillment of the requirements
for the degree of Doctor of Philosophy in Neuroscience
in the Graduate College of the
University of Illinois at Chicago, 2020

Chicago, Illinois

Defense Committee:

Ernesto Bongarzone, Anatomy & Cell Biology - Chair
Charles Abrams, Neurology & Rehabilitation - Advisor
Michael Carrithers, Neurology & Rehabilitation
Gerardo Morfini, Anatomy & Cell Biology
Leon Tai, Anatomy & Cell Biology

DEDICATION

To my parental unit, thank you for the unwavering love and support as I adventure into the unknown. I truly could not have done any of this without you.

ACKNOWLEDGEMENTS

I want to begin my acknowledgements by thanking two undergraduate mentors at Augustana College, without both I would not be sitting here writing this. Firstly, Dr. Tallitsch who not only showed me the homeostatic beauty of the brain. As I know you'll read this, I wanted to directly tell you that I truly would not be the scientist I am today without your ever-loving guidance and support both academically and emotionally. You are the type of mentor and scientist I aspire to be, and I will forever be paying it forward because of you. Secondly, Dr. Harrington, for jumpstarting the Neuroscience department at Augie, and immersing my academic experience in the Biology, Psychology and Philosophy of the Brain. Having you as a Neuroscience advisor pushed me to pursue every question my research has brought to me. Being able to touch base every year at SfN has been such an incredible reminder of how far I've come. I will forever be a proud Augie Neurd!

Next, I would like to acknowledge and thank the Graduate Neuroscience Program at UIC, specifically Dr. Larson for ensuring that everything that UIC had to offer was available. To my graduate student advisor, Dr. Charles Abrams, thank you for offering me the opportunity to pursue research interests that stretched beyond the scope of connexins and into the unknown realms of glia. Similarly, to my lab mentors Dr. Mona Freidin and Dr. Alejandro Peinado, I could not have completed this project without the advice, listening ear, and helping hands of you both. To my thesis committee advisors, Drs. Ernesto Bongarzone, Gerardo Morfini, Leon Tai, and Michael Carrithers, thank you for your continual support and encouragement as I push myself to better understand both the science and more importantly, how to effectively communicate it. Your guidance has been critical in the progression and development of my thesis work, and I am truly a better scientist as a result.

I want to especially thank our post-baccalaureate, Gabe Dungan. Gabe, this project would not be possible without you. Thank you for supporting my scientific inquiry, consistent experimental planning requests and most importantly my coffee addiction. Without your meticulous scientific rigor, my project would assuredly not be what it is. You are a light in my science life, and I am so incredibly grateful to have you as my lab family.

In line with my project's success, I would like to thank the department of Neurology and Rehabilitation, particularly Dr. Loeb, for providing the space and equipment in which to investigate my studies. To UIC's Genomics Core including Dr. Zarema, and her Research Technologist Manager, Nina Los, for their involvement with our incredibly productive RNA-Seq results. To the Lutz lab, specifically to Dr. Sarah Lutz for not only providing me the space to section my tissue, but for also breeding a continually exciting and inquisitive lab space.

And finally, but most importantly, I want to acknowledge the family I've built both here at UIC, and in life. Words cannot truly ever convey how thankful I am for you all. To my favorite sister Hayley, for always supporting my scientific adventures and for being a listening ear especially when I didn't know how to ask for it. I love you. To my oldest and truest friend, Chef Eryn, growing up here in Chicago would not have been possible without you. Thank you for seeing me through every single stage of every single degree. To my fastest friend and confidant, Nicole, I'm so grateful to have had you as a support system as I grew into science and Chicago. Thank you for seeing me through the best and the worst of it all. To my cohort humans, Dr. Samantha Corwin, Dr. Evan Kyzar (Kyzar et al., 2019), and Dr. Jennifer Melbourne (Melbourne et al., 2019). Each of you have played an integral role in my success here at UIC, as well as in life. I am so lucky to have had each of you by my side throughout this experience, to push me in my science but also support me when I needed it the most. Shot ski on me when this is all said and done! To Dr.

Antonia Savarese (Savarese & Lasek, 2018), you were a fast friend and mentor even before I started the program, and I cannot wait for what the PNW has in store for us both. To Drs. Sarah Schram (Schram et al., 2019) and Dr. Sineadh Conway (Conway et al., 2019), thank you for continually encouraging me to pursue graduate school and for pushing me to be a bad ass woman in STEM. To Dr. Eliza Jacobs-Brichford (Jacobs-Brichford et al., 2019) and Dr. Kana Hamada (Hamanda & Lasek, 2020) for encouraging me as we each became better teachers and mentors. To my favorite double Docs, Dr. Cory Reiter (Reiter & Bongarzone et al. 2019), Dr. Matthew Tobin (Tobin et al., 2019), and soon to be Dr. Joseph Geraghty (Geraghty et al., 2019), Dr. Rachael Smith, and Dr. Jane Ivakhnitskaia (Ivakhnitskaia et al., 2016), you are the future of medical research and I have been so lucky to grow into science alongside each of you. Finally, to the also soon to be Dr. Zachary Melton (Melton & Motyl, 2018), you have been an unfailing support system for my statistical analysis and throughout my entire graduate student experience, thanking you could never be enough.

TABLE OF CONTENTS

TABLE OF CONTENTS (CONTINUED)

TABLE OF CONTENTS (CONTINUED)

TABLE OF CONTENTS (CONTINUED)

TABLE OF CONTENTS (CONTINUED)

LIST OF TABLES

LIST OF FIGURES

FIGURE PAGE

LIST OF ABBREVIATIONS or NOMENCLATURE

µg	microgram
µL	microliter
µm	micrometer
A/A	astrocyte/astrocyte
AF	Alexa Fluor
Akt	protein kinase B
AMP	adenosine triphosphate
ANOVA	analysis of variance
ASPA	aspartoacylase
B27	proprietary cell culture supplement
BAER	brainstem auditory evoked response
BBB	blood brain barrier
bFGF	basic fibroblast growth factor
BSA	bovine serum albumin
C	Celsius
cm	centimeter
cAMP	cyclic adenosine monophosphate
CD45	cluster of differentiation 45
CMT	Charcot-Marie-Tooth disease
CMT1X	X-linked Charcot-Marie-Tooth disease
CNS	central nervous system
Cx	connexin
DAPI	4’,6-diamidino-2-phenylindole
dKO	double knockout
EAE	experimental autoimmune encephalomyelitis
EEG	electroencephalogram
ELISA	enzyme-linked immunosorbent assay

ERK	extracellular signal-related kinases
FasL	FAS ligand
GFAP	glial fibrillary acidic protein
GJA1	gap junction protein alpha 1
GJB1	gap junction protein beta 1
GJB6	gap junction protein beta 6
GJC2	gap junction protein gamma 2
Iba1	ionized calcium-binding adapter molecule 1
ICC	immunocytochemistry
IFN-γ	interferon-gamma
IL-x	interleukin (e.g. IL-4, IL-6, etc)
IGF-1	insulin-like growth factor
iNOS	inducible nitric oxide synthase
IP	intraperitoneal injection
IP3	inositol 1,4,5-triphosphate
Kg	kilogram
Ki67	monoclonal antibody for proliferation
KO	knockout
LPS	lipopolysaccharide
M	molar
MAPK	mitogen activated protein kinase
MBP	myelin basic protein
mL	milliliter
MOG	myelin oligodendrocyte glycoprotein
mRNA	messenger ribonucleic acid
NO	nitric oxide

LIST OF ABBREVIATIONS or NOMENCLATURE CONTINUED

NOS	nitric oxide synthase
NF-κB	nuclear factor kappa B
NT3	neurotrophin-3
O/A	oligodendrocyte/astrocyte
O/O	oligodendrocyte/oligodendrocyte
O4	oligodendrocyte marker 4
OCT	optimal cutting temperature compound
OL	oligodendrocyte
OPC	oligodendrocyte progenitor cell
PAP	Peroxidase-Antiperoxidase
PBS	phosphate buffered saline
PDGF	platelet-derived growth factor
PDGFRα	platelet-derived growth factor receptor alpha
PDL	poly-d-lysine
PFA	paraformaldehyde
pH	potential hydrogen
PI3K	Phosphatidylinositol 3-kinase
PLP	proteolipid protein 1
PMD	Pelizaeus Merzbacher disease
PMLD1	Pelizaeus Merzbacher Like disease 1
PNS	peripheral nervous system
qRT-PCR	quantitative reverse transcription polymerase chain reaction
RMT	room temperature
RNA	ribonucleic acid
ROS	reactive oxygen species
SC	Schwann cell

SEM	standard error of the mean
SEP	somatosensory evoked potential
siRNA	small interfering ribonucleic acid
Sox10	SRY-Box Transcription Factor 10
TBS	tris buffered saline
TGFB-1	transforming growth factor-beta-activated kinase 1
TLR	toll-like receptor
TNF-α	tumor necrosis factor alpha
TUNEL	Terminal deoxynucleotidyl transferase dUTP nick end labeling
VEP	visual evoked potential

SUMMARY

A study of the effect of oligodendrocyte connexin knockout was carried out with two main aims: to determine surrounding glial response to connexin knockout and identify the role inflammation may play in oligodendrocyte development after connexin knockout. Oligodendrocytes, oligodendrocyte precursor cells, astrocytes, and microglia were evaluated for evidence of apoptosis and proliferation in mixed glial cell cultures derived from WT, connexin 32 knockout (Cx32KO), and connexin 47 knockout (Cx47KO) pups. Total oligodendrocyte and microglial cell counts were also assessed at the corpus callosum level *in vivo*. Pro-inflammatory glial response was evaluated in mixed glial cultures via the inhibition of pro-inflammatory microglial factors, and in tissue using staining for microglia. Bulk RNAseq analysis of brain extracts from each group was performed at baseline and after lipopolysaccharide treatment to investigate differential transcript changes after Cx knockout.

Cx32KO and Cx47KO altered oligodendrocyte proliferation and programmed terminal differentiation resulting in decreased $O4^+$ oligodendrocyte development and significant decreases in proliferation ($p<0.0001$) at 6 days *in vitro* (6DIV). Additionally, $O4^+$ oligodendrocytes from both Cx32KO and Cx47KO showed significantly fewer intersections and arborization via Sholl analysis when compared to WT. At 8-weeks, both Cx32KO and Cx47KO cortical tissue staining showed decreased $ASPA^+$ expression (a marker of more mature oligodendrocytes) when compared to WT though this was significant only for Cx32 KO ($p<0.05$). Interestingly, knockout did not significantly alter oligodendrocyte progenitor cell expression or proliferation. Together these results suggest that Cx knockout alters oligodendrocyte development throughout later stages of oligodendrocyte lineage. Additionally, both astrocytes and microglia appear to be differentially activated after Cx knockout, with increased fluorescence intensity (FI) in $GFAP^+$ and $Iba1^+$ at

6DIV. Although neither Cx32 or Cx47 knockout resulted in increased astrocytic expression in culture, both showed a significant upregulation of microglia at 6DIV with 11.69% ($p<0.05$) and 35.83% ($p<0.0001$) when compared to 4.62% in WT, respectively. *In vivo*, Cx32KO tissue also shows increased microglial expression ($p<0.05$), while Cx47KO does not show upregulation in the corpus callosum, suggesting that microglia play differential roles in response to Cx32 and Cx47 knockout.

Given the increase in microglia and microglial activation, additional mixed glial culture experiments were performed evaluating the response to minocycline, an inhibitor of pro-inflammatory microglia. The expectation was that utilizing minocycline would inhibit the expression of inflammatory factors known to be detrimental to oligodendrocyte proliferation and differentiation. If pro-inflammatory microglial factors are inhibiting oligodendrocyte development after Cx knockout, minocycline treatment could potentially reverse those changes. Our results suggest that the factors released by "pro-inflammatory" microglia may be critical for oligodendrocyte differentiation, regardless of genotype. During treatment with minocycline, all experimental groups show a decrease in $O4^+$ cells and an increase in PDGFRα^+ cells, suggesting that in this treatment group, oligodendrocytes are no longer differentiating into a more mature state.

Interestingly, minocycline treatment differentially alters $Sox10^+$ expression in Cx32KO and Cx47KO, causing a significant downregulation of $Sox10^+$ expression ($p<0.05$) in Cx32KO and a significant upregulation in Cx47KO cultures ($p<0.01$). These results suggest that pro-inflammatory microglial factors may have different effects on the regulation of oligodendrocyte development after Cx knockout. Evaluation of pro-inflammatory factors utilizing an ELISA Cytokine array and bulk RNA-seq found Cx32KO tissue appears to be expressing factors crucial

for developmental regulation rather than an overtly inflammatory phenotype. Meanwhile, Cx47KO tissue appears to be expressing factors suggesting oligodendrocyte developmental inhibition and immune response upregulation.

Overall, this investigation found that Cx32 and Cx47 are critical for ensuring efficient oligodendrocyte development. Activation of astrocytes and microglia following oligodendrocyte Cx loss, are likely involved in their developmental inhibition.

INTRODUCTION

1.1 Background

Gap junction channels, formed by transmembrane proteins called connexins (Cx), provide a diffusion pathway for the small messenger molecules and ions crucial for efficient cellular development, differentiation, synchronization, and immune response. Mutated connexins can become mislocalized or degraded, leading to a wide range of cell and tissue-specific disease states throughout the body. Within the central nervous system (CNS), mutations to oligodendrocyte Cx32 and Cx47 cause the myelin-related diseases X-linked Charcot-Marie-Tooth (CMT1X) and Pelizaeus-Merzbacher-Like disease 1 (PMLD1), respectively. Alterations in these connexins result in varying degrees of myelin malformation, degradation, and motor system impairment with heterogeneous phenotypes.

1.2 Premise

Previous studies have utilized several genetic models with specific Cx32 and Cx47 mutations, as well as Cx knockout (KO), to determine the role each connexin plays in oligodendrocyte communication and myelination. In mice, Cx32KO predominantly causes peripheral neuropathy, with subtle CNS myelin defects, including a decrease in myelin volume and myelin sheath thickness. (Sargiannidou et al., 2009; Sutor et al., 2000). Comparatively, Cx47KO mice may also display subtle CNS myelin deficits with increased sporadic myelin vacuolation (Odermatt et al., 2003), though this seems to be model specific (Menichella et al., 2003). Cx32/Cx47 double knockout (dKO) causes severe CNS abnormalities with myelin vacuolation, axonal loss, oligodendrocyte cell death, action tremor, tonic-colonic seizure, and early mortality (Magnotti et al., 2011; Menichella et al., 2003). Together, these models suggest that

Cx32 and Cx47 are critical for CNS myelin formation and overall cortical function, making connexin knockout and mutation a relevant research model for both their respective disease mechanisms.

Along with effects on myelin itself, the loss of myelinating glial connexins causes an upregulation of pro-inflammatory factors within the central and peripheral nervous systems. In Cx32KO specifically, there is a progressive elevation of T-cell and macrophage infiltration within the PNS (Kobsar et al., 2003; Groh et al., 2010) as well as increased microglial activation within the CNS (Markoullis et al., 2012). Moreover, Cx32/Cx47 dKO mice have increased B-, T-cell, and macrophage infiltrate, with increased astrogliosis and microglial activation within the CNS (Wasseff & Scherr, 2015). Comparatively, the Cx32/Cx43 dKO mouse (eliminating one oligodendroglial and one astrocytic connexin), displays significant microglial activation along cortical white matter tracts and myelinated fibers (May et al., 2013). This microglial activation appears highest during cortical myelination periods (between P10-P60), while severe and progressive astrogliosis occurs throughout the cortex and cingulum regardless of age (May et al., 2013).

Experiments with connexin mutant and KO animals have investigated the effects of connexin dysfunction on responses to neuroinflammatory stimuli. Utilizing lipopolysaccharide (LPS) to mimic the inflammatory events that can lead to encephalopathy in CMT1X patients, researchers found that Cx32KO mice were more vulnerable to neuroinflammation than their WT counterparts. (Olympiou et al., 2016). Similarly, when applying the experimental autoimmune encephalomyelitis (EAE) model of MS, researchers found that Cx32KO and Cx47KO mice have a more severe clinical and inflammatory phenotype after treatment, with more extensive

myelination and axon loss. EAE induction also resulted in extensive microglial activation and oligodendrocyte death in all groups, with the most significant changes in Cx47KO animals (Markoullis et al., 2012; Papaneophytou et al., 2018).

1.3 Hypotheses

We hypothesize that knockout of oligodendrocyte connexins disrupts effective communication with surrounding glial cells, resulting in pro-inflammatory glial activation and oligodendrocyte developmental dysregulation evident by the decrease in the proliferation and differentiation of oligodendrocytes (Figure 1A). We also hypothesize that pro-inflammatory microglial activation hinders the development and remyelinating capacity of these Cx-deficient oligodendrocytes and that inhibition of pro-inflammatory microglia will ameliorate some of these developmental changes (Figure 1B).

1.4 Objectives

1.4.1 Aim 1

Evaluate oligodendrocyte development and glial response after Cx32 or Cx47 knockout, evident via $TUNEL^+$ apoptosis, $Ki67^+$ proliferation, and $Sox10^+$ expression in oligodendrocytes, oligodendrocyte progenitor cells, astrocytes and microglia within mixed glial cultures and cortical tissue.

1.4.2 Aim 2

Investigate the pro-inflammatory response after oligodendrocyte connexin knockout through comparison of minocycline treated cultures. Evaluate Cx32KO and Cx47KO cortical

tissue for expression of pro-inflammatory transcript alterations compared to WT, before and after Lipopolysaccharide treatment.

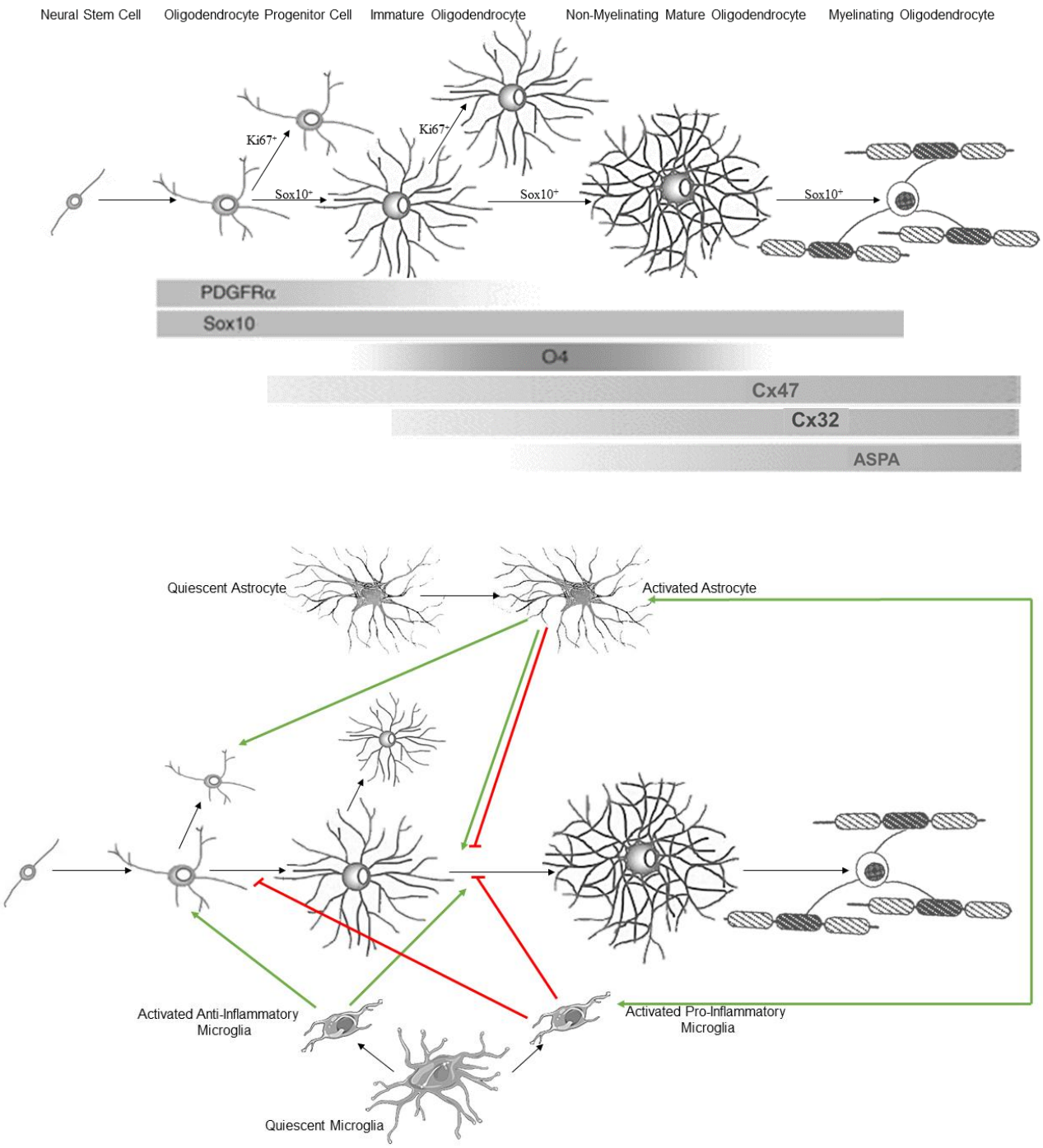

Figure 1. Oligodendrocyte Development Schematic. A. Oligodendrocyte developmental schematic portraying factor expression across lineage maturity. Abbreviations: Proliferation marker Ki67(Ki67); Platelet-derived growth factor-alpha (PDGFRα); SRY-Box Transcription Factor 10 (Sox10); Oligodendrocyte Marker 4 (O4); Connexin 47 (Cx47); Connexin 32 (Cx32); Myelin Basic Protein (MBP). B. Glial activation and oligodendrocyte development. Activation (Green) and Inhibition (Red) with astrocytes and microglia as labeled.

1.5 Methods and Results Overview

1.5.1 Aim 1 Methods: Identify glial response to oligodendrocyte connexin knockout in the CNS

Oligodendrocytes, oligodendrocyte precursors, astrocytes, and microglial cell type changes were characterized in mixed glial coverslips and tissue sections of WT, Cx32KO and Cx47KO animals utilizing immunohistochemistry. Apoptosis (TUNEL), proliferation (Ki67), and programmed terminal differentiation (Sox10) were accessed in the context of these cell types. Morphologic changes in oligodendrocytes, indicative of developmental dysregulation, were analyzed via Sholl analysis. Western blot analysis of pro-inflammatory markers inducible nitric oxide synthase (iNOS) and neuronal nitric oxide synthase (nNOS) were performed to investigate the level of inflammation in the tissue.

1.5.2 Aim 1 Results

1.5.2.1 Effect of Cx32 Knockout

Cx32KO mixed glial cultures appeared to express a developmental deficit, with a significant decrease in overall culture proliferation ($p<0.01$). There was a blunted increase in $O4^+$ expression between 3 and 6DIV, with a significant decrease in apoptosis ($p<0.05$), proliferation ($p<0.0001$), and arborization Sholl analysis ($p<0.0001$) in these oligodendrocytes. Tissue analysis also showed a significant decrease in $ASPA^+$ expression when compared to WT ($p<0.05$). Together these results suggest that oligodendrocytes lacking Cx32 are developmentally altered. Although the loss of Cx32 does not appear to alter the astrocytic expression significantly, it does result in a significant upregulation of $Iba1^+$ microglial in culture ($p<0.05$) and in tissue ($p<0.05$), with an increased fluorescence intensity in culture ($p<0.0001$), suggesting that microglia are playing a pivotal role in response to Cx32 knockout.

1.5.2.2 Effect of Cx47 Knockout

Cx47KO has a dramatic effect on global cell viability in culture with a significant decrease in total cell count ($p<0.0001$) as well as a significant decrease in proliferation ($p<0.0001$). Similar to Cx32KO, Cx47KO cultures expressed a blunted increase in $O4^+$ oligodendrocytes at 6DIV. These $O4^+$ cells were significantly more apoptotic at 3DIV ($p<0.001$), and significantly less proliferative ($p<0.0001$). Cx47KO oligodendrocytes expressed significantly lower $Sox10^+$ expression and were significantly less arborized ($p<0.05$), suggesting that these cells are developmentally less mature ($p<0.0001$). In tissue, Cx47KO also expressed a trend toward fewer $ASPA^+$ oligodendrocytes when compared to WT. This data suggests that the loss of Cx47 dramatically affects oligodendrocyte viability and developmental capacity. Additionally, the loss of Cx47 appears to cause a blunted proliferation in astrocytes, with increased FI at 6DIV ($p<0.0001$), potentially suggesting that the loss of Cx47 may alter astrocytic phenotype due to the lack of communication of Cx47/Cx43. Finally, in mixed culture, Cx47KO increases the expression of $Iba1^+$microglia ($p<0.0001$), while decreasing their proliferative capacity ($p<0.05$) and increasing their FI in culture ($p<0.0001$). In tissue, Cx47KO microglia appear ameboid, with few process extensions, suggesting these microglia are potentially in a pro-inflammatory state in response to the absence of Cx47.

1.5.2.3 Summary

Together, the changes in oligodendrocyte development and surrounding glia suggest that connexin knockout is not only altering the state of the oligodendrocytes in the CNS but is also more broadly altering glial activation. Investigating the differential role astrocytes and microglia play in response to Cx32 and Cx47 knockout may provide insight into the best therapeutic

approach to ameliorate any changes in oligodendrocyte proliferation, development and overall myelin maintenance that occurs after connexin mutation.

1.5.3 Aim 2 Methods: Inflammatory Effects of Oligodendrocyte Connexin Knockout

In this aim, the mixed glial cultures from Cx32KO, Cx47KO, and WT animals were treated with minocycline, a known inhibitor of microglial inflammatory activation. Treatment lasted for either a full 6 days of culture or 3 days with a 3-day recovery period. Treatment groups were compared to baseline mixed glial cultures, with the hypothesis that pro-inflammatory microglial inhibition would increase oligodendrocyte developmental capacity measured by increases in oligodendrocyte proliferation and $Sox10^+$ expression. Culture media was evaluated for the presence of inflammatory markers at baseline and after treatment via an ELISA cytokine array.

In parallel with minocycline treated cultures, bulk RNA-seq analysis was performed on WT, Cx32KO, Cx47KO mouse cortical tissue to investigate the presence of inflammatory factors after connexin knockout. Animals were also treated with LPS to evaluate the change in tissue after additional neuroinflammatory insult. Each comparison was analyzed for differential gene expression, cell-type-specific transcript expression, and gene ontology (GO) enrichment analysis, with specific focus applied to factors indicative of developmental and pro-inflammatory pathways.

1.5.4 Aim 2 Results

1.5.4.1 Minocycline Treatment After Connexin Knockout

Treatment with minocycline for 6 days resulted in decreased $O4^+$ expression across all genotypes, as well as an increase in $Pdgfr\alpha^+$ cells. This change is reversible in WT cultures after 3-day treatment followed by 3-day recovery but does not return to baseline in either Cx32KO or

Cx47KO cultures, suggesting that connexin knockout hinders oligodendrocyte developmental capacity. Oligodendrocyte proliferation also significantly decreases during minocycline treatment but is not changed in either Cx32KO or Cx47KO across treatments, suggesting that the significantly inhibited oligodendrocyte proliferation after knockout is not the result of pro-inflammatory microglial factors.

Minocycline treatment does not alter the percentage of $GFAP^+$ astrocytes or astrocytic proliferation in any genotype but does differentially affect FI, potentially suggesting an interactive role of pro-inflammatory microglial factors in astrocytic activation after Cx knockout. Comparatively, the percentage of $Iba1^+$ microglia is highest during treatment across all genotypes, with differential changes in FI of those microglia.

Cumulatively, these results suggest that factors released by pro-inflammatory microglia may have a role in the development and differentiation of oligodendrocytes. Similarly, the differential changes in glial response after pro-inflammatory inhibition, suggests that there are phenotypic differences in the state of the glia at baseline in culture. Although minocycline did not act as expected on glial cultures, these results provide insight into the glial interactions affecting oligodendrocyte viability.

1.5.4.2 Cytokine Elisa Array

Given the robust increase in microglial percentage after Cx32 knockout in both mixed glial culture and tissue, Qiagen's Mouse Autoimmune Response Multi-Analyte ELISArray was utilized to investigate the inflammatory state of the microglia in culture. Minocycline treatment, as well as genotype, alters the chemokine expression profile of Cx32KO cultures when compared to WT. There was no detectable expression of TNFα, IL-1β, or IL-6. Instead, there was a robust change in

chemokines CCL2 and CCL3 at 3-days and CCL2, CCL3, and CCL4 at 6-days in culture. Most interestingly, CCL2 seems to have an inverse response at baseline and after minocycline treatment, suggesting it plays a direct mechanistic role in response to Cx32. These results are somewhat contradictory to our hypothesis, which predicted pro-inflammatory microglial activation in Cx32KO cultures.

1.5.2.3 RNA-Seq Analysis

RNA-seq analysis was used to determine differential expression, cell-type-specific expression, and pathway analysis via Ingenuity Pathway Analysis (IPA) software. Results were validated with qPCR. Knockout of Cx32 and Cx47 has differential effects on the CNS, with novel pathway involvement in comparisons at baseline. LPS treatment was used to assess transcription under conditions of neuroinflammation with the expectation that Cx knockout would lead to a pattern of differential expression consistent with an inflammatory state. Contrary to expectation, differential expression analysis did not yield any apparent pro-inflammatory transcriptional alterations in Cx32KO tissue, Cx47KO tissue did show a pattern of differential expression suggestive of oligodendrocyte developmental inhibition and injury response when compared to WT.

1.6 Summary of Results

The loss of Cx32 and Cx47 significantly decreases the developmental and proliferative capacity of the oligodendrocytes, while altering microglial and astrocytic activation. These glial alterations are most robust in Cx47KO, likely due to the presence of Cx47 during earlier stages of oligodendrocyte differentiation.

Microglial presence and activation are upregulated in both KO models, but contrary to previous assumptions, the activation state does not appear to be inherently pro-inflammatory. Morphologically, Cx32KO microglia in tissue were significantly upregulated but appear ramified, suggesting they may not be in a pro-inflammatory state. Additionally, RNA-seq analysis of Cx32KO found no apparent pro-inflammatory upregulation, with changes that may be indicative of developmental alterations within the cortex. Conversely, Cx47KO microglia appear ameboid, with little to no process extension (a sign of increased activation). RNA-seq analysis found differential expression of genes broadly associated with both oligodendrocyte development and injury response. Together, Cx32KO and Cx47KO results suggest that culture and tissue response to Cx knockout is differentially regulated.

Pro-inflammatory inhibition of microglia with minocycline differentially altered oligodendrocyte responses at 3 and 6 days of treatment, hindering the development of mature oligodendrocytes as evidenced by the significant decrease in $O4^+$ cells and increasing the percentage of $Pdgfr\alpha^+$cells in all genotypes. These changes indicate that pro-inflammatory factors are required in oligodendrocyte differentiation and maturity. Cytokine Elisa Array found only a small number of chemokines to be differentially expressed, as described above. RNA-seq analysis of brain tissue suggests that loss of Cx32 alters cellular developmental pathways, and loss of Cx47 affects developmental pathways and increases injury state responses throughout microglia and astrocytes.

These experiments contribute to the overall understanding of the complicated effect of Cx deficiency in the disruption of CNS homeostasis. Understanding the role these oligodendrocyte

connexins play within the CNS will help to outline their role in demyelinating disorders and will provide a basis for developing rational therapies for both CMT1X and PMLD1.

1.7 Conclusion

The loss of Cx32 and Cx47 alters the developmental capacity of oligodendrocytes within the CNS via changes in surrounding glia. While *in vivo* data suggest compensation between Cx32 and Cx47, the results presented here emphasize the differential roles of these connexins. Microglial responses, previously thought to be inflammatory, appear to be more related to developmental regulation after Cx knockout. Our results highlight the complex and dynamic interaction across glia cell types in connexin related diseases.

BACKGROUND AND SIGNIFICANCE

Homeostatic balance within the central nervous system depends on a vast network of neuronal and glial communication. This communication is reliant, in part, on the intercellular channels created by a family of integral membrane proteins called connexins (Cxs). These channels, known as gap junctions, allow for the diffusion of ions, metabolites, and second messenger molecules between cells. Connexins also form hemichannels connecting the intracellular and extracellular compartments (Söhl et al., 2004; Nualart-Marti et al., 2013; Zoidl et al., 2010). The connexins themselves are cell- and tissue-type specific and are found in most cell types throughout the body. Neurons and glia within the central nervous system (CNS) each have specific patterns of connexin expression, allowing each cell to effectively carry out the functions critical for homeostatic balance within the brain.

2.1 Connexins

2.1.1 Connexin Protein and Gap Junction Formation

Structural studies show connexins are comprised of four α-helical membrane-spanning domains (TM1-TM4), intracellular N- and C-termini, a cytoplasmic loop connecting TM2 and TM3 and two extracellular loops connecting TM1 to TM2 and TM3 to TM4 (Yeager and Nicholson, 1996; Harris, 2001; Thévenin et al., 2017; Lapato and Tiwari-Woodruff 2017). They are translated and folded in the endoplasmic reticulum and oligomerize into ringed hexameric hemichannels (also called connexons) that are inserted into the plasma membrane (Vanslyke et al., 2009). Once inserted at the membrane, a connexon can then either join with a connexon hexamer of an apposed cell and then aggregate with other connexin channels to create densely packed intercellular gap junction plaques; or remain uncoupled as a hemichannel, facilitating connectivity between the intracellular and extracellular space (Lapato and Tiwari-Woodruff 2017; Goodenough

and Paul 2009). Homomeric hemichannels are comprised of six identical subunits, while heteromeric hemichannels contain one or more Cx subunits which differ from the others. Gap junction channels formed from two identical hemichannels are homotypic or heterotypic when the connexons are different (El-Sabban et al., 2003). Once formed, gap junctions play a critical role in both developmental and mature physiologic functions including calcium signaling (Stout et al., 2002; Scemes and Giaume, 2006), apoptosis (Lin et al., 2003), and proliferation (Omori and Yamasaki, 1998; Moorby and Patel, 2001; Qin et al., 2002; Doble et al., 2004; Freidin et al., 2009; Belousov et al., 2017; Thévenin et al., 2017).

These multifunctional complexes are the product of different connexin encoding genes, with twenty-one identified in humans and twenty in mice (Beyer and Berthoud et al., 2009). In vertebrates, connexins are the only known intercellular channels, providing a direct cytoplasmic exchange of ions and small hydrophilic molecules (<1200 Da) including glutamate, glutathione, glucose, adenosine triphosphate (ATP), cyclic adenosine monophosphate (cAMP), inositol 1,4,5-triphosphate (IP3), (Bruzzone et al., 1996; Belousov et al., 2017, Alexander and Goldberg 2003). Each gap junction has differing permeability characteristics, reflected in their single-channel conductance and selective permeabilities to specific metabolites and signaling molecules (Koval 2006). The differentiation between channels formed from different connexin isoforms also creates differential responses to specific modulatory factors. For example, most gap junction channels close in response to elevations in cytoplasmic Ca2+ or decrease in pH, but the sensitivities of different GJ isoforms vary (Hermans et al., 1995; Siegelbaum and Kandel et al., 2013). This responsivity may play a role in the decoupling of damaged cells from healthy cells since damaged cells are more acidified and have elevated levels of Ca2+ (Siegelbaum and Kandel et al., 2013).

The modulation of coupling and decoupling of these gap junctions determines the efficiency of the gap junction-mediated intercellular communication (GJIC) required for homeostatic functions including the exchange of metabolic substrates, coordination of activity, migration, proliferation, and differentiation (Thévenin et al., 2017; Orthmann-Murphy et al., 2008; Giaume et al., 2010). While structural studies have identified these channels in gap junction plaques, connexins may also be involved in non-junctional cellular processes (Bennett et al., 2003; Sosinsky and Nicolson 2003; Kreuzberg et al., 2006). For this reason, the factors and mechanisms that regulate the function of these structures are an ongoing and rapidly expanding area of research (Nualart-Marti et al., 2013; Pogoda et al., 2016; Lilly et al., 2016).

2.1.2 Connexins in the Central Nervous System

In the central nervous system, neurons and microglia have been found to express nine of the identified connexin encoding genes (Söhl et al., 2004; Beyer and Berthoud, 2009), with at least six of these genes (*GJB1, GJC3, GJC2, GJA1, GJB2,* and *GJB6)* found in oligodendrocytes and astrocytes. Oligodendrocytes express Cx29 (*GJC3*), Cx32 (*GJB1*), and Cx47 (*GJC2*) (Dermietzel et al., 1989; Micevych and Abelson, 1991; Scherer et al., 1995; Li et al., 1997; Altevogt et al. 2002; Menichella et al., 2003; Nagy et al., 2003a, 2003b; Odermatt et al. 2003; Kleopa et al., 2004), while astrocytes express Cx43 (*GJA1*), Cx30 (*GJB6*) (Dermietzel et al., 1989; Yamamoto et al., 1990; Kunzelmann et al. 1999; Rash et al. 2001; Nagy et al., 2003b; Altevogt & Paul, 2004); some astrocytes likely express Cx26 (*GJB2*) as well (Paul, 2004). Each connexin likely plays a unique role within the cell in which it is expressed, together providing a functional syncytium for macroglial cells across the brain (Mugnaini 1986; Rash et al., 2001). These panglial networks appear to be formed primarily via astrocytic Cx43 and Cx30, and oligodendrocytic Cx32 and Cx47; astrocytic Cx26 expression appears limited to a subset of gray matter astrocytes (Nagy et

al. 2001, 2003b; Altevogt and Paul 2004), while *in vitro* data suggest that neither mouse oligodendrocytic Cx29 nor its human homolog Cx31.3 form gap junction channels (Ahn et al., 2008, Sargiannidou et al., 2009; Giaume and Theis 2010; Liang et al., 2011; Nagy et al., 2011).

Specific pairings enable gap junction channel formation between neighboring oligodendrocytes (O/O), neighboring astrocytes (A/A), or a neighboring oligodendrocyte and astrocyte (O/A) (Magnotti et al., 2011; Orthmann-Murphy et al., 2007a). In oligodendrocytes, gap junction-forming connexins, Cx32 and Cx47, are generally localized to the cell somata and outer aspects of myelin sheaths. These connexins enable O/O communication and formation of O/A gap junctions with astrocytic connexins (Mugnaini 1986; Rash et al., 1997, 2001; Orthmann-Murphy et al., 2008). This intercellular communication is believed to assist in homeostatic maintenance by specifically restoring membrane potential after axonal activity (Nualart-Marit et al., 2013). O/A communication is facilitated by three functional heterotypic O/A channels in the CNS: Cx47-Cx43, Cx32-Cx30, and rarely Cx32-Cx26 (Nagy et al., 2007; Rash et al., 1997; Orthmann-Murphy et al., 2008). It has also been suggested that Cx30-Cx47 may form functional heteromeric O/A channels (Magnotti et al., 2011). Mutation of any one of these connexin proteins may impact the homeostatic regulation required during developmental and disease processes. Although the exact function of each connexin channel remains unclear, their prevalence throughout the brain and involvement in disease processes make them excellent candidates for scientific investigation.

2.1.3 Connexins in CNS Disease

The functional importance of these glial connexins is illuminated in a variety of human disease states. Mutations in at least nine of the twenty-one connexin-encoding genes have been found to cause human diseases (Zoidl and Dermietzel 2010). These include a wide variety of conditions including deafness (Wingard and Zhao 2015), skin disorders (Lilly et al., 2016), atrial

fibrillation (Molica et al., 2014), cataracts (Beyer and Berthoud 2014), oculodentodigital dysplasia (Paznekas et al., 2003), hereditary lymphedema (Ferrell et al., 2010), and myelin-related disorders of the peripheral (PNS) and central nervous system (Abrams and Scherer 2011).

2.2 Connexin 32

2.2.1 Connexin 32 CNS Expression and Localization

Connexin 32, encoded by gene *GJB1*, is expressed in both oligodendrocytes and Schwann cells throughout the early stages of myelination, with increased cellular expression in adulthood (Scherer 1995, Parenti et al., 2010; Ahn et al., 2008). Single-cell RNA sequencing found that Cx32 expression is highest in myelin-forming oligodendrocytes and only minimally expressed in earlier oligodendrocyte developmental stages (Marques et al., 2016). Confocal immunofluorescence microscopy and freeze-fracture replica immunogold labeling have shown that in both CNS and PNS myelin, Cx32 localizes between the layers of non-compact myelin found in paranodal loops and Schmidt-Laterman incisures in the PNS (Kamasawa et al., 2005; Kleopa et al., 2004), and within the oligodendrocyte somata and throughout myelinating fibers in the CNS. Unlike Cx47, the gap junctions formed by Cx32 are thought to form predominantly reflexive pathways, mediating transfer between different myelin layers of the same cell (Nualart-Marti et al., 2013). These reflexive pathways shorten the distance of diffusion between the abaxonal and adaxonal myelin layers, creating a radial short circuit communication pathway across what would otherwise be a much longer distance (Oh et al., 1997; Kamsawa et al., 2005).

2.2.2 Charcot-Marie-Tooth Disease

Charcot Marie Tooth (CMT) disease is a genetically heterogeneous group of hereditary sensory-motor neuropathies (HSMN). Estimated to affect ~1:2500 people worldwide (Eggerman et al., 2018; Braathen et al., 2011; Skre 2008; Nicolaou et al., 2010), CMT encompasses a

genetically and pathogenically diverse group of disorders which primarily cause progressive deterioration of peripheral nerves (Ahn et al., 2008; Nualart-Marti et al., 2013). Subtypes include CMT1, with autosomal dominant inheritance and demyelinating pathophysiology; CMT2, with autosomal dominant/autosomal recessive inheritance and axonal pathophysiology; CMT4, with autosomal recessive inheritance and demyelinating pathophysiology; and CMTX, with X-linked inheritance and intermediate or axonal pathophysiology (Morena et al., 2019). Demyelinating subtypes are classified with nerve conduction velocity in the range of 15-38 m/s, while axonal is greater than 39 m/s, and intermediate CMT is associated with velocities between 35 and up to 45 m/s (Saporta et al., 2011). Each subtype of CMT has been linked to mutations in one of over 80 genes or loci (Pareyson et al., 2017; Fonseca and Zanoteli 2018). Many of these mutations cause pathogenic mechanisms involving dysfunctional protein synthesis, posttranslational processing, intracellular trafficking, ion channels, and mitochondrial function (Morena et al., 2019, Jerath and Shy 2015; Rossor et al., 2013). Despite this diversity, over 90% of the genetically confirmed cases of CMT are associated with four genes: *PMP22, MPZ, GJB1*, and *MFN2* (Saporta et al., 2011).

Patients with CMT typically present with progressive, length-dependent, sensorimotor polyneuropathies. Many patients develop pes cavus, and most also experience progressive distal muscle weakness manifesting as progressive foot drop and atrophy in lower greater than upper extremities; some patients may also have scoliosis, hip dysplasia, restless legs syndrome, tremor or hearing loss (Fonseca and Zanoteli 2018; Morena et al., 2019; Harding and Thomas 1980; Horacek et al., 2007; Bamford et al., 2009; Werheid et al., 2016; Saifee et al., 2015; Anzalone et al., 2018; Lerat et al., 2019; Sambuughin et al., 2003; Papadakis et al., 2003).

2.2.3 X-Linked Charcot-Marie-Tooth Disease

X-linked Charcot-Marie-Tooth disease (CMT1X) is the second most common type of CMT, representing 7-18% of all CMT patients (Braathen et al., 2011). CMT1X can be caused by any of over 400 different mutations in the Cx32 encoding gene, *GJB1* (though some of these mutations may be due to polymorphisms) (Scherer and Kleopa 2012). Since Cx32 affects development and function in both Schwann cells and oligodendrocytes, CMT1X symptoms are phenotypically similar to other forms of CMT type 1, with occasional clinical or subclinical CNS-manifesting phenotypes (Fonseca and Zanoteli 2018; Abrams 2017). Peripheral neuropathy symptoms generally begin between 5 and 25 years of age and include slowly progressing weakness and atrophy starting in distal limb muscles, as well as absent deep tendon reflexes and sensory loss (Abrams, 2020). The PNS effects of CMT1X are relatively uniform in males (Shy et al. 2007), with more variable presentations in female patients due to random X-chromosome inactivation (Scherer et al., 1998; Nicholson and Nash 1993).

Despite the predominant PNS phenotypes, subclinical CNS abnormalities are not uncommon in patients with Cx32 mutations (Kassubek et al., 2005; Zambelis et al., 2008). In studies on CMT1X patients, Nicholson and colleagues found that nearly all patients presented with prolonged brainstem auditory evoked responses (BAERs) in their central auditory pathway, with a wave I delay and interpeak latency prolongations indicating slowed conductance in both the PNS and CNS (Nicholson et al., 1996). These findings have been confirmed and extended by others; individual CMT1X patients have presented with prolonged visual evoked potential (VEP), prolonged central motor evoked potential (CMEP) (Bähr et al., 1999), prolonged central somatosensory evoked potential (SEP) latencies (Kawakami et al., 2002), and prolonged transcranial magnetic stimulation (TMS)-evoked central motor conduction (Zambelis et al., 2008).

A subset of the mutation-specific CNS phenotypes includes both transient and chronic manifestations, with overt CNS symptoms typically presenting in early to late childhood (Abrams, 2017). These are often collectively referred to as $CMT1X_{CNS}$ phenotypes. Clinically, CMT1X patients have shown other transient and permanent CNS symptoms including extensor and flexor plantar responses, asymmetric muscle atrophy, difficulty hearing, dysarthria and ataxia, facial weakness, hyperreflexia, cranial nerve paralysis (Zambelis et al., 2008; Caramins et al., 2013; Kleopa et al., 2006; Siskind et al. 2009; Fusco et al., 2010; Halbrich et al., 2008) and/or evidence of pathology found in brain magnetic resonance images (MRI) of the myelinated tracts of the brain (Ahn et al., 2008; Kassubek et al., 2005; Kleopa et al., 2006; Marques et al., 1999). In most cases, this encephalopathy begins after a period of metabolic stress such as return to sea level after traveling to high altitudes, febrile illness, hyperventilation, or concussion (Scherer et al. 2012).

The *GJB1* mutations that are known to cause chronic corticospinal tract dysfunction resulting in spasticity, extensor plantar responses and hyperactive reflexes include A39V, T55I (Panas et al., 1998), M93V, R164Q, R164W, R183H, T191 frameshift and L143P mutations (Orthmann-Murphy et al., 2008; Kleopa et al., 2006; Lee et al., 2002; Taylor et al., 2003). Similarly, CMT1X patients carrying the M1L (Sargiannidou et al., 2015), T55I (Panas et al., 1998), R75W (Taylor et al., 2003), E102del (Hanemann et al., 2003), R142W (Paulson et al., 2002), R142Q (Fusco et al., 2010), R164W, R164Q, C168Y (Paulson et al. 2002) and V177A (Aand et al., 2010) mutations can present with a florid syndrome characterized by acute transient encephalopathy and MRI changes (Taylor et al., 2003; Panas et al., 2001) MRI evaluation in all CMT1X patients with the transient CNS phenotype showed diffuse subcortical white matter hyperintensities sometimes accompanied by an increased signal in the corpus callosum in both diffusion-weighted and T2 images. Signal changes of this type often reflect cytotoxic edema

(Dijkhuizen et al., 1998; Voříšek et al., 2002), which results from an uncompensated influx of cations into the cell due to energy failure (Liang et al., 2007). The T2 white matter changes, although often transient, can take months to resolve; well after the resolution of clinically expressed symptoms (Fusco et al., 2010; Halbrich et al., 2008; Hanemann et al., 2003; Aand et al., 2010; Kim et al., 2014).

Investigating the molecular basis of CMT1X mutant phenotypes, Sargiannidou and colleagues (Sargiannidou et al. 2009) determined that R75W and T55I mutations in a *GJB1*-null background have a phenotype similar to the knockout, suggesting that these mutations cause a loss of function (LoF) mutation in the PNS. Furthermore, no progressive peripheral neuropathy was present in mice expressing both the mutation and endogenous Cx32, suggesting a lack of gain of function. However, patients with a complete absence of *GJB1* have been found to express PNS symptoms with no CNS phenotype. Some CMT1X mutations are much more prevalent in patients with CNS symptoms than would be predicted by their population frequencies (Abrams, 2020), suggesting that mutations causing CNS symptoms are gain of function (GoF) mutations (Takashima et al., 2003; Olympiou et al., 2016). The mechanism involved in GoF mutations remains unclear (Abrams, 2017).

2.3 Connexin 47

2.3.1 Connexin 47 CNS Expression and Localization

Cx47, encoded by *GJC2*, is expressed in oligodendrocytes throughout the CNS. Single-cell RNA sequencing found that Cx47 expression is upregulated in newly formed, pre-myelinating oligodendrocytes and continues to increase in expression throughout development (Marques et al., 2016). Cx47 expression in mice is highest during early embryonic periods, with temporally specific expression in the corpus callosum, the striatum, the cerebellum, and the spinal cord in

adult animals (Nualart-Marti et al., 2012, Menichella et al., 2003, Parenti et al., 2010). Punctate immunofluorescence labeling shows Cx47 expression in oligodendrocyte somata in white and grey matter, with lower expression of Cx47 in myelinating fibers when compared to Cx32 (Kamasawa et al., 2005). Freeze-fracture replica immunogold labeling (FRIL) in specific brain regions determined that, when compared to Cx32, Cx47 is expressed in a 7:1 ratio for somata associated gap junctions and processes and in a 5:1 ratio for myelin-associated junctions (Kamasawa et al. 2005). Inter-oligodendrocytic coupling within the corpus callosum relies predominantly on Cx47 gap junctions. In contrast, heterologous O/A coupling is almost wholly dependent on Cx47/Cx43 junctions throughout the brain (Maglione et al. 2010; Kamsawa et al., 2005; Wassef et al., 2011; Odermatt et al., 2003). Using an *ex vivo* dye transfer in cortical slice preparation, Maglione and colleagues found that with the ablation of Cx47, O/A coupling was completely abolished and O/O coupling within the corpus callosum was reduced by up to eighty percent, suggesting that Cx47 is critical for O/O and O/A coupling (Maglione et al., 2010). Comparatively, Wasseff and Scherer (Wassef & Scherer, 2011) found that within the corpus callosum, oligodendrocytes were coupled almost exclusively to other oligodendrocytes O/O, with coupling mediated by Cx32 predominantly. Meanwhile, in the neocortex, oligodendrocytes were almost exclusively coupled to astrocytes via Cx47 coupling (Wassef & Scherer, 2011).

2.3.2 Pelizaeus-Merzbacher Disease

Pelizaeus-Merzbacher disease (PMD) is an X-linked recessive hypomyelinating leukodystrophy affecting 1.45-1.9:100,000 male births and characterized by dysmyelination throughout the CNS (Bonkowsky et al., 2010, Numata et al., 2014, Inoue, 2019). PMD is caused by a variety of mutations to proteolipid protein one gene, *PLP1*, and shows a heterogeneous and mutation dependent phenotype. (Inoue, 2019; Henneke et al., 2008). As a result of abnormal

myelination, patients with PMD experience global developmental delays with motor and sometimes cognitive function (Inoue, 2019). They present with symptoms including nystagmus by six months of age, cerebellar ataxia by four years, and spasticity by six years of age (Uhlenber et al., 2004; Diekmann et al., 2010; Salviati et al., 2007; Wolf et al., 2007). Patient MRIs also show diffuse T2 signal hyperintensities in white matter, further supporting the idea that *PLP1* is involved in the development and maintenance of myelinating oligodendrocytes (Inoue, 2019).

2.3.3 Pelizaeus-Merzbacher Like Disease 1

Rarely, patients present with the PMD phenotype without mutation or duplications in *PLP1;* these patients are clinically diagnosed with the autosomal recessive Pelizaeus-Merzbacher-like disease (PMLD1). About eight percent of PMLD patients carry autosomal recessive mutations in *GJC2*, the gene which encodes Cx47 (Uhlenberg et al., 2004; Henneke et al., 2008). First identified in 2004, these patients present with early-onset leukodystrophy, nystagmus, poor head and trunk control during early infancy, delayed and impaired motor development, facial weakness, focal epileptic seizures, hypertonia, progressive spasticity, and ataxia (Uhlenberg et al., 2004; Kammoun et al., 2013). Recessive *GJC2* mutations have also been associated with hereditary spastic paraplegia (SPG44), which has a milder phenotype with later onset and normal cognition (Orthmann-Murphy et al., 2009) and subclinical leukodystrophy (Abrams, 2014). Autosomal dominant *GJC2* mutations are the cause of hereditary lymphedema (Ferrell et al., 2010; Finegold et al., 2012).

To date, at least 33 mutations in the coding region of *GJC2* have been associated with PMLD1 (Salviati et al., 2007; Orthmann-Murphy et al., 2009; Bugiani et al., 2006; Biancheri et al., 2013; Ji et al., 2016; Uhlenberg et al., 2004). Mutations include missense, frameshift, nonsense, and micro-insertions; as well as two promoter mutations and one mutation in the 5’ noncoding

region at a highly conserved splice site (Salviati et al., 2007; Wolf et al., 2007; Bianchei et al., 2013; Wang et al., 2010; Combes et al., 2012; Osaka et al., 2010; Henneke et al., 2010). Homozygous Cx47 deficient mice express no clinical and only minimal (Tress et al., 2011) or no (Menichalla et al., 2003) histological abnormalities, suggesting that missense Cx47 mutations may produce an element of GoF). On the other hand, the autosomal recessive inheritance pattern of this disorder suggests a possible LoF mechanism. One possibility is that these mutations may confer both loss of normal Cx47 function and gain of abnormal function with phenotypes that are dependent on mutant dosage (Uhlenber et al., 2004).

Similar to PMD patients, PMLD1 patients experience early onset hypomyelination, with a uniform expression of increased intensity of white matter signal in T2-weighted images by MRI (Bugiani et al., 2006), consistent with hypomyelinating leukoencephalopathy (Orthmann-Murphy et al. 2009). CNS conduction velocity and nerve function are also progressively altered in patients as evidenced by variable delay in visual evoked potentials (VEP), distortion of brainstem auditory evoked responses (BAER), and delayed latency in somatosensory evoked potentials (SEP) (Hennecke et al., 2010).

White matter damage seen in PMLD1 patients may be the direct result of the loss of Cx47-mediated coupling within oligodendrocytes. These mutations can cause defective cellular localization and disrupted channel formation and function (Orthmann-Murphy et al., 2007; Maglione et al., 2010; Diekmann et al., 2010). It is also possible that myelin damage is secondary to misfolding of Cx47, resulting in altered protein trafficking and activation of the unfolded protein response (UPR) in patients with PMLD1, similar to what has been seen in PMD (Southwood et al., 2002; Gow et al., 1998; Gow and Lazzarini et al., 1996). The UPR is a group of cellular signaling pathways that can lead to apoptosis (Zhang and Kaufman 2006; Zhang and Kaufman

2006). Research investigating PLP mutants showed they accumulated in the endoplasmic reticulum (ER) and activated CCAAT enhancer-binding protein homologous protein (CHOP) (Southwood et al., 2002), a downstream effector of the unfolded protein response (UPR) transcription factor phosphorylated extracellular response kinase (PERK)(Orthmann-Murphy et al., 2007). Although the three missense Cx47 mutations associated with PMLD1 did not activate CHOP when expressed in cell lines, (Orthmann-Murphy et al., 2007). unpublished data from the Abrams lab suggest that PMLD1 associated mutants do activate CHOP while a milder spastic paraparesis (SPDG44) mutation does not

2.4 Mouse Models of Connexin Diseases Within the CNS

Through the utilization of connexin single and double knockout (dKO) mouse models, researchers have been able to investigate the role these channels play in brain homeostasis and myelin production and function. To directly model the effects of oligodendrocyte connexin dysfunction, Cx32KO (Anzini et al. 1997; Scherer et al., 1998), Cx47KO (Odermatt et al., 2003), and Cx32/Cx47 dKO (Odermatt et al., 2003; Menichella et al., 2003) mice have been developed. The Abrams lab is also using CRISPR technology to investigate the effects of several specific Cx32 mutations on CNS function. Additionally, to investigate potential roles of O/A coupling on oligodendrocyte function and myelin formation, Cx32/Cx43 and Cx47/Cx30 dKO mice have also been examined. A Cx43/Cx30 dKO mouse has also been utilized to examine the effects of astrocyte connexin knockout (Lutz et al., 2012).

2.4.1 Connexin 32 Knockout

Mice deficient of Cx32 display predominantly late-onset and progressive peripheral neuropathy, similar to CMT1X patients, supporting the causative role of Cx32 in the disease state (Anzini et al., 1997; Scherer et al., 1998). Peripheral myelin deficits, indicative of demyelination

and remyelination, begins at ~P90 with abnormally thin myelin sheaths, onion bulb formation, and enlarged periaxonal collars (Anzini et al. 1997; Scherer et al., 1998). Heterozygous females have fewer demyelinated and remyelinated axons than their age-matched *GJB1*-null females or males, similar to the clinical phenotype (Scherer et al., 1998). This demyelination appears to be preceded by progressive axonal cytoskeletal alterations associated with slowing of axonal support, including a reduced diameter of axons with increased dephosphorylation and dense packing (Vavlitou et al., 2010). In the CNS, myelin volume density in the ventral and dorsal funiculus of the spinal cord and myelin sheath thickness in the neocortex are reduced. (Sargiannidou et al., 2009; Sutor et al., 2000). Additionally, Cx32 deficient mice have a significant reduction in body and brain weight (~17%) when compared to WT controls (Nelles et al., 1996), with mild conduction decreases and increased M-latency in the sciatic nerve (Anzini et al., 1997) as well as increased intrinsic neuron excitability in the neocortex (Sutor et al., 2000)

Along with demyelinating and axonal effects, the loss of Cx32 within myelinating glia is also marked by the upregulation of pro-inflammatory factors within the central and peripheral nervous systems. In the PNS, there is a progressively increasing elevation of T-cell and macrophage infiltration (Kobsar et al., 2003; Groh et al., 2010) as well as increased microglial activation within the CNS (Markoullis et al., 2012). In both the CNS and PNS, the number of immune cells increases, suggesting at least a baseline up-regulation in the inflammatory response within the tissue.

Additional experimental paradigms have been used to investigate the inflammatory response of Cx32KO mice with added immune and neurologic insults. Utilizing lipopolysaccharide to mimic the inflammatory events that can lead to encephalopathy in CMT1X patients, researchers found that Cx32KO mice were more vulnerable to neuroinflammation than

their WT counterparts, expressing more severe motor dysfunction after treatment (Olympiou et al., 2016). Similarly, when applying the experimental autoimmune encephalomyelitis (EAE) model of MS, the Abrams lab and collaborators found that Cx32KO mice have a more severe clinical and inflammatory phenotype after treatment with more severe myelin loss and axonal loss than WT animals (Markoullis et al., 2012, Papaneophytou et al., 2018). In the PNS, the Abrams lab found that the gene expression profile in WT mouse sciatic nerve after crush injury was similar to the found in Cx32 KO animals at baseline (Freidin et al., 2015).

2.4.2 Connexin 47 Knockout

Similar to Cx32KO animals, the Cx47KO mice displayed no obvious gross morphologic or behavioral abnormalities with subtle CNS dysmyelination seen in one of the two Cx47KO mouse strains (Odermatt et al., 2003). Specifically, CNS white matter shows significant sporadic vacuolation of the myelinated nerve fibers of the optic nerve (Odermatt et al., 2003). Li and colleagues (Li et al., 2008) evaluated the Cx47-deficient mouse for disruption of specific regulatory proteins in the absence of Cx47 gap junction formation. They found that Cx47 loss alters connexin-accessory protein composition, resulting in the absence of MUPP1 and ZONAB at the oligodendrocyte soma, which in generally co-localized with puncta for Cx47. Cx47 knockout also caused a total loss of Cx30, Cx32, and Cx43 puncta labeling at the oligodendrocyte soma, with a large increase in Cx32 along myelinated fibers (Li et al., 2018). Together, these findings suggest that myelination deficits caused by Cx47 loss may be compounded by the subsequent loss of other gap junction channels and regulatory proteins at the soma. However, in some areas, this dysfunction may be partially compensated by Cx32 (Li et al., 2008).

In experiments comparing WT, Cx32KO, and Cx47KO subjected to the MOG35-55 experimental autoimmune encephalomyelitis (EAE) model of MS, both Cx32KO and Cx47KO

mice were more severely affected than WT, with Cx47KO more affected than Cx32KO for a variety of measures. Cx47KO animals were more severely clinically affected, showing the most extensive myelin loss, axonal loss, and oligodendrocyte apoptosis (Papaneophytou et al. 2018). EAE also resulted in a significant increase in microglial activation and inflammatory infiltration of macrophages, B- cells, and T-cells in Cx47KO mice compared to WT (Markoullis et al., 2012, Papaneophytou et al., 2018). Pro-inflammatory cytokine upregulation, including FasL, IL-2, IL-3, and CCL2, was highest during peak inflammation and persisted in later stages of EAE for the Cx47KO compared to WT animals (Papaneophytou et al., 2018). These results suggest that Cx47 loss can disrupt the integrity of the blood-spinal cord barrier (Papaneophytou et al., 2018), potentially due to microglial and astrocyte activation and inflammatory response.

Liu and colleagues (Liu et al., 2017) utilized astrocyte/OPC co-cultures and found that oligodendrocytes appear to utilize Cx47-mediated transfer of proliferative factors from astrocytes and demonstrated that the loss of Cx47 alters oligodendrocyte developmental pathways. Additionally, treatment with a siRNA for Cx47 decreased proliferation, and altered cell cycles of OPCs, evident by Ca^{2+} activation and ERK1/2 pathway alterations (Liu et al., 2017). Comparatively, Papaneophytou and colleagues (Papaneophytou et al., 2018) found that Cx47 loss resulted in increased astrocytic apoptosis and increased OPC proliferation after EAE treatment. Together suggesting, that the loss of Cx47 plays a dynamic role in oligodendrocyte development and remyelination.

2.4.3 Double Connexin Knockout Models

2.4.3.1 Connexin 32/Connexin 47 Double Knockout

As described above, loss of either oligodendrocytic Cx32 or Cx47 results in mild or no myelin defects in adult mice (Scherer et al., 1998; Sutor et al., 2000; Odermatt et al., 2003;

Menichella et al., 2003; Sargiannidou et al., 2009). On the other hand, the double knockout (dKO) of Cx32 and Cx47 causes severe CNS dysmyelination followed by demyelination with myelin vacuolation, axonal loss, oligodendrocyte death, action tremor, tonic-colonic seizures, and early mortality at ~P35 (Odermatt et al., 2003; Menichella et al., 2003; Maglione et al., 2010; Wasseff and Scherer, 2011). This dKO mouse was the first connexin knockout in which oligodendrocyte death is prominent, though it is unclear whether the demyelination is the primary cause (Menichella et al., 2003). This dKO also affects other glial and inflammatory cells with increased B-, T-cell and macrophage infiltrate, and increased astrogliosis and microglial activation (Wasseff & Scherer, 2015). Thus, while either of these oligodendrocytic Cxs might be partially dispensable, in the aggregate, these Cxs play vital roles in the formation and maintenance of myelin in the CNS. Deciphering their roles is paramount to understanding how Cx gene mutations result in CNS dysfunction.

2.4.3.2 O/A Connexin Double Knockout

Double knockout astrocytic gap junction forming connexins, Cx43 and Cx30, results in mild myelin defects and normal viability, despite complete A/A coupling loss and reduction in O/A coupling in mice (Wallraff et al., 2006; Lutz et al., 2009).

Similar to the Cx32/Cx47 dKO mouse, Cx32/Cx43 dKO mice experience progressive motor impairment with subsequent onset of progressive seizure-like activity, as well as early-onset mortality ~P140 (Magnotti et al., 2011), albeit at a much later time point than for the Cx32/Cx47 dKO. Sagittal sections showed marked vacuolation associated with white matter in the corpus callosum, anterior commissure, and cerebellum. With onset around P35, this vacuolation appears similar, albeit less severe than that found in the Cx32/Cx47 dKO (Magnotti et al., 2011). Electron microscopy also revealed a significant microglia activation aligned with white matter tracts and

myelinated fibers (Magnotti et al., 2011; May et al., 2013). This microglial activation appears during cortical myelination ~P10-P60, though an overall increase in Iba1+ cells in other areas of the brain was not observed until after P119 (Magnotti et al. 2011, May et al., 2013). The Cx32/Cx43 dKO also causes cause severe and progressive astrogliosis throughout the cortex and the cingulum (May et al., 2013).

In contrast, the Cx47/Cx30 dKO mouse examined by Tress and colleagues (Tress et al., 2012) found that loss of Cx47 and Cx30 resulted in a loss of functional O/A coupling within white matter tissue after P10, accompanied by vacuole formation, myelin lesions, and early mortality (P42-P90) in ~40% of animals. The remaining mice, which survived for a "normal life expectancy", expressed less severe action tremor and mild ataxia (Tress et al., 2012), suggesting there might be variability in the remaining Cx functionality. In the Cx47/Cx30 dKO, no compensatory response from the remaining astrocytic Cx43 and oligodendrocytic Cx32 is noted, suggesting that the roles each of these oligodendrocytic connexins play glial function and communication may be distinct (Tress et al., 2012). Together, these results suggest that panglial networks are critical for proper myelin development and function in later developmental stages.

2.5 Rationale and Hypothesis for Current Studies

The work outlined above demonstrates that Cx32 and Cx47 are both critical to myelinating glial cell function and are required for normal myelination throughout the central nervous system. Previous experiments (electron-microscopic and immunofluorescence) suggest that the roles each connexin plays may be related but are likely functionally distinct. While previous Cx knockout studies have investigated the overall changes in coupling function, myelination deficits, and potential immune response, a more specific investigation into the surrounding glial response after the loss of either Cx32 or Cx47 should elucidate the role each connexin plays in engaging the

panglial syncytium in oligodendrocyte development. Insight into the cellular and mechanistic changes with Cx knockout may also provide a better understanding of their respective disease states.

OLIGODENDROCYTIC CONNEXIN KNOCKOUT CAUSES ALTERATIONS IN OLIGODENDROCYTE DEVELOPMENT AND SURROUNDING GLIAL ACTIVATION

3.1 MACROGLIAL DEVELOPMENT

3.1.1 Oligodendrocytic Development and Glial Interaction

The central nervous system relies on oligodendroglial myelination to maintain axon integrity and fast saltatory nerve conduction for axons throughout the brain (Nave and Werner, 2014). In humans, most of this myelination occurs throughout the first two decades of life, providing temporal myelination as neurologic structures mature (Yakovlev and Lecours, 1967; Lebel et al., 2008). Outside of development, myelination occurs throughout life to replace dysfunctional oligodendrocytes and myelin or to myelinate previously unmyelinated axons (Bartzokis et al., 2012; Young et al., 2013). This constant and continual oligodendrocyte turnover and myelination relies on complex networks of surrounding macroglia and is critical for maintaining effective and efficient neurologic function.

Many neurologic disease states have characteristic demyelination caused by the loss or inability of oligodendrocyte progenitor cells and mature oligodendrocytes to develop remyelinating capacity. Though myelination and oligodendrocyte generation occur continuously in healthy brains, the potential for development and remyelination does not rely exclusively on oligodendroglial health. Instead, a complex interplay of transcription factors, regulatory proteins, and mechanistic pathways initiated and inhibited by surrounding macroglia controls myelination.

In the context of oligodendrocyte Cx32 and Cx47 loss or mutation, there are diffuse changes in myelination and conduction velocity throughout the central (and in the case of Cx32, peripheral) nervous system. These changes may be cell-autonomous, i.e., exclusively the result of

oligodendrocyte dysfunction and the lack of remyelinating and developmental capacity but may also involve inhibitory and inflammatory factors from surrounding macroglia. Prior work has shown that astrocytes and microglia play a role in oligodendrocyte development and function, (Noble et al., 1988; Richardson et al., 1988; Nicholas et al., 2001; Nicolas et al. 2002; Kumar et al., 2007; Nash et al., 2011; Pasquini et al., 2011; Pang et al., 2013; Hoyos et al. 2014; Domingues et al., 2016) but connexin involvement in this process is unclear.

3.1.2 Astrocytes, Oligodendrocytes, and Connexins

As the most abundant cell within the central nervous system, astrocytes express morphologic and physiologic heterogeneity that is still being characterized (Mugnaini et al., 1986; Montgomery, 1994; Daginakatte et al., 2008; Sonfroniew et al., 2010; Cunngingham et al., 2019). They are heterogeneous in nature and involved in the maintenance of the blood-brain barrier, support of neuronal function, surveillance of synaptic formation, and modulation of immune responses (Nash et al., 2011; Domingues et al., 2016). Astrocytes are dispersed throughout the brain, presumably carrying out different roles in the gray and white matter. Fibrous astrocytes, named for their morphology, presumably provide neuronal regulation via neuron-glia contact at nodes of Ranvier and blood vessels within white matter heavy regions (Barres, 2014).

Cx47 and Cx32 form O/A gap junctions via astrocytic Cx43 and Cx30, respectively (Mugnaini 1986; Rash et al., 1997, 2001; Orthmann- Paul, 2004; Murphy et al., 2008). These O/A gap junctions are thought to transport cytosolic contents between astrocytes and oligodendrocytes, suggesting that astrocytes maintain a role in the metabolic support of the oligodendrocytes to which they are coupled (Fasciani et al., 2018). In a Cx47/Cx30dKO, where Cx47/Cx43 and Cx32/Cx30 channels would presumably both be affected, there was diffuse disruption within the myelin integrity, supporting a role for O/A gap junctions in glial interaction and myelin

maintenance (Tress et al., 2012). Connexins may also mediate astrocyte influence on oligodendrocyte proliferation and differentiation (Nash et al., 2011; Domingues et al., 2016). Physical contact with astrocytes facilitates maturation and survival of oligodendrocytes through a variety of mechanisms (Sakurai et al., 1998; Corley et al., 2001). Notably, oligodendrocytes co-cultured with astrocytes express higher levels of myelin related genes, as well as higher levels of Cx47 (Iacobas and Iacobas, 2010).

Astrocytes regulate surrounding oligodendrocyte progenitors and oligodendrocytes by releasing factors essential for proliferation and differentiation into more mature myelinating states (Kumar et al., 2007). Certain growth factors have differential effects depending on whether they are applied singularly or in conjunction with other factors. For example, astrocytic production of platelet-derived growth factor-alpha (PDGF-AA) and basic fibroblast growth factor (bFGF) each inhibit OPC differentiation throughout development (Noble et al., 1988; Richardson et al., 1988), but together, these growth factors may enhance proliferation of progenitors in a regionally specific way (Wolswijk 1992; Bogler et al., 1990). Similarly, the combination of astrocytic neurotrophin-3 (NT3) (also shown to increase OPC proliferation), and PDGF-AA promote the expansion of OPCs and drives oligodendrocyte development (Barres et al., 1994). In fact, following cuprizone-induced demyelination, Kumar and colleagues found that a combination of PDGF-AA, bFGF, NT3, and IGF-1 encouraged OPC proliferation, differentiation, and remyelination (Kumar et al., 2007).

In conjunction with ATP release after axon firing, astrocytes produce leukemia inhibitory factor (LIF), encouraging increased myelination and oligodendrocyte survival (Bhat and Pfeiffer, 1986; Gard et al., 1995; Ishibashi et al., 2006). Similar myelin enhancement occurs with the

regional and temporal increase of astrocytic type III neuregulin-1 (NRG1) (Taveggia et al., 2008; Brinkmann et al. 2008), insulin-like growth factor 1 (IGF-1) (Zeger et al., 2007), and astrocytic gamma-secretase (Watkins et al., 2002). These factors are also known to be critical for activation of PI3K/Akt and MEK/ERK1/2/MAPK pathways, which can lead to decreased myelin thickness when not properly activated (Rubinfeld and Seger, 2005; Furusho et al., 2012).

3.1.3 Microglia and Oligodendrocyte Development

Microglia, which comprise 10-20% of the brain's cells (Soulet and Rivest, 2008; Popovich et al., 2009), are known as the brain's resident immune cells, reacting quickly in response to CNS injury and disease. Singularly, and in conjunction with astrocytes, these cells fluctuate between a range of phenotypes, releasing factors critical for CNS homeostasis. Microglial form and function are inextricably connected and morphologically range between a ramified resting state and an activated amoeboid state. This amoeboid state can be further divided into pro-inflammatory "M1" cells and anti-inflammatory "M2" cells. However, microglia also adopt intermediate phenotypes (Alliot et al., 1999; Streit et al., 1999; Bernhardi and Nicholls, 1999; Karperien et al., 2013). In an uninjured brain, microglia are known to scan the extracellular space, allowing for constant dynamic surveillance of surrounding glia (Popovich et al., 2009). However, recent research suggests that microglia also play a role in oligodendrocyte development.

In co-culture with oligodendrocytes, microglia express increased myelin related sulfatide, MBP, and PLP, suggesting a role in oligodendrocyte maturation (Hamilton and Rome, 1994). This MBP expression may be tied to microglial galectin-3 both in culture and after cuprizone demyelination (Pasquini et al., 2011; Hoyos et al. 2014). Conditioned microglial media enhanced OPC survival and differentiation by activation of the PDGF-a receptor signaling pathway, insulin-like growth factor-2 dependent inhibition of TNFα, and modulation of the NF-kB signaling

pathway (Nicholas et al., 2001; Nicolas et al. 2002; Pang, 2013). Additionally, conditioned media from both primary astrocytes and primary microglia encouraged OPC proliferation, while the conditioned microglial media encouraged differentiation, further supporting the role of microglia in oligodendrocyte development (Pang et al., 2013).

Although microglia are not known to directly form gap junction channels with oligodendrocytes, their role in oligodendroglial migration, proliferation and differentiation might be differentially affected in oligodendrocytes lacking either Cx32 or Cx47.

3.2 Rationale and Hypothesis for Baseline Effect of Connexin Knockout

We hypothesized that the mutation or loss of these oligodendrocyte connexins disrupts effective communication with surrounding glial cells, resulting in glial activation at baseline and subsequent hindrance of proliferation and differentiation of oligodendrocytes.

In this chapter, we investigated the glial response to oligodendrocyte connexin knockout in the CNS. Oligodendrocytes, oligodendrocyte precursors, astrocytes, and microglia were characterized in mixed glial cultures derived from WT, Cx32KO, and Cx47KO animals. Apoptosis (TUNEL) and proliferation (Ki67) were assessed for each cell type, while Sox10 evaluated terminal differentiation programming in oligodendrocytes. Morphologic changes, indicative of developmental immaturity, were analyzed via Sholl analysis. Microglia and oligodendrocyte numbers were also evaluated in tissue sections from WT, Cx32KO, and Cx47KO animals. Western blot analysis of pro-inflammatory markers iNOS and nNOS evaluated the level of inflammation in the tissue.

3.3 Materials

3.3.1 Chemicals and Reagents

Antibodies used for immunocytochemistry and immunohistochemistry are listed in Appendix 1 and detailed in each pertinent methods section. Blocks and reagents used in culture experiments and immunohistochemistry are described below.

3.3.2 Animals

All animal experiments were approved by the University of Illinois at Chicago's Institutional Animal Care and Use Committee. All animals were housed and maintained in standard housing conditions (12/12-hour light/dark cycle) with access to food and water *ad libitum.* For neonatal mixed glial cell cultures, WT, Cx32KO, and CX47KO P0-P2 mouse pups were obtained from in-house breeders. All mice were fully backcrossed on a C57BL/6N background. Immunohistochemistry was performed on 8-week-old male mice, age-matched, and obtained from in-house breeders.

3.4 Methods

3.4.1 Mixed Glial Cell Culture

Mouse pups (P0-P2) were decapitated, the cortex was separated from the brainstem and cerebellum and incubated for 35-45 minutes at 37 ºC in Neural Basal A media supplemented with B27(B27NBMA) and Papain (30U/ml). The enzyme reaction was stopped with the addition of 0.25 volume Bovine Growth Serum (BGS). The brains were mechanically dissociated with using a sequential series of 10mL, 5mL, and 1mL pipets 4-6 times, with 2-3 minutes rest before supernatant removal and pooling. Cell pellets were resuspended at each step with an additional

3mL B27NBM+10% BGS and filtered through a 70 μm Nylon filters. The final cell suspension was pelleted at low-speed centrifugation (300Xg, 5 minutes), filtered a second time, and plated. Suspensions were seeded on Poly-D-Lysine coated coverslips at four brains per 24-well plate. Cultures were maintained at 37 ºC + 5% CO_2. The media was changed the next day to B27NBMA without BGS, and cultures were fed every three days.

3.4.2 Immunocytochemistry

Mixed glial cultures were evaluated at 3 and 6-days *in vitro* (DIV). Cell cultures were washed once with PBS and fixed in 4% paraformaldehyde for 15 minutes at room temperature. After fixation, cells were washed and blocked for 30-60 minutes in ICC block (1% BSA, 0.1% fish gelatin, 0.1% Triton-X-100, 0.05% Tween-20, 1X PBS), or 2% BSA/PBST.05 block (2% BSA, 0.05% Tween-20, 1xPBS) with antibody specific necessity. Cultures were incubated in the primary antibody solution for 60 minutes at room temperature or overnight at 4ºC, washed in PBST.05, and incubated with Alexa-Fluor conjugated secondary antibody (Life Technologies) before mounting. Labeling with O4 antibody was performed on live cells for 1 hour before fixation and incubation with secondary antibody. Primary antibodies utilized included: rabbit anti-Ki67 (1:300; Cell Signaling), rabbit anti-sex determining region Y-box 10 (Sox10) (1:250; Aviva Systems Biology), mouse anti-glial fibrillary acidic protein (GFAP) (1:650; Cell Signaling), rabbit anti-ionized calcium-binding adaptor molecule 1 (Iba1) (1:750; WAKO), mouse anti-platelet-derived growth factor receptor alpha (PDGRF-α) (1:100; Cell Signaling), and mouse anti-O4 (Gift from Dr. Grinspan, 1:24). Anti-O4 is a live cell stain and was diluted in cell media and incubated for 1hr at 37 ºC before fixation. After washing, cells were labeled with secondary antibodies, as

listed in Appendix 1, for 1hr at room temperature. Samples were mounted with Vectashield or Vibrance containing DAPI (Vector Laboratories).

3.4.3 TUNEL Staining

For apoptosis studies, TUNEL staining was performed before immunolabeling using Click-iT™ TUNEL Alexa Fluor™ Imaging Assay (Catalog # C10245; Alexa Fluor 488; Thermofisher, USA) as per manufacturer's coverslip protocol. Briefly, cells were fixed with 4% paraformaldehyde and permeabilized with 0.25% TritonX-100 in PBS. Apoptotic cells were labeled by TdT reaction containing EdUTP and incubated for overnight at room temperature. Detection was completed by Click-it Reaction for 30 minutes at room temperature. Following TUNEL labeling, cultures were washed and processed for additional antibody staining.

3.3.4 Whole Coverslip Imaging

Immunofluorescence images were obtained using Leica CTR DMB 5500 microscope and Surveyor Objective Imaging software. 11 X 11 block mosaic images were scanned from the center of each coverslip at 20X magnification. Three images were randomly selected for image analysis. Images were pseudo-colored for display.

3.4.5 Sholl Analysis

Sholl analysis was performed on WT, Cx32KO, and Cx47KO oligodendrocytes utilizing ImageJ's Fiji6 software (https://imagej.net/Fiji). Images were taken on an Olympus BX61 Microscope with epifluorescence at 60x and manually traced. Once traced, oligodendrocyte images were calibrated to a 0.37mm image diameter. The center of the soma was identified for each cell, and linear method Sholl analysis was performed after drawing 35 concentric circles at

10μm intervals, critical value, critical radius, and Schoenen Ramification Index (SRI) of each oligodendrocyte (Schoenen, 1982; https://imagej.net/Sholl_Analysis) was determined. 2-Way ANOVA was performed as a function of distance and genotypes, with individual t-tests performed at specific intervals. This analysis was utilized to investigate complexity within each genotype.

3.4.6 Tissue Extraction, Perfusion, and Sectioning

8-week old male mice were anesthetized with isoflurane and transcardially perfused with 60 mL of ice-cold saline followed by 30 mL of ice-cold 4% PFA. Brains were removed and post-fixed in 4% PFA overnight at 4°C, washed once with PBS, and transferred to 30% sucrose for cryoprotection. Once fully immersed in sucrose solution (12-48 hours), the brains were rinsed once with PBS before mounting in optimal cutting temperature compound (OCT; Fisher Scientific, USA) in fixing blocks on dry ice. OCT blocks were maintained at -80°C until sectioning. 12 μm cortical sections were taken from bregma area 1.5 and 3 to ensure corpus callosum-was obtained and mounted on Superfrost Plus slides (Fisherbrand) with a drop of fresh RMT PBS to assist with unfolding. Slides were serially sectioned across 20 slides with 4 sections each to ensure selection of the same region while staining. Slides were then heat-dried at 55°C for 20-30 minutes, to ensure tissue fixation and adherence.

3.4.7 Immunohistochemistry

Oligodendrocyte staining was performed with rabbit anti-aspartoacylase (ASPA) (1:200; Genetex) and mouse anti-O4 (Gift from Dr. Grinspan, 1:4). Tissue was submersed in sodium citrate (pH 6.0) in a plastic slide staining container and boiled for 35 minutes at 95°C for antigen retrieval. Once boiled, tissue was returned to room temperature by irrigating the slide staining box with room temperature water. Slides were then partially dried, and tissue was encircled with a

liquid blocker (PAP) pen and blocked for one hour at room temperature in PBST (PBS with 0.1% Triton X-100) with 10% goat serum (S-1000-20; Vector, USA). Slides were incubated overnight at 4°C with diluted ASPA and O4 antibodies and were subsequently washed 3x for 15 minutes with PBST and incubated with diluted Goat anti-Rabbit Alexa Fluor 594, and Goat anti-Mouse Alexa Fluor 488 (1:500; Invitrogen), for one hour. Tissue was washed 3x for 5 minutes each after secondary antibody incubation and fixed with Vectashield containing DAPI (Vector Laboratories).

Microglial staining was performed with rabbit anti-ionized calcium-binding adaptor molecule 1 (Iba1) (1:500; WAKO). Once slides cooled back to room temperature, tissue was encircled with the PAP pen. Tissue was rehydrated with PBS 3x for 5 minutes and blocked for one hour at room temperature in PBS/0.1% triton/10% goat serum/0.5% BSA, followed by incubation with diluted primary antibody overnight at 4°C. Tissue was again washed 3x with PBS for 15 minutes and incubated with diluted secondary antibody Goat-anti Rabbit Alexa Fluor 594 for one hour at room temperature (in the dark) and was washed with PBS 3x for 5 minutes and mounted with Vectashield containing DAPI (Vector Laboratories)

3.4.8 Metamorph Multi-wavelength Cell Scoring Immunofluorescence Analysis

Integrated fluorescence values were obtained using the Multi-Wavelength Cell Scoring applet in Metamorph 7.10 imaging analysis software (Molecular Devices). Thresholds were determined using negative control images such that unlabeled cellular integrated fluorescence was less than 10% of positively scored cells. Image analysis for cultured cells was performed on total $DAPI^+$ cell count, $O4^+$ oligodendrocytes, $Pdgfr\alpha^+$ oligodendrocyte progenitor cells, $GFAP^+$ astrocytes, $Iba1^+$ microglia, $Ki67^+$ nuclei, $Sox10^+$ nuclei/cytosol, and $TUNEL^+$ nuclei. For cultures being evaluated for proliferation, differentiation, and apoptosis, colocalization was assessed for

any cell that showed both a cell-type-specific stain and any of the respective cellular development/death markers. Analysis of tissue sections was based on total $DAPI^+$ cells, $ASPA^+$ oligodendrocyte nuclei, and $Iba1^+$ microglial cells.

3.4.9 Western Blotting

Cortical tissue extracts from 8-week old WT, Cx32KO, and Cx47KO mice were collected in Lysis Buffer (50mM Tris, 0.5 mM EDTA, 10% glycerol, 150mM NaCl) containing 1% DDM and freshly added protease inhibitors. Total protein was determined by BradfordPlus assay (Expedeon, USA). Samples were processed for Western blot, denaturing for 30 minutes at room temperature. 20µg of each sample was loaded into GenScript ExpressPlus™ PAGE Gels 4-20% run with Tris-MOPS SDS Buffer and transferred to PVDF membranes. Membranes were activated in ethanol, stained with Ponceau S for 5 minutes at room temperature to confirm protein transfer, and destained with PBST before blocking. Blocking and antibody dilutions were made using Advan-Chemi Block (Advansta) solution, and blots were washed with TBST (Tris-buffered saline. 0.05% Tween-20).

Western blots were probed with rabbit anti-induced nitric oxide synthase (iNOS) (1:750; Protein Tech) and rabbit anti-neuronal nitric oxide synthase (nNOS) (1:750; Cell Signaling Technology). Blots were stripped and reprobed using mouse-anti-Actin (Genscript). WesternBright Quantum HRP Substrate (Advansta) was used for detection, and digital images were acquired with the AlphaEaseFC (FluorChemSP Version 6) imaging system. Blots were analyzed using GelQuant.Net software (http://biochemlabsolutions.com/GelQuantNet.html) and normalized to actin signal. Fold change was calculated relative to untreated WT signals for each probe.

3.4.10 Statistical Analyses

All statistical analyses were performed with GraphPad Prism (Version 8.3; GraphPad Software Inc). All data represent mean ± SEM, and the null hypothesis was rejected at $p<0.05$. Individual statistical analyses (t-test, ANOVA) are described under their respective figures.

3.5 Results: Effect of Connexin 32 Knockout

3.5.1 Effect of Connexin 32 Knockout *In Vitro*

3.5.1.1 Overall Cell Count

Total cell count in mixed glial cultures was determined by the total $DAPI^+$ cells per image. Between 3DIV and 6DIV, the total cell count in culture for both WT and Cx32KO increased significantly (Figure 2A) ($p <0.0001$). At 3DIV, there was a trend towards a higher cell count in Cx32KO, but this effect was variable. WT cultures increased from an average of 409 cells to 4621 per image, and Cx32KO cultures increased from an average of 958.5 cells to 5002 cells. These results suggest that Cx32KO cell cultures are growing and developing similarly to WT.

3.5.1.2 Apoptosis

Global apoptosis was measured utilizing a TUNEL assay to assess nuclear DNA fragmentation. There was no significant difference in overall apoptosis, with an average of 4.69% in WT and 3.25% in Cx32KO cultures at 3DIV (Figure 2B).

3.5.1.3 Proliferation

Proliferation was evaluated in mixed glial culture via the percentage of $Ki67^+$ nuclei and showed a significant increase in cellular proliferation between 3day and 6-day cultures for both

genotypes. WT cultures increased in proliferation, with an increase from 7.087% $Ki67^+$ at 3DIV to 35.92% at 6DIV in culture (Figure 2C) ($p<0.0001$). Comparatively, Cx32KO cultures showed a reduced increase in proliferation with time, increasing from 11.05% at 3DIV in culture to 20.86% at 6DIV in culture ($p=0.042$). At 6DIV, Cx32KO cultures showed significantly less proliferation than WT ($p=0.0013$).

3.5.1.4 Oligodendrocytes

Oligodendrocytes undergo several developmental stages between progenitor cells and mature myelinating cells. Here, oligodendrocyte stain anti-O4 was used, as it identifies a range of late-stage progenitors to early-stage myelinating oligodendrocytes. Total $O4^+$ cell count was evaluated at both 3 and 6DIV in culture. As a follow-up to this experiment, the oligodendrocyte precursor antibody anti-Pdgfrα was used to assess early-stage oligodendrocytes known to differentiate into myelinating oligodendrocytes. Each oligodendrocyte marker was also co-stained with anti-Ki67, anti-Sox10, and TUNEL for proliferation, differentiation, and apoptosis, as described below.

3.5.1.4.1 $O4^+$ Oligodendrocytes

As discussed above, the percentage of oligodendrocytes was determined by the cells that were $O4^+$ cells in culture. WT oligodendrocytes significantly increased from an average of 3.01% at 3DIV to 9.14% at 6DIV (Figure 3A) ($p=0.0242$). In contrast, the percentage of Cx32KO oligodendrocytes was not significantly different across time or in comparison to WT, with 4.66% $O4^+$ cells at 3DIV and 5.64% at 6DIV in culture. The percentage of Cx32KO oligodendrocytes showed a trend toward being lower than WT at 6DIV.

3. 5.1.4.2 Oligodendrocyte Apoptosis

The level of apoptosis within oligodendrocytes was determined by the percentage of $O4^+$ oligodendrocytes with $TUNEL^+$ nuclei at 3DIV. Despite the overall level of apoptosis being comparable between WT and Cx32KO cultures, the percentage of apoptotic oligodendrocytes was unexpectedly lower in Cx32KO cultures (Figure 3B) ($p=0.021$). About 2.21% of WT oligodendrocytes and 0.80% of Cx32KO oligodendrocytes were $TUNEL^+$. This decrease in Cx32KO apoptosis is surprising but may account for the trend toward higher numbers of $O4^+$ cells at 3DIV.

3. 5.1.4.3 Oligodendrocyte Proliferation

Oligodendrocyte proliferation, determined as the percentage of colocalized $O4^+$ cells and $Ki67^+$ nuclei, increased within both genotypes from 3DIV to 6DIV in culture. While WT oligodendrocyte proliferation increased from 0.574% to 30.73%, Cx32KO proliferation showed a blunted increase from 2.17% to 11% (not significant) (Figure 3C). At 6DIV, the Cx32KO oligodendrocytes are proliferating significantly less than WT ($p<0.0001$). Oligodendrocyte proliferation would be expected to increase in culture as cells become stable, and neurons begin to develop, requiring more mature oligodendrocytes for trophic support. This significantly lower proliferation in Cx32KO cultures may represent a blunted increase in proliferation as oligodendrocytes mature may reflect increased Cx32 expression as oligodendrocytes develop (Mareques et al., 2016).

3. 5.1.4.4 $Sox10^+$ Expression

Terminal differentiation to mature myelinating oligodendrocytes can be monitored by transcription factor Sox10. When localized with $O4^+$ cells, it suggests that these oligodendrocytes

are programmed toward a mature myelinating state. As O4 covers oligodendrocytes from late-stage progenitors through early-stage myelination, $Sox10^+$ cells allow evaluation of differentiation in culture. Evaluated at 6DIV, there was a trend towards a significant increase in Sox10 expression within Cx32KO cultures in comparison to WT. Cx32KO cultures expressed 6.645% while WT expressed 2.98% (Figure 3D) ($p=0.0803$). This expression suggests that cells are primed for differentiation into maturity but are not necessarily developing into maturity. Confirmation should be performed with later stage oligodendrocyte markers for confirmation.

3. 5.1.4.5 Sholl Analysis

Sholl analysis provides a quantitative measurement of oligodendrocyte arbor complexity, utilizing arbor length, primary branching totals, and assessment of ramification of oligodendrocyte processes (Murtie et al., 2007). As oligodendrocyte lineage maturity increases, the number of primary branches, and the complexity of the processes increases (Trapp et al., 1997). Similarly, the average number of intersections per Sholl ring and the absolute number of crossings is indicative of increased oligodendrocyte maturity (Gensel et al., 2011). Here we assessed oligodendrocyte branching and arborization in WT and Cx32KO $O4^+$ oligodendrocytes. WT ($n=12$) and Cx32KO ($n=16$) cells were randomly selected over four experiments, manually traced, and analyzed with ImageJ Sholl Analysis software. Based on this analysis, Cx32KO oligodendrocytes express significantly fewer intersections by distance and by genotype (Figure 4A) ($p<0.0001$). This decrease in intersections was maintained as a factor of distance at 80μm, 130μm, and 180μm from the cell soma (among other distances) ($p=0,0256$; $p=0.0194$; $p=0.0308$) (Figure 4B, C, D). Although the critical radius (radius with maximum intersections) and the number of intersections at that radius (critical value) were not significantly different, Cx32KO

arborization appears to be significantly altered, as the number of primary branches leaving from the soma is significantly lower at 7.07 compared to 17 in WT oligodendrocytes ($p<0.0001$). As such, Cx32KO expresses a significantly higher Schoenen ramification index (SRI) (Garcia-Segura & Perez-Marquez, 2014; Schoenen, 1982), with an SRI of 1.835 in WT and 3.879 in Cx32KO oligodendrocytes ($p=0.0001$). Taken together, it appears that the Cx32KO oligodendrocytes are less mature with significantly lower intersections (Gensel et al., 2011), significantly fewer primary processes releasing from the soma (Murtie et al., 2007), and a significantly higher SRI, which is indicative of the number of primary processes and intersections (Schoenen, 1982).

3. 5.1.4.6 Pdgfrα^+ Oligodendrocyte Progenitor Cells

In contrast to the $O4^+$ oligodendrocytes results, there was no significant difference across genotypes in the percentage of Pdgfrα^+ oligodendrocyte progenitor cells. There was a significant decrease in oligodendrocyte progenitor cells for both genotypes between 3DIV and 6DIV (Figure 5A) ($p<0.0001$), decreasing from 24.03% to 4.24% for WT, and from 31.61% to 3.68% in Cx32KO. The decrease is not surprising as progenitors are expected to differentiate with time. Additionally, the expression of Cx32 is not as prevalent in oligodendrocytes until later in the oligodendrocyte maturity lineage (Mareques et al., 2016), and thus the absence of Cx32 should not be expected to affect progenitor cell total.

3. 5.1.4.7 Pdgfrα^+ Proliferation

Unlike $O4^+$ proliferation, oligodendrocyte progenitor cell proliferation (determined by the percentage of Pdgfrα^+ and $Ki67^+$ cells) significantly decreased within WT cultures between 3 and 6DIV (Figure 5B) ($p=0.0004$). There was also a non-significant decrease in Cx32KO cultures ($p=0.0562$). This overall proliferative decrease may be representative of progenitor proliferation

switching to differentiation and may be represented by $Sox10^+$ cells. The lack of a significant difference between WT and Cx32KO cultures may again be the result of no significant expression of Cx32 until more mature oligodendrocyte stages (Mareques et al., 2016).

3. 5.1.5 Astrocytes

3.5.1.5.1 $GFAP^+$ Astrocytes

The percentage of $GFAP^+$ astrocytes significantly increased in both genotypes between 3 and 6DIV (Figure 6A). WT cultures increase from 11.93% at 3DIV to 26.90% at 6DIV ($p=0.0042$). Similarly, the average percentage of astrocytes in Cx32KO cultures started at 10.13% at 3DIV and increased to 21.18% at 6DIV ($p=0.0085$). The significant increase in astrocytes is likely indicative of astrocytic development with culture. No significant decrease in WT vs. Cx32KO astrocyte percentage suggests astrocytes in these cultures are developing normally after Cx32 knockout.

3. 5.1.5.2 Astrocyte Apoptosis

The overall level of apoptosis in 3day cultures was not significantly different in Cx32KO when compared to WT (Figure 2B). This remained true in WT and Cx32KO astrocytes, with no significant difference in apoptosis within astrocytes at 3DIV (Figure 6B) ($p=0.1589$). Both cultures expressed very low levels of astrocytic apoptosis, with an average of 0.29% in WT compared to 0.598% in Cx32KO.

3. 5.1.5.3 Astrocyte Proliferation and Activation

Both WT and Cx32KO cell cultures expressed increased astrocytic proliferation between 3 and 6DIV, with an increase in $Ki67^+$ nuclei from 2.92% to 35.10% in WT (Figure 6C) ($p<0.0001$) and 1.20% to 19.62% in Cx32KO cultures ($p<0.0090$). Astrocytic proliferation was not

significantly different between genotypes, though there was a blunted increase in proliferation within Cx32KO astrocytes when compared to WT, suggesting that these astrocytes may be affected by the loss of Cx32. Astrocytic proliferation generally increases in conditions where astrocytes are activated and inflammatory (Nash et al., 2011), suggesting that any phenotypic change within Cx32KO astrocytes may not be pro-inflammatory.

Astrocytic activation in vitro was evaluated by an increase of $GFAP^+$ fluorescence intensity (FI) relative to baseline. Increased cellular activation can be denoted by an increase in fluorescence emission (Montgomery, 1994; Brodie et al., 1997; Kang et al., 2014), and is generally attributed to higher levels of immune and anti-inflammatory response. The $GFAP^+$ fluorescence intensity significantly decreased within each genotype, with WT FI decreasing from 24500 at 3DIV to 11442 at 6DIV (Figure 6D), and Cx32KO decreasing from 34246 to 101766($p=0.0040$). This FI decrease suggests that the astrocytes in both WT and Cx32KO cultures are becoming more quiescent with time. This significant decrease in Cx32KO cultures, suggests that these astrocytes may be more activated earlier in development. Whatever phenotypic activation differences that occur due to Cx32KO, seem to be leveled at 6DIV.

3.5.1.6 Microglia

3. 5.1.6.1 $Iba1^+$ Microglial Cells

The percentage of microglia increased in both genotypes between 3 and 6DIV, with WT increasing from 0.568% to 4.616%, while Cx32KO increased from 6.90% to 11.69% (Figure 7A). The percentage of microglia was significantly higher in Cx32KO when compared to WT at 6DIV ($p=0.0298$). This increase in Cx32KO cultures suggests that the microglia may play an

inflammatory role in response to Cx32 knockout. Alternatively, the microglia may play a role in oligodendrocyte monitoring and development, which is altered by the loss of Cx32.

3. 5.1.6.2 Microglial Proliferation and Activation

Microglial proliferation, evaluated 6DIV in culture, was determined by $Iba1^+$ and $Ki67^+$ positive cells. Although lower in Cx32KO (22.44%), microglial proliferation was not significantly different from WT cultures (31.67%) (Figure 7B). Changes in proliferative capacity and overall numbers may be indicative of phenotypic differences for microglia within these cultures.

Microglial activation *in vitro* can be evaluated by an increase in fluorescence intensity (FI) of the $Iba1^+$ staining. There was a downregulation in microglial FI for both genotypes between timepoints. WT microglia expressed an average FI of 67400 at 3DIV and 52463 at 6DIV ($p<0.0001$), while Cx32KO microglia expressed an average FI of 87741 at 3DIV and decreased to 60415 at 6DIV ($p<0.0001$) (Figure 7C). Although these decreases in FI suggest that microglia are more activated at earlier time points in culture, Cx32KO expressed a significantly higher FI at both time points, suggesting microglia within Cx32KO cultures are more activated. Increased microglial activation may be consistent with an increased immune response after Cx32 knockout (Markoullis et al., 2012; Olympiou et al., 2016). Follow-up experiments are required to determine pro- or anti-inflammatory activation. Previous peripheral nerve studies in Cx32KO animals (Kobsar et al., 2003; Groh et al., 2010; Freidin et al., 2015), as well as other connexin knockout data, suggests that these activated microglia reflect a pro-inflammatory immune response.

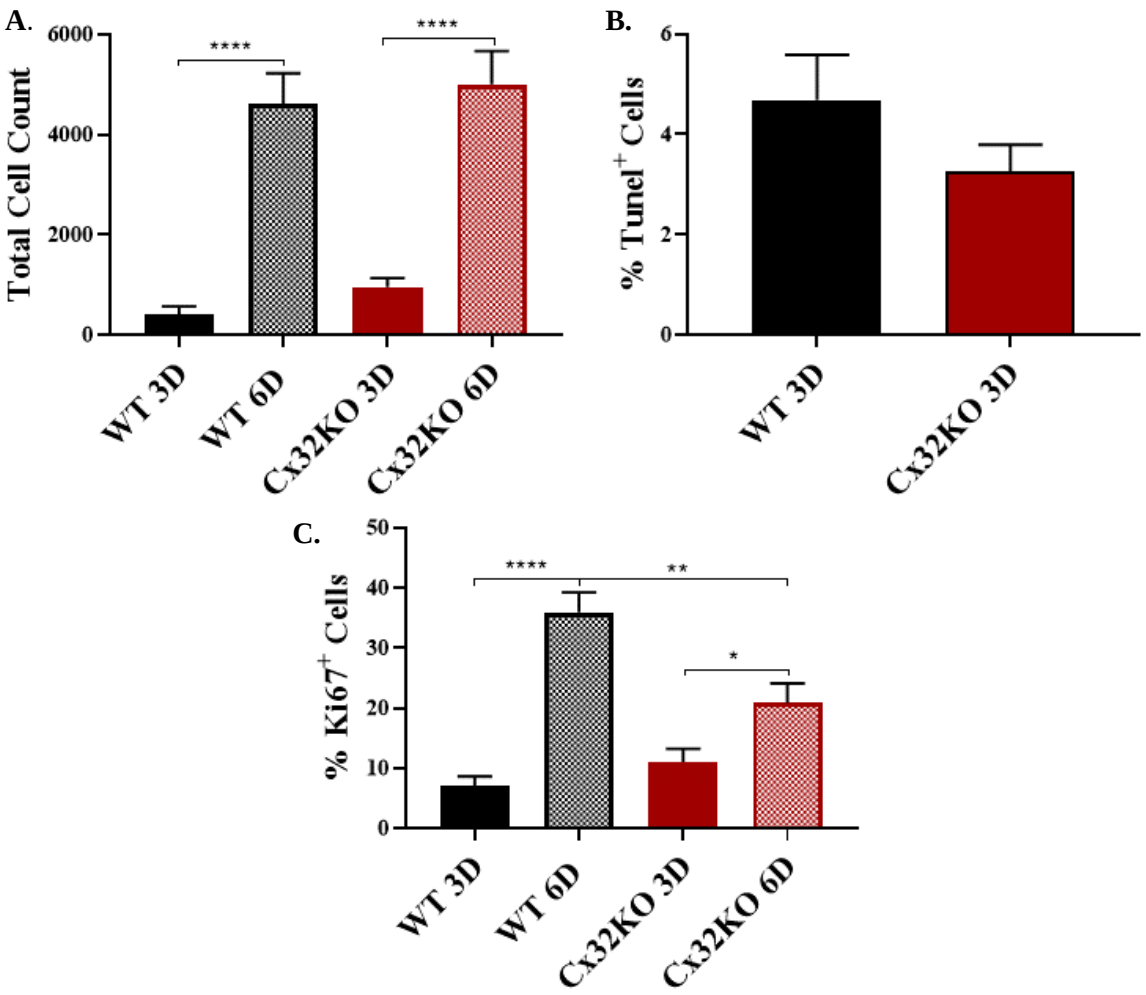

Figure 2. Baseline Cell Type Changes WT vs. Cx32KO. Evaluation of mixed glial cell cultures at 3 and 6DIV. A. Total cell count ($DAPI^+$ nuclei) per image. There was no significant difference between genotypes, but there was a significant increase at 6DIV when compared to 3DIV in both ($F_{3,51}$=28.79) by one-way ANOVA. B. No significant difference by two-tailed t-test in the percentage of $TUNEL^+$ nuclei WT versus Cx32KO C. Percentage of $Ki67^+$ of total cells shows a significant increase in both genotypes from 3 to 6DIV in culture. Proliferation is significantly lower in 32KO cultures at 6DIV compared to WT ($F_{3,46}$=21.11) by one-way ANOVA. Data represent mean ±SEM derived from n=8-24 coverslips per group. *p<0.05, **p<0.01, ***p<0.001, ****p<0.0001.

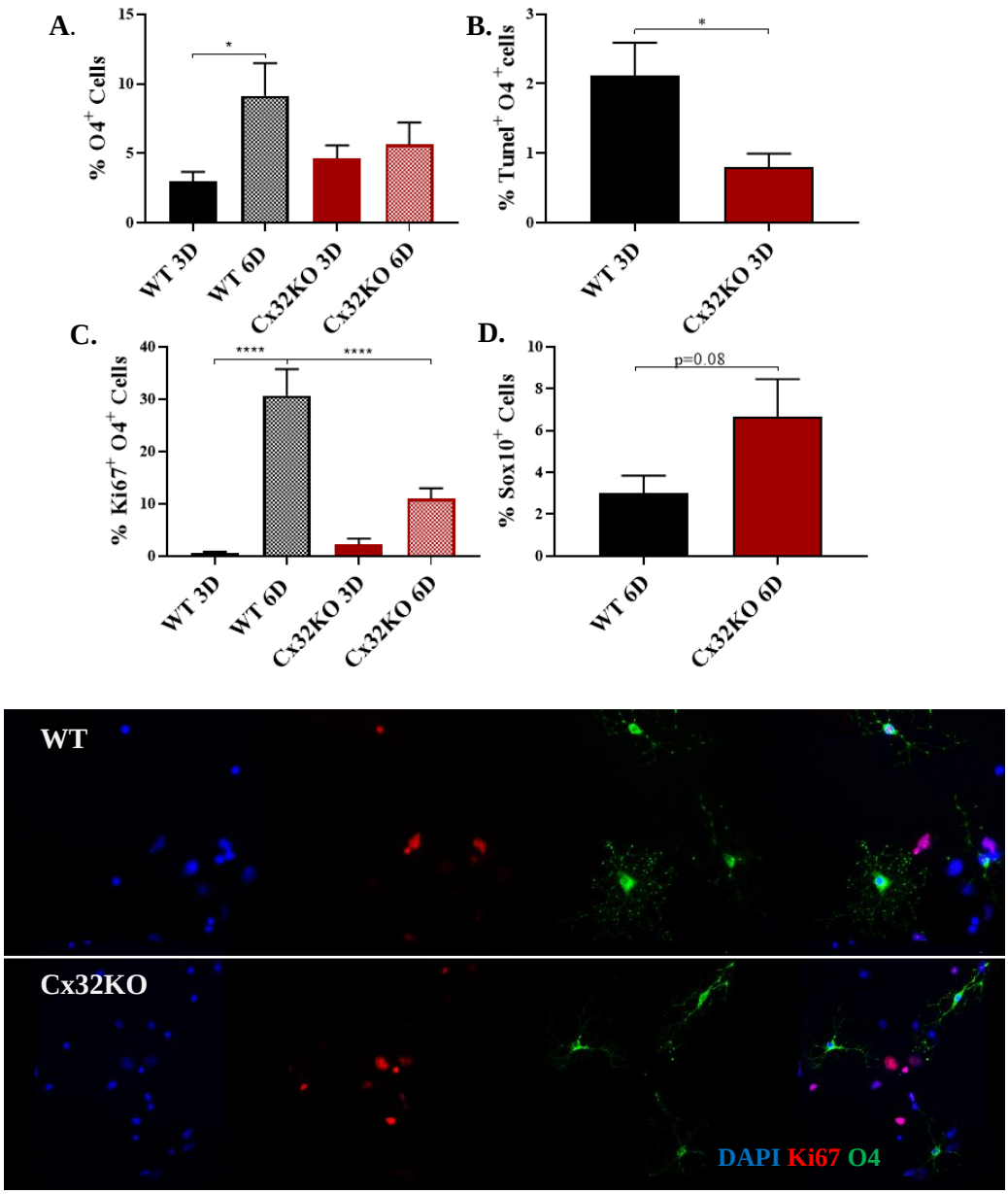

Figure 3. Oligodendrocytes in WT and Cx32KO Cultures. Evaluation of oligodendrocytes within mixed glial cell cultures at 3 and 6DIV. A. Percentage of $O4^+$ cells per image, showing an increase in the percentage of oligodendrocytes within both genotypes, significant in WT. *($F_{3,26}$=3.085)* by one-way ANOVA B. Percentage of apoptotic oligodendrocytes at 3DIV determined by $O4^+$ with $TUNEL^+$ nuclei, was significantly lower in Cx32KO cells (*t (14)* =2.599) by two-tailed t-test C. Proliferating oligodendrocytes, determined by $O4^+$ with $Ki67^+$ nuclei significantly increases between 3 and 6DIV in WT cultures, and is significantly lower at 6DIV in Cx32KO cultures when compared with WT *($F_{3,19}$=25.82)* by one-way ANOVA. D. Cellular programming for terminal oligodendrocyte differentiation, determined by the percentage of $Sox10^+$ cells, was non-significantly higher in Cx32KO cells by a two-tailed t-test E. Representative images of $O4^+$ $Ki67^+$ cultures at 40X, with DAPI, Ki67(AF594), O4(AF488). Data represent mean ±SEM derived from n=5-10 in each group. *p<0.05, ****p<0.0001.

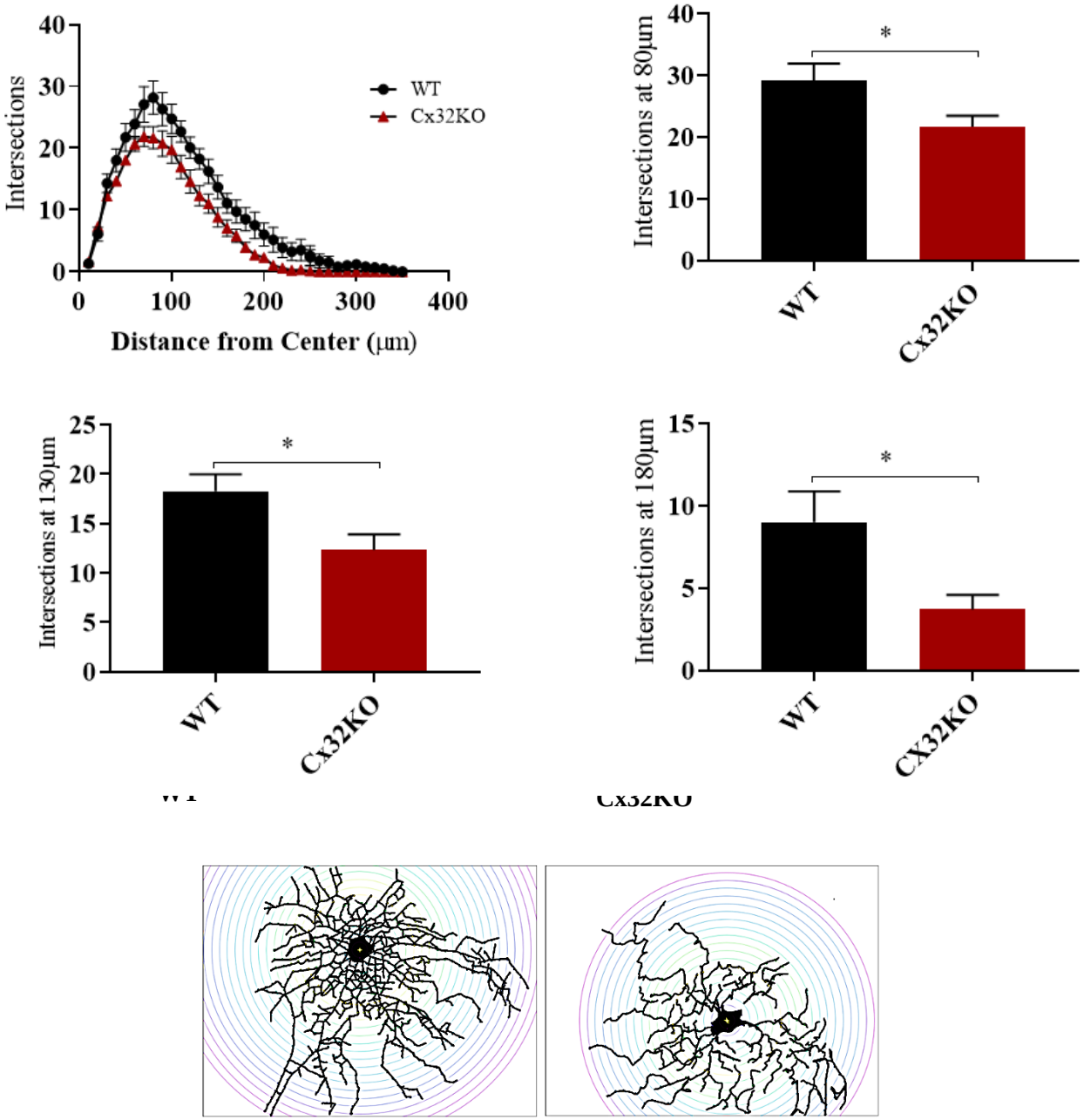

Figure 4. Oligodendrocyte Sholl Analysis WT versus Cx32KO. Sholl analysis performed on 60x images of Oligodendrocytes in 6-day Mixed Glial Cultures. A. Plot of average intersections at 10µm intervals for the entire oligodendrocyte. Cx32KO oligodendrocytes express significantly fewer intersections by 2-Way ANOVA *(F(Distance)*$_{35,936}$=87.21); *F(Genotypes)*$_{1,936}$=93.91*)*. B-D. Average intersections at specific distances from the cell soma are significantly lower in Cx32KO when compared to WT at 80µm, 130µm, and 180µm (among others). (t (27) =2.363; t (26) =2.493; t (21) =2.315) by two-tailed t-test E-F. Representative images of traced oligodendrocytes for WT and Cx32KO. Data represent mean ±SEM derived from n=15-24 in each group. *p<0.05, ****p<0.0001.

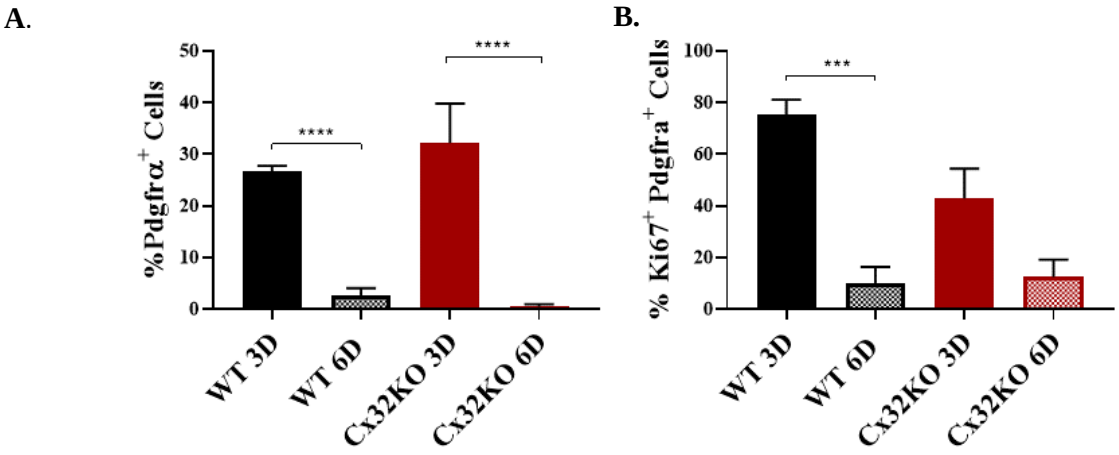

Figure 5. Oligodendrocyte Progenitor Cells in WT and Cx32KO Cultures. A. Percentage of oligodendrocyte progenitor cells, determined by Pdgfrα^{+} cells, significantly decreased both genotypes between 3 and 6DIV in culture *($F_{3,12}$=29.20)* by one-way ANOVA. B. OPC proliferation measured by the percentage of Pdgfrα^{+} cells with Ki67^{+}nuclei, which was significantly lower between 3 and 6DIV in WT cultures at 6DIV ($F_{3,14}$=12.60*)* by one-way ANOVA. Data represent mean ±SEM derived from n=4-6 in each group. ***p<0.001, ****p<0.0001.

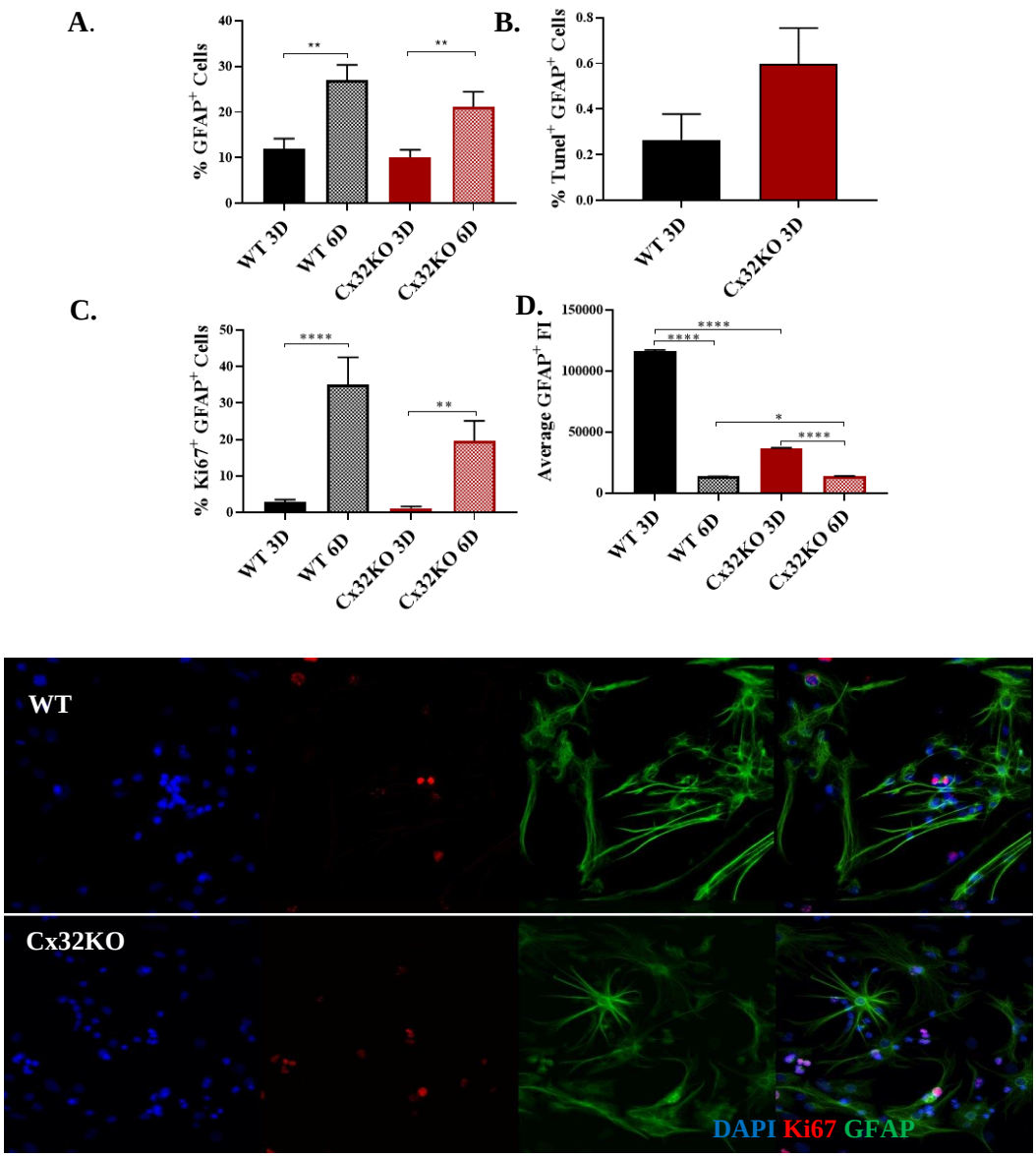

Figure 6. Astrocytes in WT and Cx32KO Cultures. Evaluation of GFAP$^+$ astrocytes within mixed glial cell cultures at 3- and 6DIV. A. Percentage of GFAP$^+$ cells per image significantly increases in both genotypes between 3- and 6DIV in culture. *($F_{3,39}$=7.856)* by one-way ANOVA B. Percentage of apoptotic astrocytes at 3DIV determined by GFAP$^+$ cells with Tunel$^+$ nuclei per image, was not significantly different across genotype at 3DIV by two-tailed t-test. C. The percentage of proliferating astrocytes determined by GFAP$^+$ cells with Ki67$^+$ nuclei significantly increased between 3- and 6DIV for both genotypes. *($F_{3,21}$=15.32)* by one-way ANOVA D. Average integrated fluorescence intensity of GFAP$^+$ cells by cell. FI significantly decreased for both WT and Cx32KO between 3- and 6DIV in culture but was comparatively lower at 3DIV and higher at 6DIV in Cx32KO cultures when compared with WT *($F_{3,41518}$=20705)* by one-way ANOVA. E. Representative GFAP Ki67 40x images, DAPI, Ki67(AF594), and O4(AF488). Data represent mean ±SEM derived from n=15-24. *p<0.05, **p<0.01, ****p<0.0001

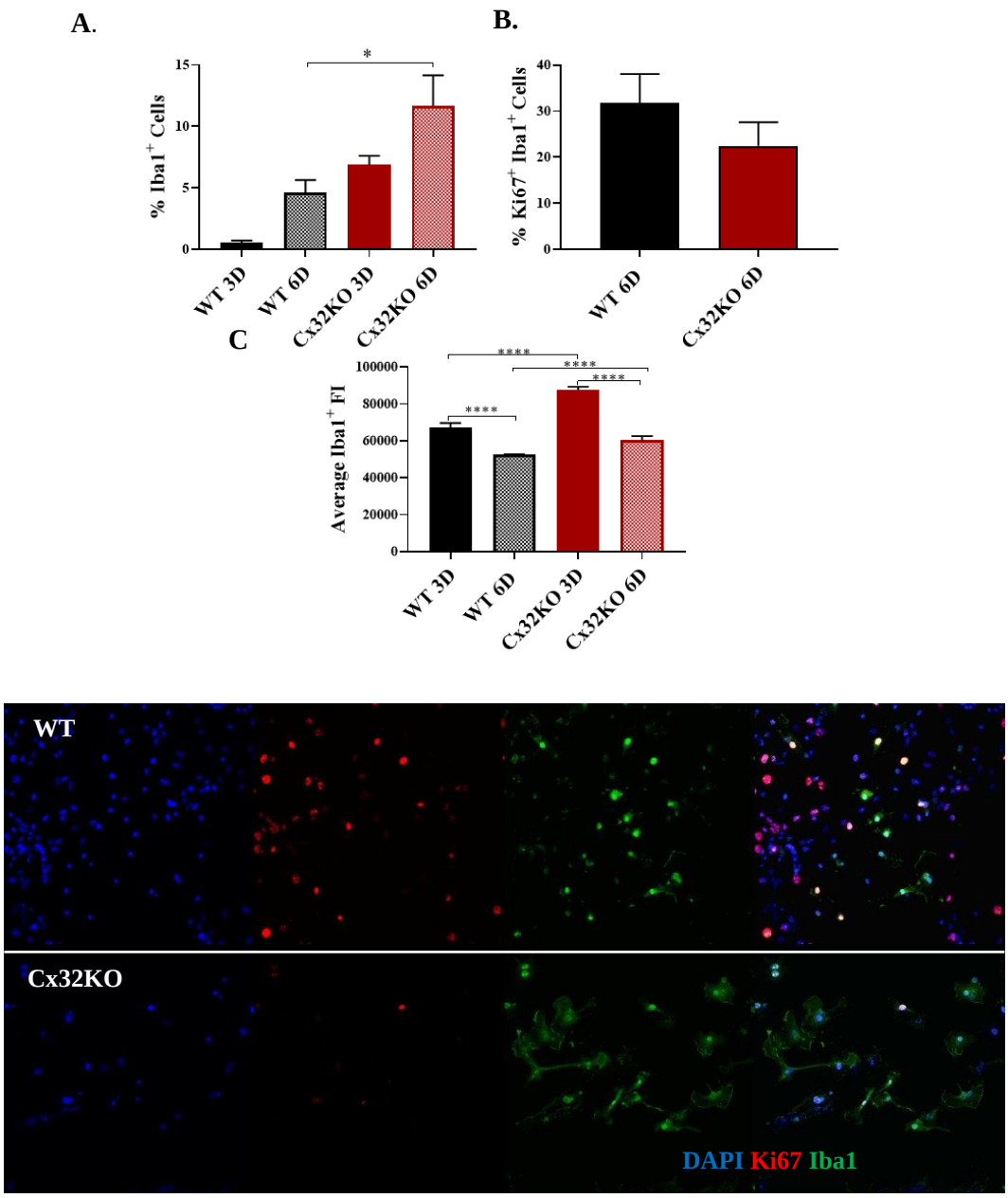

Figure 7. Microglia in WT and Cx32KO cultures. Evaluation of Iba1$^+$ microglia within mixed glial cell cultures at 3 and 6DIV. A. Percentage of Iba1$^+$ cells per image was significantly higher in Cx32KO at 6DIV when compared to WT *($F_{3,22}$=7.674)* by one-way ANOVA B. Percentage of proliferating microglia determined by Iba1$^+$ cells with Ki67$^+$ nuclei, was lower in Cx32KO but not significantly different than WT. C. Average integrated fluorescence intensity of Iba1$^+$ cells. FI significantly decreased in WT cultures but not Cx32KO between 3 and 6DIV *($F_{3,16}$=6.560)* by one-way ANOVA D. Representative 40x images Ki67$^+$ Iba1$^+$, with DAPI, Ki67 (AF594), and O4(AF488). Data represent mean ±SEM derived from n=4-8 coverslips in each group. *p<0.05, ****p<0.0001

3.5.2 Effect of Connexin 32 Knockout *In Vivo*

3.5.2.1 $ASPA^+$ Cells

ASPA is a highly specific polyclonal antibody associated with oligodendrocyte cell bodies, nuclei, and some processes (Moffett et al., 2011; Hershfield et al., 2006). It also co-localizes with oligodendrocyte marker CC1 (Madhavarao et al., 2004), making it an excellent marker for the identification of mature oligodendrocytes.

Cortical tissue, coronally sectioned at 12μm, was prepared from WT and Cx32KO 8-week old animals and evaluated for $ASPA^+$ staining, as described above. In agreement with the decreased oligodendrocyte expression in culture, cortical tissue sections in Cx32KO (7.11%) animals showed a significantly lower oligodendrocyte expression via $ASPA^+$ cell count when compared to WT (13.23%) ($p=0.0238$; n=4-5) (Figure 8A-D). No noticeable difference appeared in the oligodendrocyte pattern or expression. One interpretation of these findings is that the loss of Cx32 affects the development of oligodendrocytes in these animals. This decrease in ASPA expression supports that the knockout of Cx32 affects the development of oligodendrocytes in these animals. Thus, Cx32-containing gap junctions may be critical for growth factor uptake, or their loss may affect surrounding glia in a way that inhibits further oligodendrocyte development.

3.5.2.2 $Iba1^+$ Microglia in the Corpus Callosum

Tissue sections were also stained to determine the percentage of microglia and their morphologic state. Consistent with cell culture findings, Cx32KO tissue sections have a significantly higher percentage of $Iba1^+$ cells in the corpus callosum sections than WT tissue, with an average of 5.47% in Cx32KO and 1.525% in WT ($p=0.0260$) (Figure 9A-C).

3.5.2.3 Nitric Oxide Synthase Production

With a significant increase in activated microglia in culture as well as a significant increase in microglia in cortical tissue, the next question is whether or not these microglia are in a pro-inflammatory state. A known marker for pro-inflammatory microglial activation is inducible nitric oxide synthase (iNOS) (Kim et al., 2006; Marques et al., 2008; Sierra et al., 2014; Lisi et al., 2017), which results in a cascade of inflammatory events in the surrounding environment. As lipopolysaccharide (LPS) is known to activate microglia and increase levels of iNOS (Zhang et al., 2012; Olajide et al., 2013; Lively & Schlichter, 2018; Zhao et al., 2019), western blot analysis was performed on brain homogenates of WT and Cx32KO animals at baseline or after LPS treatment (Figure 10A, C). Although there was upregulation after LPS treatment, there was no significant difference in levels of iNOS between WT and Cx32KO. Neuronal nitric oxide synthase, which may be upregulated by neurons in an inflammatory environment, was also evaluated (Figure 10B, D). It was also not significant between WT and Cx32KO at baseline but was significantly lower in Cx32KO after treatment ($p=0.0056$). Together, these data suggest that the microglia in Cx32KO tissue are not in an activated pro-inflammatory state.

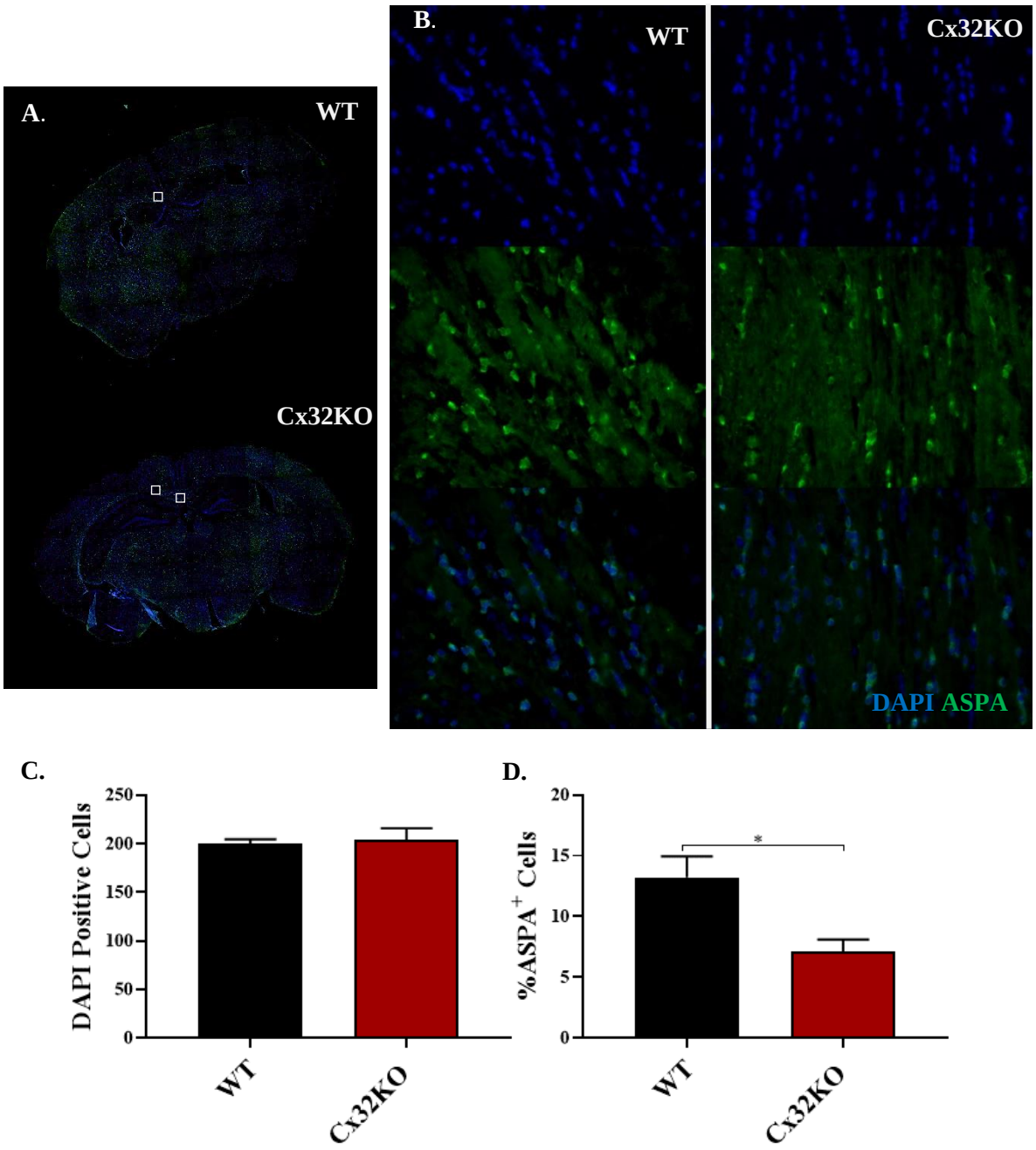

Figure 8. Oligodendrocytes in WT and Cx32KO Tissue. Percentage of oligodendrocytes in tissue section determined by the percentage of $ASPA^+$ nuclei in cortical tissue (n=5,4 animals, 5 images each). A. WT and Cx32KO 12µm coronal tissue sections stained with DAPI and ASPA (AF488). White boxes indicate where representative 40x images were sampled. B. Subdivided DAPI, ASPA, and overlay images at 40x for WT and 32KO. C. Average total cell count, not significant between WT and Cx32KO by a two-tailed t-test. D. Significant decrease in $ASPA^+$ nuclei found in Cx32KO tissue (*t (7)* =0.0238) by two-tailed t-test. Data represent mean ±SEM *p<0.05

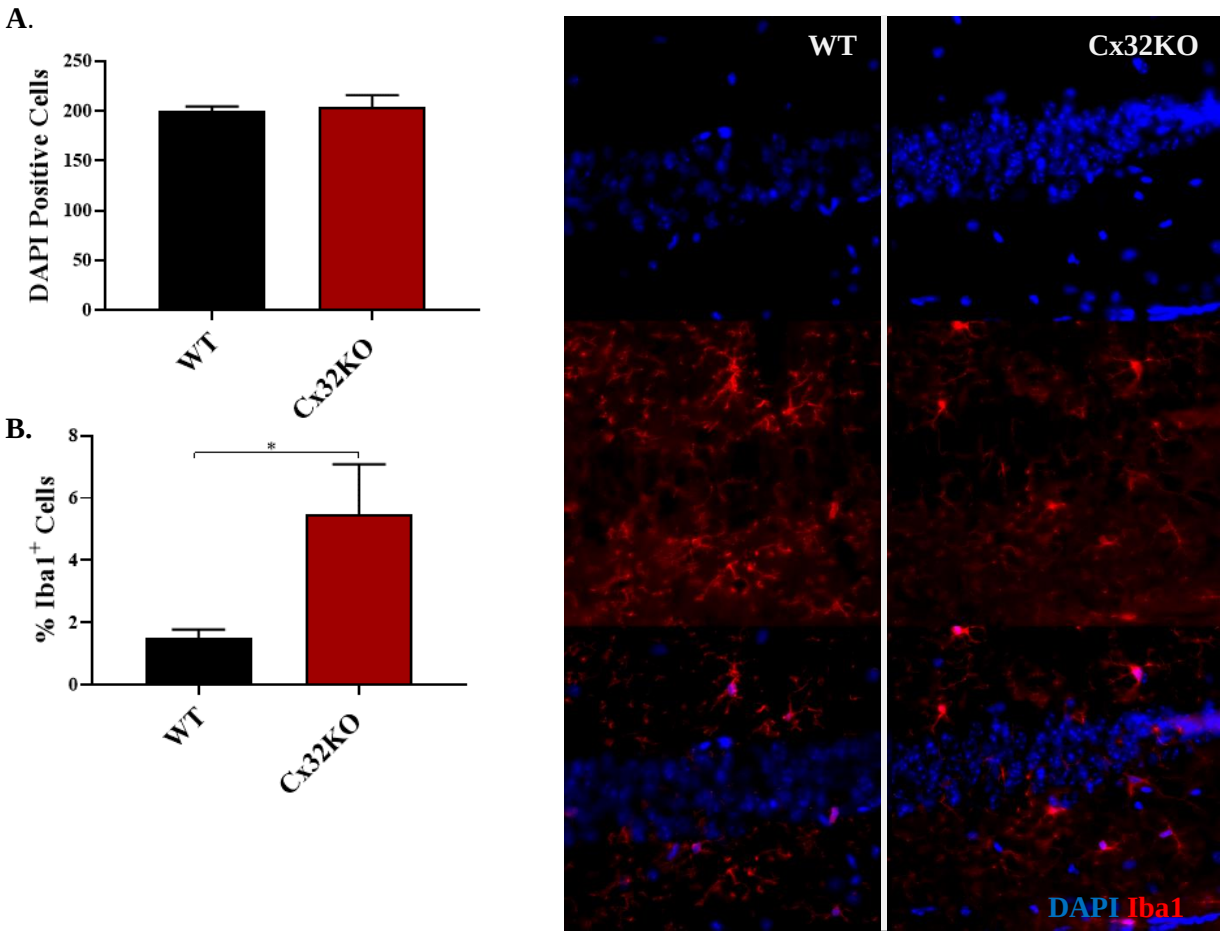

Figure 9. Microglia in WT and Cx32KO Tissue. The percentage of microglia in tissue section determined by the percentage of Iba1$^+$ cells in cortical tissue (n=5-11). A. WT and Cx32KO 12µm coronal tissue sections stained with DAPI and Iba1(AF594). A. Average total cell count, not significant between WT and Cx32KO by two-tailed t-test B. Percentage of Iba1$^+$ cells are significantly higher in Cx32KO tissue (t *(9)* = 2.662) by two-tailed t-test. C. Representative 40x images subdivided into DAPI, Iba1, and overlay for WT and Cx32KO tissue. Data represent mean ±SEM *p<0.05.

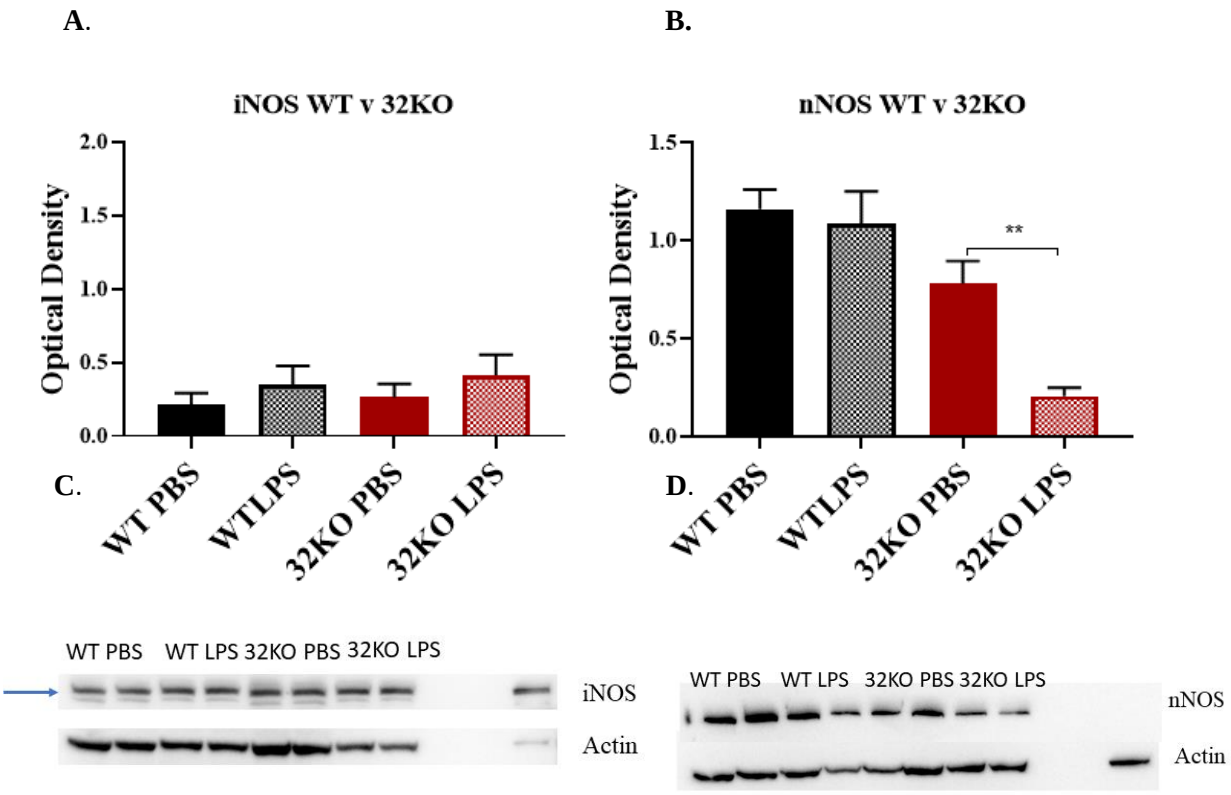

Figure 10. Nitric Oxide Synthase WT vs. Cx32KO. Western blot analysis of both iNOS and nNOS in WT and Cx32KO cortical tissue after PBS and LPS treatment. A. iNOS levels increase but not significantly in both WT and Cx32KO after LPS treatment by one-way ANOVA. (n=6) B. nNOS levels do not change after LPS treatment in WT but do decrease in Cx32KO after LPS treatment ($F_{3.20}$=14; n=6) by one-way ANOVA C. Representative iNOS Western Blot and Actin Control, treatment as marked., iNOS 130kDa. D. Representative nNOS Western Blot and Actin Control, treatment as marked, nNOS 150kDa.

3.6 Results: WT vs. Cx47KO

3.6.1 Effect of Connexin 47 Knockout *In Vitro*

3.6.1.1 Overall Cell Count

Although overall cell count in WT cultures increased from an average of 409 cells at 3DIV to 4621 cells at 6DIV (Figure 11A) ($p<0.0001$), Cx47KO total cell count did not significantly change, with an average of 505.5 at 3DIV and 1095 at 6DIV. Though Cx47KO and WT cultures were similar at 3DIV, Cx47KO cultures show blunted increase and are significantly lower at 6DIV ($p<0.0001$). This cell count decrease suggests that cells are not proliferating and developing as they would in WT, or there is increased cell death with increased DIV. The loss of Cx47KO seems to be detrimental to overall culture development, which will be examined below.

3.6.1.2 Apoptosis

Apoptosis in culture was evaluated by TUNEL positive cell count, reflecting apoptotic DNA-breaks within the nuclei. One possible explanation for the lower total cell counts in Cx47KO cultures could be increased apoptotic activity. However, at 3DIV, we found no significant change in TUNEL positive cell count, with an average of 4.69% in WT and 5.01% in Cx47KO cultures (Figure 11B).

3.6.1.3 Proliferation

In WT cultures, levels of proliferation increased from 7.09% to 35.92% of total cells between 3DIV and 6DIV (Figure 11C) ($p<0.0001$). Comparatively, proliferation within Cx47KO cultures did not significantly increase with an average of 5.21% at 3DIV and 10.31% at 6DIV. At 6DIV Cx47KO cultures expressed a significantly lower percentage of $Ki67^{+}$ cell when compared

to WT ($p<0.0001$). The lack of an increase in proliferation with culture time-point suggests that the knockout of Cx47 creates an environment that is not conducive to continued cellular growth.

3.6.1.4 Oligodendrocytes

3.6.1.4.1 $O4^+$ Oligodendrocytes

Cultures were probed with anti-O4, an oligodendrocyte marker spanning late-stage progenitors through early myelinating oligodendrocytes. There was a significant increase in the percentage of $O4^+$ cells between 3 and 6DIV for WT ($p=0.0157$), increasing from 3.01% to 9.14%. Cx47KO cultures did show a non-significant increase in $O4^+$ percentage from 2.08% to 7.05% ($p=0.0821$) (Figure 12A). It is possible that the overall cell count decrease at 6DIV after Cx47 loss is affecting multiple cell types, including oligodendrocytes, and should be evaluated further.

3.6.1.4.2 Oligodendrocyte Apoptosis

To investigate the levels of apoptosis within Cx47KO and WT oligodendrocytes, we evaluated the percentage of cells which were $O4^+$ / $TUNEL^+$ at 3DIV in culture. Despite the overall level of apoptosis being comparable between WT and Cx47KO cultures, the percentage of apoptotic oligodendrocytes was significantly increased in Cx47KO cultures, with only 2.21% of oligodendrocytes expressing TUNEL in WT cultures and 17.73% in Cx47KO cultures (Figure 12B) ($p=0.0006$). This increase in oligodendrocyte apoptosis suggests that the loss of Cx47 in oligodendrocytes is critical to the overall oligodendrocyte viability.

3.6.1.4.3 Oligodendrocyte Proliferation

Ki67^{+} staining was used to determine the percentage of proliferating O4^{+} oligodendrocytes. As was discussed previously, WT oligodendrocytes express a significant increase in proliferation from 3 to 6DIV ($p<0.0001$). Comparatively, in Cx47KO cultures, oligodendrocytes show only a trend toward increased proliferation from 0.30% to 3.96%. Similar to global proliferation in Cx47KO cultures, this increase appears blunted in comparison to WT, which proliferate at 30.73% and is significantly lower at 6DIV (Figure 12C) ($p<0.0001$). This decrease in oligodendrocyte proliferation may suggest that Cx47 knockout decreases oligodendrocyte viability, potentially hindering their developmental capacity.

3.6.1.4.4 Sox10^{+} Expression

We evaluated the percentage of Sox10^{+} oligodendrocytes at 6DIV. Unlike Cx32KO cultures, the percentage of Sox10^{+} cells were significantly lower in Cx47KO (0.14%) compared to WT (2.98%) (Figure 12D) ($p=0.0362$). This Sox10 decrease is not entirely surprising considering the decrease in total O4^{+} cells, the extremely high level of apoptosis, and reduced level of proliferation. These findings suggest that the loss of Cx47 is altering the viability and developmental capacity of the oligodendrocytes, though a direct interaction between Cx47 with Sox10 cannot be ruled out.

3.6.1.4.5 Sholl Analysis

To investigate arbor and branching characteristics, Sholl Analysis was performed on O4^{+} oligodendrocytes were randomly chosen from WT (n=12) and Cx47KO (n=10) cultures, manually traced and analyzed using ImageJ's Sholl Analysis software. Cx47KO has significantly fewer branching intersections, by distance and genotype (Figure 13A) ($p<0.0001$). The critical Value

(maximum intersections) was not significantly different between WT and Cx47, with an average of 29.33 and 25 respectively, though the critical radius (radius of the circle with maximum intersections) occurred at a significantly shorter distance in Cx47KO oligodendrocytes (67μm compared to 91.67μm) (Figure 13D) (p=0.0189). Cx47KO oligodendrocytes also have significantly fewer primary branches than WT with an average of 11.4 primary branches compared to 17 (p=0.0152). Evaluation of arborization, performed using the SRI (Garcia-Segura & Perez-Marquez, 2014), was not significantly different between the two, with WT at 1.835 and Cx47KO at 2.361. Taken together, the significant decrease in branching intersections (Gensel et al., 2011), the significantly fewer primary branches (Trapp et al., 1997), and the significantly shorter critical radius (Murtie et al., 2007), suggest that the Cx47KO oligodendrocytes are significantly less mature and developed.

3.6.1.4.6 Pdgfrα^{+} Oligodendrocyte Progenitor Cells

Oligodendrocyte progenitor cells are characterized by Pdgfrα^{+} staining. There was no significant difference between Cx47KO and WT cultures, though there was a trend toward reduction at 6DIV. Both WT and Cx47KO cultures expressed a significant decrease in OPC expression with development, decreasing from 26.67% to 2.64% in WT (p<0.0001) and 22.94% to 0.23% in Cx47KO (p=0.0005) (Figure 14A) (p<0.0001).

3.6.1.4.7 Pdgfrα^{+} Proliferation

Oligodendrocyte progenitor proliferation, determined by the percentage of Pdgfrα^{+} and Ki67^{+} cells, significantly decreased within both WT and Cx47 genotypes between 3 and 6DIV (Figure 14B) (p=0.0001, p=0.0003). No differences were seen between genotypes.

3.6.1.5 Astrocytes

3.6.1.5.1 GFAP $^{+}$ Astrocytes

Astrocyte positive cell count, determined by the percentage of $GFAP^{+}$ cells in culture, significantly increased within both genotypes. While WT increased from 11.93% to 26.90% ($p=0.0096$), Cx47KO astrocytic percentage increased from 10.12% to 37.99% at 6DIV($p=0.0003$) (Figure 15A). Though the increase within Cx47KO is not significant in comparison to WT at 6DIV, the trend may be indicative of more severe gliosis after the loss of Cx47 and Cx47/Cx43 mediated communication between oligodendrocytes and astrocytes.

3.6.1.5.2 Astrocyte Apoptosis

Globally, there was no significant difference in the percentage of $TUNEL^{+}$ apoptotic cells within the WT and Cx47KO cultures at 3DIV. While this remains true within astrocytes, there was a non-significant upregulation of $TUNEL^{+}$ astrocytes within Cx47KO cultures (3.21%) compared to 0.21% in WT (Figure 15B). This finding may again reflect the loss of Cx47/Cx43 mediated intercellular O/A coupling in these astrocytes (Maglione et al. 2010, Kamsawa et al., 2005; Wassef et al. 2003, Odermatt et al., 2003).

3.6.1.5.3 Astrocyte Proliferation and Activation

$Ki67^{+}$staining was used to determine the percentage of proliferating $GFAP^{+}$ astrocytes. Both WT and Cx47KO astrocytes increase in proliferation between 3 and 6DIV, with WT increasing from 2.92% to 35% ($p=0.0005$) and Cx47KO increasing from 2.15% to 14.78% (Figure 15C). This blunted upregulation in Cx47KO cultures at 6DIV may suggest that these astrocytes

are affected by the loss of Cx47 and fit with the significant decrease in proliferation within Cx47KO cultures globally.

As described above, $GFAP^+$ FI increase has been used as an indicator of increased astrocytic activation (Montgomery, 1994; Brodie et al., 1997; Kang et al., 2014). Similar to microglial FI in culture, the higher the FI, the more activated/inflammatory these cells can be considered. As with Cx32KO cultures, the $GFAP^+$ FI decreased in both WT and Cx47KO cultures, with WT decreasing from 24500 to 11442 at 6DIV ($p=0.0011$) and Cx47KO decreasing from 25627 to 13875 at 6DIV ($p=0.066$) (Figure 15D). This decrease in FI suggests astrocytes are less reactive/activated the longer they grow in culture. Comparable but slightly elevated FI in Cx47KO cultures at both 3 and 6DIV may suggest that these astrocytes are slightly more activated after the loss of Cx47. As stated previously, although FI intensity is a proxy measurement of activation, these results should be pursued via transcript and protein evaluation specific to astrocytes.

3.6.1.6 Microglia

3.6.1.6.1 $Iba1^+$ Microglia

Measured by the percentage of $Iba1^+$ cells in culture, there was an increase in microglia in both genotypes between 3DIV and 6DIV. The increase in microglial percentage within WT cultures was non-significant (0.57% at 3DIV and 4.62% at 6DIV), and the increase within Cx47KO cultures was robust with 2.18% at 3DIV and 35.83% at 6DIV ($p<0.0001$) (Figure 16A). Although there is an increase in Cx47KO microglia when compared to WT at both time points, only the increase at 6DIV was significant ($p<0.0001$). The global decrease in overall cell count within Cx47KO cultures only accounts for about half the increase in the fraction of microglia.

Thus, the loss of oligodendrocyte Cxs seems to have a direct effect on cortical microglial upregulation and potentially suggests that these cultures are in an elevated state of gliosis.

3.6.1.6.2 Microglial Proliferation and Activation

Microglial proliferation, assessed at 6DIV, was determined by the percentage of $Iba1^+$ cells with $Ki67^+$ nuclei. Unlike Cx32KO cultures, which showed a trend toward lower proliferation, the proliferative capacity of Cx47KO microglia was significantly lower when compared to WT. While WT microglia were proliferating at 31.67% in 6-day cultures, Cx47KO microglia only expressed a 9.01% proliferation (Figure 16B) ($p=0.017$). This decrease in proliferation, as well as the percentage increase in total microglia, suggests that cultured Cx47KO microglia are phenotypically different from those in WT culture.

Microglial activation, determined by increased FI of $Iba1^+$ staining relative to baseline, was decreased with development in both WT and Cx47KO cultures. WT FI decreased from 145405 at 3DIV to 19643 at 6DIV ($p=0.0266$), while the decrease in Cx47KO from 72475 at 3DIV to 14406 at 6DIV is non-significant. (Figure 16C). The decrease in FI with time suggests that microglia become more quiescent with time in culture. Unlike astrocytic FI in culture, these microglia appear to be less FI than WT across time points, suggesting an altered phenotype of microglia within Cx47KO mixed glial cultures.

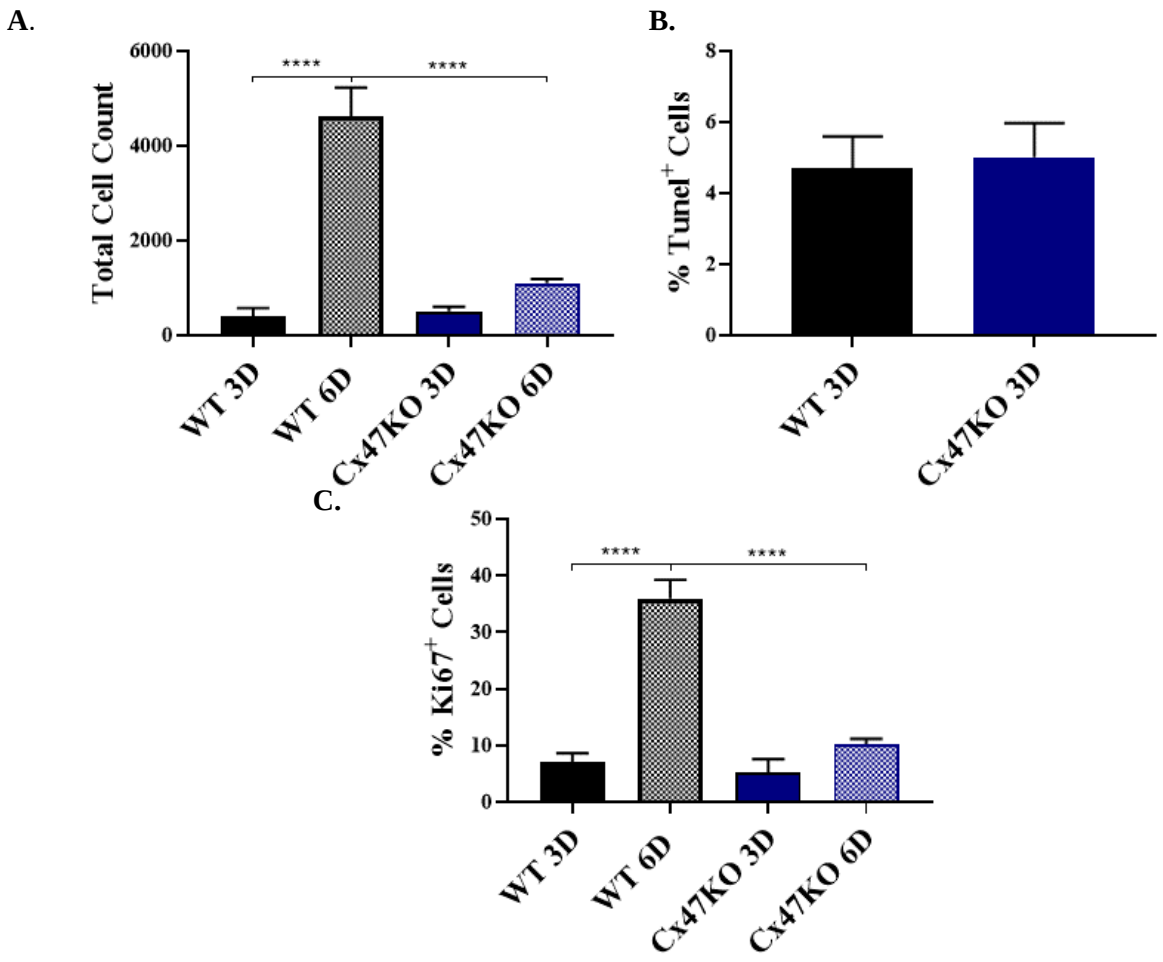

Figure 11. Baseline Cell Type Changes WT vs. Cx47KO. Evaluation of mixed glial cell cultures at 3 and 6DIV. A. Total cell count measured by $DAPI^+$ nuclei per image. There was a significant increase in total cell count for WT cells between 3 and 6DIV, with a significant decrease in total cells in Cx47KO when compared to WT at 6DIV ($F_{3,33}$ = 36.31*)* by one-way ANOVA. B. No significant difference in the percentage of $TUNEL^+$ nuclei WT versus Cx47KO was seen. C. Percentage of $Ki67^+$ of total cells showed a significant increase in WT from 3 to 6DIV in culture, as well as a significantly lower percentage of proliferating cells in Cx47KO cultures at 6DIV compared to WT *($F_{3,28}$*=34.91*)* by one-way ANOVA. Data represent mean ±SEM derived from n=4-15 in each group. ****p<0.0001.

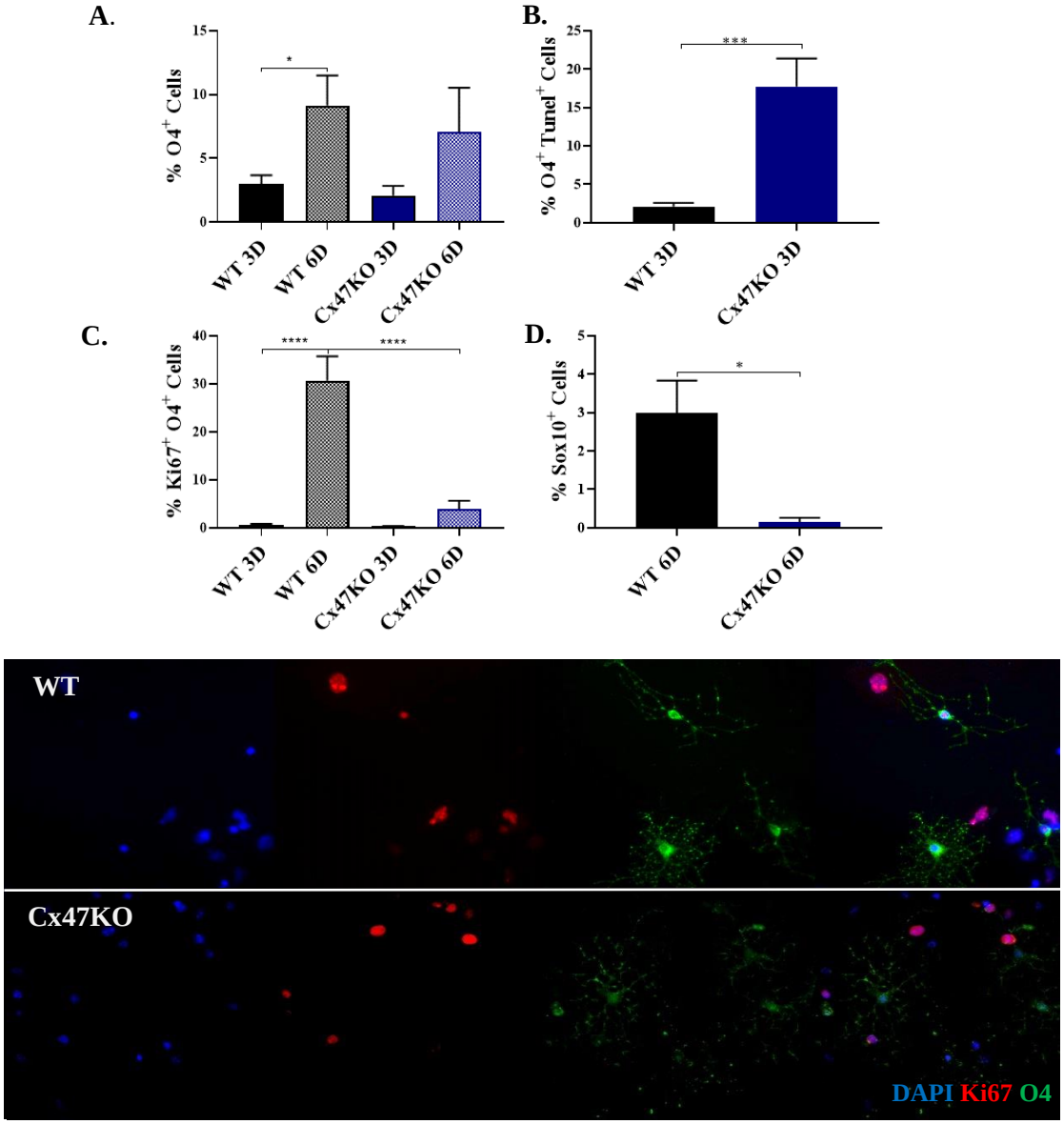

Figure 12. Oligodendrocytes in WT and Cx47KO Cultures. Evaluation of oligodendrocytes within mixed glial cell cultures at 3 and 6DIV. A. The percentage of $O4^+$ cells per image increased in both genotypes between 3 and 6DIV. The increase was significant in WT ($F_{3,18}$=3.631) by one-way ANOVA. B. The percentage of apoptotic oligodendrocytes at 3DIV determined by $O4^+$ with $TUNEL^+$ nuclei is significantly higher in Cx47KO cells (*t (13)* = 4.536) by two-tailed t-test. C. Oligodendrocyte proliferation, determined by the percentage of $O4^+$ with $Ki67^+$ nuclei, significantly increased between 3 and 6- days in WT cultures, and is significantly lower at 6DIV in Cx47KO cultures when compared with WT ($F_{3,17}$=34.64) by one-way ANOVA D. The percentage of $Sox10^+$ cells, is significantly lower in Cx47KO cells (t (9) =2.460) by two-tailed t-test E. Representative WT and Cx47KO $O4^+$ $Ki67^+$ images with DAPI. Ki67 (AF594), and O4 (AF488). Data represent mean ±SEM derived from n=4-10. *<p0.05, **p<0.01, ****p<0.0001.

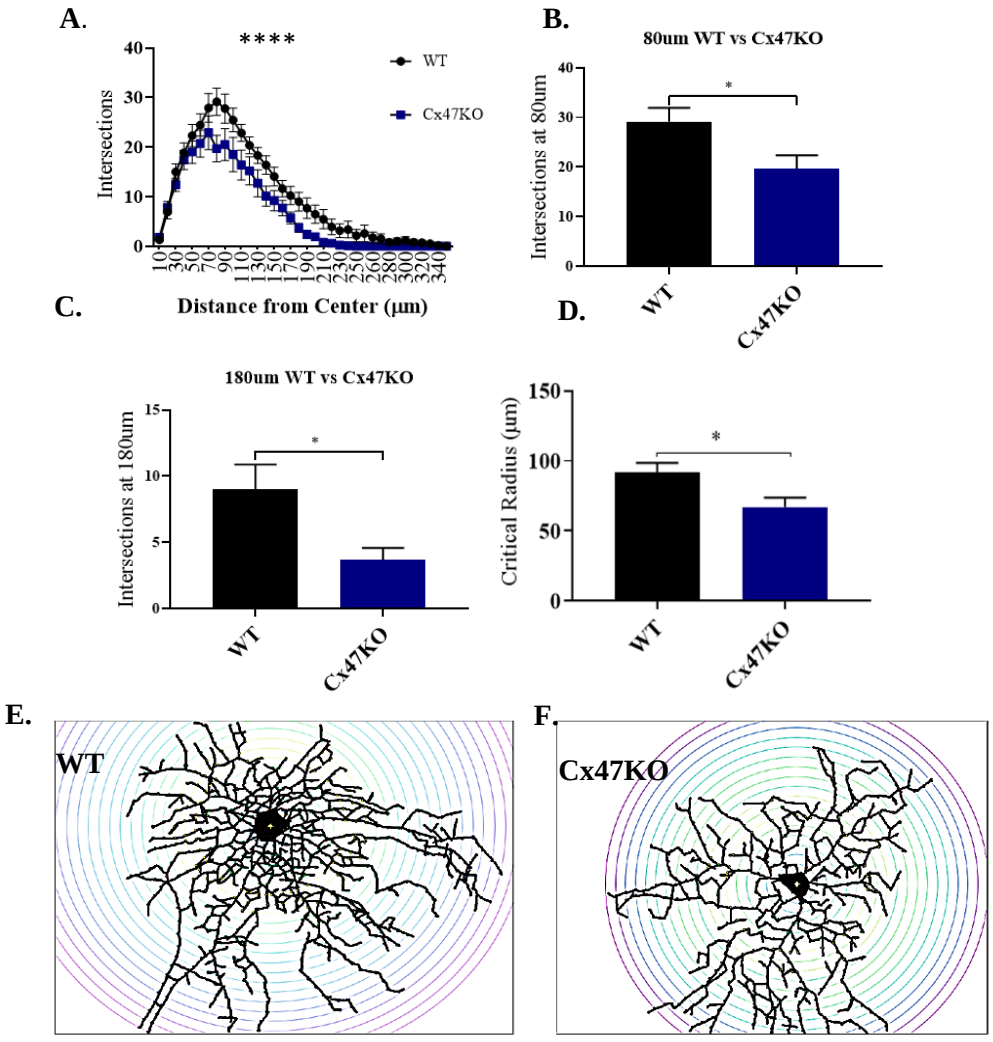

Figure 13. Oligodendrocyte Sholl Analysis WT versus Cx47KO. Sholl analysis performed on 60x images of Oligodendrocytes in Mixed Glial Culture. A. A plot of average intersections at 10µm intervals for the entire oligodendrocyte. Cx47KO oligodendrocytes express significantly fewer intersections by 2-Way ANOVA *(F(Distance)*$_{35,720}$=53.40; *F(Genotype)*$_{1,720}$=56.59*).* B & C. Average intersections at specific distances from the cell soma are significantly lower in Cx47KO when compared to WT at 80µm, 180µm (among others). Showing significantly less branching the farther from the cell soma. (t (20) =2.164; t (21) =2.315) by a two-tailed t-test. D. The critical radius is significantly lower in Cx47KO oligodendrocytes (t (20) =2.554) by a two-tailed t-test. E-F. Representative images of traced oligodendrocytes for WT and Cx47KO. Data represent mean ±SEM derived from n=15-24 in each group. *p<0.05, ****p<0.0001.

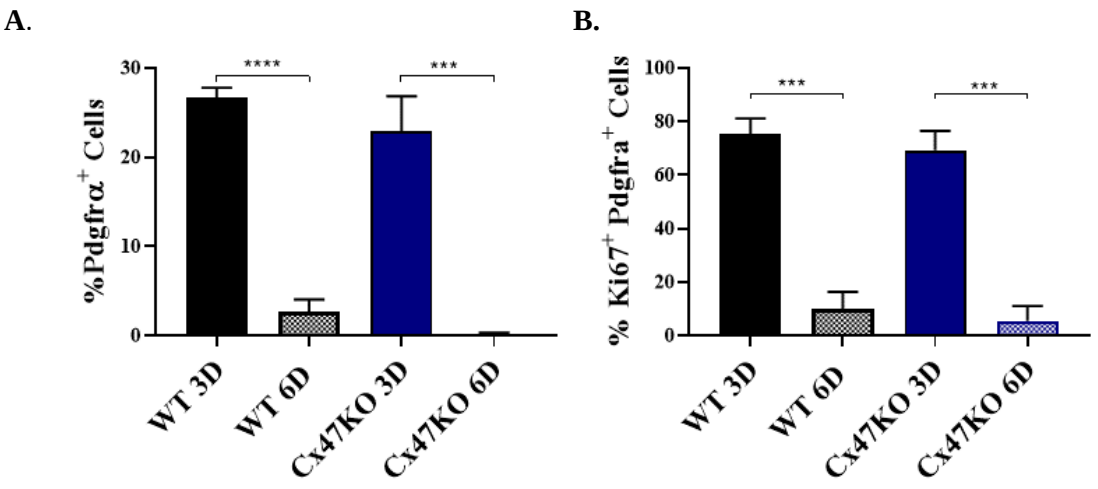

Figure 14. Oligodendrocyte Progenitor Cells in WT and Cx47KO Cultures. A. Percentage of oligodendrocyte progenitor cells, determined by Pdgfrα^{+} cells, significantly decreased in both genotypes between 3 and 6DIV in culture *($F_{3,9}$=37.12)* by one-way ANOVA B. OPC proliferation measured by the percentage of Pdgfrα^{+} cells with Ki67^{+}nuclei significantly decreased between 3 and 6DIV in both genotypes (*$F_{3,10}$*=31.10*)* by one-way ANOVA. Data represent mean ±SEM derived from n=36 in each group. ***p<0.001, ****p<0.0001.

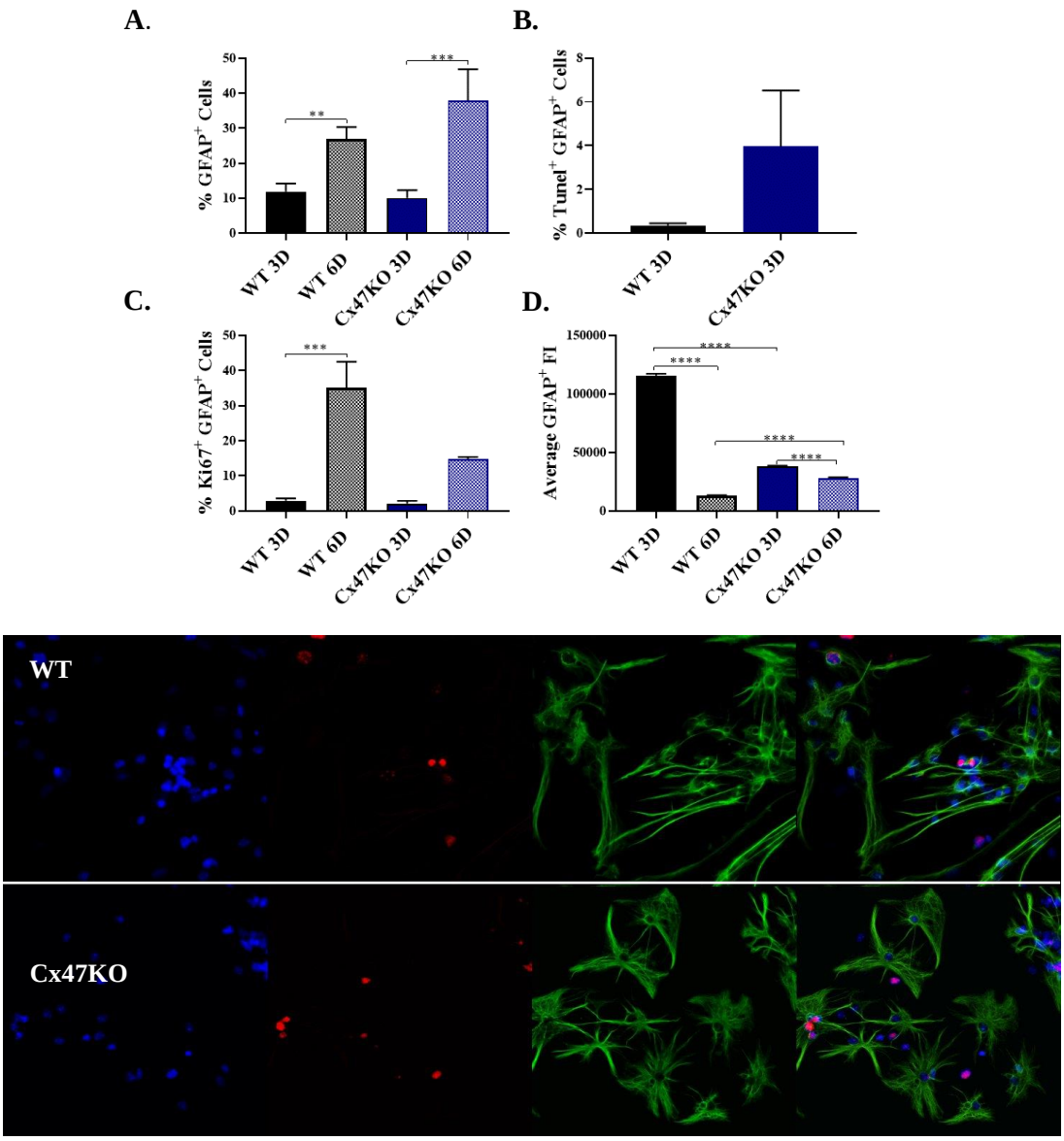

Figure 15.. Astrocytes in WT and Cx47KO Cultures. Evaluation of GFAP$^+$ astrocytes within mixed glial cell cultures at 3 and 6DIV. A. Percentage of GFAP$^+$ cells per image significantly increased in both genotypes between 3 and 6 days *($F_{3,25}$ = 11.45)* by one-way ANOVA. B. The percentage of apoptotic astrocytes at 3DIV was determined by GFAP$^+$ cells with TUNEL$^+$ nuclei and is higher though not significantly in Cx47KO cells by a two-tailed t-test C. Percentage of proliferating astrocytes determined by GFAP$^+$ cells with Ki67$^+$ nuclei significantly increased between 3 and 6DIV in WT. *($F_{3,12}$=12.14)* by one-way ANOVA. D. The average integrated fluorescence intensity of GFAP$^+$ cells. FI decreased between 3 and 6DIV, significantly in WT and non-significantly in Cx47KO cultures*($F_{3,14}$=11.26)* by one-way ANOVA E. Representative GFAP$^+$ Ki67$^+$ 40x images with DAPI, Ki67(AF594), and O4(AF488) are shown. Data represent mean ±SEM derived from n=310 in each group. *p<0.05, ***p<0.001. 5, ***p<0.001.

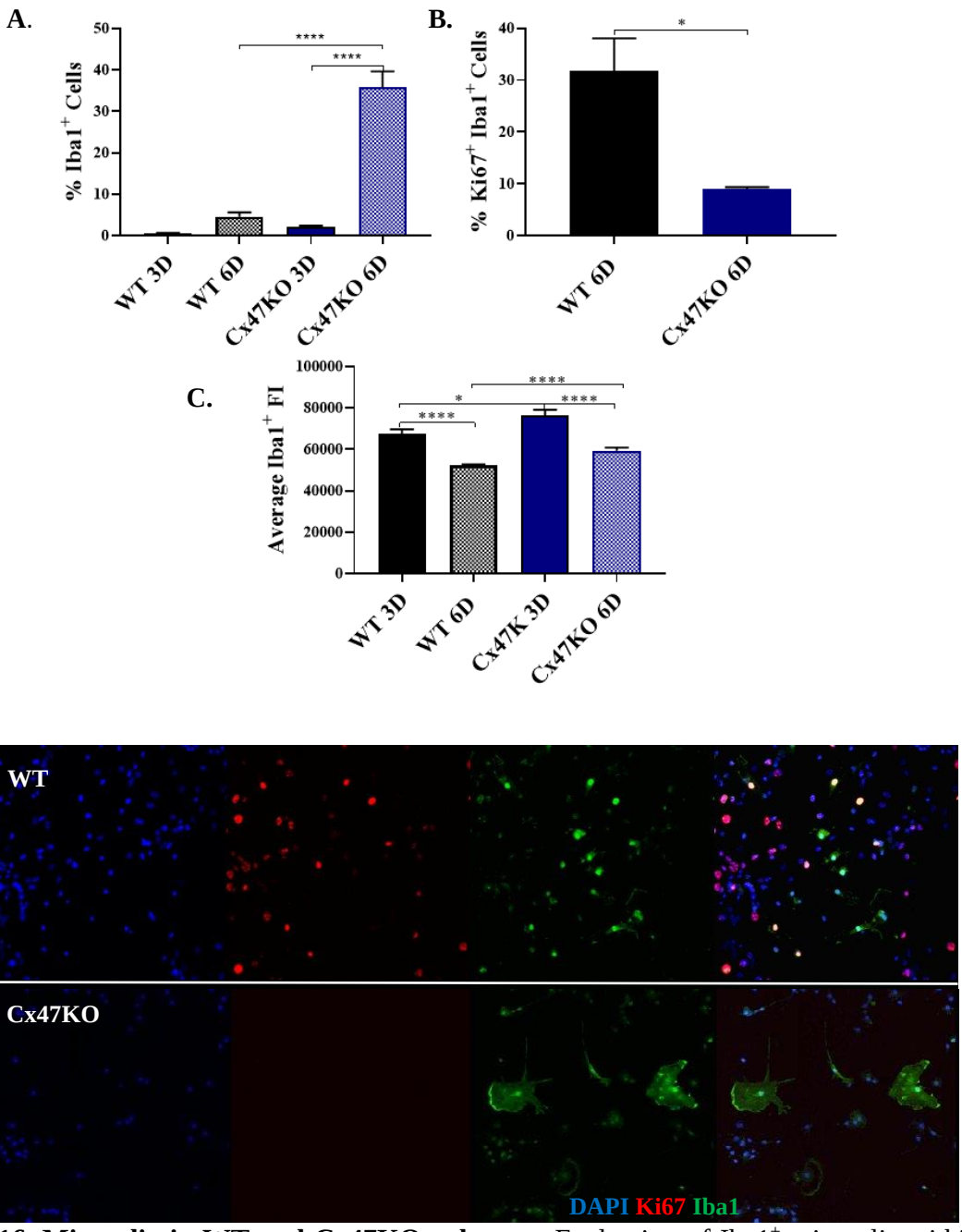

Figure 16. Microglia in WT and Cx47KO cultures. Evaluation of Iba1$^+$ microglia within mixed glial cell cultures at 3 and 6DIV. A. Percentage of Iba1$^+$ cells per image was significantly higher in Cx47KO cultures between 3 and 6DIV, and significantly higher than WT at 6DIV *($F_{3,16}$=97.94)* by one-way ANOVA. B. The percentage of proliferating microglia determined by Iba1$^+$ cells with Ki67$^+$ nuclei was significantly lower in Cx47KO cultures (t (7) = 3.131) by two-tailed t-test. C. Average integrated fluorescence intensity of Iba1$^+$ cells significantly decreased in WT between 3 and 6DIV *($F_{3,13}$=4.529)* by one-way ANOVA. D. Representative 40x Ki67$^+$ Iba1$^+$ images with DAPI, Ki67(AF594), and O4(AF488). Data represent mean ±SEM derived from n=38 in each group. *p<0.05, ****p<0.0001.

3.6.2 Effect of Connexin 47 Knockout *In Vivo*

Oligodendrocyte and microglial percentage in cortical tissue sections were evaluated in tissue sectioned from about bregma area 2.5 (http://www.mbl.org/atlas170/atlas170_frame.html) and sectioned at 12μm to ensure the cortical thickness of approximately one cell nucleus in diameter. While comparing WT and Cx47KO tissue sections (n=5-10), there is a significantly higher cell count per 40x image with an average of 219.7 cells in Cx47KO tissue and 199.8 in WT (Figure 17D) ($p=0.0100$).

3.6.2.1. $ASPA^+$ Cells

As was described previously, cortical tissue sections from WT and Cx47KO were evaluated for $ASPA^+$ staining to quantify oligodendrocytes in the corpus callosum (Figure 17A-C). Within the corpus callosum region of the cortex, Cx47KO had a decreased percentage of $ASPA^+$ oligodendrocytes when compared to WT ($p=0.0820$) (Figure 17E). Although this decrease was not significant, there was a trend towards significance with WT expressing 13.23% $ASPA^+$, while Cx47KO sections had an average of 9.012% $ASAP^+$ cells. This decrease in oligodendrocytes in cortical tissue supports *in vitro* results suggesting that the loss of Cx47 may alter the developmental capacity of the oligodendrocytes or decreases their viability.

3.6.2.2 $Iba1^+$ Microglia in the Corpus Callosum

As was described in the Cx32KO tissue results, Cx47KO and WT tissue were probed for microglial presence sections adjacent t to those stained for oligodendrocytes (Figure 18A-C). Unlike the Cx32KO tissue sections, the Cx47KO tissue did not express a higher percentage of $Iba1^+$ in corpus callosum sections when compared to WT tissue (Figure 18B). Morphologically, these Cx47KO microglia appeared ameboid in shape, potentially in a pro-inflammatory activated

phenotype (Giulian, 1987; Kaur et al., 2017). This finding would support similar results showing increased Iba1^{+} activation in the cerebellum and pons after the loss of Cx47 (Tress et al., 2012; Wassef & Scherer, 2015).

3.6.2.3 Nitric Oxide Synthase

The inflammatory state of the WT and Cx47KO cortical tissue was assessed via Western blot analysis. Brain homogenates were evaluated at baseline and after LPS treatment for levels of both iNOS and nNOS. With a significant increase in activated microglia in culture, as well as the activated morphology of the microglia in tissue, there was an expectation of an increase in iNOS protein levels at baseline in Cx47KO tissue (Figure 19 A-D). As was observed in Cx32KO tissue, there was no significant difference in iNOS levels after LPS treatment (Figure 19A, C). Sister blots showed no significant difference in nNOS levels in Cx47KO tissue when compared with WT tissue at baseline or after LPS treatment (Figure 19B, D). Together, this data suggests that the microglia in Cx47KO tissue are not in an activated pro-inflammatory state, though further investigation will be made in the next chapter. It is possible that the intraperitoneal injection of LPS, as well as the 6-hour time-point, was not long enough to upregulate iNOS and nNOS levels.

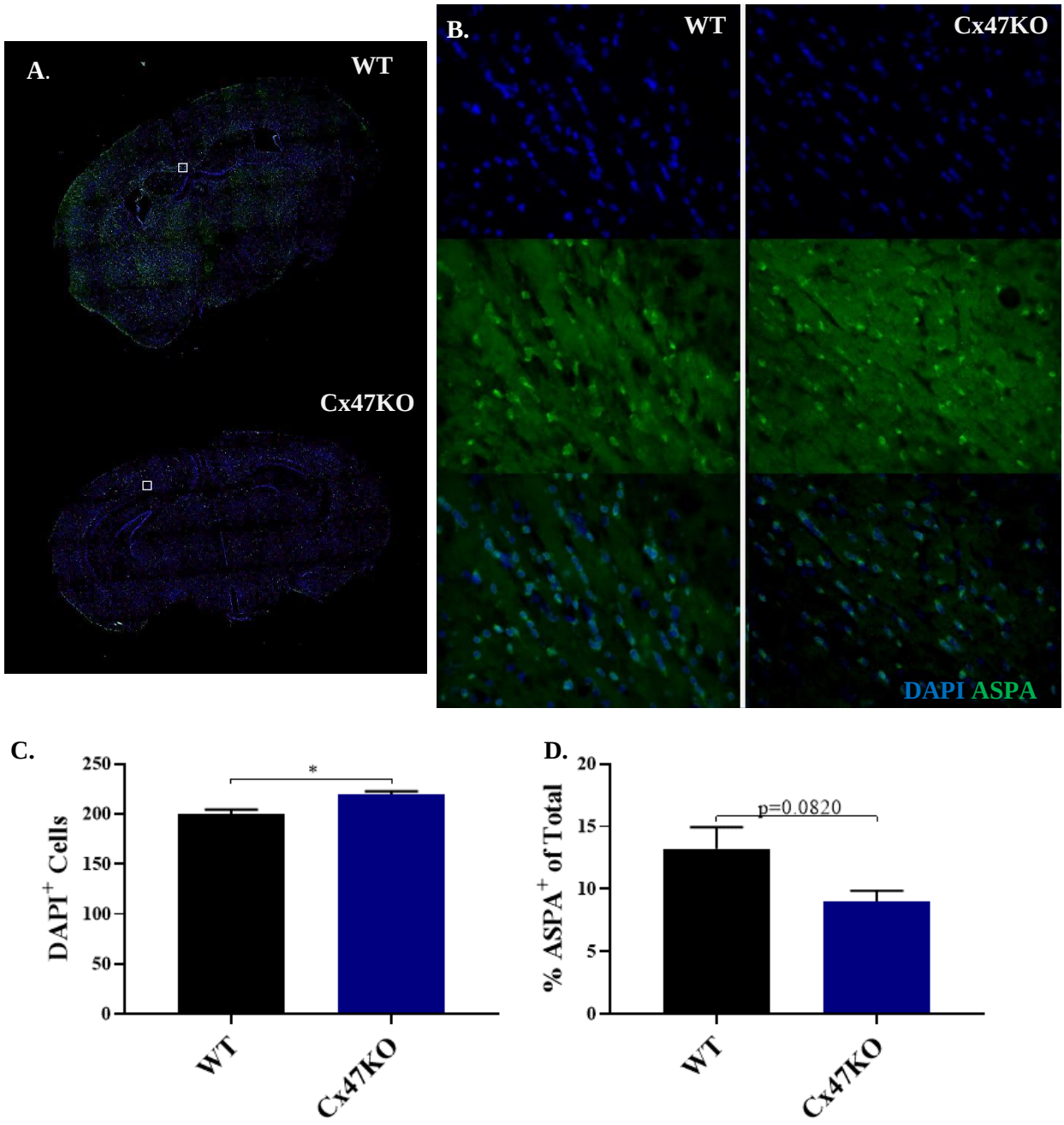

Figure 17. Oligodendrocytes in WT and Cx47KO Tissue. The percentage of oligodendrocytes in tissue section was determined by the percentage of $ASPA^+$ nuclei in cortical tissue (n=4-10). A. WT and Cx47KO 12µm coronal tissue sections were stained with DAPI and ASPA (AF488). White boxes indicate where the representative 40x image was sampled. B. DAPI, ASPA, and overlay images at 40x for WT and Cx47KO tissue. C. Average total cell count, significantly higher in Cx47KO ($t(15) = 2.945$). D. A non-significant decrease in $ASPA^+$ nuclei was found in Cx47KO tissue (two-tailed t-test). Data represent mean $\pm$SEM *$p<0.05$.

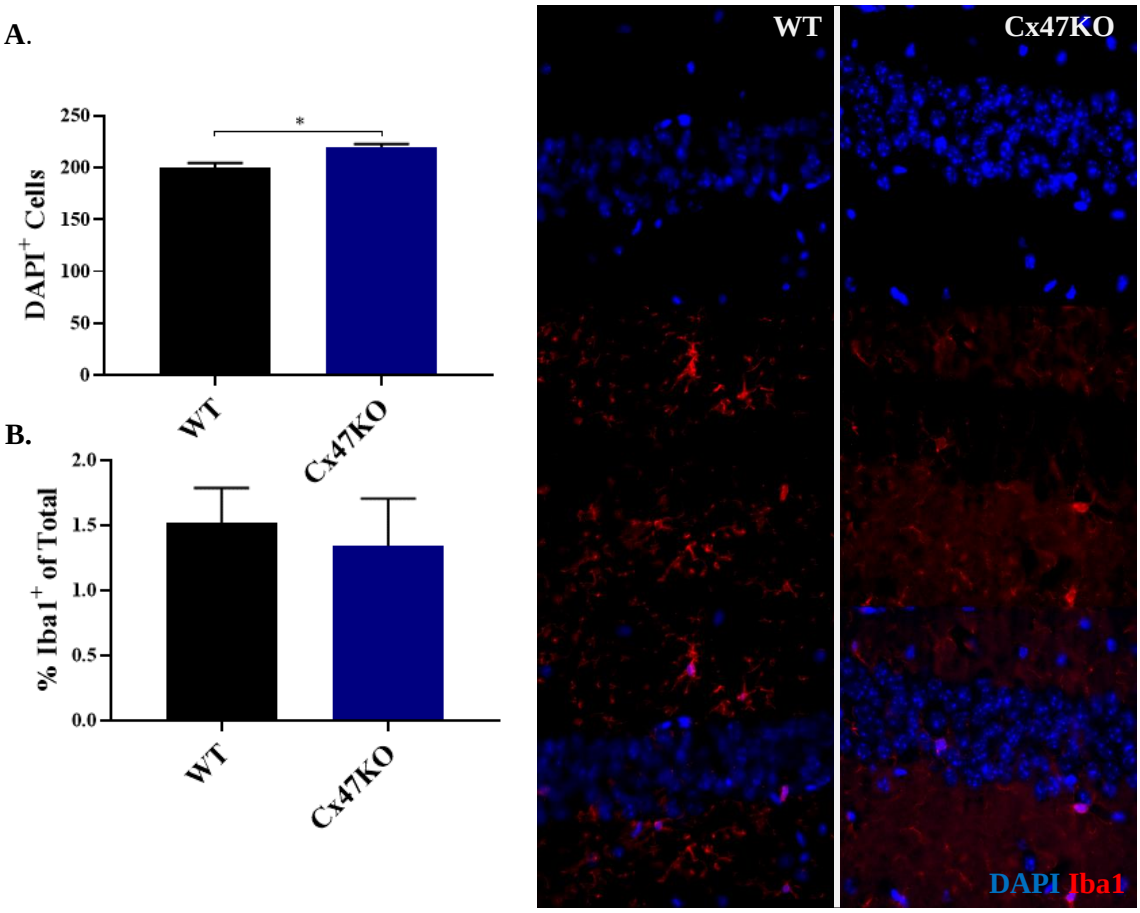

Figure 18. Microglia in WT and Cx47KO Tissue. The percentage of microglia in tissue section determined by the percentage of Iba1$^+$ cells in cortical tissue (n=4-10 animals). A. WT and Cx47KO 12µm coronal tissue sections stained with DAPI and Iba1(AF594). A. Average total cell count was significantly higher between WT and Cx47KO ($t\ (15)$ = 2.945) by two-tailed t-test B. The percentage of Iba1$^+$ cells between Cx47KO and WT was not significantly different, but Cx47KO microglia appear morphologically less ramified. Data represent mean ±SEM derived ***p<0.05. C. Representative 40x images subdivided into DAPI, Iba1, and overlay for WT and Cx47KO tissue.

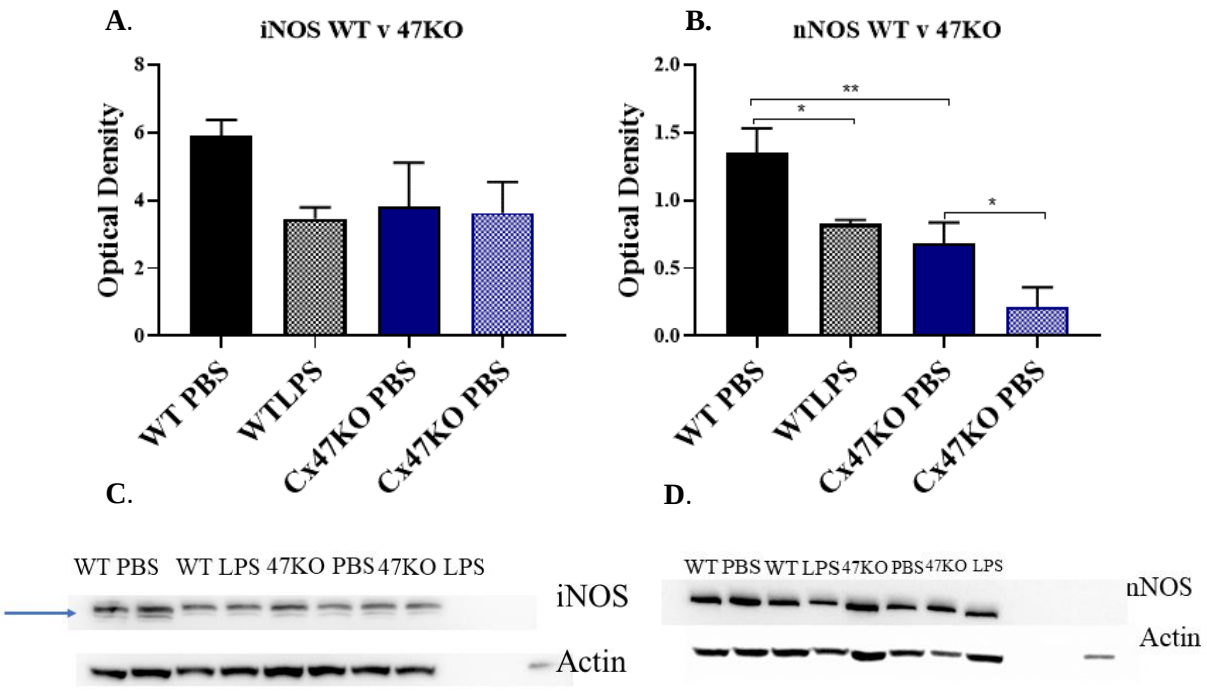

Figure 19. Nitric Oxide Synthase WT vs. Cx47KO. Western blot analysis of both iNOS and nNOS in WT and Cx47KO cortical tissue after PBS and LPS treatment. A. iNOS was not significantly different between WT and Cx47KO tissue. (n=6) B. nNOS levels were not significantly different between genotypes or after LPS treatment C. Representative iNOS Western Blot and Actin Control, treatment as marked., iNOS 130kDa. D. Representative nNOS Western Blot and Actin Control, treatment as marked, nNOS 150kDa.

3.7 Discussion

3.7.1 Effect of Cx32 Knockout

In this study, I showed the knockout of Cx32 appears to affect CNS glia by altering oligodendrocyte development and potentially causing glial activation in surrounding astrocytes and microglia. Analysis of P0-P2 mixed glial cell cultures at 3 and 6DIV found that the knockout of Cx32 blunted oligodendrocyte development when compared to WT at 6DIV. These oligodendrocytes were significantly less apoptotic at 3DIV, and significantly less proliferative at 6DIV when compared to WT oligodendrocytes. Meanwhile, there was a trend toward an increase in Sox10 expression in Cx32KO cultures, suggesting there is a differential change after Cx32KO that may be altering oligodendrocyte development (Stolt e al., 2002; Lü et al., 2008; Bauer and ffrench-Constant, 2009; Lourenço et al., 2016). Sholl analysis of these $O4^+$ oligodendrocytes showed that Cx32KO cells have significantly decreased arborization and branch intersection and significantly higher SRI. These changes indicate that Cx32KO oligodendrocytes are significantly less mature and developed when compared to WT oligodendrocytes (Trapp et al., 1997; Murtie et al.,2007; Gemsel et al., 2011; Garcia-Segura & Perez-Marquez, 2014). Meanwhile, there was no significant difference in the percentage of $Pdgfr\alpha^+$oligodendrocyte precursor cells between Cx32KO and WT cultures, likely due to the lack of Cx32 expression in early oligodendrocyte lineages (Marques et al., 2016). In 8-week old mice, coronal tissue sections revealed that the knockout of Cx32 significantly decreases the percentage of $ASPA^+$ oligodendrocytes in the corpus callosum, suggesting the possibility that altered developmental capacity after Cx32 loss continues throughout later stages of cortical development. Together these findings indicate that Cx32 may play an essential role in the efficient and effective maturity in these myelinating cells.

It remains to be seen if Cx32 knockout causes global or regionally-specific decreases in oligodendrocytes, and whether these developmental deficits persist when comparing normal cortical development to remyelinating paradigms. Future studies should investigate conditional time-point specific knockouts of Cx32 in the context of both developmental myelination as well as remyelination. Furthermore, additional immunohistochemistry should be performed on other alternative brain regions, including the subventricular zone as OPCs are recruited from this region (Menn et al., 2006; Maki et al., 2013).

Despite being localized exclusively in oligodendrocytes, the loss of Cx32 also appears to affect surrounding glia in both culture and tissue. While the percentage of $GFAP^+$ astrocytes was not significantly changed in culture, astrocytes expressed a blunted elevation in proliferation and a significant decrease in FI, suggesting Cx32 alters the astrocytic phenotype in culture. Any astrocytic fluctuation may be the direct result of losing communication provided by the Cx32/Cx30 gap junction or as a homeostatic response to other factors after Cx32 loss (Nash et al., 2011; Talbott et al., 2005; Nobula et al., 2012; Back et al., 2005; Sloane et al., 2010). Additionally, we found that Cx32 knockout resulted in a significant increase in the percentage of $Iba1^+$ microglia both in culture and in tissue. Given the previous evidence for pro-inflammatory and immune responses to connexin knockout (Markoullis et al., 2012; Freidin et al., 2015), it would be hypothesized that this significant increase in microglia, indicative of gliosis, is a pro-inflammatory response. However, in culture, these microglia were less proliferative and showed less FI at 6DIV, and in tissue, these microglia appear to be in a ramified state, together suggesting the microglia in Cx32KO samples may not be playing a phagocytotic or pro-inflammatory role (Harry & Kraft, 2008; Karperien et al., 2013). This observation should be pursued via Sholl analysis for morphologic alterations, as well as via protein and tissue expression of inflammatory factors.

These data suggest that both astrocytes and microglia play an active role in response to the loss of Cx32. In culture, the significant decrease in $Ki67^+$ and increased expression of Sox10 in oligodendrocytes may implicate microglial response (Pang et al., 2013) and warrants continued investigation into modulatory factors of differentiation such as PDGF-a, IGF-2, and NF-kB (Nicholas et al., 2001; Nicolas et al., 2002). Further investigation into the pro- or anti-inflammatory involvement may provide insight into this interaction.

3.7.2 Effect of Cx47 Knockout

In contrast, the loss of Cx47 seems to detrimentally alter oligodendrocyte viability while simultaneously causing astrocytic and microglial activation. In P0-P2 mixed glial cultures, Cx47KO expressed a significantly lower cell count and a significantly lower percentage of $Ki67^+$ proliferation, but no significant difference in the percentage of $TUNEL^+$ apoptotic cells when compared to WT, suggesting that the loss of Cx47 affects the capacity for proliferation within the culture environment. Similar to Cx32KO cultures, Cx47KO cultures expressed a blunted increase in $O4^+$ oligodendrocytes, which were strikingly more apoptotic, less proliferative, and less $Sox10^+$, suggesting the loss of Cx47 alters oligodendrocyte viability in culture. Sholl analysis revealed that $O4^+$ cells in culture expressed significantly lower arborization with a shorter critical radius, suggesting that Cx47KO cells are significantly less mature and developed then WT oligodendrocytes (Trapp 1997; Murtie et al., 2007; Gensel et al., 2011). As seen with Cx32 knockout, Cx47 does not appear to affect oligodendrocyte progenitor percentage or proliferative capacity, likely due to its lack of expression at early oligodendrocyte time-points (Marques et al., 2016). Comparatively, 8-week old cortical tissue showed that after Cx47 knockout, the corpus callosum is hypercellular, with a similar trend towards a decrease in $ASPA^+$ oligodendrocytes. In

a cuprizone model of demyelination, a similar increase in cellularity and a decrease in oligodendrocytes was observed within the demyelinated corpus callosum (Remington et al., 2007), which suggests that Cx47KO tissue cellular changes may also be compensatory for the continued lack of oligodendrocyte viability within the brain. Together, culture and tissue data indicate that Cx47 is vital for oligodendrocyte survival.

Cx47 knockout also altered astroglial response in culture by with a nonsignificant increase in astrocytic expression from 3 to 6DIV. These astrocytes also expressed a non-significant increase in astrocytic apoptosis at 3DIV and substantially decreased astrocytic proliferation, suggesting astrocytes are phenotypically responding to the loss of Cx47 in culture. The lack of significance with some of these measures may have been attributable to the small sample size. These may reflect the reliance of O/A coupling predominantly on Cx47/Cx43 gap junctions (Maglione et al. 2010, Kamsawa et al., 2005; Wassef et al. 2011; Odermatt et al., 2003). My data suggests a role for Cx47 in mutual trophic support between oligodendrocytes and astrocytes and potentially for inflammatory regulation. Follow-up experiments should attempt to investigate the full extent of astrocyte and oligodendrocyte reliance on this communication, possibly via a study of Cx47/Cx43 and Cx43/Cx30dko mice, which could elucidate differences between the loss of this functional channel and all O/A channels without altering O/O communication.

Similarly, in culture, loss of Cx47 resulted in a robust increase in the percentage of microglia within Cx47KO. These microglia were significantly less proliferative and showed reduced Iba1 expression, suggesting the loss of Cx47 alters microglial phenotype with development. The robust increase in microglia, with a significant decrease in overall cell count, may be indicative of a toxic environment after the loss of Cx47. This increase in microglial

expression was not found in the corpus callosum, as was expected. However, *in vivo*, the microglia did appear ameboid with little to no ramification, potentially indicating a pro-inflammatory or phagocytotic phenotype after the loss of Cx47 (Giulian 1987; Karperien et al., 2013; Kaur et al., 2017). These morphologic changes should be pursued with Sholl analysis and analysis for the expression of pro-inflammatory/immune factors. Furthermore, these glial activation responses warrant follow-up experiments investigating the effects of loss of Cx47 on expression profiles of both astrocytes and microglia, given the possibility that their dysregulation might both be contributing to the decreased oligodendrocyte viability (Harry & Kraft, 2008; Peferoen et al., 2014; Wang et al., 2011).

INFLAMMATORY RESPONSE TO OLIGODENDROCYTE CONNEXIN KNOCKOUT

4.1 Glial Activation and Oligodendrocytes

4.1.1 Oligodendrocyte Development and Results of Connexin Knockout

As was discussed in Chapter 3, knockout of both Cx32 and Cx47 affects oligodendrocyte development and surrounding glial activation and phenotype. Results for the two connexins are similar, but the unique differences suggest that each connexin plays a different role within the CNS.

The loss of Cx32 altered oligodendrocyte development and increased the percentage of microglia, with a significant increase in activation of both astrocytes and microglia in culture. Most importantly, in tissue, the loss of Cx32 significantly decreased the percentage of oligodendrocytes, while increasing the percentage of microglia within the corpus callosum. Together, this suggests that loss of Cx32 affects oligodendrocyte development and that microglia may play a role in their regulation. Given our previous findings suggesting increased immune response after Cx32 knockout in the CNS and periphery (Freidin et al., 2015), the microglial response found in Cx32KO culture and cortical tissue will be investigated further in this chapter.

In contrast, the loss of Cx47 resulted in a global decrease in cellular development and proliferation in culture, with decreased oligodendrocyte viability, increased microglial expression, and increased activation of both astrocytes and microglia. In tissue, Cx47KO showed decreased oligodendrocyte presence, similar to culture. Although the total increase in microglia was not maintained in tissue, the phenotype of the microglia appeared to be ameboid, suggesting that these microglia are either in an activated inflammatory state or are underdeveloped as the result of Cx47 knockout. Considering Cx47 plays a prominent role with O/A interactions through the brain, the

microglial response may be the result of cyclic activation with reactive astrocytes after Cx loss (Figure 1B; Boche et al., 2013; Mayo et al., 2014; Savarin et al., 2015; Liddelow et al., 2017; Kery et al., 2020). This chapter will describe investigations into possible pro-inflammatory roles for both astrocytes and microglia.

4.1.2 Astrocytic Activation and Oligodendrocyte Development

In response to inflammatory environments, quiescent astrocytes will change phenotype, becoming activated and reactive to protect the environment and encourage a pro-inflammatory cascade in surrounding glia (Nash et al., 2011). Activated astrocytes release the modulatory factors necessary to regulate OPC and oligodendrocyte survival and development (Talbott et al., 2005) in a variety of neurologic disorders. For example, reactive astrocytes surrounding multiple sclerosis (MS) lesions release the chemo-attractants CXCL8, CXCL1, and CXCL10. These factors promote OPC migration to the site of injury, encouraging remyelination (Omari et al. 2005). After cuprizone-induced demyelination, astrocytic expression of TNFR2 induces increased expression of CXCL12. CXCL12 binds to CXCR4 and leads to increased OPC proliferation and differentiation (Patel et al., 2012).

Astrocytic ciliary neurotrophic factor (CNTF) expressed by activated astrocytes encourages myelin repair by increasing the total myelinating fibers (Stankotf et al., 2002; Nash et al., 2011). In adult traumatic brain injury, an increase in astrocytic IGF-1 leads to Akt phosphorylation, causing a reduction in demyelination, neurodegeneration, and cellular overgrowth (Ye et al., 2004; Zeger et al., 2007; Madathil et al., 2013). Similarly, in neonatal brain injury, the astrocytic release of STAT3 inhibits pro-inflammatory microglia from impairing oligodendrocyte maturation (Nobula et al., 2012). Studies utilizing EAE have also shown that

inhibition of astrocytic NF-κB helps increase myelin preservation, myelin compaction, and remyelination (Brambilla et al., 2014). In response to injury, activated astrocytes also release inhibitory factors, reducing OPC proliferation and developmental potential and thereby curbing remyelinating capacity. For example, after traumatic spinal cord injury, activated astrocytes release bone morphogenetic proteins (BMP2/4), leading to inhibition of OPC differentiation while encouraging continued astrogliosis (Wang et al., 2011). In multiple sclerosis, hyaluronan produced by activated astrocytes is known to mediate OPC maturation via hyaluronidases and the TLR2/MyD88 complex (Back et al., 2005; Sloane et al., 2010). Similarly, reactive astrocytes in demyelinated lesions increase expression of endogenous endothelin-1 (ET-1), promoting Notch activation in OPCs and negatively regulating OPC differentiation and remyelination (Hammond et al., 2014).

4.1.3 Microglial Activation and Oligodendrocyte Development

The homogenous distribution and propensity for rapid activation make microglia crucial cells in response to injury and coordination of repair in the CNS (Popovich et al., 2009). Although microglial roles throughout the brain are diverse, they play a critical role in OPC and oligodendrocyte maintenance and recruitment (Benveniste, 1997; Arnett et al., 2001; Sherwin & Fern, 2005; Butovsky et al., 2006; Horiuchi et al., 2006; Li et al., 2008; Olah et al., 2012; Nobuta et a., 2012; Goldmann et al., 2013; Miron et al., 2013; Peferoen et al., 2014)

Although less studied than the pro-inflammatory microglial phenotype, anti-inflammatory microglia provide trophic support to encourage development and homeostatic regulation between glial cells. Olah and colleagues (Olah et al., 2012) found that a subset of microglia in the corpus callosum facilitates OPC activation, migration, development, and myelin trophic support,

suggesting that the primary role of resident microglia is to repair and maintain tissue homeostasis. Under remyelinating conditions, activated microglia express a specific transcriptional signature, including transforming growth factor-β (TGFβ1), osteopenia (Spp1), and galectin-3 (Gal3). In a cuprizone demyelinating model, Arnett and colleagues (Arnett et al., 2001) found that microglial expression of tumor necrosis factor (TNF-α) is critical for oligodendrocyte regeneration specifically when bound with tumor necrosis factor receptor 2 (TNFR2). Similarly, EAE causes activated microglia to express anti-inflammatory factor interleukin-4 (IL-4), stimulating oligodendrogenesis, and improving clinical symptoms (Butovsky et al., 2006). During demyelinating conditions, "M2" polarized microglia have been shown to release activin-A, which drives oligodendrocyte differentiation to a remyelinating phenotype (Miron et al., 2013).

Alternatively, due to high metabolic activity and energy demand, oligodendrocytes are extremely susceptible to pro-inflammatory microglial modulation (Peferoen et al., 2014). When activated, microglia release a variety of pro-inflammatory modulators, including glutamate, matrix metalloproteinases, lipolytic enzymes, reactive oxygen species, reactive nitrogen species, excitotoxins, chemokines, and cytokines (Benveniste, 1997). Singularly or in combination, these factors lead to the inhibition of OPC development and oligodendrocyte apoptosis (Baud et al., 2004; Yang et al., 2009). For example, during periods of neuroinflammation microglia respond by expressing excess transforming growth factor-β- activated kinase 1 (TAK1), interferon-y (IFNG), tumor necrosis factor (TNF-α), and interleukin- β (IL-1β), thereby halting OPC development and apoptosis (Sherwin & Fern, 2005; Horiuchi et al., 2006; Li et al., 2008; Nobuta et a., 2012; Goldmann et al., 2013).

4.1.4 Minocycline and Inflammatory Regulation

Minocycline (7-dimethylamino-6-dimethyl-6-deoxytetracycline), a semi-synthetic tetracycline analog used initially for its antibiotic function (Garrido-Mesa et al., 2013), has recently been investigated for secondary anti-inflammatory (Good & Hussey, 2003; Gough et al., 1996), anti-apoptotic (Noble et al., 2009), glutamate modulating (Darman et al., 2004), and neuroprotective properties (Zemke et al., 2004; Koistinaho et al., 2005; Kielian et al., 2007; Lampl et al., 2007; Jin et al., 2015). As a lipophilic compound, minocycline easily crosses the blood-brain barrier (Brogden et al., 1975), making it an excellent candidate for neurodegenerative disease states and inflammation. It has been studied in a variety of neurologic disorders including Alzheimer's disease (Choi et al., 2007), amyotrophic lateral sclerosis (Zhu et al., 2002), Huntington's (Chen et al., 2000; Thomas et al., 2004), multiple sclerosis (Metz et al., 2004; Brundula et al., 2002; Nessler et al., 2002), spinal cord injury (Golub et al., 1991; Yong et al., 2004; Festoff et al., 2006; Sonmez et al., 2013), and traumatic brain injury (Sanchez Mejia et al., 2001; Zhao et al., 2011). Though its mechanism of action is unclear, it is thought to inhibit microglial activation after neurologic insult resulting in reduced oligodendrocyte loss, OPC proliferation, and white matter protection (Fan et al., 2006; Cai et al., 2006; Cho et al., 2006). Additionally, experiments performed by Ma and colleagues (Ma et al., 2015), found that after a right unilateral common carotid artery occlusion (rUCCAO) minocycline administration suppressed microglial activation (as evidenced by $Iba1^{+}$ expression), increased MBP production, increased OPC proliferation, and reduced mature oligodendrocyte apoptosis. Similarly, Faheem and colleagues found that after transient middle cerebral artery occlusion (tMCAO), minocycline decreased total $Iba1^{+}$ expression and significantly reduced white matter injury (Faheem et al.,

2019). Together these experiments suggest that minocycline use may be a novel therapeutic target for alleviating the detrimental effect of microglial activation.

4.2 Rationale and Hypothesis for Inflammatory Evaluation

Given the glial response to oligodendrocyte connexin knockout described in chapter 3, we hypothesized that the reduction in $O4^+$ oligodendrocytes and the significant change in oligodendrocyte development is modulated by activated pro-inflammatory microglia. If pro-inflammatory microglial activation is hindering the development of these Cx-deficient oligodendrocytes, we also hypothesize that inhibition of pro-inflammatory microglia might ameliorate some of these changes.

In this aim, mixed glial cultures from WT, Cx32KO and Cx47KO animals were treated with minocycline, a known inhibitor of microglial inflammatory activation. Treatment lasted for either a full 6 days or 3 days with a 3-day recovery period. After treatment, oligodendrocytes, oligodendrocyte precursors, astrocytes and microglia were assessed for changes in proliferation and, for oligodendrocytes, terminal differentiation. Culture media was evaluated for the presence of inflammatory markers at baseline and after treatment via a cytokine assay.

Inflammatory activation was also assessed *in vivo* via whole-brain RNA-seq analysis of cortical tissue for all genotypes, both at baseline and after LPS treatment. LPS treatment in WT animals was performed to evaluate any pro-inflammatory upregulation that may be expected in Cx32KO and Cx47KO tissue. RNA-seq analysis provided insight into differential gene expression, gene ontology analysis, and cell-type-specific response/involvement within each treatment group.

4.3 Materials

4.3.1 Chemicals and Reagents

All cell culture experiments were performed utilizing B27 supplemented Neural Basal Media with an additional 0.5mM glutamax (Invitrogen, USA), 10mM Hepes, and primocin. Papain suspension (Worthington, USA) and bovine growth serum (Hyclone, USA) was used during dissociation and initial seeding. Cultures were treated for either 0, 3, or 6DIV with 10μg/mL minocycline. Culture media was harvested for enzyme-linked immunosorbent assay (ELISA) performed utilizing Mouse Autoimmune Response Multi-Analyte ELISArray™ Kit (catalog # MEM-005A; Qiagen, USA). Antibodies for immunocytochemistry were used as described above, and as detailed in Appendix 1.

Lipopolysaccharide (LPS) (L5668; Sigma, USA) was intraperitoneally injected at 5mg/kg, and cortical tissue was evaluated for transcript changes indicative of pro-inflammatory response. Control animals were treated with phosphate-buffered saline.

4.3.2 Animals

All animal experiments were approved by the University of Illinois at Chicago's Institutional Animal Care and Use Committee. Mice were housed and maintained in standard housing conditions (12/12-hour light/dark cycle) with access to food and water *ad libitum* before experimental use. Animals were treated with lipopolysaccharide as described in the methods below and underwent behavioral evaluation before sacrifice.

For neonatal mixed glial cell cultures, P0-P2 mouse pups were obtained from in-house breeders. Immunohistochemistry was performed on 8-week-old male mice, age-matched, and obtained from in-house breeders.

4.4 Methods: *In Vitro* Assessment of Inflammation

4.4.1 Mixed Glial Cell Culture with Minocycline Treatment

Mouse pups (P0-P2) were decapitated, the cortex was separated from the brainstem and cerebellum and incubated for 35-45 minutes at 37 ºC in Neural Basal A media supplemented with B27(B27NBMA) and Papain (30U/ml). The enzyme reaction was stopped with the addition of 0.25 volume Bovine Growth Serum (BGS). The brains were mechanically dissociated with a 10mL pipet. Dissociation was performed using a sequential series of 10mL, 5mL, and 1000 μL pipets 4-6 times sequentially, with 2-3 minutes rest before supernatant removal and pooling. Cell pellets were resuspended at each step with an additional 3mL B27NBM+10% BGS and filtered through a 70 μm Nylon filters. The final cell suspension was pelleted at low-speed centrifugation (300Xg, 5 minutes), filtered a second time, and plated. Suspensions were seeded on Poly-D-Lysine coated coverslips at four brains per 24-well plate. Cultures were maintained at 37 ºC + 5% CO_2. The media was changed the next day to B27NBMA without BGS and fed every three days.

Dose-response to minocycline was evaluated at 3DIV in culture for WT animals. Subsequent cultures of all genotypes were treated with 0μg or 10μg/mL of minocycline for 6DIV, or for the first 3DIV with recovery in normal media conditions for the subsequent 3DIV. Cells were fed at 3DIV, and media was collected from both 3- and 6-DIV in cultures. These cultures were labeled by genotype and treatment: 6D 0μg T (treatment), 6D 10μg T, and 6D 10μg R. All cultures were washed one time with fresh PBS and fixed with 4% PFA for 15 minutes. Antibody

staining was performed as described below, with O4 staining performed on live cells for 1-hr before fixation.

4.4.2 Immunocytochemistry

As described in Chapter 3, cell cultures were washed once with PBS and fixed with 4% PFA for 15 minutes at RMT. After fixation, cells were washed and blocked for 30-60 minutes in blocked and probed as described in the previous chapter. Primary antibodies utilized included: rabbit anti-Ki67 (1:300; Cell Signaling), rabbit anti-sex determining region Y-box 10 (Sox10) (1:250; Aviva Systems Biology), mouse anti-glial fibrillary acidic protein (GFAP) (1:650; Cell Signaling), rabbit anti-ionized calcium-binding adaptor molecule 1 (Iba1) (1:750; WAKO), mouse anti-platelet-derived growth factor receptor alpha (Pdgrfα) (1:100; Santa Cruz), and mouse anti-O4 (Gift from Dr. Grinspan, 1:24) (Appendix 1). Anti-O4 is a live cell stain and was diluted in cell media and incubated for 1hr at 37 ºC before fixation. After washing, cells were labeled with secondary antibodies for 1hr at room temperature. Secondary antibodies, as listed in Appendix 1. Samples were mounted with Vectashield containing DAPI (Vector Laboratories).

4.4.3 ELISA Cytokine Array

Cytokine levels were evaluated with Mouse Autoimmune Response Multi-Analyte ELISArray™ Kit (catalog # MEM-005A; Qiagen), enabling detection of 12 factors including: interleukin-1β (IL-1β), interleukin-4 (IL-4), interleukin-6 (IL-6), interleukin-10 (IL-10), interleukin-12α (IL-12α), interleukin-17α (IL-17 α), tumor necrosis factor-alpha (TNFα), interferon-gamma (IFNγ), transforming growth factor β (TGFβ1), monocyte chemotactic protein-1 (MCP-1; CCL2), macrophage inflammatory protein 1- α (MIP1-α; CCL3), and macrophage inflammatory protein 1-β (MIP1β; CCL4). This kit allowed for pro- and anti-inflammatory

cytokine evaluation of culture media harvested from WT and Cx32KO cultures under the following conditions: 3D 0μg treatment and 3D 10 μg treatment, as well as 6D 0/0 μg treatment, 6D 10μg treatment and 6D 10ugR treatment. The ELISArray was carried out according to the protocol, with a 1:3 dilution of each sample.

4.4.4 Metamorph Multi-Wavelength Cell Scoring

As described in Chapter 3, multi-wavelength cell scoring was used to analyze all immunofluorescence images. Integrated fluorescence values were obtained using the Multi-Wavelength Cell Scoring applet in Metamorph 7.10 imaging analysis software (Molecular Devices, USA). Thresholds were determined using negative control images such that unlabeled cellular integrated fluorescence was less than 10% of the level of positively scored cells. Image analysis for cultured cells was performed on total $DAPI^+$ cell count, $O4^+$ oligodendrocytes, $Pdgfr\alpha^+$ oligodendrocyte progenitor cells, $GFAP^+$ astrocytes, $Iba1^+$ microglia, $Ki67^+$ nuclei, $Sox10^+$ nuclei/cytosol. Analysis of tissue sections was based on total $DAPI^+$ cells, $ASPA^+$ oligodendrocyte nuclei, and $Iba1^+$ microglial cells.

4.4.5 Statistical Analyses

All statistical analyses were performed with GraphPad Prism (Version 8.3; GraphPad Software Inc). All data represent mean ± SEM, and the null hypothesis was rejected at $p<0.05$. Individual statistical analyses (t-test, ANOVA) are described under their respective figures.

4.5 Methods: *In Vivo* Inflammatory Investigation

4.5.1 Lipopolysaccharide Treatment

Age-matched, 8-week-old WT, Cx32KO, and Cx47KO males were moved into the surgical/behavioral testing space 24-hours treatment. Each mouse was weighed before treatment to provide specific dose/weight LPS treatment. Each animal received either a dose of PBS or Lipopolysaccharide 5mg/kg via intraperitoneal injection, assigned randomly across the cohort at the time of injection. Animals were assessed at every hour over a period of 6 hours post-injection for signs of motor dysfunction, and behaviorally tested at 4-hours post injection. Animals were divided into 3 blocks. Tissue was collected for a total of n =5-9 animals from each genotype and condition.

4.5.2 Behavioral Assessment

Each animal was assessed according to an EAE scoring paradigm at each hour post-injection. At 4 hours post-injection, each mouse was evaluated for changes in rearing and foot-slip behavior after treatment. Rearing was performed in a 1L beaker and determined as the number of times each mouse reared onto its' hind legs in 60 seconds. Foot-slip behavior was evaluated in a laboratory-made 15cm X 15cm X 15cm polyurethane box, with 1.25cm coated metal grid suspended 1.25cm above the floor. Slips were scored as, slip/no-touch = 1and slip with touch = 2. Each task was video recorded for 1 minute and evaluated by an observer blind to treatment.

4.5.3 Tissue Extraction, Sample Preparation

Animals were sacrificed by cervical dislocation, followed by decapitation 6-hours after treatment. A 2mm segment of cortex from bregma -1 to -3 was extracted utilizing a Stoelting acrylic coronal brain matrix (#51380 https://www.stoeltingco.com/acrylic.html). The right

hemisphere was separated off, and tissue was flash frozen and maintained at -80ºC before RNA-seq preparation by UIC's Core Genomics Facility.

4.5.4 RNA-sequencing

4.5.4.1 RNA-seq Sample Preparation

Total RNA was isolated by the UIC Genomics Core Facility using Maxwell® RSC simplyRNA Tissue Kit (#AS1340; Promega). RNA samples were quantified and checked for purity using NanoDrop™ One Spectrophotometer (Thermo Scientific), and integrity was checked using Agilent 4200 TapeStation.

RNA-seq library preparation was completed using NuGen's Universal Plus mRNA-seq kit, per User Guide M01485 v3. RNA inputs into library preparation were between 360-818ng per sample. In brief, library construction steps included poly(A) RNA selection, RNA fragmentation and double-stranded cDNA generation using a mixture of random and oligo(dT) priming, followed by end repair to generate blunt ends, ligation of UDI adaptors, strand selection, and 14 cycles of PCR amplification to produce the final libraries. The number of cycles for PCR library amplification was determined by qPCR using the KAPA Library Quantification Kit (KAPA Biosystems), with the Prime Pro 48 Real-Time PCR system (Techne).

Amplified libraries were analyzed on the 2200 TapeStation system (Agilent) and quantified using a Qubit 2.0 Fluorometer (Life Technologies). Individual libraries were normalized and pooled in equimolar amounts, and concentration of the final pool was determined by the PCR quantification method using KAPA Library Quantification Kit (KAPA Biosystems). Sequencing was carried out on NextSeq 500 (Illumina), 2x42 nt reads, high output, to achieve approximately 20x10^6 clusters per sample.

4.5.4.2 RNA-seq Analysis

4.5.4.2.1 Differential Gene Expression

All the PE100 bp reads were processed with the Trimmomatic (version 0.36)1 QC pipeline, where all the bases in the reads that were below the quality score of 15 were trimmed using a sliding window of 4 bp. All reads that were less than 35 bp in length were discarded. The trimmed PE100 bp reads were aligned to the GRCm38.primary_assembly mouse genome using STAR (version 2.4.2) 2 software using the default parameters, and the gene counts were obtained by adding the parameter ---quantMode GeneCounts. The edgeR pipeline for multifactorial analysis was used to identify significant differences across treatments. The pipeline involved the following steps: 1) the raw gene counts generated using the STAR were set up for each contrast analysis, 2) the low expressed genes were filtered off by selecting for genes with more than 10 counts in at least one sample across the sample set, 3) The filtered counts were normalized using the weighted trimmed mean of M-values (TMM) method, 4) A design matrix was generated to test various genotypes and treatments; in total, nine different design matrices included wild type (PBS), 32KO (PBS),47KO (PBS), wild type (LPS), 32KO (LPS) and 47KO (LPS). The generalized linear models (GLM) were fitted with the data, and the significant gene clusters in different treatments were determined using the likelihood ratio test (LR test). The final sets of genes in each test were determined using an FDR of 0.1. The differentially expressed set of genes were annotated using the annotations available for the most recent mouse genome.

4.5.4.2.2 Cell-Type Specific Sorting

The differentially expressed gene sets from various treatments and genotypes were further classified into different cell types by overlaying them with the cell-type specific RNA-seq data from https://web.stanford.edu/group/barres_lab/brain_rnaseq.html using custom Perl scripts.

4.5.4. 2.3 SYBR Green Quantitative Real-Time PCR

Initial gene expression analysis of differentially expressed oligodendrocyte transcripts was executed through a quantitative real-time polymerase chain reaction (qPCR). Transcripts assessed include gap junction beta-1 (GJB1; Cx32), gap junction gamma-2 (GJC2; Cx7), myelin oligodendrocyte glycoprotein (MOG), N-myc downstream regulated-1 (Ndrg1), and a disintegrin-like and metalloprotease with thrombospondin motifs 4 (ADAMTS4). Primers for each transcript assessment can be found in Appendix Tables A4 & A6.

Total RNA was prepared and evaluated as described for RNA-seq. 2.5µg of total RNA from each sample was reverse transcribed to cDNA using a SuperScript IV Vilo Kit (#11766050; Invitrogen) according to the manufacturer's instructions. A no reverse transcription control was also included. The resultant cDNA was stored at -20°C before qPCR analysis. Primers used to analyze genes of interest (GOI) were first assayed on WT cDNA using a SYBR Green qPCR method to determine reaction efficiency and ideal cDNA mass input. Amplification specificity was confirmed by melt curve analysis. After primer validation, 25 ng of each sample was assayed in triplicate for each GOI, and the reference genes β-actin and GAPDH. Quantitative real-time PCR was performed with a Chromo4 Real-Time PCR Detector (CFB-3240; Bio-Rad) using a 2x SsoAdvanced Universal SYBR Green Supermix (#1725270; Bio-Rad). The following thermal cycling protocol was used: [95°C for 30 s] – 1 cycle, [95°C for 20 s, 55°C for 30 s, 72°C for 15 s]

– 40 cycles, followed by a heating regimen to generate a qPCR product melt curve. All GOI results were normalized to the geometric mean of the corresponding reference gene results using the Pfaffl relative quantification method in Excel (Microsoft). Resultant fold changes were graphed and statistically examined for significance (GraphPad Prism).

4.6 *In Vitro* Results

4.6.1 Minocycline Treatment WT vs. Cx32KO

We hypothesized that pro-inflammatory microglia inhibit the development of oligodendrocytes within Cx knockout cultures, and that minocycline treatment within these cultures would modulate these deficits. A 10μg/mL dose was utilized throughout, after trial experiments at 3DIV showed this dose both increased cell count and proliferation, presumably by inhibition of inflammatory microglia (Figure 20A-B). Minocycline treated cells were analyzed after 6DIV with no treatement, after full 6-day treatment, or after 3-day treatment followed by a 3-day recovery. Treatment groups were compared to baseline 6DIV cultures.

4.6.1.1 Cellular Development and Overall Cell Count

The total cell count after minocycline treatment in mixed glial cultures was evaluated by the total $DAPI^+$ cell count at 6 DIV under the following treatment conditions: 0μg treatment (6D 0μg), 10μg treatment (6D 10μg), and 10 μg treatment with a 3-day recovery (6D 10μg R). There was no significant difference in total cell counts across genotypes at baseline, but minocycline treatment and recovery appeared to differentially effect global cell expression. WT cultures showed a decrease in cell count during treatment, with a significant decrease to 1194 total cells

during recovery (p=0.0441). Comparatively, the Cx32KO cell total significantly decreased during treatment (p=0.0270) and returned closer to baseline during recovery. (Figure 21A).

4.6.1.2 Ki67^{+}Proliferation

Cellular proliferation was differentially altered with minocycline treatment across genotypes. Cx32KO cultures proliferated significantly less than WT at 19.62% compared to 35.92% at baseline at 6DIV (Figure 21B) ($p<0.0008$). Meanwhile, minocycline treatment had opposite effects on WT and Cx32KO cultures, significantly decreasing the percentage of proliferative cells in WT to 23.12% (p=0.0174) and increasing the percentage of proliferation to 30.33% in Cx32KO cells (p=0.0375). The proliferative capacity returned to 36.93% in WT cultures when in recovery and remained elevated in Cx32KO at 28.58%. This alteration in proliferation suggests that the inhibition of pro-inflammatory microglia plays a role in the proliferative capacity of these cells in culture with a suppressive effect on WT and a stimulatory effect in the Cx32KO by minocycline treatment.

4.6.1.3 O4^{+} Oligodendrocytes

Minocycline treated cultures were evaluated for the percentage of oligodendrocytes via the percentage of cells that were both DAPI^{+} and O4^{+}. Minocycline treatment resulted in a significant decrease in the percentage of oligodendrocytes in culture, with WT decreasing from 5.91% to 0.72% (p=0.0029) and Cx32KO decreasing from 4.78% to 0.40% (p=0.0049) (Figure 22A). This change was reversed in WT cultures during recovery, while Cx32KO had a blunted recovery of oligodendrocytes at 1.95%. This decrease in oligodendrocytes suggests one of two things: either 10μg/mL minocycline treatment is toxic to oligodendrocytes, or the inhibition of pro-inflammatory microglial factors alters effective oligodendrocyte development and maintenance. Visually, the

treated oligodendrocytes to have fewer processes than mature oligodendrocytes at baseline, which suggests that oligodendrocyte maturation may be compromised during treatment.

4.6.1.4 $O4^+$ Oligodendrocyte Proliferation

The proliferative capacity of oligodendrocytes in 6-day cultures were evaluated by $O4^+$ cells with $Ki67^+$ nuclei. The knockout of Cx32 significantly lowered proliferation within oligodendrocytes at baseline, with WT oligodendrocytes proliferating at 30.73% and Cx32KO proliferating at 11% ($p<0.0001$) (Figure 22B). Minocycline treatment significantly decreased oligodendrocyte proliferation in WT culture to 2.67% ($p<0.0001$), while oligodendrocyte proliferation was closer to baseline at 25.78% after recovery. Comparatively, Cx32KO oligodendrocyte proliferation was not significantly altered across treatments. The lack of alteration during treatment suggests that the decrease in Cx32KO proliferation may not be the result of pro-inflammatory microglial factors.

4.6.1.5 $Sox10^+$ Expression

Changes in the percentage of $Sox10^+$ expression was also evaluated *in vitro*. There was an increase in $Sox10^+$ expression after Cx32KO at baseline (as expressed in Chapter 3), but after minocycline treatment, both genotypes expressed a lower percentage of $Sox10^+$ cells. The percentage decreased from 4.79% to 0.55% in WT ($p=0.0530$) and 6.64% to 1.51% in Cx32KO cultures ($p=0.0486$). Although the percentage of $Sox10^+$ cells rebounded in WT cultures during recovery, it remained inhibited in Cx32KO cultures at 1.62% (Figure 22C). These results are qualitatively similar to those obtained for $O4^+$ cells.

4.6.1.6 Pdgfrα^{+} Oligodendrocyte Progenitor Cells

Oligodendrocyte progenitor cells in culture were evaluated by the percentage of cells that were Pdgfrα^{+}. At baseline, 6-day cultures showed no significant difference regardless of genotypes, with WT expressing 2.64% and Cx32KO expressing 1.18% OPCs. During treatment, there was an increase in OPC percentage across genotype, rising to 7.26% in WT and 11.44% in Cx32KO cultures ($p=0.0036$) (Figure 22D). This significant increase during treatment is inverse to the decrease of O4^{+} cells, suggesting that while treated with minocycline, oligodendrocytes are not differentiating into more mature states.

4.6.1.7 Pdgfrα^{+} Proliferation

As was discussed in the previous chapter, there is no significant difference between WT and Cx32KO in the percentage of proliferating oligodendrocyte progenitors, evaluated by Pdgfrα^{+} and Ki67^{+} cells. There is no significant difference across treatment types, as the percentage of proliferating cultures varies widely across the small percentage of OPCs present at baseline. In WT cultures, proliferation increased from 9.94% to 13.56% after treatment, returning to 9.7% during recovery. Cx32KO OPC proliferation was 12.57% at baseline, showing a trend toward an increase to 33.14% during treatment and decreasing to only 3.34% during recovery (Figure 22E).

4.6.1.8 GFAP^{+} Astrocytes

The percentage of astrocytes in cultures treated with minocycline was evaluated by the percentage of total GFAP^{+} cells. At baseline, 26.90% of cells in WT cultures and 26.60% of cells in Cx32KO cultures expressed GFAP. There was a decrease to 15.46% astrocytes in WT cultures with minocycline treatment ($p=0.0875$), while Cx32KO cultures expressed a non-significant

decrease to 21.86% during treatment (Figure 23A). The lack of significant alteration in astrocytic expression suggests pro-inflammatory microglial factors are not involved in the astrocyte response to Cx knockout.

4.6.1.9 $GFAP^+$ Astrocyte Proliferation and Activation

Astrocytic proliferation after minocycline treatment was determined by the percentage of $GFAP^+$ cells with $Ki67^+$ nuclei. As was discussed in the previous chapter, WT astrocytes were more proliferative than Cx32KO at baseline, with 35.10% of astrocytes proliferating versus 14.78% in Cx32KO cultures (Figure 23B). While being treated with minocycline, WT astrocytes became less proliferative at 14.18% ($p=0.0914$). Interestingly, in WT cultures, this proliferative capacity returns during recovery, suggesting the presence of pro-inflammatory microglial factors plays a role in the astrocytic capacity for proliferation. The treatment of Cx32KO cultures decreases astrocyte proliferation, which increases closer to a level comparative to WT at baseline during recovery. These results suggest pro-inflammatory microglial factors and Cx32 may affect astrocytic proliferation in culture.

As was discussed in chapter 3, astrocytic activation in culture can be measured by the increase in $GFAP^+$ fluorescence intensity (FI) relative to baseline, with the expectation that the higher the activation state, the more fluorescence emission (Montgomery, 1994; Brodie et al., 1997; Kang et al., 2014). After 6DIV in culture, baseline astrocyte $GFAP^+$ FI was slightly elevated in Cx32KO cultures as compared to WT ($p=0.0014$) (Figure 23C). Both genotypes had an elevation of FI during minocycline treatment ($p<0.0001$). This increased activation continues to elevate in WT cultures during recovery ($p<0.0001$), while Cx32KO cultures returned closer to

baseline ($p<0.0001$). These data suggest that inhibition of microglial inflammatory factors alters astrocytic activation and that Cx32 recovers from this treatment more readily than WT.

4.6.1.10 Iba1$^+$ Microglia

The presence of microglia in the minocycline treated cultures was determined by the percentage of Iba1$^+$ cells. As was discussed previously, there is a significant increase in the percentage of microglia within Cx32KO 6-day cultures when compared to WT at baseline ($p=0.0685$). While treated with minocycline, both genotypes show a significant upregulation in the percentage of microglia, increasing from 4.62% to 22.17% in WT ($p=0.0006$), and 11.7% to 20.68% in Cx32KO ($p=0.0238$) (Figure 24A). Both genotypes appear to return closer to baseline levels during recovery with WT at 6.08% and Cx32KO at 8.11%. This result may suggest that microglia are proliferating more when they are not pro-inflammatory. However, when corrected for total cell count, there is little change in absolute Iba1$^+$ cell counts, which suggests instead that microglia are the most resilient glial cells in these cultures.

4.6.1.11 Iba1$^+$ Microglial Proliferation and Activation

Microglial proliferation was evaluated in minocycline treated cultures by the percentage of Iba1$^+$ cells that have Ki67$^+$ nuclei. As was stated before, baseline microglial proliferation in Cx32KO was non-significantly reduced compared to WT, with 22.44% of microglia proliferating in Cx32KO cultures and 31.67% of microglia proliferating in WT. Minocycline treatment did not significantly change the proliferation of WT microglia, which proliferated 29.92% with full treatment, and 36.79% in the recovery. Conversely, minocycline treatment increased proliferative capacity in Cx32KO microglia, increasing to 37.75% with treatment ($p=0.0447$) and 42.14% while recovering from treatment ($p=0.0608$) (Figure 24B). This increase in microglial proliferation

suggests that the phenotype of Cx32KO microglia was significantly altered after minocycline treatment.

Increases in relative Iba1^{+} FI, indicative of microglial activation in culture, were also evaluated in the context of minocycline treatment. Previously, we found that the FI of microglia in Cx32KO cultures at 6DIV was significantly higher than that of WT at baseline ($p<0.0001$), suggesting that Cx32KO microglia are more activated than WT. When treated with minocycline, WT microglial FI significantly increases from an average of 52463 to 79890 ($p<0.0001$) and continues to increase after treatment withdrawal with an average FI of 115118 ($p<0.0001$) (Figure 24C). Conversely, Cx32KO cultures decreased significantly in FI during minocycline treatment to 37337 ($p<0.0001$) but rebounded closer to baseline (with a still significantly lower FI) during recovery, with an average FI of 50898 ($p<0.0001$). These alterations in FI may support our hypothesis that microglial activation occurs in response to Cx32 knockout, and the significant decrease in FI during minocycline treatment suggests that this activation is pro-inflammatory.

4.6.1.11 Elisa Cytokine Array

The Mouse Autoimmune Response Multi-Analyte ELISArray™ Kit (catalog # MEM-005A; Qiagen) was used to investigate the state of inflammation within WT and Cx32KO cultures at 3- and 6DIV for each treatment type. Considering the microglial response found and discussed in chapter 3, we expected to find that Cx32KO cultures were expressing higher levels of pro-inflammatory factors at baseline, and that minocycline treatment would lower these levels. Of the 12 cytokines and chemokines within this array, at 3DIV, mixed glial cultures expressed detectable levels of MCP-1(CCL2) (Figure 25A) and MIP-1α (CCL3) (Figure 25B). WT cultures expressed higher levels of CCL2 than Cx32KO cultures at baseline, and this change was inverted after

minocycline treatment (Figure 25A). Meanwhile, Cx32KO cultures expressed higher levels of CCL3 at baseline and after treatment, when compared to WT (Figure 25B).

Comparatively, 6DIV cultures expressed detectable levels of MCP-1 (CCL2), MIP-1α (CCL3), and MIP-1β (CCL4) (Figures 25C-E). Replicating 3-day levels, 6-day levels of CCL2 were lower at baseline in Cx32KO cultures. This relationship inverted while minocycline treated and returned to baseline levels during recovery (Figure 25C). CCL3 levels were also replicated at 6DIV in Cx32KO and WT cultures and inverted during recovery (Figure 25D). Unlike 3-day cultures, 6-day cultures showed detectable levels of CCL4, which increased in both genotypes during treatment, but inversely reacted to recovery with a decrease in Cx32KO and an increase in WT cultures (Figure 25E).

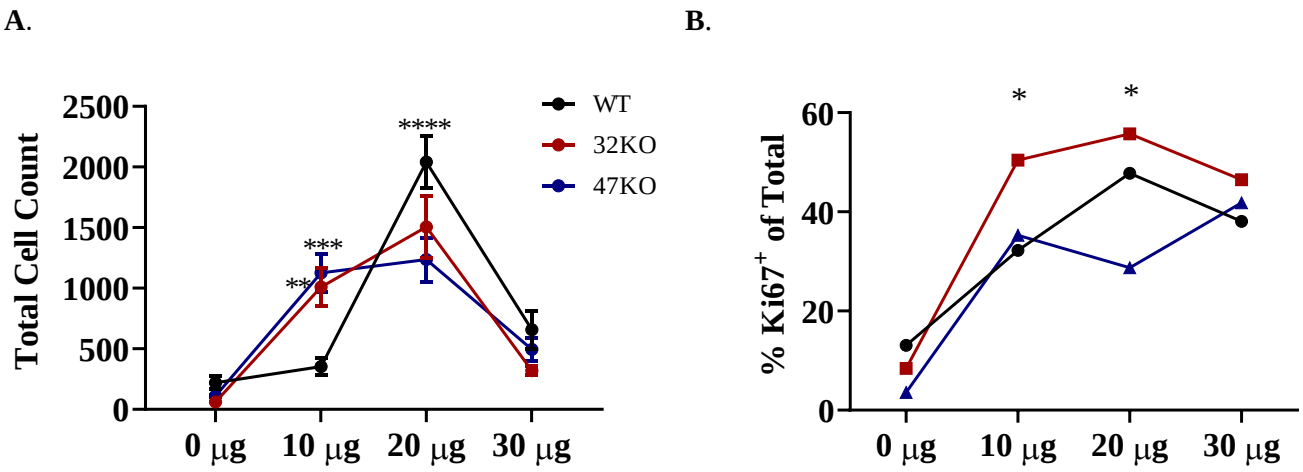

Figure 20. Dose-Response to Minocycline Treatment at 3DIV. Evaluation of mixed glial cell cultures with 0μg, 10μg, 20μg, and 30μg treatment for 3DIV in WT, Cx32KO, and Cx47KO cultures. A. Total cell count in $DAPI^+$ nuclei per image showed significant upregulation in total cells under 10μg, 20μg, and 30 μg treatment conditions for all genotypes ($F(_{7,46})=17.94$; $F(_{7,52})=19.26$) by one-way ANOVA B. The percentage of $Ki67^+$ of total cells significantly increases in 10μg and 20μg treatment conditions for Cx32KO compared to WT. Data represent mean ±SEM derived from n=6-12 in each group. **p<0.01, ***p<0.001, ****p<0.0001.

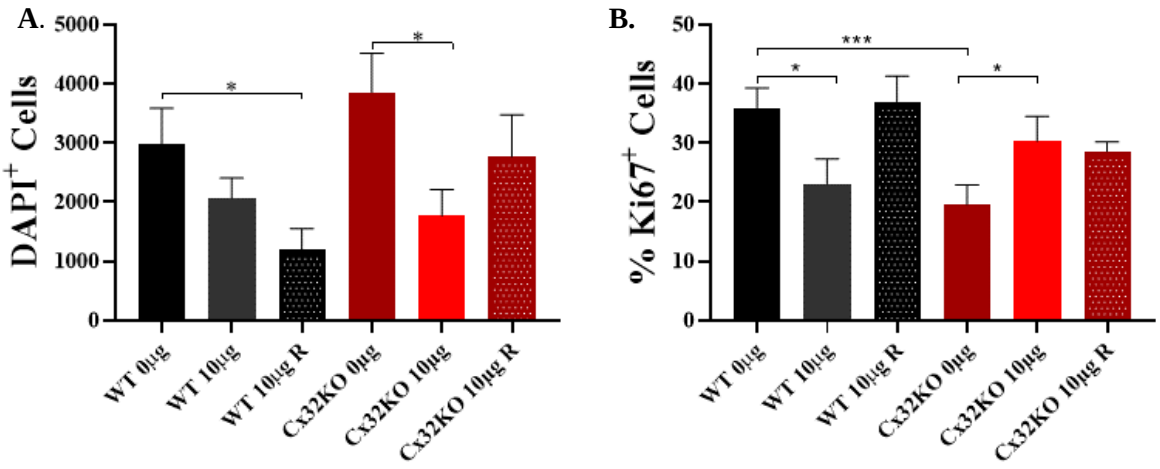

Figure 21. Overall Cell Type Changes WT vs. Cx32KO After Minocycline. Evaluation of mixed glial cell cultures 6 DIV at baseline, after 6-day treatment (10µg), and after 3DIV treatment with 3-day recovery (10µg R). A. Total cell count in DAPI^{+} nuclei per image showing significantly lower cell count after recovery in WT and during treatment in Cx32KO ($F_{5,66}$=2.501) by one-way ANOVA. B. The percentage of Ki67^{+} cells show a significant decrease in WT proliferation during treatment and between WT and Cx32KO at baseline. Comparatively, Cx32KO cultures expressed higher levels of Ki67^{+} during minocycline treatment *($F_{5,38}$=3.657)* by one-way ANOVA. Data represent mean ±SEM derived from n=4-18 in each group, specific groups, and treatments located on the x-axis. *p<0.05, ***p<0.001

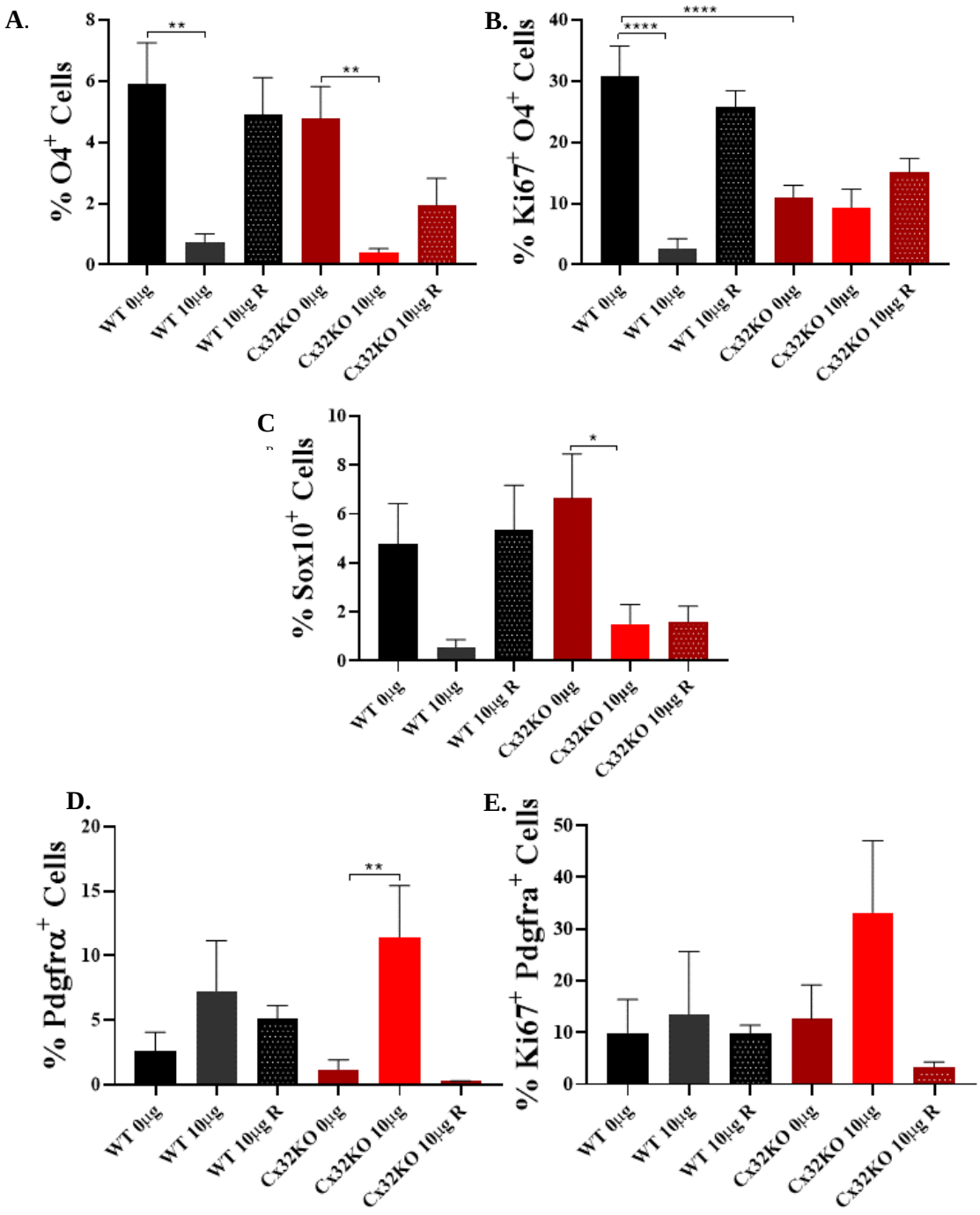

Figure 22. Oligodendrocytes after Minocycline in WT and Cx32KO Cultures. Mixed glial cell cultures were evaluated for oligodendrocytes and oligodendrocyte precursor cells at baseline, during minocycline treatment, and after recovery. A. The percentage of $O4^+$ cells significantly decreased after minocycline treatment in both genotypes and remained lower in Cx32KO after recovery. ($F_{5,47}$=4.468) by one-way ANOVA. B. The percentage of proliferating $O4^+$ cells were significantly lower during treatment in WT cultures, and in Cx32KO cultures compared to WT at baseline ($F_{5,19}$=10.01) by one-way ANOVA. C. The percentage of $Sox10^+$ cells after minocycline treatment was lower in Cx32KO

during treatment and remained low during recovery ($F_{5,27}$=2.089) by one-way ANOVA. D. The percentage of Pdgfrα^{+} cells under minocycline treatment was higher in both genotypes during treatment, significantly increased in Cx32KO cultures. Levels returned close to baseline in recovery *($F_{5, 14}$=1.329)* by one-way ANOVA. E. The percentage of Ki67^{+} Pdgfrα^{+} did not significantly change during minocycline treatment. Data represent mean ±SEM derived from n=2-12 in each group, specific groups, and treatments located on the x-axis. *p<0.05, **p<0.01, ****p<0.0001.

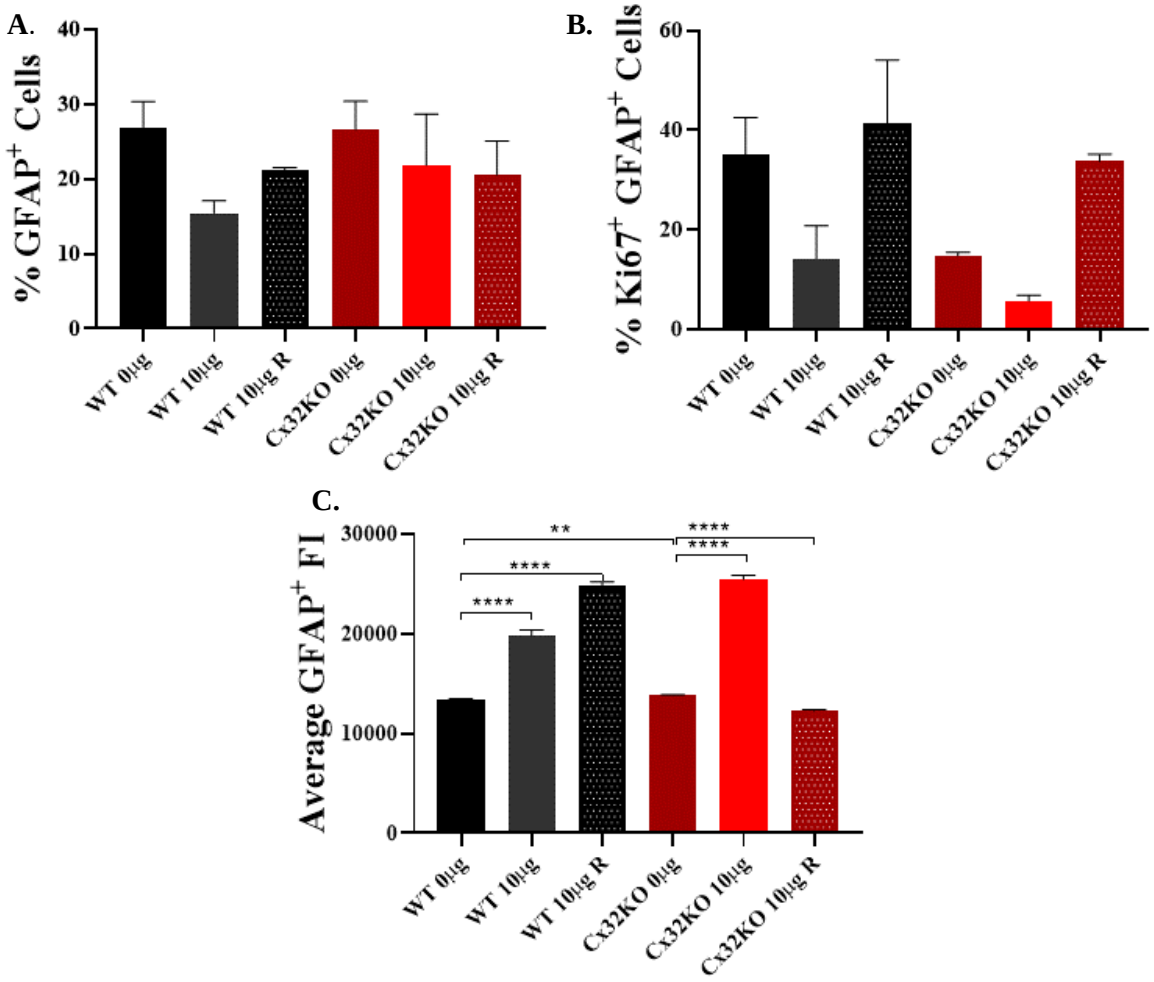

Figure 23. Astrocytes after Minocycline in WT and Cx32KO Cultures. Mixed glial cell cultures were evaluated for GFAP$^+$ astrocytes at baseline, during minocycline treatment, and after recovery. A. The percentage of GFAP$^+$ cells was not significantly altered during minocycline treatment by one-way ANOVA. B. The percentage of Ki67$^+$ GFAP$^+$ cells was not significantly altered by minocycline treatment by one-way ANOVA. C. Average integrated fluorescence intensity of each GFAP$^+$ cells after minocycline treatment showed a significant increase of FI in WT during treatment and further after recovery. The Cx32KO GFAP$^+$ FI was higher than WT at baseline, significantly increased during treatment, and significantly decreased after recovery *($F_{5, 50217}$=944.9)* by one-way ANOVA. Data represent mean ±SEM derived from n=2-8 images in each group, specific groups, and treatments located on the x-axis. **p<0.01, ****p<0.0001.

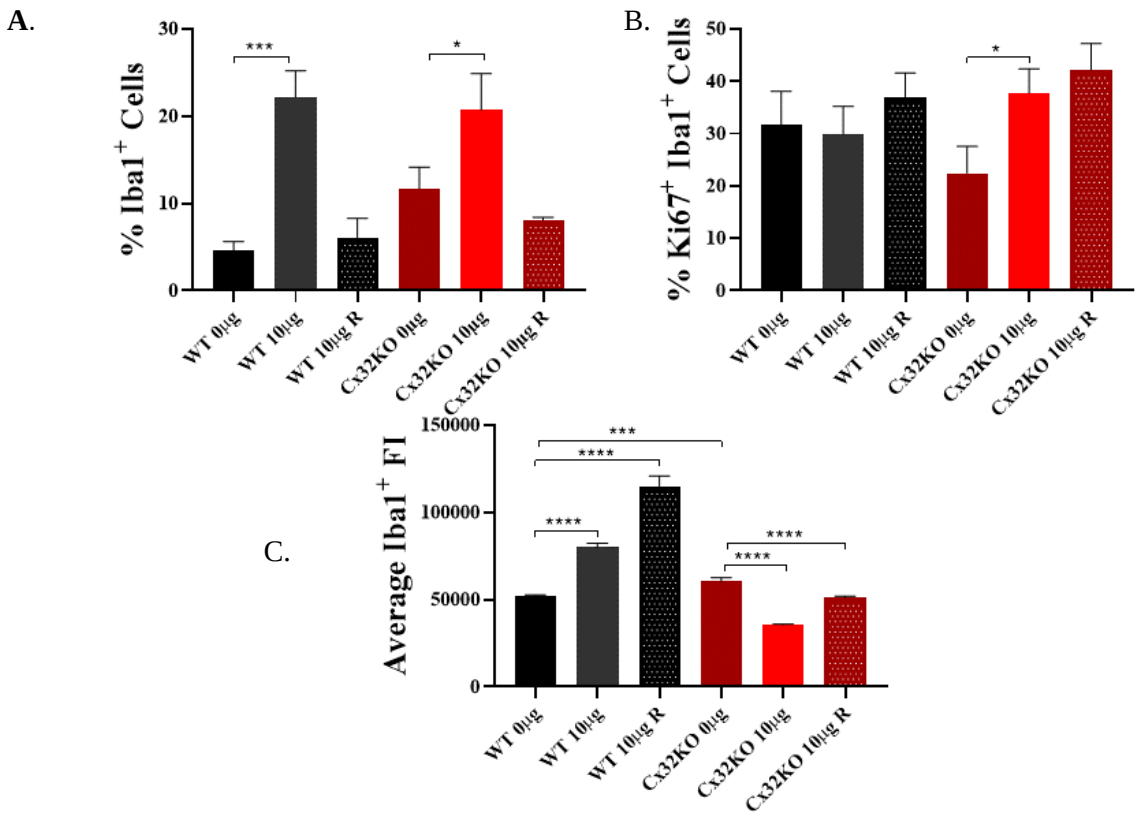

Figure 24. Microglia after Minocycline in WT and Cx32KO Cultures. Mixed glial cell cultures were evaluated for Iba1$^+$ microglia at baseline, during minocycline treatment, and after recovery. A. The percentage of Iba1$^+$ cells significantly increased while treated with minocycline in both genotypes ($F_{5,20}$=5.489) by one-way ANOVA. B. The percentage of Ki67$^+$ Iba1$^+$ cells after minocycline treatment was not significantly changed in WT cultures regardless of treatment but increased during treatment in Cx32KO cultures ($F_{5,20}$=1.445) by one-way ANOVA. C. Average integrated fluorescence intensity of each Iba1$^+$ cell after minocycline treatment showed a significant increase in FI in WT during treatment and further after recovery. The Cx32KO Iba1$^+$ FI, which was significantly higher than WT at baseline, decreased during treatment, and remained significantly lower during recovery *($F_{5,14904}$=213.9)* by one-way ANOVA. Data represent mean ±SEM derived from n=2-8 images in each group specific groups, and treatments located on the x-axis. *p<0.05, ***p<0.001, ****p<0.0001.

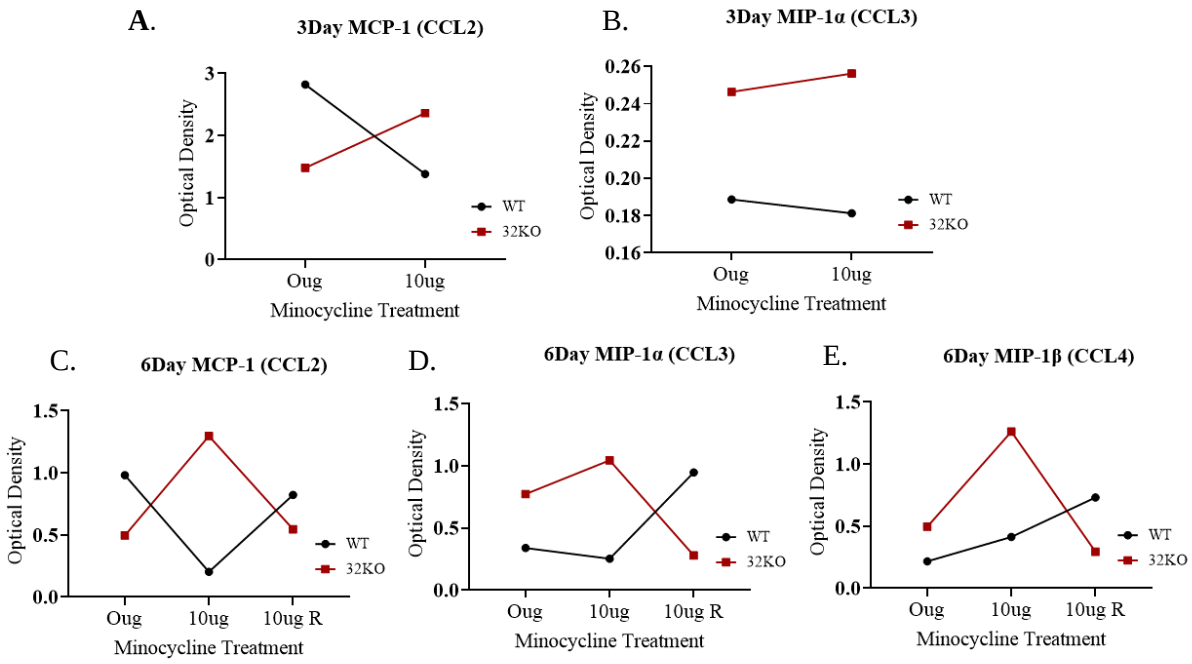

Figure 25. ELISA Array After Minocycline in WT and Cx32KO Cultures. Mouse Autoimmune Response Multi-Analyte ELISArray™ Kit evaluated WT and Cx32KO cultures for pro- and anti-inflammatory factors at baseline and during treatment and recovery from minocycline treatment. A. 3-day cultures at baseline express lower levels of CCL2 in Cx32KO cultures compared to WT, which inverses after minocycline treatment, as seen at 6DIV. B 3-day levels of CCL3 replicated in 6DIV, with CCL3 levels higher in Cx32KO cultures compared to WT. C. 6-day cultures show inverse expression of CCL2 in WT and Cx32KO cultures at baseline, during treatment and recovery. D. 6-day cultures express detectable levels of CCL3, which was higher in Cx32KO compared to WT cells at baseline but inversed during recovery from minocycline. E.6-day detectable levels of CCL4 are also higher in Cx32KO compared to WT and inverse during recovery.

4.6.2 Minocycline Treatment WT vs. Cx47KO

4.6.2.1 Cellular Development and Overall Cell Count

The effect of minocycline treatment on total cell count in WT and Cx47KO mixed glial cultures was evaluated by the total $DAPI^+$ cells under the following treatment conditions: 0μg treatment (6D 0μg), 10μg treatment (6D 10μg), and 10μg treatment with a 3-day recovery (6D 10μgR). As was seen previously, Cx47KO cultures have significantly fewer cells than WT, with an average of 957 cells per image, compared to 2983 ($p<0.0001$) (Figure 26A). Minocycline treatment appears to alter WT cell culture development, resulting in a significant decrease in total cell count with an average of 2074 cells per image during treatment and 1194 during recovery ($p<0.0001$). Cx47KO cultures were not significantly changed by treatment, though there was a trend towards an increase with an average of 1895 cells while treated. These levels returned closer to baseline at 1178 during recovery. Together, these cell changes suggest that minocycline plays a role in overall cultural viability either by a direct effect or through inhibition of pro-inflammatory microglial expression.

4.6.2.2 $Ki67^+$ Proliferation

Overall $Ki67^+$ cell proliferation was affected by minocycline treatment in both WT and Cx47KO cultures. As discussed in chapter 3, Cx47KO glia were proliferating significantly less at 12.08% compared to WT at 35.92% ($p<0.0001$) (Figure 26B). While treated, WT cultures proliferated significantly less at 23.12% ($p=0.0084$), though this change was reversed with recovery. Cx47KO cultures also decreased in proliferative capacity during treatment to 6.33% but increased to 29.20% proliferation during recovery ($p=0.0072$). This change in proliferation

suggests that pro-inflammatory microglia might be regulating developmental and proliferative factors in culture.

4.6.1.2 $O4^+$ Oligodendrocytes

WT and Cx47KO cultures were monitored for changes in percent of $O4^+$ cells after minocycline treatment. Treated cultures showed a decreased expression of $O4^+$ expression in both genotypes, with WT cultures showing a significant decrease from 5.91% to 0.72% ($p=0.0002$), and Cx47KO cultures decreasing non-significantly from 4.77% to 1.93% (Figure 27A). These Cx47KO oligodendrocytes appear to express a similar albeit blunted expression pattern during treatment to that of WT, suggesting that the inhibition of pro-inflammatory microglial factors has a similar effect in Cx47KO cultures. This oligodendrocyte response may suggest that oligodendrocytes are less capable of developmental recovery after the loss of Cx47. It cannot yet be determined if the 10μg/mL of minocycline treatment may be toxic to oligodendrocytes or if the inhibition of pro-inflammatory microglial factors alters oligodendrocyte viability and developmental capacity.

4.6.2.3 $O4^+$ Oligodendrocyte Proliferation

The percentage of proliferating $O4^+$ oligodendrocytes at 6DIV was evaluated by $Ki67^+$ nuclei. Knockout of Cx47 resulted in a significantly lowered proliferative capacity, with 30.73% in WT and 3.96% in Cx47KO ($p<0.0001$) (Figure 27B). While treated oligodendrocytes in WT cultures become less proliferative, down to 2.67% in WT cultures ($p<0.0001$). This proliferative deficit reverted back to baseline during recovery 25.78%. Meanwhile, there were no significant changes in the proliferative capacity of Cx47KO oligodendrocytes when treated with minocycline.

This low level of proliferation at Cx47KO is maintained throughout recovery, suggesting that pro-inflammatory microglial factors may not be playing a role inhibiting oligodendrocyte proliferation.

4.6.2.4 $Sox10^+$ Expression

The percentage of $Sox10^+$ oligodendrocytes was higher in WT when compared to Cx47KO cultures, expressing 4.79% and 0.42%, respectively at baseline (Figure 27C). Sox10 expression was not significantly different at baseline between WT and Cx47KO cultures, and while WT Sox10 levels were not altered across treatments, minocycline significantly upregulated $Sox10^+$ expression in Cx47KO cultures to 10.27% ($p=0.0080$). This elevation was maintained during recovery at 6.3% ($p=0.0256$). Together an increase in $Sox10^+$ expression and decrease in $O4^+$ expression during minocycline treatment may suggest that pro-inflammatory microglial factors alter programming for terminal oligodendrocyte differentiation. It is possible that after Cx47 knockout, oligodendrocyte precursors are programmed for terminal differentiation but are potentially not capable of transitioning.

4.6.2.5 $Pdgfr\alpha^+$ Oligodendrocyte Progenitor Cells

The percentage of oligodendrocyte progenitor cells after minocycline treatment was evaluated by the percentage that were also $Pdgfr\alpha^+$ cells. At baseline, there was no significant difference in OPCs between WT and Cx47KO though the number for Cx47 was substantially lower. While treated, both genotypes expressed a non-significant increase in the percentage of OPCs from 2.64% to 7.26% in WT and 0.23% to 6.63% in Cx47KO cultures (Figure 27D). These increases coincide with a decrease in $O4^+$ cells during minocycline treatment and may suggest that there is a buildup of OPCs due to an inhibition of oligodendrocyte differentiation during while pro-inflammatory microglial inhibition. These developmental patterns do not, however, rule out

minocycline toxicity within oligodendrocytes. During recovery, WT Pdgfrα$^+$ remains elevated and may contribute to the recovery of O4$^+$ cells.

4.6.2.6 Pdgfrα$^+$ Proliferation

There is no significant difference between WT and Cx47KO oligodendrocyte progenitor proliferation by Ki67$^+$ staining across treatment groups. Similarly, there was no significant difference across treatments within genotypes, though it should be noted that 0% of oligodendrocytes were proliferating during Cx47KO recovery and only 1.28% were proliferating after treatment (Figure 27E). Although the OPCs that are present may be influenced by pro-inflammatory microglial expression and inhibition, it is also possible that this proliferative expression is the result of the limited number of progenitors within cultures.

4.6.2.7 GFAP$^+$ Astrocytes

The average percentage of astrocytes in minocycline treated cultures was determined by cells that were GFAP$^+$. At baseline, there was no significant difference in the percentage of astrocytes between genotypes (Figure 28A). Although minocycline treatment and recovery appear to alter this expression differentially, there was also no significant difference across treatment types for either genotype.

4.6.2.8 GFAP$^+$ Astrocyte Proliferation and Activation

Similarly, astrocyte proliferation was not significantly altered by genotype or treatment. While treated, both genotypes showed trend toward decreases in proliferation, dropping from 35.02% to 14.78% in WT ($p=0.0522$), and 14.87% to 5.93% in Cx47KO cultures (Figure 28B). Recovery cultures showed WT astrocytes returned to baseline proliferative capacity at 41.37%,

while Cx47KO increased from baseline at 33.72%. These proliferative alterations, albeit nonsignificant, may reflect a relationship between pro-inflammatory microglial factors and astrocytic phenotype (Figure 1B; Boche et al., 2013; Mayo et al., 2014; Savarin et al., 2015; Liddelow et al., 2017; Kery et al., 2020).

Similar to Cx32KO cultures, Cx47KO astrocytes express a significantly higher $GFAP^+$ FI when compared to baseline at 6DIV ($p<0.0001$). During minocycline treatment, both genotypes show an increase in FI ($p<0.0001$) (Figure 28C). Comparatively, during recovery, Cx47KO astrocytes express significantly lower FI ($p<0.0001$), while WT astrocytes appear to increase activation ($p<0.0001$). This decrease in Cx47KO FI may suggest that pro-inflammatory microglial factors are regulating the astrocytic phenotype in oligodendrocytes lacking Cx47. These changes in glial activation support inverse activation of astrocytes and microglia in Cx47KO.

4.6.2 $Iba1^+$ Microglia

The microglial presence within minocycline-treated mixed glial cultures was represented by the percentage of $Iba1^+$ cells in both WT and Cx47KO cultures. As discussed in chapter 3, Cx47KO cultures expressed a significantly higher percentage of $Iba1^+$ cells when compared to WT at baseline, with WT cultures expressing 4.62% versus 35.83% in knockout ($p<0.0001$) (Figure 29A). During minocycline treatment, there was an increase in microglia across genotypes, to 20.71% in WT ($p=0.0004$) and 42.65% (non-significant) in Cx47KO cultures. This number returned toward baseline in WT during recovery, while in Cx47KO cultures, microglia were reduced below baseline to 15.65% ($p=0.0010$). As was discussed previously, the high percentage of microglia in Cx47KO is partially but not entirely attributable to the decreased total cell count at

6DIV. The minocycline dependent microglial increase suggests that microglia are resilient in minocycline-containing environments when other cell types are not.

4.6.2 Iba1$^+$ Microglial Proliferation and Activation

Microglial proliferation was evaluated by the percentage of Iba1$^+$ cells that were also Ki67$^+$ after minocycline treatment. Baseline assessment at 6DIV found that microglial proliferation was significantly lower in Cx47 knockout cultures, resulting in 9.01% proliferation compared to 31.67% in WT cultures ($p<0.0059$) (Figure 29B). Inhibition of pro-inflammatory microglial activation by minocycline did not alter the proliferative capacity of the microglia in WT culture, suggesting that the microglia are not inherently inflammatory within these cultures. Meanwhile, recovery from minocycline treatment caused an increase (non-significant) in Cx47KO cultures to 27.05%. This proliferative capacity in Cx47KO cultures may be reflective of the total microglial percentage. The baseline microglial percentage may have reached a critical threshold above which it may become more challenging to proliferate.

Microglial activation, represented in culture by an increase in relative Iba1$^+$ FI, was assessed in the context of minocycline treatment. At baseline, Cx47KO microglial FI was significantly higher than WT with an average 59345 but decreased significantly during treatment with an average FI of 40001 ($p<0.0001$). Iba1$^+$ FI returned to baseline levels during recovery with an average FI of 60709 in Iba1$^+$ cells. In contrast, microglial activation increased significantly during treatment in WT from an average FI of 52463 to 79890 and continued to increase while in recovery with an average FI of 115118 ($p<0.0001$) (Figure 29C). The decrease in activation during minocycline treatment within Cx47KO cultures supports our hypothesis that these microglia are in an activated state in the Cx47 knockout. Comparatively, upregulation in the FI intensity in WT

microglia suggests that minocycline treatment leads to differential microglial activation, alternate to the pro-inflammatory ‘M1’ activation which should be inhibited while treated (Kobayashi et al., 2014).

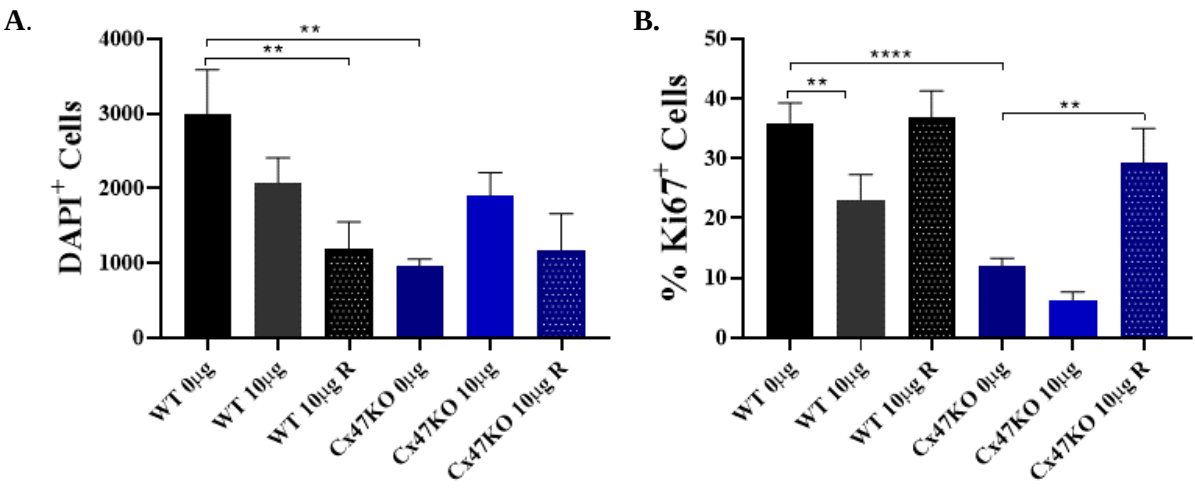

Figure 26. Overall Cell Type Changes WT vs. Cx47KO After Minocycline. Evaluation of mixed glial 6DIV at baseline, after 6DIV 10µg T, 6DIV 10µg R. A. Total cell count in $DAPI^+$ nuclei per image was significantly lower after recovery in WT and at baseline in Cx47KO cultures compared to WT ($F_{5,53}$=2.891) by one-way ANOVA. B. The percentage of $Ki67^+$ of total cells showed a significant decrease in WT proliferation during treatment and between WT and Cx47KO at baseline. Comparatively, Cx47KO cultures expressed higher levels of $Ki67^+$ during recovery ($F_{5, 29}$=10.09) by one-way ANOVA. Data represent mean ±SEM derived from n=4-16 images in each group, ***p<0.001, ****p<0.0001.

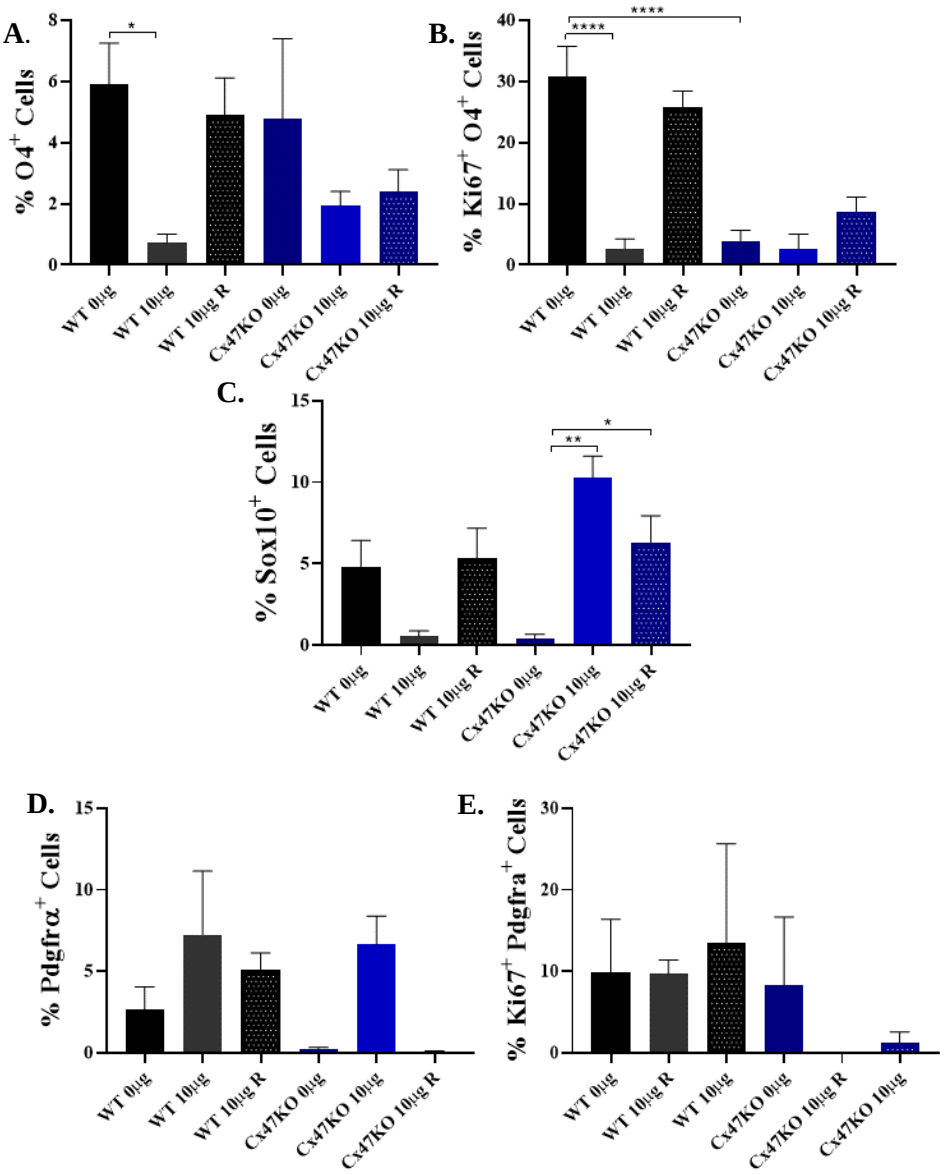

Figure 27. Oligodendrocytes after Minocycline in WT and Cx47KO Cultures. Mixed glial cell cultures were evaluated for oligodendrocytes and oligodendrocyte precursor cells at baseline, during minocycline treatment, and after recovery. A. The percentage of $O4^+$ cells significantly decreased after minocycline treatment in WT cultures ($F_{5,13}$=12.41) by one-way ANOVA B. The percentage of $Ki67^+$ $O4^+$ cells are significantly downregulated during minocycline treatment in WT, as well as at baseline in Cx47KO cultures when compared to WT ($F_{5,51}$=14.99) by one-way ANOVA. C. The percentage of $Sox10^+$ cells after minocycline treatment and during recovery was significantly upregulated in Cx47KO cultures ($F_{5,26}$=2.5858) by one-way ANOVA. D. The percentage of $Pdgfr\alpha^+$ cells showed a trend towards an increase during treatment but was not significantly altered across genotypes. E. The percentage of $Ki67^+$ $Pdgfr\alpha^+$ did not significantly change during minocycline treatment. Data represent mean ±SEM derived from an n=2-11 in each group. *p<0.05, **p<0.01, p<0.0001.

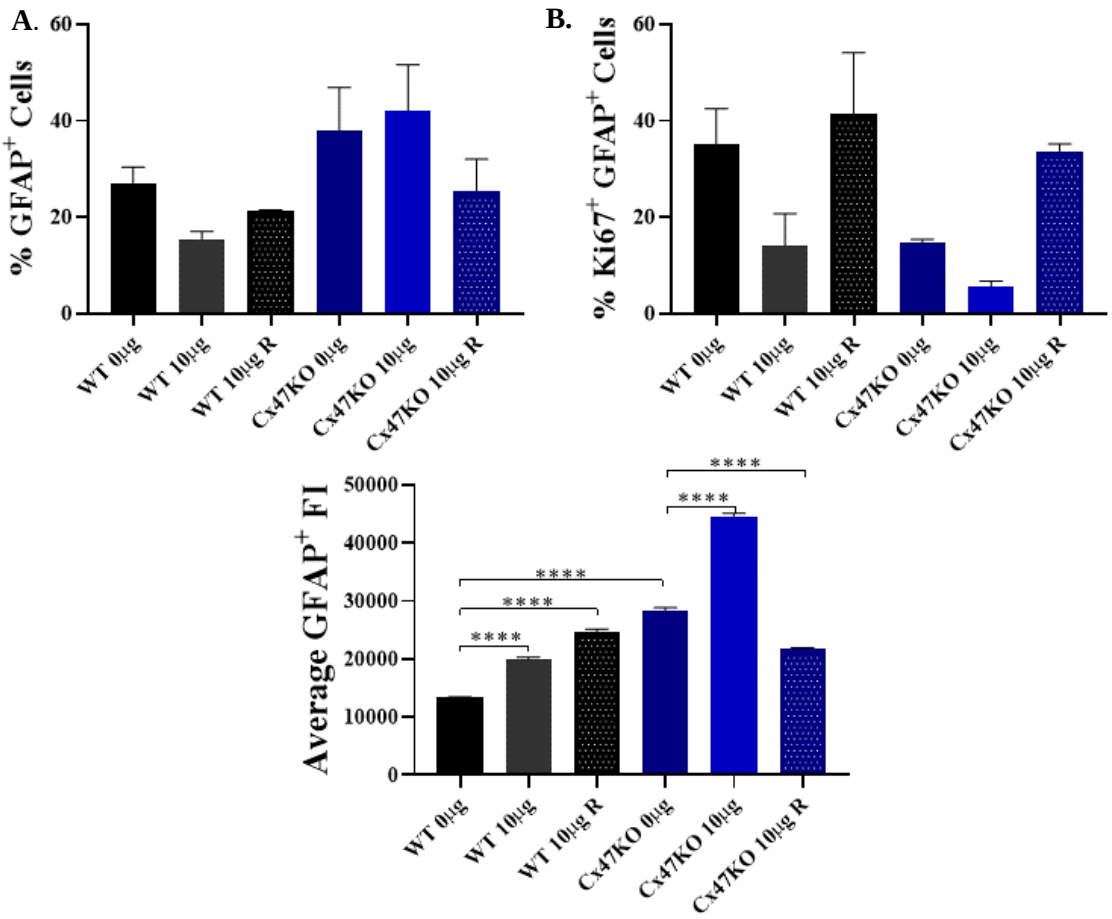

Figure 28. Astrocytes after Minocycline in WT and Cx47KO Cultures. Mixed glial cell cultures were evaluated for GFAP$^+$ astrocytes at baseline, during minocycline treatment, and after recovery. A. There was no significant alteration in the percentage of GFAP$^+$ astrocytes across treatments or genotypes by one-way ANOVA. B. The percentage of Ki67$^+$ GFAP$^+$ cells was not significantly altered after treatment in either genotype but showed a trend towards a decrease during treatment. C. The average integrated fluorescence intensity of each GFAP$^+$ cells after minocycline treatment showed significantly increased FI in WT during treatment and further after recovery. The Cx47KO GFAP$^+$ FI was higher than WT at baseline, and significantly increased during treatment and significantly decreased after recovery *($F_{5,30693}$=2010)* by one-way ANOVA. Data represent mean ±SEM derived from n=2-5 images in each group unless otherwise noted. *p<0.05, **p<0.01, ***p<0.001, ****p<0.0001.

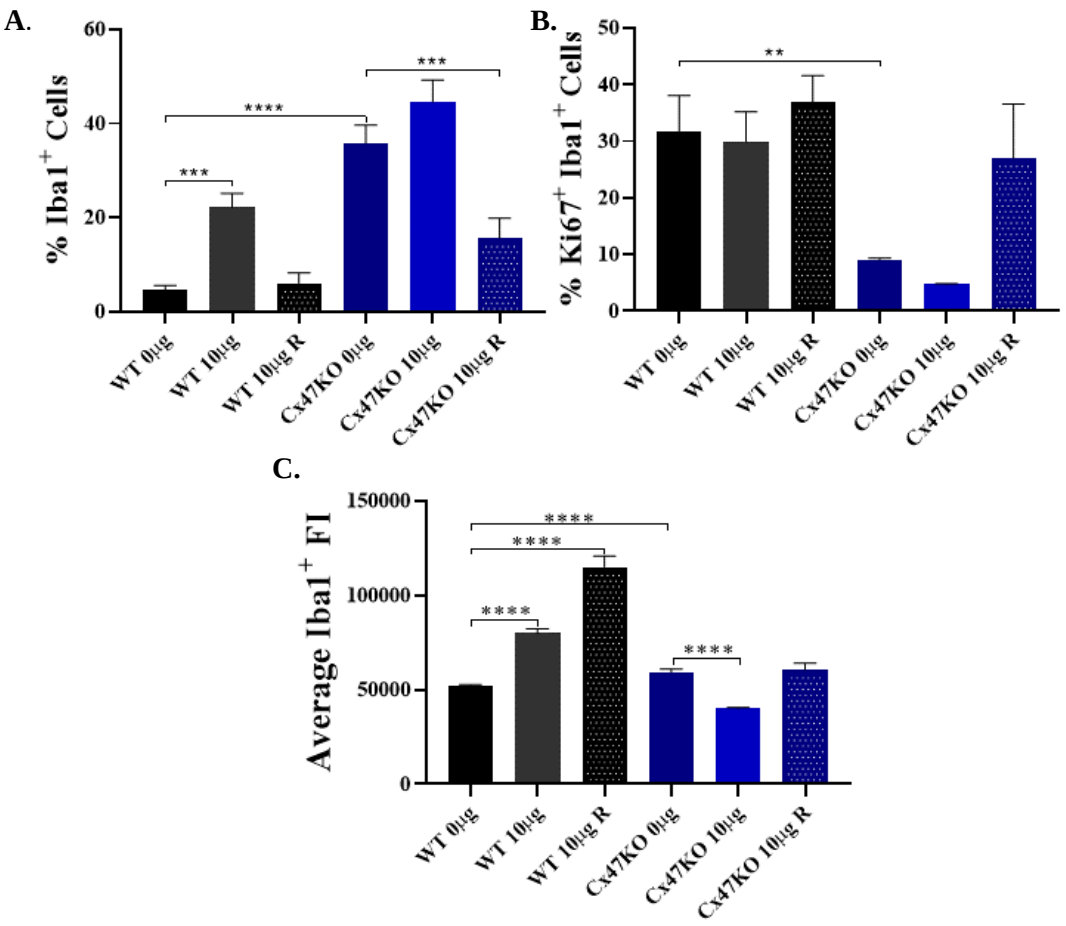

Figure 29. Microglia after Minocycline in WT and Cx47KO Cultures. Mixed glial cell cultures were evaluated for Iba1$^+$ microglia at baseline, during minocycline treatment, and after recovery. A. The percentage of Iba1$^+$ cells significantly increased in WT cultures while treated and was significantly higher in Cx47KO cultures at baseline. Cx47KO microglial expression significantly decreased during recovery ($F_{5,13}$=25.44) by one-way ANOVA. B. The percentage of Ki67$^+$ Iba1$^+$ cells after minocycline treatment was significantly lower in Cx47KO cultures compared to WT at baseline ($F_{5,13}$=4.589) by one-way ANOVA. C. Average integrated fluorescence intensity of each Iba1$^+$ cell after minocycline treatment showed a significant FI increase in WT during treatment and further after recovery. The Cx47KO Iba1$^+$ FI was significantly higher at baseline when compared to WT, and became significantly lower during treatment *($F_{5,19822}$=178.6)* by one-way ANOVA. Data represent mean ±SEM derived from n=2-5 images in each group unless otherwise noted. **p<0.01, ****p<0.0001.

4.7 RNA Sequencing Analysis

4.7.1 WT-PBS vs. Cx32KO-PBS

4.7.1.1 Differential Expression Analysis

To address the role of Cx32 within the central nervous system, we compared the gene expression profiles of cortical tissue from WT and Cx32KO mice at baseline. The comparative analysis found 120 differentially expressed genes (DEGs) (FDR < 0.1) between baseline WT and Cx32KO samples, with 66 downregulated and 54 upregulated (Appendix 5). The relative expression of several differentially expressed oligodendrocyte genes was validated via QC-PCR using RNA collected from the cortical tissue, as seen in Figure 40A (Appendix 4).

4.7.1.2 Gene Ontology Analysis

Gene ontology (GO) enrichment analysis was performed with Ingenuity Pathway Analysis (IPA) and utilized the DEGs to assess biological, functional, and canonical pathway involvement. With the deficits in oligodendrocyte development and increases in microglial presence in both culture and tissue, particular focus was given to inflammatory and developmental pathways. Unexpectedly, IPA results did not show distinct pro-inflammatory canonical pathways (detailed chart shown in Tables 1-2), suggesting that the role of Cx32 connexins and gap junctions within oligodendrocytes is novel and that, in spite of the upregulation of microglia the response to knockout does not appear to leave the tissue in an inherently pro-inflammatory state. Top Network analysis suggests that the response to Cx32 knockout may affect developmental pathways, as a variety of genes that are upregulated in Cx32KO tissue are involved in cellular interaction and the proliferation and differentiation of oligodendrocytes (Figure 30).

4.7.1.3 Cell Type-Specific Analysis

The DEGs were comparatively analyzed in conjunction with the Barres single-cell mouse cortex database (Zhang et al., 2014), to provide insight into glial involvement after Cx32 knockout. As can be seen in Table 3 and the associated heat map (Figure 32), a majority of DEGs are not oligodendrocytic. There is considerable involvement of other cell types, suggesting a network of cellular involvement relying on and regulating Cx32. Moreover, 51 DEGs could not be associated with one specific cell type and could be differentially regulated by one or more cell types (Figure 31).

4.7.2 WT-LPS and Cx32KO-LPS

4.7.2.1 Behavioral Assessment

Animals utilized for RNA-seq analysis were treated with intraperitoneal PBS or LPS 6-hours before sacrifice to investigate the inflammatory response within the central nervous system. Male mice were age-matched at 8-weeks, and weight was distributed evenly among genotypes/treatments, with an average of 25.06g and 23.86g in WT PBS and LPS treated animals, and 22.70g and 22.13g in Cx32KO treated animals respectively (Figure 33). At four hours, the mice were behaviorally assessed to ensure that LPS treatment was effective. They were monitored for motor deficits by assessing foot-slip and rearing behavior.

The foot-slip score measured over a total of one minute found a significant decrease in overall movement and total foot-slips after LPS when compared to PBS in both WT (n=15) and Cx32KO (n=15) animals ($p=0.0005$). There was no significant difference in overall foot-slips between genotypes. Conversely, when assessed for rearing behavior, WT animals rear significantly fewer times after LPS treatment with 9.38 in verses 0.57 rears with LPS onto their

hind legs (p=0.0005). Meanwhile, Cx32KO rear an average of 9 times in the PBS group and 6.13 in the LPS group, which is not significant. After LPS treatment, Cx32KO mice rear significantly more times than the WT mice (p=0.0256).

4.7.2.2 Differential Expression Analysis

Differential gene expression was assessed within each genotype after LPS treatment to assess differential expression caused by acquired neuroinflammatory stress. Based on the prediction that lack of Cx32 increases inflammatory stress at baseline, it was expected that WT would express a more robust response to LPS than Cx32KO, evident by a larger number of differentially expressed transcripts in the WT. Comparative analysis between WT-PBS and WT-LPS determined 2533 genes were differentially expressed in WT, with 1203 downregulated and 1330 upregulated after LPS treatment (FDR < 0.1). In contrast, differential expression between Cx32KO-PBS and Cx32KO-LPS resulted in a more robust response of 3677 DEGs, with 1700 downregulated and 1977 upregulated genes (Figure 33). The intersecting DEGs are depicted in the Venn diagram in Fig 33. (https://bioinfogp.cnb.csic.es/tools/venny/index2.0.2.html). Additionally, DEGs expressed in the WT-PBS vs. WT-LPS comparison (Appendix 7), were compared to WT-PBS vs. Cx32KO-PBS (Appendix 5), to evaluate comparable expression indicative of pro-inflammatory factors you might expect if the loss of Cx32 causes inflammatory upregulation (Appendix 8). This comparison suggests that Cx32KO may not be in an inflammatory state at baseline, which will be further addressed in the discussion.

4.7.2.3 Gene Ontology Analysis

GO analysis was performed on the differentially expressed genes from both the WT LPS treated and Cx32KO LPS treated samples. The genes upregulated after LPS treatment in the WT

cortex were further used to characterize what a baseline inflammatory response might look like in tissue. If cortical tissue was inflammatory at baseline after Cx32 knockout, we might expect to see similar differential regulation. However, this was not the case. As was expected, LPS treatment in both WT and Cx32KO expressed differential patterns with canonical pathways and disease states related to an inflammatory response (Tables 4 & 5).

4.7.2.4 Cell-Type Specific Analysis

Utilizing the Linnarsson Lab single-cell expression database (Zeisel et al., 2015), we evaluated some cell-type-specific responses to LPS treatment in both WT and Cx32KO tissue. Of the 2533 DEGs expressed after LPS in WT tissue, 1052 were assigned a cell type (Table 6). Similarly, in the assessment of Cx32KO tissue after LPS, 1081 of the 3677 DEGs had a cell type-specific association (Table 7). Genotype differences in the DEGs may provide some insight into the cellular response after a neuroinflammatory insult.

T1.

WT PBS vs 32KO PBS

Canonical Pathways		
Name	p-Value	Overlap
Hepatic Fibrosis/Hepatic Stellate Cell Activation	4.88E-04	6 of 186
Agranulocyte Adhesion and Diapedesis	5.77E-04	6 of 192
Choline Degradation I	1.06E-02	1 of 2
Sulfate Activation for Sulfonation	1.06E-02	1 of 2
Granulocyte Adhesion and Diapedesis	1.55E-02	4 of 179
Diseases and Disorders		
Name	p-Value Range	# Molecules
Neurological Disease	1.57E-02 - 6.40E-05	43
Organismal Injury and Abnormalities	1.59E-02 - 8.17E-05	114
Psychological Disorders	1.49E-02 - 8.17E-05	26
Skeletal and Muscular Disorders	1.47E-02 - 9.83E-05	49
Hereditary Disorder	1.59E-02 - 1.34E-04	38

T2.

Top Networks	
Associated Network Function	Score
Developmental Disorder, Cell-To-Cell Signaling and Interaction, Nervous System Development and Function	55
Nucleic Acid Metabolism, Cellular Development, Cellular Growth and Proliferation	44
Cell-To-Cell Signaling and Interaction, Hematological System Development and Function, Inflammatory Response	33
Cell Cycle, Cancer, Neurological Disease	31

Table 1-2: GO Enrichment Analysis WT-PBS vs. Cx32KO-PBS. T1. Top canonical pathways and top diseases and disorders that may involve the differentially expressed gene patterns that occur with the knockout of Cx32. T2. Top Networks and their associated functions which have similar gene transcript changes seen in the differentially expressed genes between WT and Cx32KO cortical tissue.

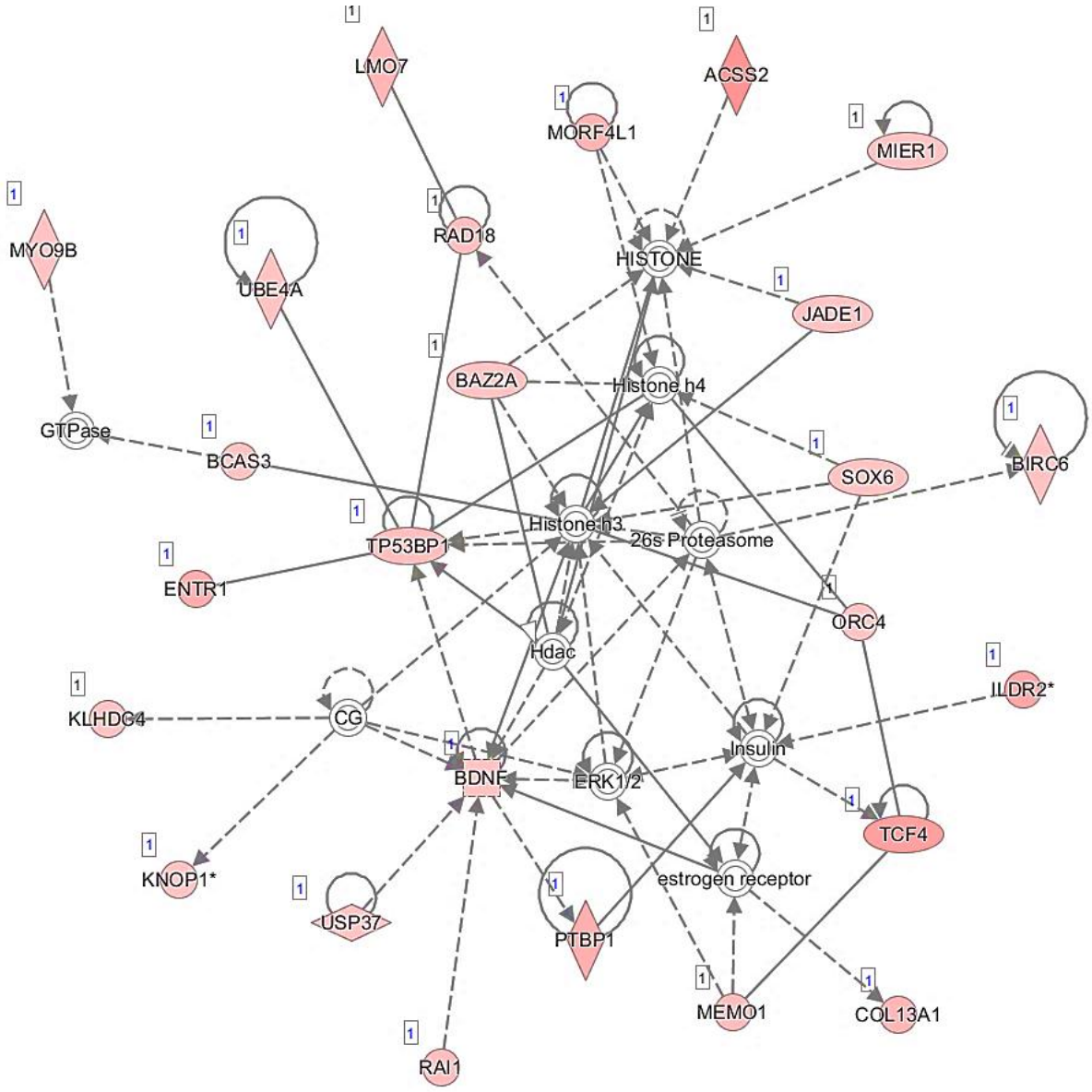

Figure 30. Network Within GO Enrichment Analysis After Cx32 Knockout. The Top Network associated with DEGs after Cx32KO. This network is associated with developmental disorders and alterations in cell-to-cell signaling and interaction. Though not all these genes may not be significantly differentially expressed, those in red are upregulated in Cx32KO tissue when compared to WT (Refer to Appendix 5).

WT vs 32KO PBS						
	Upregulated		Downregulated		Total	
Cell Type	Genes	% of Total	Genes	% of Total	Genes	% of Total
Astrocyte	5	9.26	4	6.06	9	7.96
Neuron	4	7.41	2	3.03	6	5.31
Oligodendrocytes	21	38.89	13	19.70	34	30.09
Microglia	3	5.56	6	9.09	9	7.96
Endothelial	2	3.70	9	13.64	11	9.73
Unassociated	19	35.19	32	48.48	51	45.13
	54		66		**113**	

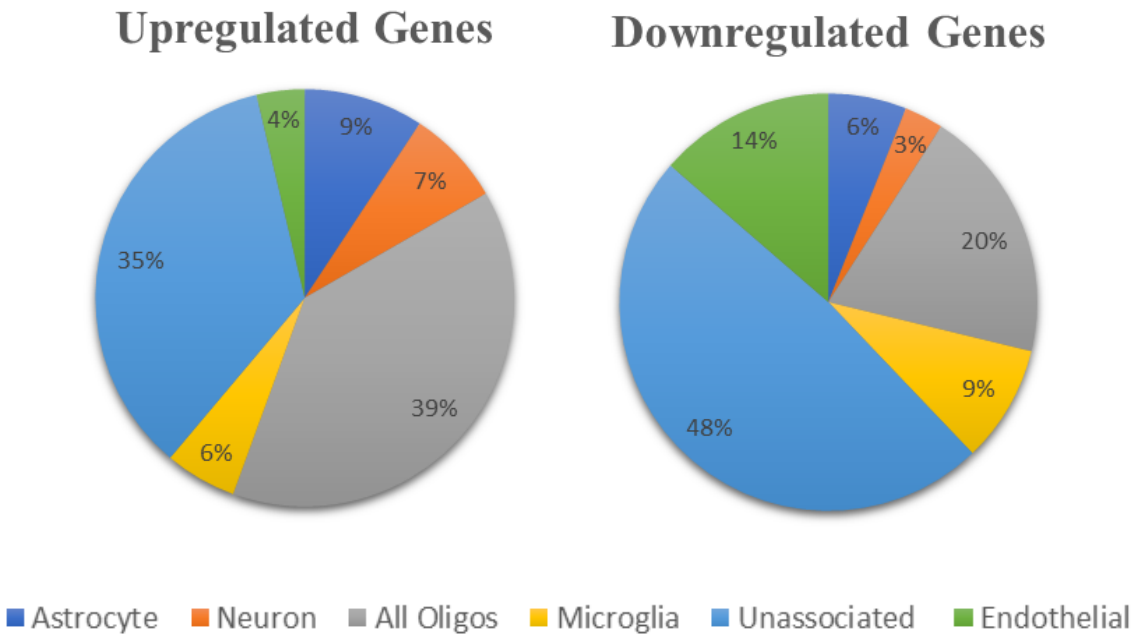

Table 3: Cell-Type Specific Gene Association of DEG WT-PBS vs. Cx32KO-PBS. T3. Differentially expressed genes categorized into those expressed in astrocytes, neurons, OPCs, newly formed oligodendrocytes, myelinating oligodendrocytes, all oligodendrocytes, microglia, and endothelial cells by percentage of association. Unassociated genes also included.

Figure 31. Pie-Chart of Cell-Sorted DEGs WT vs. Cx32KO. Representative pie-charts of differentially expressed genes, both up and down-regulated for WT-PBS vs. Cx32KO-PBS. Unassociated genes are also included.

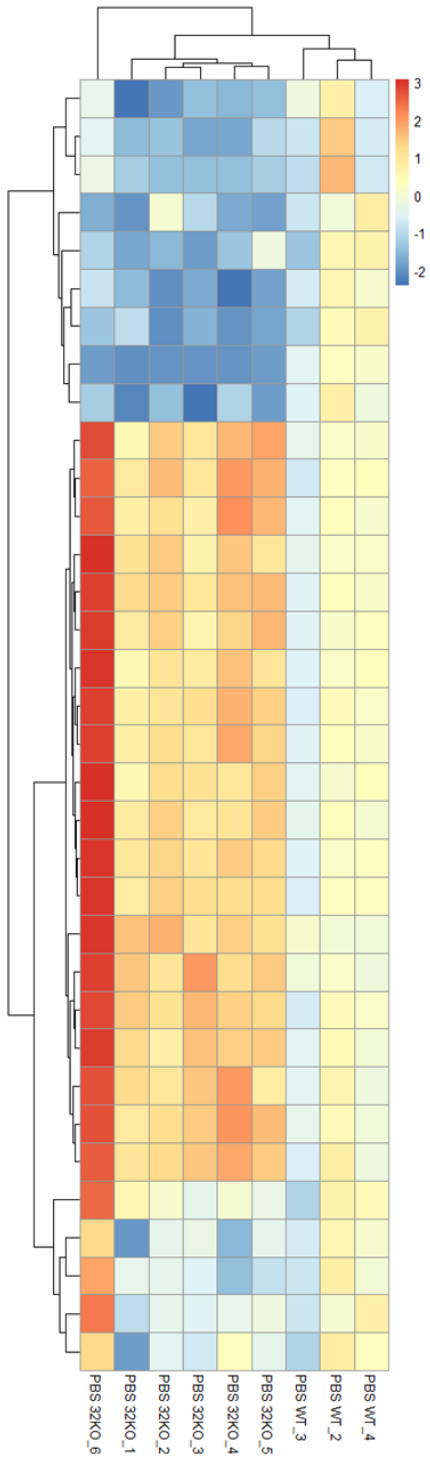

Figure 32. Oligodendrocyte DEG Heatmap WT and Cx32KO. Heatmap of WT-PBS and Cx32KO-PBS oligodendrocyte associated genes, both down and upregulated. Color represents z-score averaged to the WT-PBS group.

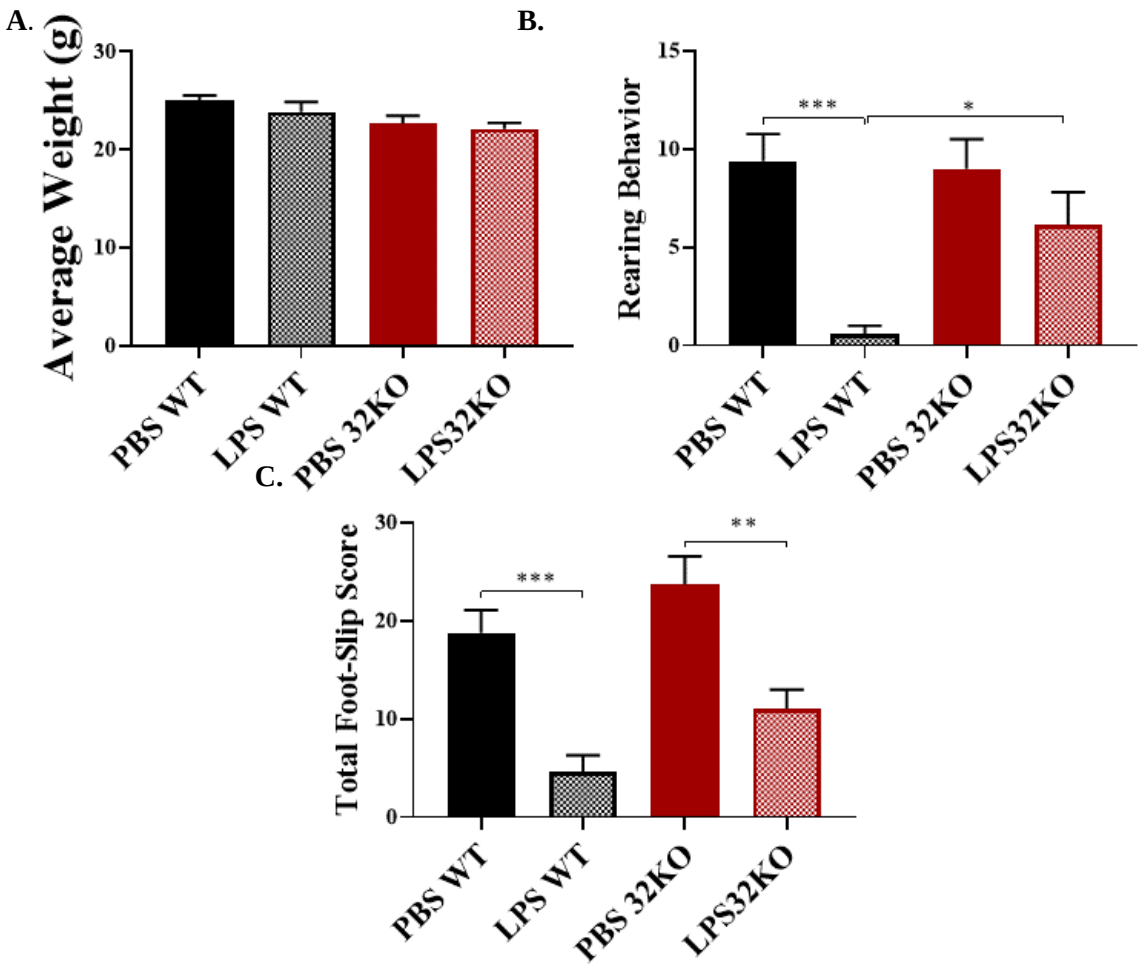

Figure 33. Behavioral Assessment WT and Cx32KO Animals Behavioral assessment after PBS and LPS treatment, before RNA-seq. A. The average weight at 8 weeks WT vs. Cx32KO, was not significant across genotype or treatment groups by one-way ANOVS. B. Rearing behavior after PBS or LPS injections counted as an average amount of hindlimb rears in one minute and was significantly lower in both genotypes after LPS injection. ($F_{3,26}$=8.340) by one-way ANOVA. C. Foot-slip test measured by the number of foot slips over one minute, was significantly lower in both genotypes after LPS acquisition. (F3,26=13.28). Data represent mean ±SEM derived from n=6-20 images in each group unless otherwise noted. *p<0.05, **p<0.01, ***p<0.001.

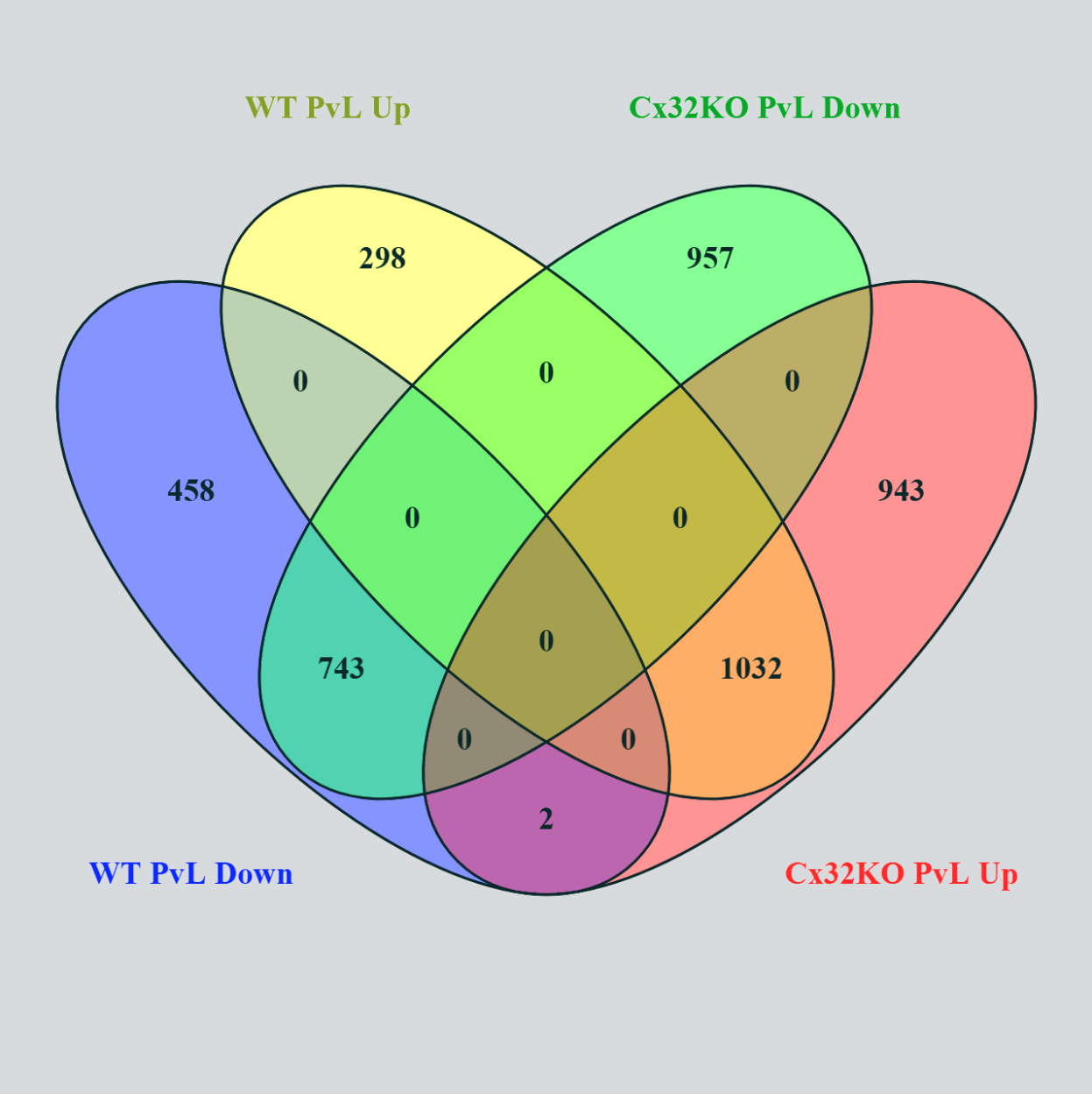

Figure 34. Venn Diagram Comparing DEG after LPS in WT and Cx32KO. Differentially expressed genes, both down and upregulated were assessed after LPS treatment. Downregulated DEGs in WT =458, Cx32KO=957 Both =743. Upregulated DEGs in WT = 298, Cx32KO=943, Both = 1032. Cfap157 and 1700024G13Rik were down-regulated in WT and up-regulated in Cx32KO.

T4.

WT PBS vs WT LPS

Canonical Pathways		
Name	p-Value	Overlap
Hepatic Fibrosis/Hepatic Stellate Cell Activation	6.25E-17	54 of 186
Role of Macrophages, Fibroblasts and Endothelial Cells in RA	2.98E-15	72 of 323
Neuroinflammation Signaling Pathway	2.03E-14	69 of 313
IL-8 Signaling	3.19E-13	51 of 204
IL-6 Signaling	4.12E-13	40 of 136
Diseases and Disorders		
Name	p-Value Range	# Molecules
Cancer	2.44E-16 - 4.69E-56	1690
Gastrointestinal Disease	2.44E-16 - 4.69E-56	1576
Organismal Injury and Abnormalities	2.44E-16 - 4.69E-56	1727
Inflammatory Response	1.80E-16 - 3.73E-46	699
Immunological Disease	1.42E-16 - 1.01E-45	810

T5.

32KO PBS vs 32KO LPS

Canonical Pathways		
Name	p-Value	Overlap
Role of Macrophages, Fibroblasts and Endothelial Cells in RA	3.34E-17	83 of 323
Neuroinflammation Signaling Pathway	5.15E-17	81 of 313
Colorectal Cancer Metastasis Signaling	3.34E-15	68 of 255
IL-8 Signaling	2.45E-13	56 of 204
Molecular Mechanisms of Cancer	2.54E-14	21 of 172
Diseases and Disorders		
Name	p-Value Range	# Molecules
Cancer	5.26E-17 - 4.75E-63	2007
Organismal Injury and Abnormalities	6.43E-17 -4.75E-63	2048
Gastrointestinal Disease	4.21E-17 - 6.76E-61	1851
Endocrine System Disorders	8.36E-20 - 3.65E-59	1696
Connective Tissue Disorders	1.03E-17 - 2.65E-41	364

Table 4-5: GO Enrichment Analysis WT-PBS vs. LPS and Cx32KO-PBS vs. LPS T4. Top canonical pathways and top diseases and disorders that may involve the differentially expressed gene patterns that occur after LPS treatment to WT tissue. T5. Top canonical pathways and top diseases and disorders that may involve the differentially expressed gene patterns that occur after LPS treatment to Cx32KO tissue.

T6.

WT PBS v LPS DEGs						
	Upregulated		Downregulated		Total	
Cell Type	Genes	% of Total	Genes	% of Total	Genes	% of Total
Astrocyte	48	7.52	96	13.08	144	13.69
Neuron	29	4.55	141	19.21	170	16.16
OPC	14	2.19	30	4.09	44	4.18
New Oligo	4	0.63	9	1.23	13	1.24
Myelinating Oligo	14	2.19	32	4.36	46	4.37
All Oligos	165	25.86	172	23.43	337	32.03
Microglia	211	33.07	85	11.58	296	28.14
Endothelial	153	23.98	169	23.02	322	30.61
	638		734		**1372**	

T7.

32KO PBS v LPS DEGs						
	Upregulated		Downregulated		Total	
Cell Type	Genes	% of Total	Genes	% of Total	Genes	% of Total
Astrocyte	78	8.63	141	15.49	219	12.07
Neuron	45	4.98	122	13.41	167	9.21
OPC	24	2.65	44	4.84	68	3.75
New Oligo	9	1.00	15	1.65	24	1.32
Myelinating Olig	16	1.77	37	4.07	53	2.92
All Oligo	260	28.76	262	28.79	522	28.78
Microglia	279	30.86	100	10.99	379	20.89
Endothelial	193	21.35	189	20.77	382	21.06
	904		910		**1814**	

Tables 6 & 7. Cell-Type Specific Gene Association of DEG WT-PBS vs. LPS and Cx32KO-PBS vs. LPS. Differentially expressed genes categorized into astrocytes, neurons, OPCs, newly formed oligodendrocytes, myelinating oligodendrocytes, all oligodendrocytes, microglia, and endothelial cells T6. WT-PBS vs. LPS Cell-type-specific sorting of DEGs after LPS treatment in WT tissue. T7. Cell-specific sorting of DEGs after LPS treatment in Cx32KO tissue.

4.7.3 WT-PBS vs. Cx47KO-PBS

4.7.3.1 Differential Expression Analysis

This study compared gene expression profiles of cortical tissue from WT and Cx47KO mice at baseline, to address the role Cx47 may play in the CNS. The comparative analysis determined 478 DEGs (Appendix 6) (FDR < 0.1) between WT and Cx47KO samples, with 157 downregulated and 320 upregulated after the loss of Cx47. Relative expression was validated for 5 differentially expressed oligodendrocyte genes via QC-PCR using RNA collected from the cortical tissue, as seen in Figure 39B (Appendix 4).

4.8.2 Gene Ontology (GO) Analysis

IPA was used to assess gene ontology. A particular focus was applied to inflammatory and developmental pathways. GO analysis of the DEG genes suggests that loss of Cx47 does resemble a number of disease states, including cancer, organismal injury, and neurological disease, as shown in Table 8 & 9. One of the Top Networks is associated with the loss of Cx47 involves multiple genes in the MEK/ERK1/2 pathway (Figure 35)

4.8.3 Cell-Type Specific Analysis

The DEGs were also analyzed with Linnarsson Lab's single-cell mouse cortex database (Zeisel et al., 2015) to provide insight into oligodendrocyte versus downstream glial regulation in response to the loss of Cx47. As can be seen in Table 10, the majority of the upregulated and downregulated genes are oligodendrocytic (Figure 37). There is, however, considerable involvement from other cell types, suggesting a network of cellular involvement relying on and regulating Cx47. Moreover, 221 DEGs could not be associated with one specific cell type and could be differentially regulated by one or more cell types. These up and down-regulated genes are also displayed in Figures 36, with the percentage of unassociated DEGs.

4.7.4 WT-LPS and Cx47KO-LPS

4.10.1 Behavioral Assessment

Animals were treated with either PBS or LPS, given intraperitoneally, and sacrificed at 6-hours. Cx47KO animals were comparable to WT in weight across treatments, weighing an average of 26.19 grams in the PBS treated group and 26.67 grams in the LPS treated group. (WT-PBS 25.06, and WT-LPS 23.86) (Figure 38A). Four hours after treatment, mice were behaviorally assessed, and monitored for motor deficits as well as foot-slip and rearing behavior indicative of impairment.

Treatment efficacy was evaluated with a foot-slip score under a novel open field paradigm and found both genotypes had a significant decrease in total foot slips after LPS treatment. WT animals decreased from an average of 18.75 to 4.57 slips after LPS treatment ($p=0.0019$), while Cx47KO animals decreased from 19.20 to 5.33 slips after treatment ($p=0.009$) (Figure 38C). In a novel context, this showed that the animals were moving significantly less after LPS treatment, either from pain or decreased motor ability. There was no significant difference between WT and Cx47KO animals. Similarly, LPS treatment significantly decreased the total amount of hind-limb rears by both WT and Cx47KO animals. As stated previously, WT animals reared an average of 9.38 times compared to 0.57 times after LPS ($p<0.0001$), while Cx47KO animals reared an average of 10.6 times after PBS and 1.5 times after LPS treatment ($p=0.0001$) (Figure 38B). Again, there was no significant difference between genotypes.

4.10.1 Differential Expression Analysis

LPS treatment was utilized to provide insight into the effects of inflammatory upregulation, and response to additional neurologic stress. DEGs were evaluated within each genotype after LPS

treatment. Comparative analysis between WT-PBS and WT-LPS determined 2533 genes were differentially expressed in WT, with 1203 downregulated and 1330 upregulated after LPS treatment (Appendix 7) (FDR < 0.1). Comparison of Cx47KO-PBS and Cx47KO-LPS found 1990 DEGs, with 898 downregulated and 1090 upregulated. (FDR <0.1). (https://bioinfogp.cnb.csic.es/tools/venny/index2.0.2.html). Additionally, DEGs expressed in the WT-PBS vs. WT-LPS comparison (Appendix 7), were compared to WT-PBS vs. Cx47KO-PBS (Appendix 6), allowing for comparative analysis of shared DEGs after LPS and Cx47KO. DEGs from each comparison were placed in the Venn diagram shown in Figure 39.

4.7.2.3 Gene Ontology Analysis

As was described above, GO analysis was performed on the differentially expressed genes from both the WT LPS treated and Cx47KO LPS treated samples. As was expected, LPS treatment in both WT and Cx47KO expressed differential patterns with canonical pathways and disease states related to an inflammatory response (Table 11 & 12).

4.7.2.4 Cell Type-Specific Analysis

Utilizing the Linnarsson Lab's single-cell RNA expression database (Zeisel et al., 2015), we assessed cell-type-specific responses to LPS treatment in both WT and Cx47KO tissue. Of the 2533 DEGs expressed after LPS in WT tissue, 1052 were assigned a cell type (Table 13). Comparatively, of the 1990 DEG genes in Cx47KO tissue after LPS, 1160 were associated with a specific cell type. A closer investigation into the similarities, differences, and trends in DEG after a neuroinflammatory insult might provide more insight into the mechanistic underpinnings of Cx47 (Table 14). In conjunction with differential expression analysis, this data provides some

insight into the potential roles that astrocytes and microglia may be playing after the loss of Cx47; this will be expanded upon in the discussion.

T8.

WT PBS vs 47KOKO PBS		
Canonical Pathways		
Name	p-Value	Overlap
Relaxin Signaling	2.54E-05	11 of 163
Adrenomedullin Signaling Pathway	5.66E-05	12 of 210
Gap Junction Signaling	5.92E-05	12 of 211
Synaptic Long Term Depression	9.75E-05	11 of 189
G-Protein Coupled Receptor Signaling	2.78E-04	13 of 286
Diseases and Disorders		
Name	p-Value Range	# Molecules
Cancer	9.16E-04 - 8.60E-18	309
Endocrine System Disorders	8.93E-04 - 8.60E-18	268
Organismal Injury and Abnormalties	9.33E-04 - 8.60E-18	311
Gastrointestinal Disease	8.93E-04 - 5.94E-15	284
Neurological Disease	8.93E-04 - 5.35E-13	142

T9.

Top Networks	
Associated Network Function	Score
Neurological Disease, Cell Death and Survival, Cellular Compromise	47
Post-Translational Modification, Cellular Movement, Neurologic Disease	44
Neurological Disease, Organismal Injury and Abnormalities, Cell Morpholgy	37
Cell-To-Cell Signaling and Interaction, Hematological System Development and function, Hypersensitivity Response	29

Table 8-9: GO Enrichment Analysis WT-PBS vs. Cx32KO-PBS. T8. Top canonical pathways and top diseases and disorders that may involve the differentially expressed gene patterns that occur with the knockout of Cx47. T9. Top Networks and their associated functions which have similar gene transcript changes seen in the differentially expressed genes between WT and Cx47KO cortical tissue.

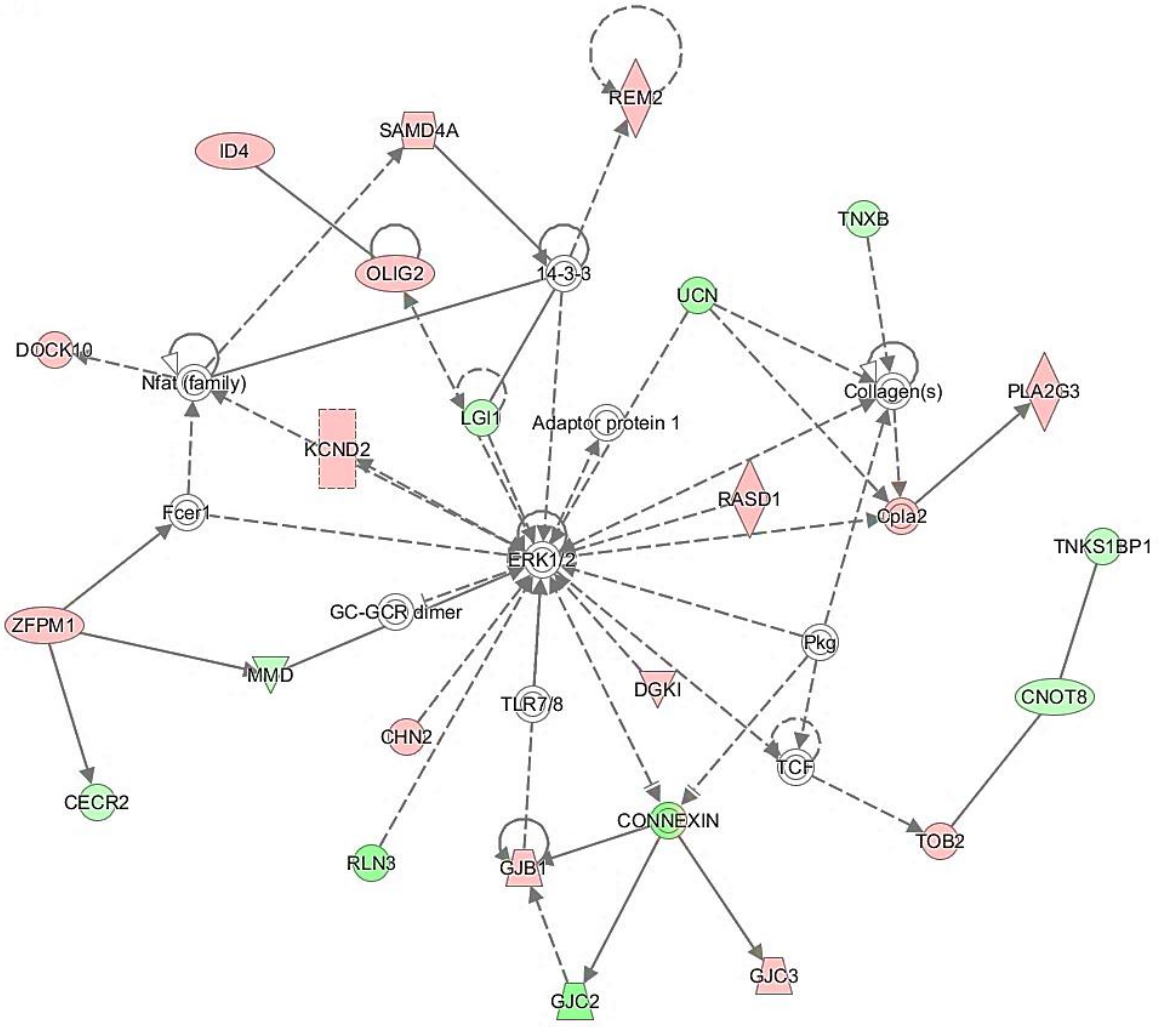

Figure 35. Network Within GO Enrichment Analysis After Cx47 Knockout. A representative network, involving DEGs after Cx47KO, is associated with post-translational modification, cellular movement, and neurologic disease. Though these genes are not all significantly regulated in Cx47KO tissue when compared to WT, those that are red are upregulated, and green are downregulated (Refer to Appendix 6 for significance values).

WT vs 47KO PBS						
	Upregulated		Downregulated		Total	
Cell Type	Genes	% of Total	Genes	% of Total	Genes	% of Total
Astrocyte	16	5.00	6	3.82	22	7.38
Neuron	44	13.75	27	17.20	71	23.83
All Oligos	112	35.00	37	23.57	149	50.00
Microglia	10	3.13	9	5.73	19	6.38
Endothelial	20	6.25	17	10.83	37	12.42
Unassociated	118	36.88	61	38.85	179	63.54
	320		157		477	

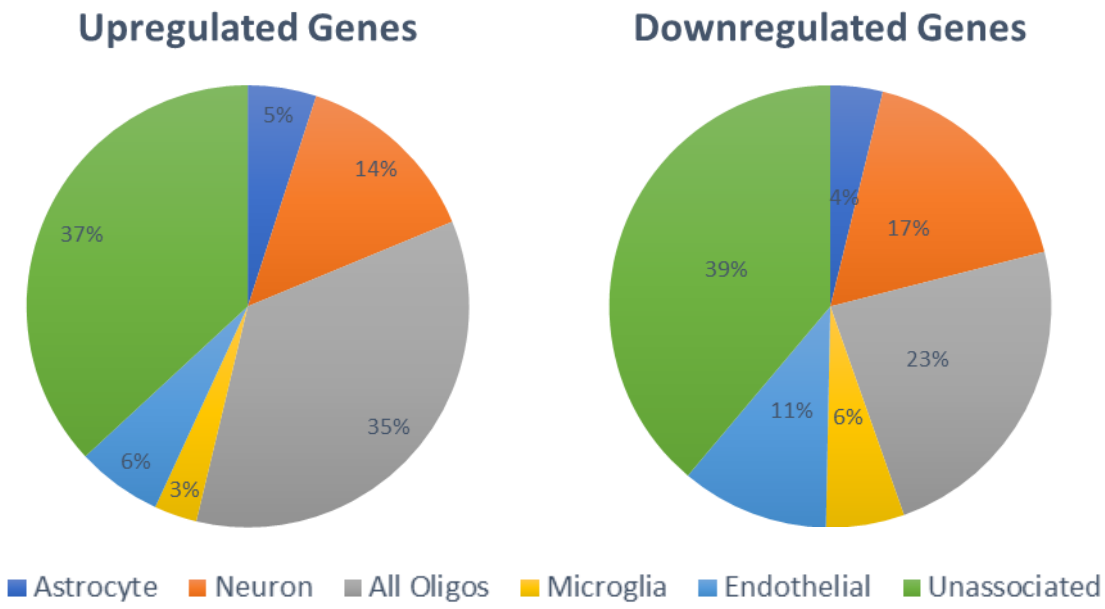

Table 10: Cell-Type Specific Gene Association of DEG WT-PBS vs. Cx47KO-PBS. Differentially expressed genes include those expressed in astrocytes, neurons, oligodendrocytes, microglia, and endothelial cells. These were subdivided into up and downregulation in Cx47KO. Unassociated genes are also included.

Figure 36. Pie Charts of Cell-Sorted DEGs. Representative pie-charts of differentially expressed genes, both up and down-regulated for WT-PBS vs. Cx47KO-PBS. Unassociated genes are also included.

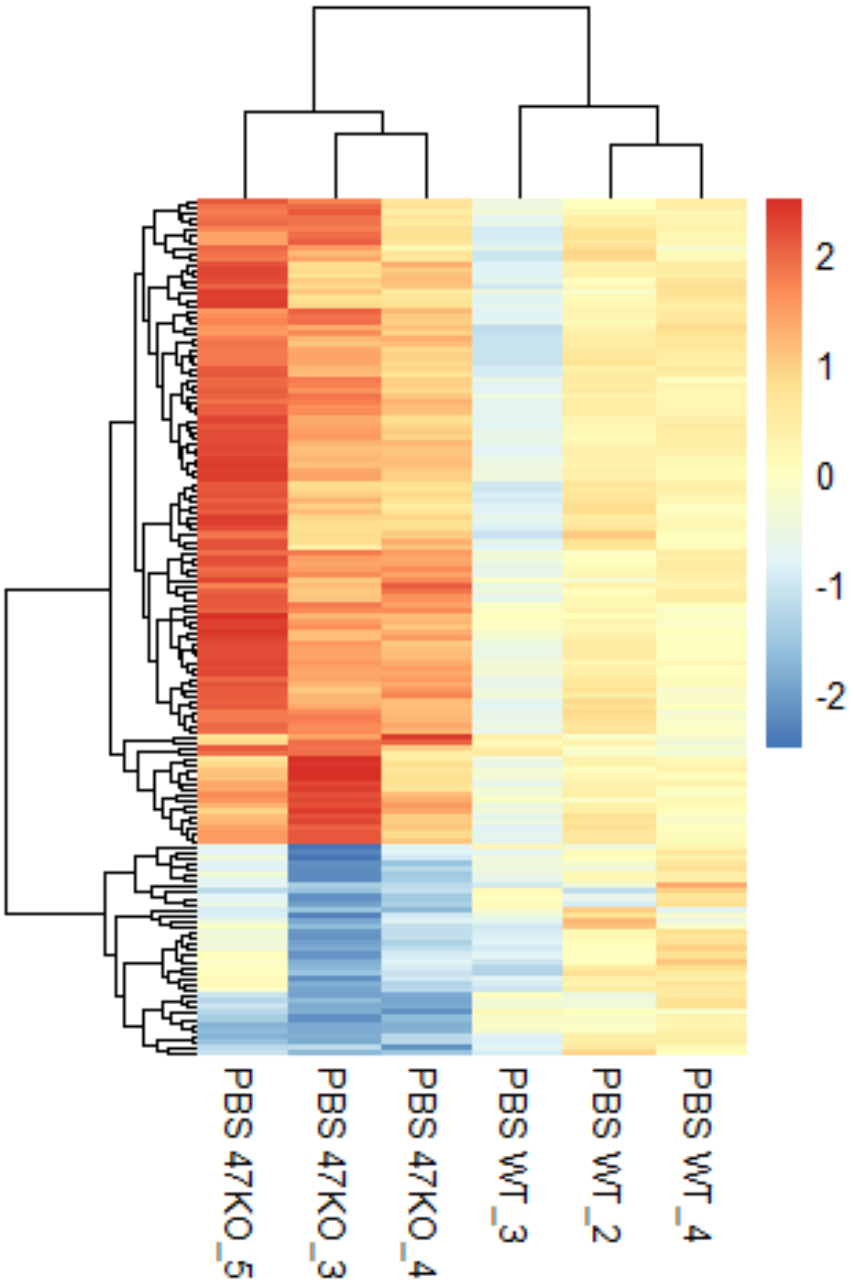

Figure 37. Oligodendrocyte DEG Heatmap WT and Cx47KO. Heatmap of WT-PBS and Cx47KO-PBS oligodendrocyte associated genes, both down and upregulated. Color represents z-score averaged to the WT-PBS group.

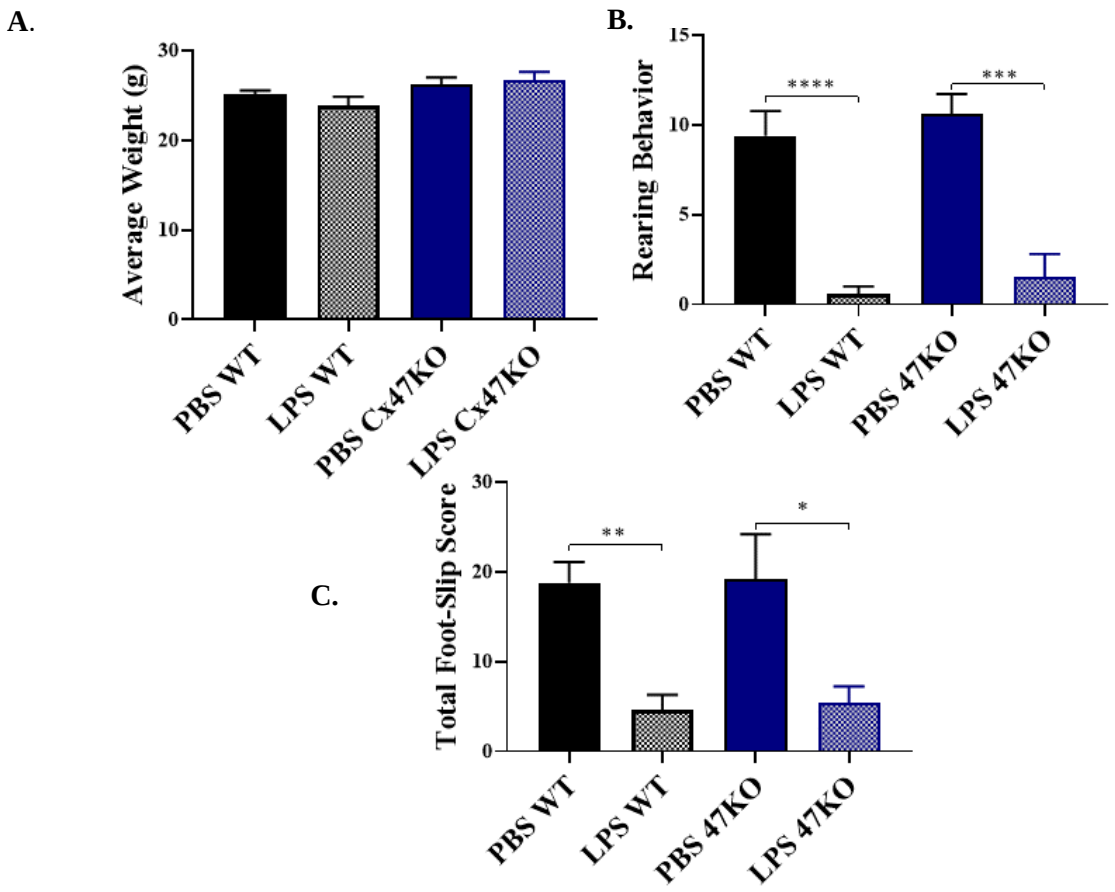

Figure 38. Behavioral Assessment WT and Cx47KO Animals After PBS and LPS Treatment. A. Average weight at 8-weeks for WT and Cx47KO was not significant across treatment groups by one-way ANOVA. B. Rearing behavior after PBS or LPS injections were counted as an average number of hindlimb rears in one minute and were significantly lower in both genotypes after LPS injection. ($F_{3,33}$=9.007). C. Foot-slip test measured by the number of foot slips over one minute were significantly lower in both genotypes after LPS. ($F_{3,22}$=8.610). Data represent mean ±SEM. *p<0.05, **p<0.01, ***p<0.001.

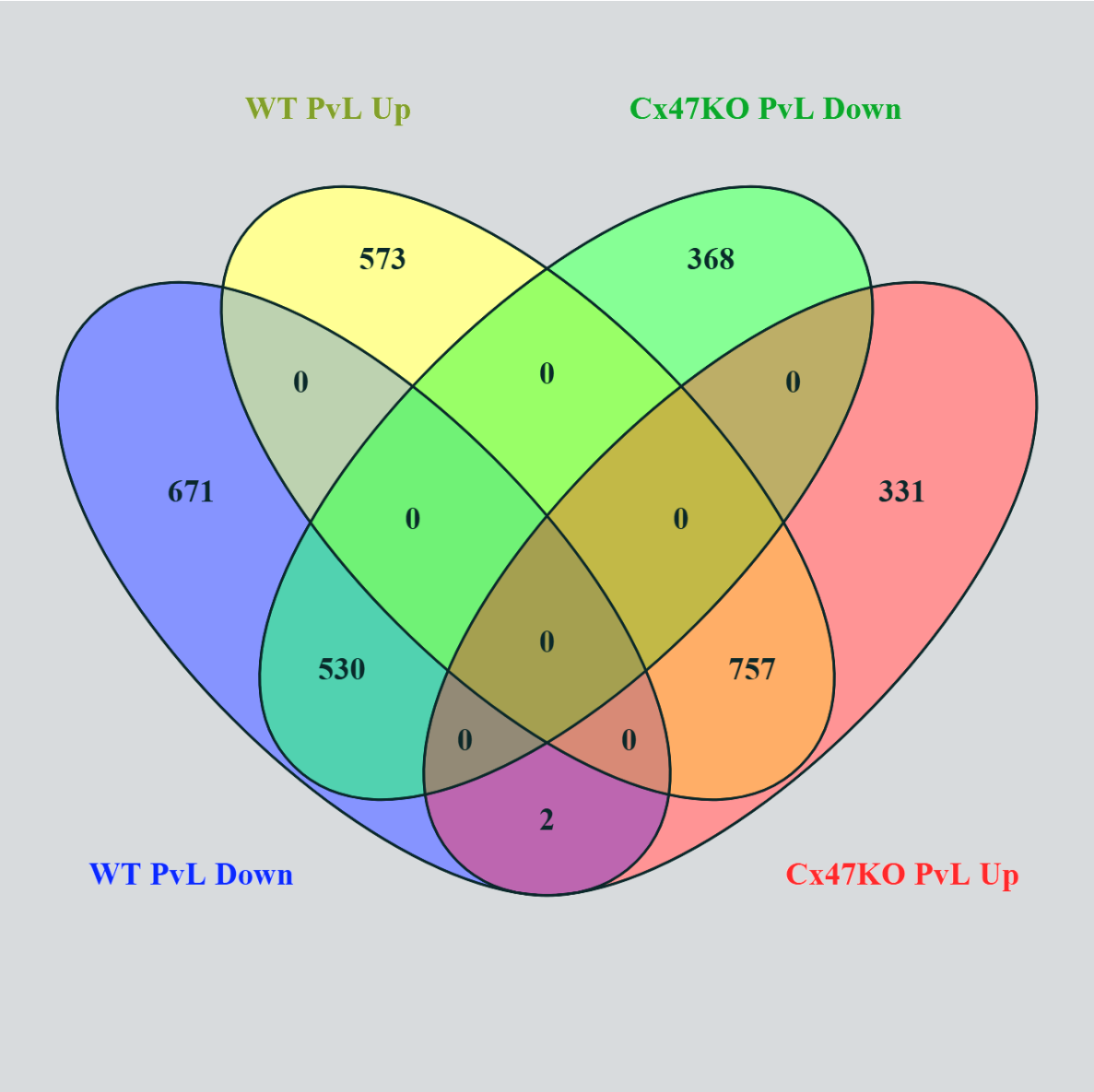

Figure 39. Venn Diagram Comparing DEG after LPS in WT and Cx47KO. Differentially expressed genes that were down, and upregulated after LPS treatment were assessed.

T11. **WT PBS vs WT LPS**

Canonical Pathways		
Name	p-Value	Overlap
Hepatic Fibrosis/Hepatic Stellate Cell Activation	6.25E-17	54 of 186
Role of Macrophages, Fibroblasts and Endothelial Cells in RA	2.98E-15	72 of 323
Neuroinflammation Signaling Pathway	2.03E-14	69 of 313
IL-8 Signaling	3.19E-13	51 of 204
IL-6 Signaling	4.12E-13	40 of 136

Diseases and Disorders		
Name	p-Value Range	# Molecules
Cancer	2.44E-16 - 4.69E-56	1690
Gastrointestinal Disease	2.44E-16 - 4.69E-56	1576
Organismal Injury and Abnormalities	2.44E-16 - 4.69E-56	1727
Inflammatory Response	1.80E-16 - 3.73E-46	699
Immunological Disease	1.42E-16 - 1.01E-45	810

47KO PBS vs 47KO LPS

T12.

Canonical Pathways		
Name	p-Value	Overlap
Neuroinflammation Signaling Pathway	1.25E-17	66 of 313
Role of Macrophages, Fibroblasts and Endothelial Cells in RA	6.74E-17	66 of 323
IL-8 Signaling	1.86E-16	50 of 204
Colorectal Cancer Metastasis Signaling	5.64E-16	56 of 255
Production of Nitric Oxide and Reactive Oxygen Species in Macrophages	7.72E-16	48 of 196

Diseases and Disorders		
Name	p-Value Range	# Molecules
Connective Tissue Disorder	3.45E-19 - 4.30E-50	299
Inflammatory Disease	4.88E-18 - 4.309E-50	400
Organismal Injury and Abnormalities	6.98E-18 - 4.309E-50	1393
Skeletal and Muscular Disorders	3.45E-18 - 4.309E-50	299
Immunological Disease	1.39E-18 - 3.65E-49	595

Table 11-12: GO Enrichment Analysis WT-PBS vs. LPS and Cx47KO-PBS vs. LPS T11. Top canonical pathways and top diseases and disorders that may involve the differentially expressed gene patterns that occur after LPS treatment to WT tissue. T12. Top canonical pathways and top diseases and disorders that may involve the differentially expressed gene patterns that occur after LPS treatment to Cx47KO tissue.

T13.

WT PBS v LPS						
	Upregulated		Downregulated		Total	
Cell Type	Genes	% of Total	Genes	% of Total	Genes	% of Total
Astrocyte	48	7.52	96	13.08	144	13.69
Neuron	29	4.55	141	19.21	170	16.16
OPC	14	2.19	30	4.09	44	4.18
New Oligo	4	0.63	9	1.23	13	1.24
Myelinating Oligo	14	2.19	32	4.36	46	4.37
All Oligos	165	25.86	172	23.43	337	32.03
Microglia	211	33.07	85	11.58	296	28.14
Endothelial	153	23.98	169	23.02	322	30.61
	638		734		1372	

T14.

Cx47KO PBS v LPS Total Gene Count						
	Upregulated		Downregulated		Total	
Cell Type	Genes	% of Total	Genes	% of Total	Genes	% of Total
Astrocyte	55	9.86	79	13.12	134	11.55
Neuron	41	7.35	62	10.30	103	8.88
OPC	16	2.87	25	4.15	41	3.53
New Oligo	6	1.08	17	2.82	23	1.98
Myelinating Olig	12	2.15	42	6.98	54	4.66
All Oligo Genes	107	19.18	144	23.92	251	21.64
Microglia	181	32.44	64	10.63	245	21.12
Endothelial	140	25.09	169	28.07	309	26.64
	558		602		**1160**	

Tables 13 & 14. Cell-Type Specific Gene Association of DEG WT-PBS vs. LPS and Cx47KO-PBS vs. LPS. Differentially expressed genes categorized into astrocytes, neurons, OPCs, newly formed oligodendrocytes, myelinating oligodendrocytes, all oligodendrocytes, microglia, and endothelial cellT13. WT-PBS vs. LPS cell-type-specific sorting of DEGs. T14. Cell-specific sorting of DEGs after LPS treatment in Cx47KO tissue.

4.8 Discussion

4.8.1 Glial Inflammatory Response After Cx32 Knockout

4.8.1.1 Minocycline Treatment Response

In this study, I investigated the potential role of pro-inflammatory microglia in the development of both Cx32 and Cx47 knockout oligodendrocytes. As discussed in chapter 3, the data show that loss of Cx32 results in an upregulation in the percentage of microglia within both culture and tissue, and Cx47KO resulted in a significant increase of microglia within culture. Though tissue microglia in the Cx47KO were not quantitatively upregulated, they did appear ameboid (and therefore potentially phagocytotic) in tissue (Giulian 1987; Donat et al., 2017; Kaur et al., 2017). Both the loss of Cx32 and Cx47 appears to result in activated microglia, though these microglia may play a differential role that will be explored below.

Our data show that while treated with minocycline, Cx32KO cultures express a global increase in the percentage of $Ki67^+$ cells that is maintained during recovery. This proliferative response was the opposite of what was seen in WT cultures, suggesting that in Cx32 knockout pro-inflammatory microglial factors may be partially inhibiting cell proliferation. Surprisingly, in both WT and Cx32KO cultures, the treatment with minocycline significantly downregulated the percentage of $O4^+$ oligodendrocytes. These oligodendrocytes expressed reduced $Ki67^+$ expression during treatment in WT cultures, but these levels returned to baseline in recovery. Comparatively, Cx32KO oligodendrocytes maintained significantly lower proliferation throughout treatment groups, and expressed a significantly lower percentage of $Sox10^+$ cells while treated, suggesting that pro-inflammatory microglial factors may be involved in oligodendrocyte determination. There are several possible explanations for the oligodendrocyte response to minocycline treatment in

culture. One is that the dose and/or time course of minocycline treatment is toxic to oligodendrocytes. Alternatively, it is possible that at 6DIV, when cells have settled into their culture environment, the microglial pro-inflammatory factors are critical to oligodendrocyte maintenance and differentiation. Experiments performed by Shigemoto-Mogami et al. suggest that at low doses, pro-inflammatory microglial factors inhibited by minocycline (IL-1β, IL-6, and TNFα) encourage increased $O4^+$ development (Shigemoto-Mogami et al., 2014). Interestingly, while the percentage of oligodendrocytes significantly decreased during minocycline treatment across genotypes, there was a significant increase in the percentage of $Pdgfra^+$ cells within Cx32KO cultures, which returned to baseline during recovery. This inverse relationship between the increased percentage of OPCs and decreased percentage of $O4^+$ oligodendrocytes suggests that while microglia are inhibited from releasing pro-inflammatory factors, oligodendrocytes are not differentiating. Follow-up experiments should include primary cell cultures to elucidate any toxic effect of minocycline but should also investigate minocycline's effect in tissue as well as in remyelinating capacity in WT and Cx knockout animals.

Assessment of both astrocytes and microglia found that response to minocycline was differentially modulated across genotypes. Minocycline treatment did not significantly alter $GFAP^+$ astrocyte percentage or proliferative capacity in cultures of either genotype but did significantly increase their FI while treated. In contrast, both genotypes expressed a significant increase in the percentage of $Iba1^+$ microglia during treatment, which appears to return to baseline during recovery. Cx32KO microglia showed significant increases in proliferation during treatment and recovery, with a significant decrease in $Iba1^+$ FI. On the other hand, the proliferative state of WT microglia was not altered, but these cells expressed significantly higher levels of activation. These findings suggest that the pro-inflammatory state of Cx32KO cultures is likely altered at

baseline when compared to WT. While the inhibition of pro-inflammatory factors appears to encourage cell growth in Cx32KO cultures, this did not occur in WT. Nonetheless, addition of minocycline to already quiescent WT cultures may disrupt homeostatic balance and activate glia, specifically if these factors are necessary for cellular development at low doses (Shigemoto-Mogami et al., 2014).

To further probe the inflammatory state of our mixed glial cultures, we performed an ELISA on WT and Cx32KO media from all treatments, enabling multi-analyte detection of the following pro- and anti-inflammatory factors: IL-1β, IL-4, IL-6, IL-10, IL-12α, IL-17α, TNFα, IFNγ, TGFβ1, MCP-1 (CCL2), MIP1-α (CCL3), and MIP1β (CCL4). In consideration of our previous pro-inflammatory findings in the periphery (Freidin et al., 2015) as well as the Cx32KO culture and tissue data, we had hypothesized that there would be a clear upregulation of pro-inflammatory cytokines in Cx32KO culture media at baseline when compared to WT (IL-1β, IL-6, TNFα). Unexpectedly, the only detectable differences in the 3- and 6DIV were the microglial chemokines CCL2, CCL3, and CCL4 (6-day only). In Cx32KO cultures, CCL2 expression was lower than WT at baseline, upregulated during minocycline treatment, and returned to baseline during recovery (Figure 25A/C). CCL3 and CCL4 expression were both higher in Cx32KO at baseline, increased further during minocycline, and decreased compared to WT during recovery (Figures 25D/E). Baseline and treatment responses were comparable at 3DIV for CCL2 and CCL3 expression (Figures 25A/B). These results may provide insight into the mechanistic response of microglia in the absence of Cx32, and potentially how this might differ in the CNS when compared to the peripheral nervous system. Of particular interest is the CCL2 expression response, as it is directly inverse of WT and appears to change when microglial pro-inflammatory factors are inhibited.

MCP-1 (CCL2), a monocyte chemokine known for macrophage/microglial recruitment, has been directly implicated in demyelination and neuropathy in Cx32KO Schwann cells (Groh et al., 2010). MCP-1 upregulation has been linked to demyelination, astrogliosis, and axonal damage in CMT1A (Kohl et al., 2010) and Cx32KO mice at baseline, and this damage was attenuated in MCP-1 knockout (Groh et al., 2010). During LPS-induced neuroinflammation, MCP-1 expression is upregulated, and this upregulation is blunted by minocycline treatment (Scholz et al., 2015; Piotrowska et al., 2016). Additionally, this MCP-1 upregulation appears to be dependent on MEK-ERK activation, as inhibitory modulation of these pathways attenuated both MCP-1 upregulation and subsequent neuropathy (Fischer et al., 2008; Groh et al., 2010).

These results are of particular interest because our mixed glial culture ELISA suggests that the baseline expression of MCP-1 in the CNS is lower in Cx32KO than in WT. Additionally, although MCP-1 levels decreased in WT minocycline treated cultures as expected (Scholz et al., 2015; Piotrowska et al., 2016), the MCP-1 levels in Cx32KO cultures increased during treatment and returned to baseline during recovery. The unexpected findings of decreased MCP-1 levels in our Cx32KO cultures (in PNS, baseline expression is higher in the 32KO) (Groh et al., 2010) and the unanticipated increase in MCP-1 in the Cx32KO in response to minocycline treatment may be related to dysregulated microglial phenotypes in Cx32KO cells (Figure 24). This chemokine alteration may represent the results of a negative feedback mechanism, by which MCP-1 both recruits and encourages microglial proliferation but then becomes downregulated once the percentage of microglia reaches a critical threshold. This may also explain the upregulation in $Ki67^{+}$ microglia in minocycline treated Cx32KO cultures. Alternatively, MCP-1 alterations may be a secondary response to altered cellular interaction between oligodendrocytes and microglia after Cx32 knockout, and these possibilities should be evaluated in future studies.

In the central nervous system, and particularly in the case of neuroinflammation, chemokine MCP-1, MIP-1α (CCL3) and MIP-1β (CCL4) upregulation has been attributed to a variety of cell types including microglia, astrocytes and neurons (Berman et al., 1996; Van Der Voorn et al., 1999; Che et al., 2001; Hinojosa et al., 2011; Lawrence et al., 2005; Dubový et al., 2018; Kohno et al., 2014). In both acute MS lesions and an EAE model of demyelination, MCP-1, MIP-1α, and MIP-1β were selectively expressed by astrocytes, macrophages, and microglia in the lesion center and surrounding white matter (Simpson et al., 1998; Ambrosini et al., 2005; Lewis et al., 2014). This suggests that the upregulation of these chemokines in the Cx32KO cultures either at baseline or during minocycline treatment could be in response to oligodendrocyte dysregulation. Follow-up with each of these chemokines and their cell-specific involvement, potentially with single-cell RNA-sequencing, would provide insight into the pro-inflammatory upregulation that occurs after Cx32 knockout.

4.8.1.1 RNA-Seq Analysis Cx32KO

We originally hypothesized that loss of Cx32 would result in a compensatory pro-inflammatory activation of surrounding glia similar to the response to Cx32KO in the periphery (Freidin et al., 2015), with the potential for alternative compensatory mechanisms that result in a minimal or non-existent CNS phenotype until after an additional neurologic insult (Sutor et al., 2000; Sargiannidou et al., 2009; Freidin et al., 2015). Our tissue and culture results showed a robust increase in microglial expression and activation. While we hypothesized these microglia were expressing a pro-inflammatory phenotype within our Cx32KO tissue, these microglia were ramified, contradictory to an ameboid pro-inflammatory state (Giulian, 1987; Kaur et al., 2017). Similarly, our cytokine ELISA found that Cx32KO cultures express no pro-inflammatory

microglial cytokines and lower CCL2 when compared to WT at baseline, which was only upregulated after minocycline treatment. The expression of CCL3 and CCL4 was increased at 6DIV after minocycline treatment, decreasing to at levels lower than WT during recovery. As CCL2, CCL3 and CCL4 are expressed in acute immune response for microglial recruitment and proliferation (Groh et al., 2010; Glass et al., 2001; Kiguchi et al., 2013), this microglial activation may not be pro-inflammatory.

To further evaluate inflammatory and developmental factors after Cx32 knockout, we performed RNA sequencing on cortical tissue from 8-week old mice. After IPA analysis, many of the significant canonical pathways were based on only a few genes, and therefore may not be relevant. However, all five Diseases and Disorder pathway hits encompass brain disorders and genetic diseases, which is essential considering Cx32 mutations cause the inherited peripheral neuropathy CMT1X (Scherer & Kleopa, 2012).

The top network generated by IPA when using DEGs from the Cx32KO vs. WT comparison revealed functions associated with developmental disorders, cell-to-cell signaling, and nervous system development and function (Figure 30). A striking feature of this IPA pathway is the presence of histones and histone-modifying proteins, including histone deacetylases (HDACs). Interestingly, HDAC1 and HDAC2 are known to regulate oligodendrocyte differentiation (Ye et al., 2009; Dai et al., 2015; Hammond et al., 2015; Berry et al., 2020), and when both are knocked the result is early mortality and severe defects in oligodendrocyte proliferation and differentiation (Ye et al., 2009). Inhibition of HDACs prevents white matter injury in animal models of TBI (Wang et al., 2015), while acetylated histone H3 is enriched in the oligodendrocytes of early white matter lesions from MS patients (Pedre et al., 2011). Together, these results suggest that histones

play a complicated role in oligodendrocyte myelination. This potential histone involvement after Cx32KO is particularly interesting, as acetylation of the C-terminal lysine residues of Cx32, mediated by HDAC6, alters Cx32 ubiquitination, stability, and turnover (Alaei et al., 2018). In a novel Cx32 CNS mutation (Trp133fx), proteasomal factors rapidly degrade Cx32 via endoplasmic reticulum (ER)-associated degradation (Sakaguchi et al., 2011). Similarly, other Cx32 CNS mutations (including A39V and T55I) appear to undergo proteasomal degradation while retained in the endoplasmic reticulum (Kleopa & Scherer, 2002). Together this suggests that our data supports involvement of previously identified Cx32 mutation pathways, possibly suggesting shared roles in oligodendrocyte developmental modulation. Our Cx32KO tissue expresses upregulation of specific chromatin-modifying and proteasomal pathway genes, including ACSS2, BAZ2A, TCF4, and UBE4A, suggesting that future studies should directly investigate the role of these genes in the pathophysiology of CMT1X and related Cx32KO models.

To further investigate our hypothesis that Cx32KO resulted in surrounding glial activation, we performed cell-type-specific analysis under comparison to Linnarsson single-cell RNA sequencing data (Zhang et al., 2014) to our DEGs both at baseline and after LPS treatment. This evaluation showed that after Cx32KO, genes associated with oligodendrocytes form the predominant differentially regulated group. There are, however, a large subset of transcripts that are associated with astrocytes, microglia, and endothelial cells, supporting both our culture and tissue findings showing there is a compensatory response in surrounding glia. Subsequent comparison of these DEGs at baseline and after LPS treatment suggests that our original hypothesis about the pro-inflammatory state in Cx32KO tissue may be incomplete. Despite the significant increase in microglial expression in both culture and tissue after Cx32 knockout, baseline comparisons between Cx32KO-PBS and WT-LPS treated tissue did not find any of the

expected pro-inflammatory gene expression changes. For example, during neuroinflammatory conditions, factors including Pdgfrα and Olig2 are upregulated to recruit OPCs during periods of remyelination (Kumar et al., 2007; Morin et al., 2011). Meanwhile, connexin expression (Markoulli et al., 2012; Lieury et al., 2014; Cepeda et al., 2015) and oligodendrocyte differentiation markers, including MBP and Sox10 are downregulated (Chew et al., 2005; Finzsch et al., 2008). During pro-inflammatory polarization, microglia upregulate cytokines and chemokines, including IL-1β, TNFα, NOS2, CCL2, CCL5, CCL7 (Kumar et al., 2013, 2016; Wang et al., 2015) while downregulating anti-inflammatory factors such as TGF-β1 (Taylor et al., 2017). Although this pro-inflammatory exacerbation was observed after LPS treatment in both WT and Cx32KO tissue, there was no significant differential expression for these pro-inflammatory factors in Cx32KO tissue at baseline.

There are 30 DEGs significantly regulated in both WT-LPS treated tissue and Cx32KO-PBS tissue when compared to WT-PBS, of which only 13 are congruently up- or down-regulated while 17 are inversely regulated (Appendix 8). Further investigation should be performed into transcriptional trends beyond significant differential expression. A few of these 17 are of particular interest and may contribute to our understanding of microglial mechanistic involvement after Cx32 knockout. The microglial gene, transglutaminase 2 (Tgm2), regulates oligodendrocyte development and is significantly downregulated in our Cx32KO tissue. When knocked out, the loss of Tgm2 results in reduced OPC proliferation, fewer mature oligodendrocytes, and hypomyelination (Giera et al., 2018). Mitochondrial uncoupling protein-2 (UCP2), also downregulated in our Cx32KO tissue compared to WT, is a critical regulatory agent of both pro- and anti-inflammatory activation of microglia (Simone et al.,2015). Plastin-1 (PLS1), an actin-binding protein associated with neurons and macrophages (Shinomiya, 2012), significantly

increases oligodendrocyte differentiation (Dugas et al., 2006). This is of particular interest as it is significantly upregulated in Cx32KO tissue and may be involved in response to Cx32 knockout.

The glial responses to minocycline and the RNA-seq analysis suggest that the microglial upregulation and activation seen after Cx32KO may be operating under an alternative biological role from our originally hypothesized pro-inflammatory state. Our results expand upon our original hypothesis, highlighting potential regulatory mechanisms that occur in the CNS after Cx32 knockout.

4.8.2 Glial Inflammatory Response After Cx47 Knockout

4.8.2.1 Minocycline Treatment Response

Compared to Cx32KO cultures and as discussed in chapter 3, Cx47KO cultures expressed significantly fewer cells than WT in culture at baseline. The total cell count did increase, albeit not significantly, during minocycline treatment, suggesting that microglial inflammatory factors may play a role in suppression of cellular growth in cultures after the knockout of Cx47. While the treatment did not increase the percentage of $Ki67^+$ cells within these cultures, recovery after treatment did show a significant upregulation of proliferation. This supports prior findings suggesting that the inhibition of pro-inflammatory microglial factors encourages cellular growth and proliferation (Kigerl et al., 2009; Tang et al., 2016).

There was a non-significant decrease in the percentage of $O4^+$ oligodendrocytes in minocycline treated Cx47KO and WT cultures. However, in WT the percentage of oligodendrocytes returned to baseline during recovery, while Cx47KO expression remained downregulated. This change supports the hypothesis that Cx47KO oligodendrocytes are developmentally inhibited in that unlike WT, they are unable to recover after withdrawal of

minocycline. (Liu et al., 2017; Papaneophytou et al., 2018). Additionally, the percentage of $Ki67^+$ oligodendrocytes, which was significantly lower than WT at baseline, remained unchanged across treatment conditions in Cx47KO cultures, suggesting that the lack of proliferation after Cx47 loss is not the result of inhibition via pro-inflammatory microglial factors. Unlike WT, Cx47KO cultures expressed a significant increase in the percentage of $Sox10^+$ cells during minocycline treatment that remained elevated during recovery. In conjunction with the lower percentage of $O4^+$ cells, this elevation of Sox10 potentially indicates a failure to complete terminal differentiation due to an underlying deficit caused by Cx47 knockout. Interestingly, the large decrease in $O4^+$ oligodendrocytes during treatment in both genotypes is paired with an upregulation of $Pdgfr\alpha^+$ cells. During recovery, the levels of OPCs returned to baseline in both genotypes, suggesting that there is an interplay between oligodendrocyte differentiation and pro-inflammatory microglial factors. In consideration of the global decrease in total cell count and proliferation after Cx47 knockout, microglia in Cx47KO cultures may be in a pro-inflammatory state (Figure 16 & 18), releasing factors discouraging cellular growth. While the inhibition of these factors promotes overall culture viability and potentially OPC proliferation, these same microglial pro-inflammatory factors are critical for OPCs to complete development (Shigemoto-Mogami et al., 2014).

Comparable to both WT and Cx32KO cultures, minocycline treatment does not significantly alter the percentage of astrocytes or microglia within Cx47KO cultures. Cx47KO $GFAP^+$ astrocytes show no significant alteration in proliferation during treatment but do show changes in FI indicative of alterations in the state of activation. Astrocytes within Cx47KO cultures became significantly more activated during minocycline treatment, returning to below baseline during recovery. Subtle changes in proliferation, as well as inverse changes in activation state

across treatment, suggests there is a phenotypic change in astrocytes after the loss of Cx47. Any astroglial response may be supported and activated via pro-inflammatory microglial factors, similar to the dual activation of both astrocytes and microglia after acute EAE in conditional Cx47KO mice (Zhao et al., 2020).

At baseline, the percentage of $Iba1^{+}$microglia was also significantly higher in Cx47KO cultures, remained elevated while treated with minocycline, but significantly decreased during recovery. While these microglia displayed increased FI at baseline, this FI significantly decreased during minocycline treatment and returned to baseline levels during recovery, supporting the hypothesis that these Cx47KO microglia may be expressing pro-inflammatory factors, and are potentially phenotypically altered by minocycline treatment. There was an upregulation of $Ki67^{+}$ in Cx47KO microglia during recovery, which may account for either a phenotypic change after minocycline treatment (Manso et al., 2018) or an increased necessity for microglia after the percentage of microglia declined. Additional culture experiments could evaluate primary and co-cultured oligodendrocytes, astrocytes, and microglia at longer time points, both with and without minocycline to observe glial interaction and potentially necessary cell-cell communication as it pertains to development.

4.8.1.2 RNA-Seq Analysis Cx47KO

We originally hypothesized that the loss of Cx47 would result in a compensatory pro-inflammatory upregulation in surrounding glia, with subsequent oligodendrocyte dysregulation. Tissue and culture results supported the idea that Cx47KO leads to significantly altered oligodendrocyte developmental capacity (Figure 11). Loss of oligodendrocyte viability was

associated with the observed activation of both astrocytes and microglia in culture suggesting that there might be pro-inflammatory upregulation after Cx47 loss.

To investigate potential inflammatory and developmental pathways regulated after the knockout of Cx47, we performed RNA sequencing on cortical tissue from 8-week old mice. Differential gene expression analysis was performed and assessed via IPA pathway analysis, which evaluated canonical pathways, disease states, and networks that may be associated with the DEGs in our tissue. Similar to Cx32KO IPA analysis, the top canonical pathways were based on a few potentially relevant genes. The third highest pathway, associated with Gap Junction Signaling, includes the significant upregulation of Cx32 and Cx29 in the absence of Cx47, potentially supporting the previous hypothesis that Cx expression in oligodendrocytes may be compensatory (Li et al., 2018). Neurological disease was the fifth top Disease and Disorder hit, which included other disease and disorder states, supporting that the loss of Cx47 differentially regulates similar injury response pathways. Three of the top networks are associated with Neurological disease, and while the top two pathways centered around JUN and AKT pathway alterations that may be pertinent in response to Cx47KO, the pathway highlighted in Figure 35 encapsulates the DEGs that are related to downregulation of Cx47 and subsequent oligodendrocyte response.

The network displayed in Figure 35 centers around extracellular signal-regulated protein kinases 1 and 2 (ERK1/2), part of a mitogen-activated superfamily that can mediate cell proliferation and apoptosis (Mebratu and Tesfaigzi, 2009). A balance between expression levels and duration of downstream pro- and anti-apoptotic signals transmitted via ERK1/2 is thought to control whether a cell proliferates or undergoes apoptosis (Pearson et al.; 2001). Downstream factors include a variety of transcripts differentially expressed in our Cx47KO data including c-

Jun (McCubrey et al., 2007), and NF-κB (Nakano et al., 1998; Zhao et al. 1999). Dynamic interaction of ERK pathway factors have also been associated with pro-inflammatory interferon-gamma (IFNγ)-induced toxicity in oligodendrocyte progenitor cells (Horiuchi et al., 2006), and oligodendrocyte differentiation in conjunction with p38-mediated Sox10 regulation and upregulation of JNK pathways (Chew et al., 2010). Utilizing conditional knockouts, Ishii and colleagues found that both MEK/ERK1/2-MAPK and P13K/Akt/mTOR intracellular signaling pathways play a critical regulatory role in myelination and oligodendrocyte integrity (Ishii et al., 2019), while Dai and colleagues found both the Akt/mTOR and Erk1/2 pathways regulate oligodendrocyte differentiation and myelin basic protein expression (Dai et al., 2014). Most interestingly, cell co-culture experiments performed by Liu and colleagues found signal activation of Ca^{2+} and ERK1/2 phosphorylation by astrocytes encourages OPC proliferation and development via Cx47 channels (Liu et al., 2017). Together, this data supports the idea the ERK1/2 signaling pathways play a dynamic role in oligodendrocyte maintenance and survival. The oligodendrocyte response found in our Cx47KO cultures and tissue may be caused in part by the loss of Cx47/Cx43 gap junction communication and subsequent dysregulation of the ERK pathway signaling.

In further investigation of our hypothesis that the loss of Cx47 results in decreased oligodendrocyte viability and surrounding glial activation, we compared the DEG list of both WTPBS-Cx47KOPBS, WTPBS-WTLPS, and Cx47KOPBS-Cx47KOLPS to a single-cell RNA sequencing database (Zhang et al., 2014) to highlighting cell-type-specific involvement after the loss of Cx47. We found that similar to the loss of Cx32, DEGs were predominantly oligodendrocytic. There is, however, a large subset of transcripts associated with neurons, suggesting that neurons within the CNS are possibly more at risk due to oligodendroglial dysfunction after the loss of Cx47 (Menichella et al., 2006; Philips and Rothstein, 2017). The

comparison of the pro-inflammatory response in WT tissue (WTPBS vs, WTLPS) to the pro-inflammatory response in tissue lacking Cx47 (WTPBS-Cx47KOPBS) (Table A8), provides support that Cx47KO tissue is differentially expressing transcripts involved in the regulation of oligodendrocyte injury. Although it would be beyond the scope of this document to individually discuss all 115 DEGs revealed by this analysis, a number of these genes play a crucial role in both injury response and oligodendrocyte regulation and will be discussed below.

Notably, both the loss of Cx47 and LPS each cause differential regulation of Wnt7b and Wnt3, ligands critical in developmental and disease processes (Eubelen et al., 2018). Along with Wnt7a, Wnt7b has been implicated in OPC-endothelial regulation of angiogenesis (Yuen et al., 2014; Wang et al., 2018; Hamanaka et al., 2018). OPCs have been found to produce TGF-β and utilize the ERK pathway parallel to Wnt regulation to increase tight junction expression and bolster the blood-brain barrier (Seo et al., 2014). The downregulation of Wnt7b suggests that this pathway is compromised in both LPS treatment and after Cx47 loss. Comparatively, Wnt3, which is upregulated in both groups, is known to directly inhibit oligodendrocyte development throughout lineage (Shimizu et al., 2005). Wnt3 upregulation may support the theory that oligodendrocyte development is inhibited in both tissues. NF-κB Inhibitor Alpha (NFκBia), upregulated in our tissue after LPS and at baseline in Cx47KO, is significantly correlated with the expression of pro-inflammatory cytokines (Ping et al., 2019). Additionally, the upregulation of dual-specificity phosphatase-1 (DUSP1) is of particular interest in our pathway analysis, as each DUSP subtype shows a particular preference for a MAPK (Ham et al., 2015). The inducible nuclear phosphatase DUSP1/MAPK1 complex has been directly associated with binding and dephosphorylation of ERK, p38, and JNK during a pro-inflammatory response (Raingeaud et al., 1995; Slack et al., 2001). This association is particularly important as the ERK pathway regulates growth factor

response via Ras. At the same time, JNK activates c-Jun response to pro-inflammatory environmental cues (Raingeuad et al., 1995), and further suggests that our Cx47 tissue is in a pro-inflammatory state.

There are also a handful of genes that are inversely regulated in our Cx47KO tissue compared to WT LPS- treated tissue, suggesting that in our Cx47KO tissue, these gene pathways may be of particular mechanistic interest. Two of these genes that are downregulated in Cx47KO at baseline but upregulated in WTLPS tissue are Mmd2 (monocyte to macrophage differentiation factor 2 (Mmd2/PAQR10) and X-linked inhibitor of apoptosis-associated factor 1 (Xaf1). Mmd2 is localized in the Golgi complex and modifies Ras signaling in a dose-dependent manner. Overexpression of Mmd2 and Mmd/PAQR11 stimulates EGF-induced ERK phosphorylation and increases the expression of ERK target genes (Jin et al., 2012). XAF1 encodes a protein that binds to IAP (inhibitor of apoptosis) (Liston et al., 2001), disinhibiting caspase activity during apoptosis. Xaf1 is upregulated by c-Jun N-terminal kinase (JNK1) (Wang et al., 2009), and can be inhibited via TGF- β (Moon et al., 2019).

There are 28 genes downregulated after LPS in WT, which are upregulated in Cx47KO tissue. Genes, including Gjb1, Gjc3, and Olig2, as well as Fgfr2, Gpr37, Nrep, Smad7, and Tnfaip6, are involved in oligodendrocyte developmental and ERK1/2 pathway regulation. Oligodendrocyte connexin genes, Gjb1, and Gjc3 are both upregulated after Cx47KO, potentially supporting the theory that connexins may play a compensatory role after knockout (Li et al., 2008). Meanwhile, significant upregulation of Olig2, an early marker for oligodendrocyte differentiation, may be a compensatory response to increase the number of mature oligodendrocytes in tissue (Liu et al., 2007; Me et al., 2013; Wegner et al., 2015). Fibroblast growth factor receptor 2 (Fgfr2), is

the receptor for astrocytic expressed FGF and is known to inhibit oligodendrocyte differentiation and modify myelin sheath thickness (Wolswijk and Noble, 1992; Rashimi et al., 2003, Funisho et al., 2012). This receptor is specifically upregulated when cells enter terminal differentiation (Bansal et al., 1996) and differentially alters MAPK activation (Bansal et al., 2003). G protein-coupled receptor 37 (Gpr37), a receptor for neuroprotective factor prosaposin, induces endocytosis and ERK phosphorylation cascade linked to negative regulation of oligodendrocyte differentiation (Donohue et al., 1998; Imai et al., 2001; Meyer et al., 2013). Neuronal regeneration related protein (Nrep), promotes axonal regeneration and regulates TGF- β, a well-known inhibitor of astrocytic and macrophage pro-inflammatory cytokine production (Barnum et al., 1994; Ashcroft et al., 1999). Similarly, SMAD Family Member 7 (Smad7) is a crucial inhibitory regulator of TGF-β and has been suggested as a therapeutic target for inflammation (Yan et al., 2009). Comparatively, tumor necrosis factor-inducable gene 6 protein (Tnfaip6/TSG6) is expressed in activated microglia and suppresses immune reactions through inhibition of p38 and MEK/ERK pathways (Um et al., 2017; Zhang et al., 2017). Our RNA-seq analysis of Cx47KO tissue provides robust support that, after the knockout of Cx47, CNS tissue is in an activated pro-inflammatory state.

LITERATURE CITED

1. Aand, Geetha; Maheshwari, Nitin; Roberts, David; Padeniya, Anuruddha; Hamilton-Ayers, Michele; Van Der Knaap, Marjo; Fratter, Carl; Jayawant S. X-linked hereditary motor sensory neuropathy (type 1) presenting with a stroke-like episode. *Dev Med Child Neurol*. 2010;52(7):677-679. doi:10.1111/j.1469-8749.2010.03674.x.
2. Abrams CK. GJB1 Disorders: Charcot Marie Tooth Neuropathy (CMT1X) and Central Nervous System Phenotypes. *GeneReviews® [Internet]*. 1998; http://www.ncbi.nlm.nih.gov/books/NBK1374/
3. Abrams CK. Model Diseases of connexins expressed in myelinating glia. *Neurosci Lett*. 2017. doi:10.1016/j.neulet.2017.05.037.
4. Abrams CK, Scherer SS. Gap junctions in inherited human disorders of the central nervous system. 2011. doi:10.1016/j.bbamem.2011.08.015.
5. Abrams CK, Scherer SS, Flores-Obando R, Freidin MM, Wong S, Lamantea E, Farina L, Scaioli V, Pareyson D, and Salsano E. A new mutation in GJC2 associated with subclinical leukodystrophy. *J Neurol.* 2014; 261(10): 1929-1938.
6. Ahn M, Lee J, Gustafsson A, et al., Cx29 and Cx32, two connexins expressed by myelinating glia, do not interact and are functionally distinct. *J Neurosci Res*. 2008;86(5):992-1006. doi:10.1002/jnr.21561.
7. Alaei SR, Abrams CK, Bulinski JC, Hertzberg EL, Freidin MM. Acetylation of C-terminal lysines modulates protein turnover and stability of Connexin-32. *BMC Cell Biol*. 2018 Sep 29;19(1):22. doi: 10.1186/s12860-018-0173-0.
8. Alexander DB and Goldberg GS. Transfer of biologically important molecules between cells through gap junction channels. *Current Medicinal Chemistry.* 2003; 10 (19). DOI: 10.2174/0929867033456927
9. Alliot F, Godin I, and Pessac B. Microglia derive from progenitors, originating from the yolk sac, and which proliferate in the brain. *Brain Res/ Dev. Brain Res.* 1999; 117: 145-152.
10. Altevogt BM, Kleopa KA, Postma FR, Scherer SS, and Paul DL. Cx29 is uniquely distributed within myelinating glial cells of the central and peripheral nervous systems. *Journal of Neuroscience.* 2002; 22: 6458–6470
11. Altevogt, BM, and Paul DL. Four classes of intercellular channels between glial cells in the CNS. *Journal of Neuroscience*. 2004; 24: 4313–4323.
12. Ambrosini E, Remoli ME, Giacomini E, Rosicarelli B, Serafini B, Lande R, Aloisi F, and Coccia EM. Astrocytes Produce Dendritic Cell-Attracting Chemokines In Vitro and in Multiple Sclerosis Lesions. *J Neuropathol Exp Neurol*. 2005; 64(8): 706-715.
13. Anzalone CL, Nuhanovic S, Olund AP, Calson ML. Cochlear implantation in charcot-marie-tooth disease: Case report and review of the literature. *Case Rep. Med.* 2018; 2018, 1760978
14. Anzini P, Neuberg DKK, Schachner M, Nelles E, Willecke K, Zielasek J, Toyka K, Suter U, and Martini R. Structural abnormalities and deficient maintenance of peripheral nerve myeling in mice lacking the ap junction protein connexin 32. *J Neurosci.*1997; 17(12): 4545-4551.
15. Arnett HA, Mason , Marino M, Suzuki K, Matsushima GK, and Ting JP. TNF alpha promotes proliferation of oligodendrocyte progenitors and remeyelination. Nat Neurosci. 2001 Nov;4(11):1116-22.

16. Ashcroft GS. Bidirectional regulation of macrphage function by TGF-β. *Microbes and Infection.* 1999; 1(5): 1275-1282.
17. Bähr M, Andres F, Timmerman V, Nelis ME, Broeckhoven V, Dichgans J. Central visual, acoustic, and motor pathway involvement in a Charcot-Marie-Tooth family with an Asn205Ser mutation in the connexin 32 gene. *J Neurol Neurosurg Psychiatry*. 1999;66:202-206. https://www.ncbi.nlm.nih.gov/pmc/articles/PMC1736220/pdf/v066p00202.pdf.
18. Bamford NS, White KK, Robinett SA, Otto RK, Gospe SM. Neuromuscular hip dysplasia in charcot-marie-tooth disease type 1a. *Dev. Med. Child Neurol.* 2009; 51:408-411.
19. Bansal R, Kumar M, Murray K, Morrison RS, and Pfeiffer SE. Regulation of FGF receptors in the oligodendrocyte lineage. *Mol Cell Neurosci.* 1996;7(4):263-75.
20. Bansal R, Lakhina V, Remedios R, Tole S. Expression of FGF receptors 1, 2, 3 in the embryonic and postnatal mouse brain compared with Pdgfralpha, Olig2 and Plp/dm20: implications for oligodendrocyte development. *Dev Neurosci.* 2003;25(2-4):83-95.
21. Barnum SR, and Jones JL. Transforming growth factor-beta 1 inhibits inflammatory cytokine-induced C3 gene expression in astrocytes. *J. Immunol.* 1994; 152(2): 765-773.
22. Barres BA. The mystery and magic of glia: a perspective on their roles in health and disease. *Neuron.* 2008; 60: 430–440. doi: 10.1016/j.neuron.2008.10.013
23. Barres BA, Raff MC, Gaese F, Bartke I, Dechant G, and Barde YA. A crucial role of neurotrophin-3 in oligodendrocyte development. Letters to Nature. 1994; 367: 371-375.
24. Bartzokis G, Lu PH, Heydari P, Couvrette A, Lee GJ, Kalashyan G, Freeman F, Grinstead JW, Villablanca P, Finn JP, Mintz J, Alger JR, and Altshuler LL. Multimodal magnetic resonance imaging assessment of white matter aging trajectories over the lifespan of healthy individuals. *Biol. Psychiatry.* 2012; 72: 1026-1034.
25. Baud O, Li J, Zhang Y, Neve RL, Volpe JJ, and Rosenberg PA. Nitric oxide-induced cell death in developing oligodendrocytes is associated with mitochondrial dysfunction and apoptosis-inducing factor translocation. *European J. Neurosci.* 2004; 20(7): 1713-1726.
26. Belousov AB, Fontes JD, Freitas-Andrade M, and Naus CC. Gap junctions and hemichannels:communicating cell death in neurodevelpment. *BMC Cell Biology*.2017, 18. DOI: 10.1186/s12860-016-0120-x.
27. Bennett MV, Contreras JE, Bukauskas FF, Saez JC. New roles for astrocytes: gap junction hemichannels have something to communicate. *Trends Neurosci.* 2003;26(11):610-617.
28. Benvenist EN. Role of macrophages/microglia in multiple sclerosis and experimental allergic encephalomyelitis. *J. Mol. Med (Berl).* 1997; 75(3): 165-173.
29. Bergoffen J, Scherer SS, Wang S, et al., Connexin Mutations in X-Linked Charcot-Marie-Tooth Disease. *Science (80-).* 1993;262:2039-2042. doi:10.2307/2882981.
30. Berman JW, Guida MP, Warren J,AmatJ, and Brosnan CF. Localization of monocyte chemoattractant peptide-1 expression in the central nervous system in experimental autoimmune encephalomyelitis and trauma in the rat. *J Immunol*. 1996; 156:3017-3023.
31. Bernhardi RV, and Nicholls JG. Transformation of leech microglial cell morphology and properties following co-culture with injured central nervous system tissue. *J. Exp. Biol.* 1999; 202(6): 723-728.
32. Berry K, Wang J, and Lu QR. Epigenetic regulation of oligodendrocyte myelination in developmental disorders and neurodegenerative diseases. *F100Res.* 2020; doi: 10.12688/f1000research.20904.1.

33. Beyer EC, Berthoud VM. Connexin hemichannels in the lens. *Front Physiol*. 2014;5:20. doi:10.3389/fphys.2014.00020.
34. Beyer EC, Berthoud VM. The Family of Connexin Genes. In: *Connexins*. Totowa, NJ: Humana Press; 2009:3-26. doi:10.1007/978-1-59745-489-6_1.
35. Bhat S, and Pfeiffer SE. Stimulation of oligodendrocytes by extracts from astrocyte-enriched cultures. *J. Neurosci. Res.* 1986; 15: 19–27. doi: 10.1002/jnr.490150103
36. Biancheri R, Rosano C, Denegri L, et al., Expanded spectrum of Pelizaeus–Merzbacher-like disease: literature revision and description of a novel GJC2 mutation in an unusually severe form. *Eur J Hum Genet*. 2013;21(1):34-39. doi:10.1038/ejhg.2012.93.
37. Boche D, Perry VH, Nicoll JA Activation patterns of microglia and their identification in the human brain. *Neuropathol Appl Neurobiol*. 2013; 39:3-18.
38. Bogler O, Wren D, Barnett SC, Land H, and Noble M. Cooperation between two growth factors promotes extended self-renewal and inhibits differentiation of oligodendrocyte-type-2 astrocyte (O-2A) progenitor cells. *Proc. Natl. Acad. Sci. U.S.A.* 1990; 87: 6368–6372. doi: 10.1073/pnas.87. 16.6368
39. Bonkowsky JL, Nelson C, Kingston JL Fillouz FM, Mundorff MB, and Srivastava R. The burden of inherited leukodystrophies in children. *Neurology*. 2010; 75:718-725
40. Braathen GJ, Sand JC, Lobato A, Høyer H, Russell MB. Genetic epidemiology of Charcot-Marie-Tooth in the general population. *Eur J Neurol*. 2011;18(1):39-48. doi:10.1111/j.1468-1331.2010.03037.x.
41. Brambilla R, Morton PD Ashbaugh JJ, Karmally S, Lambertsen KL, and Bethea JR. Astrocytes play a key role in EAE pathophysiology by orchestrating in the CNS the inflammatory response of resitdent and peripheral immune cells and by supressing myelination. *Glia*. 2014; 62: 452-467. doi: 10.1002/glia.22616
42. Brinkmann BG, Agarwal A, Sereda MW, Garratt AN, Muller T, Wence H, Stassart RM, Nawaz S, Humml C, Velanac V, Radyushkin K, Goebbels S, Fischer TM, Franklin RJ, Lai C, Ehrenreich H, Birchmeier C, Schwab MH, Nave KA. Neuregulin-1/ErbB signaling serves distinct functions in myelination of the perhipheral and central nervous system. *Neuron.* 2008; 59; 581-595.
43. Brodie C, Wiezman N, Katkoff A, Lustig S, and Kobiler D. Astrocyte activation by Sinbis virus: expression of GFAP, cytokines, and adhesion molecules. *Glia.* 1997 Apr;19(4):275-85.
44. Brogden RN, Speight TM, Avery GS. Minocycline: a review of its antibacterial and pharmacokinetic properties and therapeutic use. *Drugs.* 1975;9:251–291
45. Brundula V, Rewcastle NB, Metz LM, Bernard CC, Yong VW. Targeting leukocyte MMPs and transmigration: minocycline as a potential therapy for multiple sclerosis. *Brain*. 2002;125:1297–1308.
46. Bruzzone R, White TW, Paul DL. Connextions with connexins:the molecular basis of direct intercellular signaling. *Eur J Biochem*. 1996; 238: 1-27.
47. Bugiani M, Al Shahwan S, Lamantea E, et al., GJA12 mutations in children with recessive hypomyelinating leukoencephalopathy. *Neurology*. 2006;67(2):273-279. doi:10.1212/01.wnl.0000223832.66286.e4.
48. Butovsky O, Landa G, Kunis G, Ziv Y, Avidan H, Greenberg N, Schwartz A, Smirnov I, Pollack A, Jung S, and Schwartz M. Induction and blockage of oligodendrogenesis by differently activated microglia in an animal model of multiple sclerosis. *J Clin Invest*.

2006;116(4):905-15.
49. Cai Z, Lin S, Fan LW, Pang Y, and Rhodes PG. Minocycline alleviates hypoxic-ischemic injury to developing oligodendrocytes in the neonatal rat brain. Neuroscience. 2006;137(2):425-35.
50. Caramins M, Colebatch JG, Bainbridge MN, et al., Exome sequencing identification of a GJB1 missense mutation in a kindred with X-linked spinocerebellar ataxia (SCA-X1). *Hum Mol Genet*. 2013;22(21):4329-4338. doi:10.1093/hmg/ddt282.
51. Cepeda C, Chang JW, Owens GC, Huynh MN, Chen JY, Tran C, Vinters HV, Levine MS, and Mathern GW. In Rasmussen encephalitis, hemichannels associated with microglial activation are linked to cortical pyramidal neuron coupling: a possible mechanism for cellular hyperexcitability. *CNS Neurosci Ther.* 2015;21:152-163.
52. Che X, Ye W, Panga L, Wu DC, and Yang GY. Monocyte chemoattractant protein-1 expressed in neurons and astrocytes during focal ischemia in mice. *Brain Res*. 2001;902:171-177.
53. Chen M, Ona VO, Li M, Ferrante RJ, Fink KB, Zhu S, et al. Minocycline inhibits caspase-1 and caspase-3 expression and delays mortality in a transgenic mouse model of Huntington disease. *Nat Med.* 2000;6:797–801.
54. Chew L, King W, Kenedy A, and Gallo V. Interferon-γ inhibits cell cycle exit in differentiating oligodendrocyte progenitor cells. 2005; 52(2). https://doi.org/10.1002/glia.20232
55. Chew L, Coley W, Cheng Y, and Gallo V. Mechanisms of Regulation of Oligodendrocyte Development by p38 Mitogen-Activated Protein Kinase. *J Neurosci.* 2010; 30(33): 11011–11027. doi: 10.1523/JNEUROSCI.2546-10.2010
56. Cho KO, La HO, Cho YJ, Sung KW, and Kim SY. Minocycline attenuates white matter damage in a rat model of chronic cerebral hypoperfusion. *J Neurosci Res.* 2006 Feb 1;83(2):285-91.
57. Choi Y, Kim HS, Shin KY, Kim EM, Kim M, Kim HS, Park CH, Jeong YH, Yoo J, Lee JP, Chang KA, Kim S, and Suh YH. Minocycline attenuates neuronal cell death and improves cognitive impairment in Alzheimer's disease models. *Neuropsychopharmacology*. 2007; 32(11):2393-404.
58. Combes P, Kammoun N, Monnier A, et al., Relevance of GJC2 promoter mutation in Pelizaeus-Merzbacher-like disease. *Ann Neurol*. 2012;71(1):146-148. doi:10.1002/ana.22295.
59. Conway SM, Puttick D, Russell S, Potter D, Roitman MF, and Chartoff EH. Females are less sensitive than males to the motivational- and dopamine-suppressing effects of kappa opioid receptor activation. *Neuropharmacology*. 2019; 146:231-241. doi: 10.1016/j.neuropharm.2018.12.002.
60. Corley SM, Ladiwala U, Besson A, and Young VW. Astrocytes attenuate oligodendrocyte death *in vitro* through an alpha(6) integrin-laminin-dependent mechanism. *Glia.* 36; 281-294. oi: 10.1002/g lia.1116
61. Cunningham C, Dunne A, and Lopez-Rodriguez AB. Astrocytes: heterogeneous and dynamic phenotypes in neurodegeneration and innate immunity. *Neuroscientist.* 2019; 25(5): 455–474. doi: 10.1177/1073858418809941
62. Daginakatte GC, Gadzinski A, Emnett RJ, Stark JL, Gonzales ER, Yan P, Lee JM, Cross AH, and Gutmann DH. Expression profiling identifies a molecular signature of reactive

astrocytes stimulated by cyclic AMP or proinflammatory cytokines. *Exp Neurol.* 2008;210(1):261-7.
63. Dai J, Bercury KK, Jin W, and Macklin WB. Olig1 Acetylation and Nuclear Export Mediate Oligodendrocyte Development. *J Neurosci.* 2015; 35(48): 15875–15893. doi: 10.1523/JNEUROSCI.0882-15.2015
64. Dai J, Bercury KK, and Macklin WB. Interaction of mTOR and Erk1/2 signaling to regulate oligodendrocyte differntation. *Glia.* 2014; 62(12): 2096-109. doi: 10.1002/glia.22729.
65. Darman J, Backovic S, Dike S, Maragakis NJ, Krishnan C, Rothstein JD, Irani DN, and Kerr DA. Viral-induced spinal motor neuron death is non-cell-autonomous and involves glutamate excitotoxicity. J. Neurosci. 2004; 24 (34): 7566-7575. Doi: 10.1523/JNEUROSCI.2002-04.2004
66. Dermietzel, R., Traub, O., Hwang, T. K., et al. Differential expression of three gap junction proteins in developing and mature brain tissues. *Proceedings of the National Academy of Sciences of the United States of America*; 86: 10148–10152.
67. De Simone R, Ajmone-Cat MA, Pandolfi M, Bernardo A, De Nuccio C, Minghetti L, and Visentin S. The mitochondrial uncoupling protein-2 is a master regulator of both M1 and M2 microglial responses. *J. Neurochem.* 2015; 135(1). https://doi.org/10.1111/jnc.13244.
68. Diekmann S, Henneke M, Burckhardt BC, Gärtner J. Pelizaeus–Merzbacher-like disease is caused not only by a loss of connexin47 function but also by a hemichannel dysfunction. *Eur J Hum Genet*. 2010;18(9):985-992. doi:10.1038/ejhg.2010.61.
69. Dijkhuizen RM, Knollema S, van der Worp HB, et al., Dynamics of cerebral tissue injury and perfusion after temporary hypoxia-ischemia in the rat: evidence for region-specific sensitivity and delayed damage. *Stroke*. 1998;29(3):695-704. http://www.ncbi.nlm.nih.gov/pubmed/9506615.
70. Doble DW, Dang X, Ping P, Fandrich RR, Nickel BE, Jin Y, Cattini PA, Kardami E. Phosphorylation of serine 262 in the gap junction protein connexin-43 regulates DNA synthesis in cell-cell contact forming cardiomyocytes. *Journal of cell science*. 2004; 117: 507-514.
71. Domingues HS, Portugal CC, Socodato R, and Relvas JB. Oligodendrocyte, astrocyte, and microglia crosstalk in myelin development, damage, and repair. *Front. Cell Dev.* 2016; 4 (71) 1-16.
72. Donohue PJ, Shapira H, Mantey SA, Hampton LL, Jensen RT, and Battey JF. A human gene encodes a putative G protein-coupled receptor highly expressed in the central nervous system. *Brain Res Mol Brain Res*. 1998 Feb;54(1):152-60.
73. Dubový, K, Klusáková I, Hradilová-Svíženská I, Joukal M, and Boadas-Vaello P. Activation of Astrocytes and Microglial Cells and CCL2/CCR2 Upregulation in the Dorsolateral and Ventrolateral Nuclei of Periaqueductal Gray and Rostral Ventromedial Medulla Following Different Types of Sciatic Nerve Injury. *Front Cell Neurosci.* 2018; 12: 40. doi: 10.3389/fncel.2018.00040.
74. Dugas JC, Tai YC, Speed TP, Ngai J, and Barres BA. Functional genomic analysis of oligodendrocyte differentiation. J Neurosci. 2006 Oct 25; 26(43): 10967–10983. doi: 10.1523/JNEUROSCI.2572-06.2006
75. Eggermann K, Gess B, Hausler M, Weis J, Hahn A, and Kurth I. Hereditary neuropathies. *Dtsch Arztebl Int.* 2018; 115(6): 91-97.

76. El-Sabban ME, Abi-Mosleh LF, Talhouk RS. Developmental Regulation of Gap Junctions and Their Role in Mammary Epithelial Cell Differentiation. *J Mammary Gland Biol Neoplasia*. 2003;8(4):463-473. doi:10.1023/B:JOMG.0000017432.04930.76.
77. Eubelen M, Bostaille N, Cabochette P, Gauguier A, Tebabi P, Dumitru AC, Koehler M, Gut P, Alsteens D, Staineier DYR, Garcia-Pino A, and Vanhollebeke B. *Science.* 2018; 361(6403).. doi: 10.1126/science.aat1178
78. Faheem H, Mansour A, Elkordy A, Rashad S, Shebl M, Madi M, Elwy S, Niizuma K, and Tominaga T. Neuroprotective effects of minocycline and progesterone on white matter injury after focal cerebral ischemia. *J Clin Neurosci.* 2019; 64:206-213. doi: 10.1016/j.jocn.2019.04.012.
79. Fan LW, Lin S, Pang Y, Rhodes PG, and Cai Z. Minocycline attenuates hypoxia-ischemia-induced neurological dysfunction and brain injury in the juvenile rat. *Eur J Neurosci*. 2006; 24(2):341-50
80. Fernández-Arjona M, Grondon JM, Granados-Durán P, Fernández-Llebrez P, and López-Ávalos MD. Microglia Morphological Categorization in a Rat Model of Neuroinflammation by Hierarchical Cluster and Principal Components Analysis. Front. Cell. Neurosci. 2017; 11(235). doi.org/10.3389/fncel.2017.00235
81. Ferrell RE, Baty CJ, Kimak MA, Karlsson JM, Lawrence EC, Franke-Snyder M, Meriney SD, Feingold E, and Finegold DN. *GJC2* Missense Mutations Cause Human Lymphedema. *Am J Hum Genet*. 2010;86:943-948. doi:10.1016/j.ajhg.2010.04.010.
82. Finegold DN, Baty CJ, Knickelbein KZ, Perschke A, Noon SE, Campbell D, Karlsson JM, Huang D, Kimak MA, Lawrence EC, Feingold E, Meriney SD, Brufsky AM, and Ferrel RE. Connexin 47 mutations increase risk for secondary lymphedema following breast cancer treatment. *Clin Cancer Res.* 2012;18(8):2382-90. doi: 10.1158/1078-0432.CCR-11-230
83. Finzsch M, Stolt CC, Lommes P, and Wegner M. Sox9 and Sox10 influence survival and migration of oligodendrocyte precursors in the spinal cord by regulating PDGF receptor alpha expression. *Development.* 2008; 135, 637–646.
84. Fischer S, Kleinschnitz C, Muller M, Kobsar I, Ip CW, Rollins BJ, and Martini R. Monocyte chemoattractant protein-1 is a pathogenic componenet in a model for a herediatery peripheral neuropathy. *Mol. Cell. Neurosci.* 2008; 37: 359-366.
85. Fonseca ATQSM, and Zanoteli E. Charcot-Marie-Tooth disease. *Med. Clin. Condes.* 2008; 29 (5): 521-529.
86. Freidin M, Asche-Godin S, and Abrams CK. Gene expression profiling studies in regenerating nerves in a mouse model of CMT1X: uninjured Cx32-knockout peripheral nerves display expression profile of injured wild type nerves. *Exp. Neurol.* 2015; 263: 339-349. Doi: 10.1016/j.expneurol.2014.10.014.
87. Freidin M, Asche-Godin S. Bargiello TA, Bennett MV, Abrams CK. Connexin 32 increases the proliferative response of Schwann cells to neuregulin-1 (Nrg1). *Proc Natl Acad Sci U S A.* 2009; 106: 3567-3572
88. Furusho M, Dupree JL, NaveKA, and Bansal R. Fibroblast growth factor receptor signaling in oligodendroyctes regualtes myelin sheath thickness. *J. Neurosci.* 2012; 32: 6631-6641.
89. Fusco C, Frattini D, Pisani F, Spaggiari F, Ferlini A, Della Giustina E. Coexistent Central and Peripheral Nervous System Involvement in a Charcot-Marie-Tooth Syndrome X-linked Patient. *J Child Neurol*. 2010;25(6):759-763. doi:10.1177/0883073809344119.

90. Garcia-Segura LM, and Perez-Marquez J. A new mathematical function to evaluate neuronal morphology using the Sholl analysis. *J Neurosci Methods.* 2014; 226:103-109. doi: 10.1016/j.jneumeth.2014.01.016.
91. Gard AL, Burrell MR, Pfeiffer SE, Rudge JS, and Williams WC II. Astroglial control of oligodendrocyte survival mediated by PDGF and leukemia inhibitory factor-like protein. *Development.* 1995; 121: 2187–2197
92. Garrido-Mesa N, Zarzuelo A, Galvez J. Minocycline: far beyond an antibiotic. *Br J Pharmacol*. 2013; 169: 337-352.
93. Gensel JC, Schonberg DL, Alexander JK, McTigue DM, and Popovich PG. Semi-Automated Sholl Analysis for Quantifying Changes in Growth and Differentiation of Neurons and Glia. *J Neurosci Methods*. 2010 Jun 30; 190(1): 71–79. doi: 10.1016/j.jneumeth.2010.04.026 Geraghty JR, Davis JL, and Testai FD. Neuroinflammation and Microvascular Dysfunction After Experimental Subarachnoid Hemorrhage: Emerging Components of Early Brain Injury Related to Outcome. *Neurocrit Care.* 2019;31(2):373-389. doi: 10.1007/s12028-019-00710-x. Review.
94. Glass WG. Liu MT, Kuziel WA, and Lane TE. Reduced Macrophage Infiltration and Demyelination in Mice Lacking the Chemokine ReceptorCCR5 Following Infection with a Neurotropic Coronavirus. *Virology.* 2001; 288: 8-17. doi:10.1006/viro.2001.1050.
95. Goldmann T, Wieghofer P, Müller PF, Wolf Y, Varol S, Yona S, Brendecke SM, Kierdorf K, Staszewski O, Datta M, Luedde T, Heikenwalder M, Jung S, and Prinz M. A new type of microglia gene targeting shows TAK1 to be pivotal in CNS autoimmune inflammation. *Nature Neurosci.* 2013; 16: 1618-1626.
96. Goodenough DA, Paul DL. Gap junctions. *Cold Spring Harb Perspect Biol*. 2009;1(1):a002576. doi:10.1101/cshperspect.a002576.
97. Giaume C, Koulakoff A, Roux L et al., Astroglial networks: a step further in neuroglial and gliovascular interactions. *Nat Rev Neurosci.* 2010;11(87-99).
98. Good ML, and Hussey DL. Minocycline: stain devil? *Br. J. Dermatol.* 2003; 149 (273)
99. Gow A, Lazzarini RA. A cellular mechanism governing the severity of Pelizaeus–Merzbacher disease. *Nat Genet*. 1996;13(4):422-428. doi:10.1038/ng0896-422.
100. Gough A, Chapman S, Wagstaff K, Emery P, and Elias E. Minocycline induced autoimmune hepatitis and systemic lupus erythematosus-like syndrome. *BMJ*. 1996; 312(169).
101. Gow A, Southwood CM, Lazzarini RA. Disrupted Proteolipid Protein Trafficking Results in Oligodendrocyte Apoptosis in an Animal Model of Pelizaeus-Merzbacher Disease. *J Cell Biol*. 1998;140(4). http://jcb.rupress.org/content/140/4/925. Accessed July 11, 2017.
102. Groh J, Heinl K, Kohl B, et al., Attenuation of MCP-1/CCL2 expression ameliorates neuropathy in a mouse model for Charcot-Marie-Tooth 1X. *Human Molecular Genetics.* 2010; 19:3530-3543. Doi: 10.1093/hmg/ddq269
103. Guilin D. Ameboid microglia as effectors of inflammation in the central nervous system. J. Neurosci. Research. 1987; 18: 155-171.
104. Halbrich, M, Barnes, J, Bunge, M; Joshi C. A V139M Mutation Also Causes the Reversible CNS Phenotype in CMTX. 2008;34(3). doi:10.1017/S0317167100008994.
105. Hagemeyer N, Hanft KM, Akriditou ma, Unger N, Park ES, Stanley ER, Staszewski O, Dimou L, and Prinz Marco. Microglia contribute to normal myelinogenesis

and to oligodendrocyte progenitor maintenance during adulthood. *Acta Neuropathol.* 2018; 134(3): 441-458. doi: 10.1007/s00401-017-1747-1

106. Ham JE, Oh EK, Kim DH, and Choi SH. Differential expression profiles and roles of inducible DUSPs and ERK1/2-specific constitutive DUSP6 and DUSP7 in microglia. *Biochem Biophys Res Commun.* 2015; 467(2):254-60. doi: 10.1016/j.bbrc.2015.09.180.
107. Hamada K, and Lasek AW. Receptor Tyrosine Kinases as Therapeutic Targets for Alcohol Use Disorder. *Neurotherapeutics.* 2020 ;17(1):4-16. doi: 10.1007/s13311-019-00795-4.
108. Hamanaka G, Ohtomo R, Takase H, Lok J, and Arai K. White-matter repair: Interaction between oligodendrocytes and the neurovascular unit. *Brain Circulation.* 2018; 4(3): 1180123.
109. Hammond E, Lang J, Maeda Y, Pleasure D, Angus-Hill M, Xu J, Horiuchi M, Deng W, and Guo F. The Wnt Effector Transcription Factor 7-Like 2 Positively Regulates Oligodendrocyte Differentiation in a Manner Independent of Wnt/β-Catenin Signaling. *J Neurosci.* 2015; 35(12): 5007–5022.doi: 10.1523/JNEUROSCI.4787-14.2015
110. Hammond TR, Gadea A, Dupree J, Kerninon C, Nait-Oumesmar B, Aguirre A, Gallo V. Astrocyte-Derived Endothelin-1 Inhibits Remyelination through Notch Activation. Neuron. 2014 Mar 19;81(6):1442. doi: 10.1016/j.neuron.2014.03.007
111. Hamilton SP and Rome LH. Stimulation of in vitro myelin synthesis by microglia. *Glia*. 1994; 11:326-335. doi: 10.1002/glia.440110405
112. Hanemann CO, Bergmann C, Senderek J, Zerres K, Sperfeld A-D, LJ B. Transient, Recurrent, White Matter Lesions in X-linked Charcot-Marie-Tooth Disease With Novel Connexin 32 Mutation. *Arch Neurol*. 2003;60(4):605. doi:10.1001/archneur.60.4.605.
113. Harding AE, and Thomas PK. The clinical features of hereditary motor and sensory neuropathy types i and ii. *Brain.* 1980; 103: 259-280.
114. Harris AL. Emerging issues of connexin channels: biophysics fills the gap. *Q Rev Biophys.* 2001;34(3):325-472.
115. Harry GJ,and Kraft AD. Neuroinflammation and microglia: considerations and approaches for neurotoxicity assessment. *Expert Opin Drug Metab Toxicol.* 2008; 4(1): 1265-1277. doi: 10.1517/17425255.4.10.1265
116. Henneke M, Combes P, Diekmann S, et al., GJA12 mutations are a rare cause of Pelizaeus-Merzbacher-like disease. *Neurology*. 2008;70(10):748-754. doi:10.1212/01.wnl.0000284828.84464.35
117. Henneke M, Gegner S, Hahn A, Plecko-Startinig B, Weschke B, Gärtner J, and Brockmann K. Clinical neurophysiology in GJA12-related hypomyelination vs Pelizaeus-Merzbacher disease. *Neurology*. 2010;74(22):1785-1789. doi:10.1212/WNL.0b013e3181e0f820.
118. Hermans MMP, Kortekaas P, Jongsma HJ, and Book MB. pH sensitivity of the cardiac gap junction proteins, connexin 45 and 43. *Pflügers Archiv.* 1995; 431:138–140.
119. Hershfield J, Madhavarao CN, Moffett JR, Benjamins JA, Garbern JY, and Namboodiri MA. Aspartoacylase is a regulated nuclear-cytoplasmic enzyme. *FASEB J.* 2006;20:2139–2141.
120. Hinojosa AE, Garcia-Bueno B, Leza JC, and Madrigal JLM. CCL2/MCP-1 modulation of microglial activation and proliferation. *J Neuroinflammation.* 2011; 8(77). https://doi.org/10.1186/1742-2094-8-77

121. Horacek O, Mazanec R, Morris CE, Kobesova A. Spinal deformities in hereditary motor and sensory neuropathy: A retrospective qualitative, quantitative, genotypical and familial analysis of 175 patients. *Spine*. 2007; 32: 2502-2508.
122. Horiuchi M, Itoh A, Pleasure D, and Itoh T. MEK-ERK Signaling is involved in Interferon-γ-induced Death of Oligodendroglial Progenitor Cells. J. Bio. Chem. 2006;281(29) 20095-20106. DOI 10.1074/jbc.M603179200.
123. Hoyos HC, Rinaldi M, Mendez-Huergo SP, Marder M, Rabinovich GA, Pasquini JM et al. Galectin-3 controls the response of microglial cells to limit cuprizone-induced demyelionation. *Neurobiol. Dis.* 2014; doi: 10.1016/j.nbd.2013.10.023
124. Huang J, Upadhyay UM, and Tamargo RJ. Inflammation in stroke and focal cerebral ischemia. *Surgical Neurology*. 2006; 66: 232-245.
125. Hunter AW, Gourdie RG. The PDZ domain of zonula occludens-1 is dispensable for targeting to connexin 43 gap junctions. *Cell Commun Adhes.* 2008; 15(1):55-63.
126. Iacobas S, and Iacobas DA. Astrocyte proximity modulates the myelination gene fabric of oligodendrocytes. *Neuron Glia Biol.* 2010; 6:157–169. doi: 10.1017/S1740925X10000220
127. Imai Y, Soda M, Inoue H, Hattori N, Mizuno Y, and Takahashi R. An unfolded putative transmembrane polypeptide, which can lead to endoplasmic reticulum stress, is a substrate of Parkin. *Cell.* 2001;105(7):891-902.
128. Inoue K. Pelizaeus-Merzbacher Disease: Molecular and cellular pathologies and associated phenotypes. In: Sango K.., Yamauchi J, Ogata T, Susuki K (eds) *Myelin*. Advances in Experimental Medicine and Biology. 2019; 1190: 201-216.
129. Ishibashi T, Dakin KA, Stevens B, Lee PR, Koxlov SV, Stewart, CL, and Fields RD. Astrocytes promote myelination in response to electrical impulses. *Neuron.* 2006; 49(6): 823–832. doi: 10.1016/j.neuron.2006.02.006
130. Ishii A, Furusho M, Macklin W, and Bansal R. Independent and cooperative roles of the Mek/ERK1/2-MAPK and PI3K/Akt/mTOR pathways during developmental myelination and in adulthood. *Glia.* 2019; DOI: 10.1002/glia.23602.
131. Ivakhnitskaia E, Hamada K, and Chang C. Timing mechanisms in neuronal pathfinding, synaptic reorganization, and neuronal regeneration. *Dev Growth Differ*. 2016; 58(1):88-93. doi: 10.1111/dgd.12259.
132. Jacobs-Brichford E, Manson KF, Roitman JD. Effects of chronic cannabinoid exposure during adolescence on reward preference and mPFC activation in adulthood. *Physiol Behav.* 2019; 199:395-404. doi: 10.1016/j.physbeh.2018.12.006.
133. Janowska J, Ziemka-Nalexz M, and Sypecka J. The differentiation of rat oligodendroglial cells is highly influenced by the oxygen tension: in vitro model mimicking physiologically normoxic conditions. *Int J Mol Sci.* 2018; 19(2): 331. doi: 10.3390/ijms19020331
134. Jerath NU, and Shy ME. Hereditary motor and sensory neuropathies: Understanding molecular pathogenesis could lead to future treatment strategies. *Biochim. Biophys.* 2015; 1852: 667-678.
135. Ji T, Li D, Wu Y, et al., Identification of GJC2 gene mutations in chinese patients with Pelizaeus-Merzbacher-like disease. *Minerva Pediatr*. April 2016. http://www.ncbi.nlm.nih.gov/pubmed/27057822.
136. Jin T, Ding Q, Huang H, Xu D, Jiang Y, Zhou B, Li Z, Jiang X, He J, Liu W, Zhang Y, Pan Y, Wang Z, Thomas WG, Chen Y. PAQR10 and PAQR11 mediate Ras signaling in the Golgi apparatus. *Cell Res.* 2012;22(4):661-76. doi: 10.1038/cr.2011.161.

137. Jin Z, Liang J, Wang J, Kolattukudy PE. MCP-induced protein 1 mediates the minocycline-induced neuroprotection against cerebral ischemia/reperfusion injury in vitro and in vivo. *J Neuroinflammation.* 2015; 12: 39.
138. John GR, Lee SC, and Bronsan CF. Cytokines: powerful regulators of glial cell activation. *Neuroscientist.*2003; 9(1)10-22. DOI: 10.1177/1073858402239587.
139. Kammoun Jellouli N, Hadj Salem I, Ellouz E, et al., Molecular confirmation of founder mutation c.-167A>G in Tunisian patients with PMLD disease. *Gene*. 2013;513(2):233-238. doi:10.1016/j.gene.2012.10.070.
140. Kang W, Balordi F, Su N, Chen L, Fishell G, and Hébert JM. Astrocyte activation is suppressed in both normal and injured brain by FGF Signaling. *Proc Natl Acad Sci U S A*. 2011; 111(29): 2987-95. doi: 10.1073/pnas.1320401111.
141. Karperien A, Ahammer H, and Jelinek HF. Qauntitating the subtleties of microglial morphology with fractal analysis. *Front. Cell. Neurosci.*2013;7:3. doi: 10.3389/fncel.2013.00003
142. Kassubek J, Bretschneider V, Sperfeld A-D, Zerres K, Sperfeld AD, Heuss D. Corticospinal tract MRI hyperintensity in X-linked Charcot-Marie-Tooth Disease. *J Clin Neurosci*. 2005;12(5):588-589. doi:10.1016/j.jocn.2004.07.020.
143. Kawakami H, Inoue K, Sakakihara I, Nakamura S. Novel mutation in X-linked Charcot-Marie-Tooth disease associated with CNS impairment. *Neurology*. 2002;59(6):923-926. doi:10.1212/WNL.59.6.923.
144. Kamasawa N, Sik A, Morita M, Yasumura T, Davidson KGV, Nagy JI, and Rash JE. Connexin-47 and connexin-32 in gap junctions of oligodendrocyte somata, myelin sheaths, paranodal loops and Schmidt-Lanterman incisures: implications for ionic homeostasis and potassium siphoning. *Neuroscience*. 2005;136(1):65-86. doi:10.1016/j.neuroscience.2005.08.027.
145. Kausalya PJ, Reichert M, and Hunziker W. Connexin45 directly binds to ZO-1 and localizes to the tight junction region in epithelial MDCK cells. *FEBS Lett.* 2001; 505(1):92-96.
146. Kaur C, Rathnasamy G, and Ling EA. Biology of microglia in the developing brain. *Journal of Neuropathology & Experimental Neurology*. 2017; 76(9): 736-753. https://doi.org/10.1093/jnen/nlx056.
147. Kery R, Chen APF, and Kirschen GW. Genetic targeting of astrocytes to combat neurodegenerative diseae. *Neural Regeneration Research.* 2020; 15(2): 199-211.
148. Kielian T, Esen N, Liu S, Phulwani NK, Syed MM, Phillips N, et al. Minocycline modulates neuroinflammation independently of its antimicrobial activity in Staphylococcus aureus-induced brain abscess. *Am J Pathol.* 2007;171:1199–1214.
149. Kigerl KA, Gensel JC, Ankeny DP, Alexander JK, Donnelly DJ, and Popovich PG. Identification of two distinct macrophage subsets with divergent effects causing either neurotoxicity or regeneration in the injured mouse spinal cord. J Neurosci. 2009 Oct 28;29(43):13435-44. doi: 10.1523/JNEUROSCI.3257-09.2009.
150. Kiguchi N, Kobayashi Y, Saika F, and Kishioka S. Epigenetic upregulation of CCL2 and CCL3 via histone modifications in infiltrating macrophages after peripheral nerve injury. 2013; 64(3): 666-672. https://doi.org/10.1016/j.cyto.2013.09.019.
151. Kim GH, Kim KM, Suh S, Ki C-S, Eun B-L. Charcot-Marie-Tooth Disease Masquerading as Acute Demyelinating Encephalomyelitis-Like Illness. *Pediatrics*. 2014;134(1).

http://pediatrics.aappublications.org/content/134/1/e270. Accessed July 11, 2017.
152. Kleopa KA, Orthmann JL, Enriquez A, Paul DL, Scherer SS. Unique distributions of the gap junction proteins connexin29, connexin32, and connexin47 in oligodendrocytes. *Glia*. 2004;47(4):346-357. doi:10.1002/glia.20043.
153. Kleopa KA, Zamba-Papanicolaou E, Alevra X, et al., Phenotypic and cellular expression of two novel connexin32 mutations causing CMT1X. *Neurology*. 2006;66(3):396-402. doi:10.1212/01.wnl.0000196479.93722.59.
154. Kobayashi K, Imagama S, Ohgomori T, Hirano K, Uchimura K, Sakamoto K, Hirakawa A, Takeuchi H, Suzumura A, Ishiguro N, and Kadomatsu K. Minocycline selectively inhibits M1 polarization of microglia. *Cell & Disease*. 2014; 287.
155. Kobsar I, Berghoff M, Samsam M, Wessig C, Maurer M, Toyka KV, Martini R. Preserved myelin integrity and reduced axonopathy in connexin32-deficient mice lacking the recombination activating gene. *Brain*. 2003; 126: 804-913. https://doi.org/10.1093/brain/awg072
156. Kohl B, Fischer S, Groh J, Wessig C, and Martini R. MCP-1/CCL2 modifies axon properties in a PMP22-overexpressing mous model for Charcot-Marie-Tooth 1A neuropathy. *Am. J. Pathol.* 2010; 176:1390-1399.
157. Koistinaho M, Malm TM, Kettunen MI, Goldsteins G, Starckx S, Kauppinen RA, et al. Minocycline protects against permanent cerebral ischemia in wild type but not in matrix metalloprotease-9-deficient mice. *J Cereb Blood Flow Metab.* 2005;25:460–467.
158. Kohno H, Maeda T, Perusek L, Pearlman E, and Maeda A. CCL3 Production by Microglial Cells Modulates Disease Severity in Murine Models of Retinal Degeneration. *J Immunol*. 2014; 192 (8): 3816-3827. DOI: https://doi.org/10.4049/jimmunol.1301738
159. Koval M. Pathways and control of connexin oligomerization. *Trends Cell Biol*. 2006;16(3):159-166. doi:10.1016/j.tcb.2006.01.006.
160. Kielian T, Esen N, Liu S, Phulwani NK, Syed MM, Phillips N, et al. Minocycline modulates neuroinflammation independently of its antimicrobial activity in Staphylococcus aureus-induced brain abscess. Am J Pathol. 2007;171:1199–1214.
161. Kreuzberg MM, Willecke K, and Bukauskas FF. Connexin-mediated cardiac impulse propagation: connexin 30.2 slows atrioventricular conduction in mouse heart. *Trends Cardiovasc Med.* 2006;16(8):266-272.
162. Kumar A, Alvarez-Croda DM, Stoica BA, Faden AI, and Loane DJ. Microglial/Macrophage polarization dynamics following traumatic brain injury. J. Neurotrauma. 2016; 33, 1732–1750. 10.1089/neu.2015.4268
163. Kumar A, Barrett JP, Alvarez-Croda DM, Stoica BA, Faden AI, and Loane DJ. NOX2 drives M1-like microglial/macrophage activation and neurodegeneration following experimental traumatic brain injury. *Brain Behav. Immun.* 2016; 58, 291–309. 10.1016/j.bbi.2016.07.15
164. Kumar A, Stoica BA, Sabirzhanov B, Burns MP, Faden AI, and Loane DJ. Traumatic brain injury in aged animals increases lesion size and chronically alters microglial/macrophage classical and alternative activation states. *Neurobiol. Aging*. 2013; 34, 1397–1411. 10.1016/j.neurobiolaging.2012.11.013
165. Kumar S, Biancotti JC, Yamaguchi M, and De Vellis J. Combination of growth factors enhances remyelination in a cuprizone-induced demyelination mouse model. *Neurochem. Res.* 2007; 32: 783–797. doi: 10.1007/s11064-0 06-9208-6

166. Kunzelmann P, Schroder W, Traub O, Steinhauser C, Dermietzel R, and Willecke K. Late onset and increasing expression of the gap junction protein connexin30 in adult murine brain and long-term cultured astrocytes. *Glia.* 1999; 25, 111–119.
167. Kyzar EJ, Zhang H, and Pandey SC. Adolescent Alcohol Exposure Epigenetically Suppresses Amygdala Arc Enhancer RNA Expression to Confer Adult Anxiety Susceptibility. *Biol Psychiatry.* 2019;85(11):904-914. doi: 10.1016/j.biopsych.2018.12.021.
168. Lapato AS, Tiwari-Woodruff SK. Connexins and pannexins: At the junction of neuro-glial homeostasis & disease. *J Neurosci Res*. June 2017. doi:10.1002/jnr.24088.
169. Lawrence DMP, Seth P, Durham L, Diaz F, Boursiquot R, Ransohoff RM, and Major EO. Astrocyte differentiation selectively upregulates CCL2/monocyte chemoattractant protein-1 in cultured human brain-derived progenitor cells. *Glia.* 2005; 53(1). https://doi.org/10.1002/glia.20261
170. Lebel C, Walker L, Leemans A, Phillips L, and Beaulieu C. Microstructural maturation of the human brain from childhood to adulthood. *Neuroimage*. 2008; 40: 1044-1055.
171. Lee M-J, Nelson I, Houlden H, et al., Six novel connexin32 (GJB1) mutations in X-linked Charcot-Marie-Tooth disease. *J Neurol Neurosurg Psychiatry*. 2002;73(3):304-306. http://www.ncbi.nlm.nih.gov/pubmed/12185164.
172. Lerat J, Magdelaine C, Beauvais-Dzugan H, Espil C, Ghorab K, Latour P, Derouault P, Sturtz F, Lia AS. A novel pathogenic variant of nefl responsible for deafness associated with peripheral neuropathy discovered through next-genreation sequencing and review of the literature. *J. Peripher. Nerv. Syst.*2019; 24: 139-144.
173. Lewis ND, Hill JD, Juchem KW, Stefanopoulos DE, and Modis LK. RNA sequencing of microglia and monocyte-derived macrophages from mice with experimental autoimmune encephalomyelitis illustrates a changing phenotype with disease course. *J Neuroimmuno.* 2014; 277: 26-38.
174. Li J, Hertzberg EL, and Nagy JI. Connexin32 in oligodendrocytes and association with myelinated fibers in mouse and rat brain. *Journal of Comparative Neurology*. 1997; 379: 571–591.
175. Li J, Ramenaden ER, Peng J, Koito H, Volpe JJ, and Rosenber PA. Tumor necrosis factor α mediates lipopolysaccharide-induced microglial toxicity to developing oligodendrocytes when astrocytes are present. J Neurosci. 2008;28:5321–30.
176. Li X, Penes M, Odermatt B, Willecke K, and Nagy JI. Ablation of Cx47 in transgenic mice leads to the loss of MUPP1, ZONAB and multiple connexins at oligodendrocyte-astrocyte gap junctions. *J Neurosci.* 2008; 28 (8): 1503-1517.
177. Liang D, Bhatta S, Gerzanich V, Simard JM. Cytotoxic edema: mechanisms of pathological cell swelling. *Neurosurg Focus*. 2007;22(5):E2. http://www.ncbi.nlm.nih.gov/pubmed/17613233.
178. Liang WG, Su CC, Nian JH, Chiang AS, Li SY, and Yang JJ. Human connexin30.2/31.3 (GJC3) does not form functional gap junction channels but causes enhanced ATP release in HeLa cells. *Cell Biochem Biophys.* 2011;61(1):189-97. doi: 10.1007/s12013-011-9188-2
179. Liddelow SA, and Barres BA. Reactive Astrocytes: Production, Function, and Therapeutic Potential. *Immunity.* 2017; 46: 957.
180. Lieury A, Chanal M, Androdias G, Reynolds R, Cavagna S, Giraudon P, Confavreux C,

and Nataf S. Tissue remodeling in periplaque regions of multiple sclerosis spinal cord lesions. *Glia*. 2014 ;62(10):1645-58. doi: 10.1002/glia.22705
181. Lin JH, Yang J, Liu S, Takano T, Wang X, Gao Q, Willecke K, and Nedergaard M. Connexin mediates gap junction-independent resistance to cellular injury, *J Neurosci*. 2003; 23: 430-441.
182. Liu Z, Hu X, Cai J, Liu B, Peng X, Wegner M, and Qiu M. Induction of oligodendrocyte differentiation by Olig2 and Sox10: Evidence for reciprocal interactions and dosage-dependent mechanisms.*Dev. Biol*. 2007; 302(2): 683-693. https://doi.org/10.1016/j.ydbio.2006.10.007
183. Lilly E, Sellitto C, Milstone LM, White TW. Connexin channels in congenital skin disorders. *Semin Cell Dev Biol*. 2016;50:4-12. doi:10.1016/j.semcdb.2015.11.018.
184. Ling EA, and Wong WC. The origin and nature of ramified and amoeboid microglia: A historical review and current concepts. *Glia.* 1993; 7(1). doi.org/10.1002/glia.440070105
185. Liston P, Fong WG, Kelly NL, Toji S, Miyazaki T, Conte D, Tamai K, Craig CG, McBurney MW, and Korneluk RG. Identification of XAF1 as an antagonist of XIAP anti-Caspase activity. *Nat Cell Biol.* 2001 Feb;3(2):128-33.
186. Liu Z, Xu Dan, Wang S, Chen Y, Li Z, Gao X, Jian L, Tang Y, and Peng Y. Astrocytes induce proliferation of oligodendrocyte progenitor cells via connexin 47-mediated activation of the ERK/Id4 pathway. *Cell Cycle.* 2017; 16(7):714-722.
187. Lutz SE, Zhao Y, Gulinello M, Lee SC, Raine CS, Brosnan CF. Deletion of astroycte connexins 43 and 30 leads to a dysmyelinating phenotype and hippocampal CA1 vacuolation. *J Neurosci.* 29: 7743-7752.
188. Ma J, Zhang J, Hou WW, Wu XH, Liao RJ, Chen Y, Wang Z, Zhang XN, Zhang LS, Zhou YD, Chen Z, and Hu WW. Early treatment of minocycline alleviates white matter and cognitive impairments after chronic cerebral hypoperfusion. *Scientific Reports*. 2015; 5: 12079. DOI: 10.1038/srep12079
189. Madathil SK, Carlson SW, Brelsfoard JM, Ye P, E'Ercole AJ, and Saatman KE. Astrocyte-specific overexpression of insulin-like growth factor-1 protects hippocampal neurons and reduces behavioral deficits following traumatic brain injury in mice. PLoS One. 2013; 8(6):e67204. doi: 10.1371/journal.pone.0067204
190. Madhavarao CN, Moffett JR, Moore RA, Viola RE, Namboodiri MA, and Jacobowitz DM. Immunohistochemical localization of aspartoacylase in the rat central nervous system. *J. Comp. Neurol.* 2004; 472(3): 318-329. DOI: 10.1002/cne.20080
191. Maglione M, Tress O, Haas B, Karram K, Trotter J, Willecke K, and Kettenmann H. Oligodendrocytes in mouse corpus callosum are coupled via gap junction channels formed by connexin47 and connexin32. *Glia*. 2010;58(9):1104-1117. doi:10.1002/glia.20991.
192. Magnotti LM, Goodenough DA, Paul DL. Functional Heterotypic Interactions Between Astrocyte and Oligodendrocyte Connexins. 2011. doi:10.1002/glia.21073.
193. Manso Y, Holland PR, Kitamura A, Szymkowiak S, Duncombe J, Hennessy E, Searcy JL, Marangoni M, Randall AD, Brown JT, McColl BW, and Horsburgh K. Minocycline reduces microgliosis and improves subcortical white matter function in a model of cerebral vascular disease. Glia. 2018; 66(1):34-46. doi: 10.1002/glia.23190.
194. Maki T, Liang AC, Miyamoto N, Lo EH, and Arai K. Mechanisms in oligodendrocyte regeneration from ventricular-subventricular zone-derived progenitor cells in white matter diseases. *Front Cell Neurosi.* 2013; 7:275. doi: 10.3389/fncel.2013.00275

195. Markoullis K, Sargiannidou I, Gardner C, Hadjisavvas A, Reynolds R, Kleopa KA. Disruption of oligodendrocyte gap junctions in experimental autoimmune encephalomyelitis. *Glia*. 2012; 60(7): 1053-66. Doi: 10.1002/glia.22334
196. Marques S, Zeisel A, Codeluppi S, van Bruggen D, Falcão AM, Xiao L, Li H, Häring M, Hochgerner H, Romanov R, Gylborg D, Muñoz-Manchado AB, Manno GL, Lönnerber P, Floriddia EM Rezayee F, Ernfors P, Arenas E, Hjerling-Leffler J, Harkany T, Richardson WD, Linnarsson S, and Castel-Branco G. Oligodendrocyte heterogeneity in the mouse juvenile and adult central nervous system. *Neurodevelopment.* 2016; 352 (6269): 1326-1329. Doi: 10.1126/science.aaf6463
197. Marques W, Sweeny MG, Wood N W. LETTERS TO THE EDITOR: Central nervous system involvement in a novel connexin 32 mutation affecting identical twins. 1999. http://jnnp.bmj.com/content/jnnp/66/6/803.full.pdf.
198. May D, Oliver T, Gerald S, Willecke K. Connexin47 protein phosphorylation and stability in oligodendrocytes depend on expression of connexin43 protein in astrocytes. *JNeurosci.* 2013; 33(18) 7985-7996. Doi: https://doi.org/10.1523/JNEUROSCI.5874-12.2013
199. Mayo L, Trauger SA, Blain M, Nadeau M, Patel B, Alvarez JI, Mascanfroni ID, Yeste A1, Kivisäkk P, Kallas K, Ellezam B, Bakshi R, Prat A, Antel JP, Weiner HL, and Quintana FJ. Regulation of astrocyte activation by glycolipids drives chronic CNS inflammation. *Nat Med*. 2014; 20:1147-1156.
200. McCubrey JA, Steelman LS, Chappell WH, Abrams SL, Wong EWT, Chang F, Lehmann B, Terrian DM, Milella M, Tarfuri A, Stivala F, Libra M, Basecke J, Evangelisti C Martelli AM, and Franklin RA. Roles of the RAF/MEK/ERK pathway in cell growth, malignant trasformation and drug resistance. *Biochim Biophys Acta*. 2007; 1773(8): 1263–1284. doi:10.1016/j.bbamcr.2006.10.001.
201. Mebratu Ym and Tesfaigzi Y. How ERK1/2 activation controls cell proliferation and cell death is subcellular localization the answer? *Cell Cycle.* 2009; 8 (8): 1168-1175.
202. Meeuwsen S, Persoon-Deen C, Bsibsi M, Ravid R, and van Noort JM. Cytokine, chemokine and growth factor gene profiling of cultured human astrocytes after exposure to proinflammatory stimuli. *Glia.* 2003; 43(3): 243-53.
203. Mei F, Wang H, Liu S, Niu J, Wang L, He Y, Etxeberria A, Chan J, and Xiao L. Stage-Specific Deletion of Olig2 Conveys Opposing Functions on Differentiation and Maturation of Oligodendrocytes. *J Neurosci.* 2013; 33(19): 8454–8462.doi: 10.1523/JNEUROSCI.2453-12.2013
204. Melbourne JK, Thompson KR, Peng H, and Nixon K. Its complicated: The relationship between alcohol and microglia in the search for novel pharmacotherapeutic targets for alcohol use disorders. *Prog Mol Biol Transl Sci.* 2019; 167:179-221. doi: 10.1016/bs.pmbts.2019.06.011.
205. Melton ZJ, and Motyl M. Segregation and belief polarization as boundary conditions for when fusion leads to self-sacrifice. *Behav Brain Sci.* 2018 Jan; 41: e211. doi: 10.1017/S0140525X1800170X.
206. Menichella DM, Goodenough DA, Sirkowski E, Scherer SS, Paul DL. Connexins are critical for normal myelination in the CNS. *J Neurosci*. 2003;23(13):5963-5973. doi:23/13/5963.
207. Menichella DM, Majdan M, Awatramani R, Goodenough DA, Sirkowski E, Scherer SS, Paul DL. Genetic and physiological evidence that oligodendrocyte gap junctions contribute

to spatial buffering of potassium released during neuronal activity. *J Neurosci.* 2006 Oct 25;26(43):10984-91.

208. Menn B, Garcia-Verdugo JM, Yaschine C, Gonzalez-Perez O, Rowitch D, and Alvarez-Buyilla A. Origin of oligodendrocytes in the subventricular zone of the adult brain. J Neurosci. 2006 Jul 26;26(30):7907-18.
209. Metz LM, Zhang Y, Yeung M, Pantry DG, Bell Rb, Stoian CA, Yong VW, Patten SB, Duguette P, Antel JP, and Mitchell JR. Minocycline reduces gadolinium-enhancing magnetic resonance imaging lesions in multiple sclerosis. *Ann Neurol*. 2004 May;55(5):756
210. Meyer RC, Giddens MM, Schaefer SA, and Hall RA. Meyer RC1, Giddens MM, Schaefer SA, and Hall RA. GPR37 and GPR37L1 are receptors for the neuroprotective and glioprotective factors prosaptide and prosaposin. *Proc Natl Acad Sci U S A.* 2013;110(23):9529-34. doi: 10.1073/pnas.1219004110.
211. Micevych PE, and Abelson L. Distribution of mRNAs coding for liver and heart gap junction proteins in the rat central nervous system. *Journal of Comparative Neurology.* 1991; 305: 96–118.
212. Miron VE, Boyd A, Zhao JW, Yuen TJ, Ruckh JM, Shadrach JL, van Wijngaarden P, Wagers AJ, Williams A, Franklin RJM, and ffrench-Constant C. M2 microglia/macrophages drive oligodendrocyte differentiation during CNS remyelination. *Nat Neurosci*. 2013; 16(9): 1211-1218. doi: 10.1038/nn.3469
213. Moffett JR, Arun P, Ariyannur PS, Garbern J, Jacobowitz DM, and Namboodiri AMA. Extensive aspartoacylase expression in the rat central nervous system. *Glia*. 2011; 59 (10) 1414-1434. Doi: 10.1002/glia.21186
214. Molica F, Meens MJP, Morel S, Kwak BR. Mutations in cardiovascular connexin genes. *Biol Cell*. 2014;106(9):269-293. doi:10.1111/boc.201400038.
215. Moon JR, Oh SJ, Lee CK, Chi SG, and Kim HG. TGF-β1 protects colon tumor cells from apoptosis through XAF1 suppression. *Int J Oncol.* 2019;54(6):2117-2126. doi: 10.3892/ijo.2019.4776.
216. Moorby C, and Patel M. Dual functions for connexins: Cx43 regulates growth independently of gap junction formation. *Exp Cell Res.* 2001; 271: 238-248.
217. Montgomery DL. Astrocytes: form, functions, and roles in disease. *Vet Pathol.* 1994 Mar;31(2):145-67
218. Morena J, Gupta A, and Hoyle JC. Charcot-Marie-Tooth: From molecules to therapy. *Int. J. Mol. Sci.* 2019; 20, 3419. Doi:10.3390/ijms2043419
219. Mugnaini E. Cell junctions of astrocytes, ependyma, and related cells in the mammalian central nervous system, with emphasis on the hypothesis of a generalized functional syncytium of supporting cells. *Astrocytes.* 1986; 1: 329-371.
220. Murtie JC, Macklin WB, and Corfas G. Morphometic analysis of oliogdendrocytes in the adult mouse frontal cortex. *Neurotechnique.* 2007; 85(10):2080-6.
221. Nagy JI, Li XB, Rempel J. et al. Connexin26 in adult rodent central nervous system: Demonstration at astrocytic gap junctions and colocalization with connexin30 and connexin43. *Journal of Comparative Neurology.* 2001; 441: 302–323.
222. Nagy JI, Ionescu AV, Lynn BD, and Rash JE. Connexin29 and connexin32 at oligodendrocyte and astrocyte gap junctions and in myelin of the mouse central nervous system. *J Comp Neurol.* 2003a; 464(3): 356–370.doi: 10.1002/cne.10797

223. Nagy JI, Ionescu AV, Lynn BD, and Rash JE. Coupling of astrocyte connexins Cx26, Cx30, Cx43 to oligodendrocyte Cx29, Cx32, Cx47: Implications from normal and connexin32 knockout mice. *Glia*. 2003b; 44, 205–218.
224. Nave KA, and Werner HB. Myelination of the nervous system: mechanisms and functions. *Annu. Rev. Cell Dev. Biol.* 2014; 30: 503–533. doi: 10.1146/annurev-cellbio-100913-013101
225. Nash B, Ioannidou K, and Barnett SC. Astrocyte phenotypes and their relationship to myelination. *J. Anat.* 2011; 219: 44–52. doi: 10.1111/j.1469-7580.2010.01330.
226. Nelles E, Bützler C, Jung D, Temme A, Gabriel HD, Dahl R, Traub O, Stümpel F, Jungermann K, Zielasek J, Toyka K, Dermietzel R, and Willecke K. Defective propagation of singals generated by sympathetic nerve stimulation in the liver of the connexin32-deficient mice. *Cell Bio.* 199; 93: 9565-9570.
227. Nessler S, Dodel R, Bittner A, Reuss S, Du Y, Hemmer B, et al. Effect of minocycline in experimental autoimmune encephalomyelitis. *Ann Neurol.* 2002;52:689–690. author reply 690.
228. Nicholson G, Corbett A, Nicholson G, Corbett A. Slowing of central conduction in X-linked Charcot-Marie-Tooth neuropathy shown by brain stem auditory evoked responses. *Neurol Neurosurg Psychiatry*. 1996;6161(7):43-4643. https://www.ncbi.nlm.nih.gov/pmc/articles/PMC486455/pdf/jnnpsyc00007-0050.pdf.
229. Nicolaou P, Zamba-Papanicolaou E, Koutsou P, et al., Charcot-Marie-Tooth Disease in Cyprus: Epidemiological, Clinical and Genetic Characteristics. *Neuroepidemiology*. 2010;35:171-177. doi:10.1159/000314351.
230. Nicholas RS, Wing MG, and Compston A. Nonactivated microglia promote oligodendrocyte precursor survival and maturation through the transcriptoin factor NF-kappa B. *Eur. J. Neurosci.* 2001; 13: 959-967. doi: 10.1046/j.0953-816x.2001.01470.x.
231. Nicholas RS, Stevens S, Wing MG, and Compston DA. Microglia-derived IGF-2 prevents TNFalpha induced death of mature oligodendrocytes in vitro. *J. Neuroimmunol*. 2002; 124, 36–44. doi: 10.1016/S0165-5728(02)0 0011-5
232. Nicholson G, Nash J. Intermediate nerve conduction velocities define X-linked Charcot-Marie-Tooth neuropathy families. *Neurology*. 1993;43(12):2558-2564. http://www.ncbi.nlm.nih.gov/pubmed/8255457.
233. Noble M, Murray K, Stoobant P, Waterfield MD, and Riddle P. Platelet-derived growth factor promotes division and motility and inhibits premature differentiation of the oligodendrocyte/type-2 astrocyte pro genitor cell. *Nature*. 1988; 333, 560–562. doi: 10.1038/333560a0
234. Noble W, Garwood C, Stephenson J, Kinsey AM, Hanger DP, Anderton BH. Minocycline reduces the development of abnormal tau species in models of Alzheimer's disease. *FASEB J*. 2009;23(3):739-50. doi: 10.1096/fj.08-113795.
235. Nobuta H, Ghiani CA, Paez PM, Spreuer V, Dong H, Korsak RA, Manukyan A, Li J, Vinters HV, Huang EJ, Rowitch DH, Sofroniew MV Campagnoni AT, de Vellis J, and Wascheck JA. STAT3-mediated astrogliosis protects myelin development in neonatal brain injury. *Ann. Neurol.* 2012; 72: 750–765. doi: 10.1002/ana. 23670
236. Nualart-Marti A, Solsona C, Fields RD. Gap junction communication in myelinating glia. *BiochimBiophysActa-Biomembr*.2013;1828(1):69-78. doi:10.1016/j.bbamem.2012.01.024
237. Numata Y, Gotoh L, Iwaki A, Kurosawa K, Takanashi J, Deguchi K, Yamamoto T, Osaka

H, Inoue K. Epidemiological, clinical and genetic landscapes of hypomyelinating leukodystrophies. *J Neurol*. 2014; 261:752-758.
238. Odermatt B, Wellershaus K, Wallraff A, Seifert G, Degen J, Euwens C, Fuss B, Büssow H, Schilling K, Steinhäuser C, Willeke K. Connexin 47 (Cx47)-Deficient Mice with Enhanced Green Fluorescent Protein Reporter Gene Reveal Predominant Oligodendrocytic Expression of Cx47 and Display Vacuolized Myelin in the CNS. *J Neurosci*. 2003; 23(11):4549-4559.
239. Oh S, Ri Y, Bennett M V, Trexler EB, Verselis VK, Bargiello TA. Changes in permeability caused by connexin 32 mutations underlie X-linked Charcot-Marie-Tooth disease. *Neuron*. 1997;19(4):927-938. http://www.ncbi.nlm.nih.gov/pubmed/9354338.
240. Olah M, Amor S, Brouwer N, Vinet J, Eggen B, Biber K, Boddeke HWGM. Identification of a microglia phenotype supportive of remyelination. *Glia*. 2011; 60(2). https://doi-org.proxy.cc.uic.edu/10.1002/glia.21266
241. Olympiou M, Sargiannidou I, Markoullis K, Karaiskos C, Kagiava A, Kyriakoudi S, Abrams C, Kleopa K. Systemic inflammation disrupts oligodendrocyte gap junctions and induces ER stress in a model of CNS manifestations of X-linked Charcot-Marie-Tooth disease. *Acta Neuropathologica Communications.* 2016; 4 (1): 95. Doi: 10.1186/s40478-016-0369-5
242. Omari KM, John GR, Sealfon SC, and Raine CS. CXC cehmokine receptors on hman oligodendrocytes: implications for multiple sclerosis. *Brain*. 2005; 128: 1003-1015. doi: 10.1093/brain/awh479.
243. Omori Y, and Yamasaki H. Mutated connexin43 proteins inhibit rat glioma cell growth suppression mediated by wild-type connexin43 in a dominant-negative manner. *Int J Cancer*. 1998; 78: 446-453.
244. Orthmann-Murphy JL, Abrams CK, Scherer SS. Gap junctions couple astrocytes and oligodendrocytes. *J Mol Neurosci*. 2008;35(1):101-116. doi:10.1007/s12031-007-9027-5.
245. Orthmann-Murphy JL, Fischer, Freidin M, Scherer SS, and Abrams CK. Two distinct heterotypic channels mediate gap junction coupling between astrocyte and oligodendrocyte connexins. Journal of Neuroscience. 2007a; 27, 13949–13957
246. Orthmann-Murphy JL, Enriquez AD, Abrams CK, Scherer SS. Loss-of-function GJA12/Connexin47 mutations cause Pelizaeus–Merzbacher-like disease. *Mol Cell Neurosci*. 2007;34(4):629-641. doi:10.1016/j.mcn.2007.01.010.
247. Orthmann-Murphy JL, Salsano E, Abrams CK, et al. Hereditary spastic paraplegia is a novel phenotype for GJA12/GJC2 mutations. *Brain*. 2009;132:426-438. doi:10.1093/brain/awn328.
248. Osaka H, Hamanoue H, Yamamoto R, et al., Disrupted *SOX10* regulation of *GJC2* transcription causes Pelizaeus-Merzbacher-Like Disease. *Ann Neurol*. 2010;68(2):NA-NA. doi:10.1002/ana.22022.
249. Panas M, Charalambos K, Dimitris A, Vassilopoulos D. LETTERS TO THE EDITOR A novel de novo point mutation in the GTP cyclohydrolase I gene in a Japanese patient with hereditary progressive and dopa responsive dystonia. 1998. https://www.ncbi.nlm.nih.gov/pmc/articles/PMC2170411/pdf/v065p00947a.pdf.
250. Panas M, Kalfakis N, Karadimas C, Vassilopoulos D. Episodes of generalized weakness in two sibs with the C164T mutation of the connexin 32 gene. *Neurology*. 2001;57(10):1906-1908. doi:10.1212/WNL.57.10.1906.

251. Pang Y, Campbell L, Zheng B, Fan L, Cai Z, and Rhodes P. Lipopolysaccaride-activated microglia induce death of oligodendrocyte progenitor cells and impede their development. *Neuroscience.* 2009; 166(2) 464-475.
252. Pang Y, Fan LW, Tien LT, Dai X, Zheng B, Cai Z et al. Differential roles of astrocyte and microglia in supporting oligodendrocyte development and myelination in vitro. *Brain* Behav. 2013; 3 : 503-514. doi: 10.1002/ brb3.152
253. Papadakis CE, Hajiioannou JK, Kyrmizakis DE, Bizakis JG. Bilateral sudden sensorineural hearing loss caused by charcot-marie-tooth disease. *J. Laryngol. Otol.* 2003; 117: 399-401.
254. Papaneophytou CP, Georgiou E, Karaiskos C, Sargiannidou I, Markoullis K, Freidin MM, Abrams CK, and Kleopa KA. Regulatory role of oligodendrocyte gap junctions in inflammatory demyelintation. *Glia.* 2018. https://doi.org/10.1002/glia.23513.
255. Parenti R, Cicirata F, Zappalà A, Catania A, Delia FL, Cicirata V, Tress O and Willecke K. Dynamic expression of Cx47 in mouse brain development and in the cuprizone model of myelin plasticity. *Glia*. 2010;58(13):n/a-n/a. doi:10.1002/glia.21032.
256. Pareyson D, Saveri P, and Pisciotta C. New developments in Charcot-Marie-Tooth neuropathy and related diseases. *Curr Opin Neurol.* 2017; 30(5): 471-80.
257. Pasquini LA, Millet V, Hoyos HC, Giannoni JP, Croci DO, Marder M, et al. Galectin-3 drives oligodendrocyte diffe rentiation to control myelin integrity and function.*Cell Death Differ.* 2011; 18: 1746–1756. doi: 10.1038/cdd.2011.40
258. Paul BAD. Four Classes of Intercellular Channels between Glial Cells in the CNS. *J Neurosci*. 2004;24(18):4313-4323. doi:10.1523/JNEUROSCI.3303-03.2004.
259. Paulson HL, Garbern JY, Hoban TF, et al., Transient central nervous system white matter abnormality in X-linked Charcot-Marie-Tooth disease. *Ann Neurol*. 2002;52(4):429-434. doi:10.1002/ana.10305.
260. Paznekas WA, Boyadjiev SA, Shapiro RE, et al., Connexin 43 (GJA1) mutations cause the pleiotropic phenotype of oculodentodigital dysplasia. *Am J Hum Genet*. 2003;72(2):408-418. doi:10.1086/346090.
261. Pearson G, Robinson F, Beers Gibson T, Xu BE, Karandikar M, Berman K, et al. Mitogen-activated protein (MAP) kinase pathways: regulation and physiological functions. Endocr *Rev* 2001; 22:153-83.
262. Pedre X, Mastronardi F, Bruck W, López-Rodas G, KuhlmannT, and Casaccia P. Changed Histone Acetylation Patterns in Normal-Appearing White Matter and Early Multiple Sclerosis *Journal of Neuroscience*. 2011; 31(9): 3435-3445. https://doi.org/10.1523/JNEUROSCI.4507-10.2011
263. Peferoen L, Kipp M, Valk P, Noort JM, and Amor S. Oligodendrocytes-microglia cross-talk in the central nervous system. I*mmunology*. 2014 Mar; 141(3): 302–313. doi: 10.1111/imm.12163
264. Philips T, and Rothstein JD. Oligodendroglia: metabolic supporters of neurons. *J Clin Invest.* 2017; 127(9): 3271-3280. https://doi.org/10.1172/JCI90610.
265. Ping Z, Chen S, Hermans SJF, Kenswil KJG, Feyen J, van Dijk C, Bindels EMJ, Mylona AM, Adisty NM, Hoogenboezem RM, Sanders MA, Cremers EMP, Lindenbergh-Kortleve DJ, Samsom JN, van de Loosdrecht AA, Raaijmakers MHGP. Activation of NF-κB driven inflammatory programs in mesenchymal elements attenuates hematopoiesis in low-risk myelodysplastic syndromes. *Leukemia.* 2019;33(2):536-541. doi: 10.1038/s41375-018-0267-x.

266. Piotrowska A, Kwiatkoski K, Rojewska E, Slusarczyk, Makuch W, Basta-Kaim A, Przewlocka B, and Mika J. Direct and indirect pharmacological modulation of CCL2/CCR2 pathway results in attenuation of neuropathic pain—*In vivo and in vitro* evidence. *Journal of Neuroimmunology*. 2016; 297: 9-19. https://doi.org/10.1016/j.jneuroim.2016.04.017
267. Pogoda K, Kameritsch P, Retamal MA, Vega JL. Regulation of gap junction channels and hemichannels by phosphorylation and redox changes: a revision. *BMC Cell Biol*. 2016;17 Suppl 1(Suppl 1):11. doi:10.1186/s12860-016-0099-3.
268. Popovich PG, Jakeman LB, and McTigue DM. Glial responses to injury. *Encyclopedia of Neuroscience.* 2009; 853-859.
269. Qin H, Shao Q, Curtis H, Galipeau J, Belliveau DJ, Wang T, Alaoui-Jamali MA, Laird DW. Retroviral delivery of connexin genes to human breast tumor cells inhibits in vivo tumor growth by a mechanism that is independent of significant gap junctional intercellular communication. *J Biol Chem.* 2002; 277: 29132-29138.
270. Raingeaud J, Gupta S, Rogers JS, Dickens M, Han J, Ulevitch RJ, and Davis RJ. Pro-inflammatory cytokines and environmental stress cause p38 mitogen-activated protein kinase activation by dual phosphorylation on tyrosine and threonine. *J Biol Chem*. 1995;270(13):7420-6.
271. Rash JE, Duffy HSm Dudek FE, Bilhartz B, Whalen LR, Yasumura T. Grid mapped freeze-fracture electron microscophy of preselected neurons in spinal cord slices. *Techniques in modern biomedical microscopy.* 1997; 2: 127-150.
272. Rash JE, Yasumura T, Dudek Fem Nagy JI. Cell-specific expression of connexins, and evidence for restricted gap junctional coupling between glial cells and beween neurons. *J Neurosci*. 2001; 21:1983-2001.
273. Rashad S, Fujimura M Niizuma K, Endo H, and Tominaga T. Long-term follow-up of pediatric moyamoya disease treated by combined direct-indirect revascularization surgery: single institute experience with surgical and perioperative management. *Neurosurg Rev*. 2016; 39: 615-623.
274. Reiter CR, and Bongarzone ER. The Role of Vesicle Trafficking and Release in Oligodendrocyte Biology. *Neurochem Res*. 2019. doi: 10.1007/s11064-019-02913-2.
275. Remington LT, Babcock AB, Zehntner SP, and Owens T. Microglial recruitment, activation, and proliferation in response to primary demyelination. *American Journal of Pathology*. 2007; 170(5) 1713-1724. https://doi.org/10.2353/ajpath.2007.060783
276. Richardson WD, Pringle N, Mosley MJ, Westermark B, and Du bois-Dalcq M. A role for platelet-derived growth factor in normal gliogenesis in the central nervous system. *Cell.* 1988; 53:309–319. doi: 10.1016/0092-8674(88)90392-3
277. Rossor AM, Polke JM, Houlden H, and Reilly MM. Clinical implications of genetic advances in Charcot-Marie-Tooth disease. *Nat. Rev. Neurol.* 2013; 9, 562-571.
278. Rubinfeld H, and Seger R. The ERK cascade: a prototype of MAPK signaling. *Mol. Biotechnol.* 2005; 31:151-174.
279. Sabuughin N, deBantel A, McWilliams S, Sivakumar K. Deafness and cmt disease associated with a novel four amino acid deletion in the pmp22 gene. *Neurology*. 2003; 60:506-508.
280. Saidi Brikci-Nigassa A, Clement MJ, Ha-Duong T, Adjadj E, Ziani L, Pastre D, Curmi PA, and Savarin P. Phosphorylation controls the interaction of the connexin43 C-terminal

domain with tubulin and microtubules. *Biochemistry*. 2012; 51(21): 4331-42.
281. Saifee TA, Pareés I, Kassavetis P, Kaski D, Bronstein AM, Rothwell JC, Sadnicka A, Lunn MP, Manji H, Teo JT, et al., Tremor in charcot-marie-tooth disease: No evidence of cerbellar dysfunciton. *Clin. Nerophysiol.* 2015; 126: 1817-1824.
282. Salviati L, Trevisson E, Baldoin MC, et al., A novel deletion in the GJA12 gene causes Pelizaeus–Merzbacher-like disease. *Neurogenetics*. 2007;8(1):57-60. doi:10.1007/s10048-006-0065-x.
283. Sakaguchi H, Yamashita Sm Miura A, Hirahara T, Kimura E, Maeda Y, Terasaki T, Hirano T, and Uchino M. A novel GJB1 frameshift mutation produces a transient CNS symptom of X-linked Charcot–Marie–Tooth disease. *Journal of Neurology*. 2011; 258: 284–290.
284. Sakurai Y, Nishimura D, Yoshimura K, Tsuruo Y, Seiwa C, and Asou H. Differentation of oligodendrocyte occurs in contact with astrocyte. *J. Neurosci. Res.* 1998; 52: 17-26.
285. Sanchez Mejia RO, Ona VO, Li M, Friedlander RM. Minocycline reduces traumatic brain injury-mediated caspase-1 activation, tissue damage, and neurological dysfunction. Neurosurgery. 2001;48:1393–1399. discussion 1399–1401.
286. Saporta AS, Sottile SL, Miller LJ, Feely SM, Siskind CE, and Shy ME. Charcot-marie-tooth disease subtypes and genetic testing strategies. *Ann Neurol.* 2011; 69: 22-33.
287. Sargiannidou I, Kim G-H, Kyriakoudi S, Eun B-L, Kleopa KA. A start codon CMT1X mutation associated with transient encephalomyelitis causes complete loss of Cx32. *Neurogenetics*. 2015;16(3):193-200. doi:10.1007/s10048-015-0442-4.
288. Sargiannidou I, Ahn M, Enriguez AD, Peinado A, Reynolds R, Abrams C, Scherer SS, and Kleopa KA. Human oligodendrocytes express Cx31.3: function and interactions with Cx32 mutants. *Neurobiol Dis.* 2008; 30(2): 221–233. Doi: 10.1016/j.nbd.2008.01.009.
289. Sargiannidou I, Vavlitou N, Aristodemou S, Hadjisavvas A, Kyriacou K, Scherer SS, and Kleopa KA. Connexin32 Mutations Cause Loss of Function in Schwann Cells and Oligodendrocytes Leading to PNS and CNS Myelination Defects. *J Neurosci*. 2009;29(15). http://www.jneurosci.org.proxy.cc.uic.edu/content/29/15/4736.
290. Savarese A, and Lasek AW. Regulation of anxiety-like behavior and Crhr1 expression in the basolateral amygdala by LMO3. *Psychoneuroendocrinology.* 2018; 92:13-20. doi: 10.1016/j.psyneuen.2018.03.016.
291. Savarin C, Hinton DR, Valentin-Torres A, Chen Z, Trapp BD, Bergmann CC, and Stohlman SA. Astrocyte response to IFN-gamma limits IL-6-mediated microglia activation and progressive autoimmune encephalomyelitis. *J Neuroinflammation.* 2015; 12:79
292. Scemes E, and Giaume C. Astrocyte calcium waves: what they are and what they do. *Glia*. 2006; 54: 716-725.
293. Scherer SS, Deschênes SM, Xu YT, Grinspan JB, Fischbeck KH, Paul DL. Connexin32 is a myelin-related protein in the PNS and CNS. *J Neurosci*. 1995;15(12):8281-8294. http://www.ncbi.nlm.nih.gov/pubmed/8613761.
294. Scherer SS, Kleopa KA. X-linked Charcot-Marie-Tooth disease. *J Peripher Nerv Syst*. 2012;17 Suppl 3(0 3):9-13. doi:10.1111/j.1529-8027.2012.00424.x.
295. Scherer SS, Xu Y-T, Nelles E, Fischbeck K, Willecke K, Bone LJ. Connexin32-null mice develop demyelinating peripheral neuropathy. *Glia*. 1998;24(1):8-20. doi:10.1002/(SICI)1098-1136(199809)24:1<8::AID-GLIA2>3.0.CO;2-3.
296. Schoenen J. The dendritic organization of the human spinal cord: the dorsal horn. Neuroscience. 1982; 7: 2057-2087.

297. Scholz R, Sobotka M, Caramoy A, Stempfl T,Moehle C, and Langmann T. Minocycline counter-regualtes pro-inflammatory microglial responses in the retina and protecs from degeneration. *Journal of Neuroinflammation.* 2015; 12(209). https://doi.org/10.1186/s12974-015-0431-4
298. Schram S, Chuang D, Schmidt G, Piponov H, Helder C, Kerns J, Gonzalez M, Song F, and Loeb JA. Mutant SOD1 prevents normal functional recovery through enhanced glial activation and loss of motor neuron innervation after peripheral nerve injury. *Neurobiol Dis.* 2019; 124:469-478. doi: 10.1016/j.nbd.2018.12.020.
299. Sherwin C, and Fern R. Acute lipopolysaccharide-mediated injury in neonatal white matter glia: role of TNF-alpha, IL-1beta, and calcium. *J Immunol.* 2005 Jul 1;175(1):155-61.
300. Shigemot-Mogami Y, Hoshikawa K, Goldman JE, Sekino Y, and Sato K. Microglia enhance neurogenesis and oligodendrogenesis in the early postnatal subventricular zone. *J Neurosci.* 2014; 3(6): 2231-43. doi: 10.1523/JNEUROSCI.1619-13.2014.
301. Shimizu T, Keagawa T, Wada T, Muroyama Y, Takada S, and Ikenaka K. Wnt signaling controls the timing of oligodendrocyte development in the spinal cord. *Dev. Biol.* 2005; 282(2): 397-410. https://doi.org/10.1016/j.ydbio.2005.03.020.
302. Shinomiya H. Plastin family of actin-binding proteins: Its functions in leukocytes, neurons, intestines, and cancer. Int J Cell Biol. 2012; 2012: 213492. doi: 10.1155/2012/213492
303. Shy ME, Siskind C, Swan ER, et al., CMT1X phenotypes represent loss of GJB1 gene function. *Neurology*. 2007;68(11):849-855. doi:10.1212/01.wnl.0000256709.08271.4d.
304. Semple BD, Bye N, Rancan M, Ziebell JM, and Morganti-Kossman MC. Role of CCL2 (MCP-1) in Traumatic Brain Injury (TBI); evidence from severe TBI patients and CCL2 -/- mice. *Journal of Cerbral Blood Flow & Metabolism.* 2009. https://doi.org/10.1038/jcbfm.2009.262
305. Seo JH, Maki T, Maeda M Miyamoto N, Liang AC, Hayakawa K, Pham LD, Suwa F, Taguchi A, Matsuyama T, Ihara M, Kim K, L EH, and Arai K. Oligodendrocyte Precursor Cells Support Blood-Brain Barrier Integrity via TGF-β Signaling. *PLOS*. 2014; https://doi.org/10.1371/journal.pone.0103174.
306. Siegelbaum SA, Kandel ER. Overview of synaptic transmission. In: *Principles of Neural Science*. 5th edition, 2013.
307. Simpson JE, Newcombe J, Cuzner ML, and Woodroofe MN. Expression of monocyte chemoattractant protein-1 and other beta-chemokines by resident glia and inflammatory cells in multiple sclerosis lesions. *J Neuroimmunol.* 1998, 84: 238-249. 10.1016/S0165-5728(97)00208-7.
308. Siskind C, Feely SME, Bernes S, et al., Persistent CNS dysfunction in a boy with CMT1X. *J Neurol Sci*. 2009;279(1-2):109-113. doi:10.1016/j.jns.2008.12.031.
309. Skre H. Genetic and clinical aspects of Charcot-Marie-Tooth's disease. *Clin Genet*. 2008;6(2):98-118. doi:10.1111/j.1399-0004.1974.tb00638.x.
310. Slack DN, Seternes OM Gabrielsen M, and Keyse SM. Distinct binding determinants for ERK2/p38alpha and JNK map kinases mediate catalytic activation and substrate selctivty of map kinase phosphatase-1. *J Biol. Chem.* 2001; 276: 16491-16500.
311. Sloane JA, Batt C, Ma Y, Harris ZM, Trapp B, and Vartanian T. Hyuluronan blocks oligodendrocyte progenitor maturation and remyelination through TLR2. *Proc. Natl. Acad. Sci. USA.* 2010; 107: 11555-11560. doi: 10.1073/pnas.1006496107.
312. Sofroniew MV. Reactive astrocytes in neuronal repair and protection. *Neuroscientist.*2005;

11(5): 400-407. DOI: 10.1177/1073858405278321
313. Sofroniew MV, and Vinters HV. Astrocytes: biology and pathology. Acta Neuropathol. 2010; 119(1): 7–35. doi: 10.1007/s00401-009-0619-8
314. Söhl G, Odermatt B, Maxeiner S, Degen J, Willecke K. New insights into the expression and function of neural connexins with transgenic mouse mutants. 2004. doi:10.1016/j.brainresrev.2004.05.006.
315. Sonmez E, Kabatas S, Ozen O, Karabay G, Turkoglu S, Ogus E, Yilmaz C, Caner H, and Altinors N. Minocycline Treatment Inhibits Lipid Peroxidation, Preserves Spinal Cord Ultrastructure, and Improves Functional Outcome After Traumatic Spinal Cord Injury in the Rat. *Spine.* 2013; 38: 1253-1259.
316. Sosinsky G, Nicholson B. Structural organization of gap junction channels. *Biochim Biophys Acta.* 2005;1711:99-125.
317. Southwood CM, Garbern J, Jiang W, Gow A. The Unfolded Protein Response Modulates Disease Severity in Pelizaeus-Merzbacher Disease an X-linked recessive pediatric disorder characterized by three common genetic forms of disease: coding re- gion or splice site mutations, duplications of the wild. *Neuron.* 2002;36:585-596. http://www.cell.com/neuron/pdf/S0896-6273(02)01045-0.pdf.
318. Stankoff B, Aigrot MS, Noël F, Wattilliaux A, Zalc B, and Lubetzki C. Ciliary neurotrophic factor (CNTF) enhances myelin formation: a novel role for CNTF and CNTF-related molecules. *J. Neurosci.* 2002; 22: 9221–9227
319. Steit WJ, Walter SA, and Pennell NA. Reactive microgliosis. *Prog. Neurobiol.* 1999; 57: 563-581.
320. Stout CE, Costantin JL, Naus CC, and Charles AC. Intercellular calcium signaling in astrocytes via ATP release through connexin hemichannels. *J Biol Chem.* 2002; 277: 10482-10488.
321. Sutor B, Schmolke C, Teubner B, Schirmer C, Willecke K. Myelination defects and neuronal hyperexcitability in the neocortex of connexin 32-deficient mice. *Cereb Cortex.* 2000;10(7):684-697. http://www.ncbi.nlm.nih.gov/pubmed/10906315.
322. Takashima H, Nakagawa M, Umehara F, et al., Gap junction protein beta 1 (GJB1) mutations and central nervous system symptoms in X-linked Charcot-Marie-Tooth disease. *Acta Neurol Scand*. 2003;107(1):31-37. doi:10.1034/j.1600-0404.2003.01317.x.
323. Talbott JF1, Loy DN, Liu Y, Qiu MS, Bunge MB, Rao MS, and Whittemore SR. Endogenous Nkx2.2+/Olig2+ oligodendrocyte precursor cells fail to remyelinate the demyelinated adult rat spinal cord in the absence of astrocytes. *Exp Neurol.* 2005 Mar;192(1):11-24.
324. Tang Y, and Le W. Differential roles of M1 and M2 Microglia in Neurodegenerative Diseases. *Molecular Neurobiology.* 2016; 53: 1181-1194.
325. Taveggia C, Thaker P, Petrylak A, Caporaso GL, Toews A, Falls DL, Einheber S, Salzer JL. Type III neuregulin-1 promotes oligodendrocyte myelination. *Glia*. 2008; 56(3): 284–293. doi: 10.1002/glia.20612
326. Taylor RA, Chang C, Goods BA, Hammond MD, Grory BM, Ai Y, Steinschneider AF, Renfroe SC, Askenase MH, McCullough LD, Kasner SE, Mullen MT, Hafler DA, Love JC, and Sansing LH. TGF-β1 modulates microglial phenotype and promotes recovery after intracerebral hemorrhage. *J. Clin. Invest.* 2017; 127 (1): 280-292
327. Taylor RA, Simon EM, Marks HG, Scherer SS. The CNS phenotype of X-linked Charcot-

Marie-Tooth disease: More than a peripheral problem. *Neurology*. 2003;61(11):1475-1478. doi:10.1212/01.WNL.0000095960.48964.25.
328. Theis M, Söhl G, Eiberger J, Willecke K. Emerging complexities in identity and function of glial connexins. *Trends Neurosci*. 2005;28(4):188-195. doi:10.1016/j.tins.2005.02.006.
329. Thévenin AF, Kowal TJ, Fong JT, Kells RM, Fisher CG, Falk MM. Proteins and Mechanisms Regulating Gap-Junction Assembly, Internalization, and Degradation. *Physiology*. 2013;28(2). http://physiologyonline.physiology.org/content/28/2/93.
330. Thomas M, Ashizawa T, Jankovic J. Minocycline in Huntington's disease: a pilot study. *Mov Disord*. 2004;19:692–695
331. Tobin MK, Musaraca K, Disouky A, Shetti A, Bheri A, Honer WG, Kim N, Dawe RJ, Bennett DA, Arfanakis K, Lazarov O. Human Hippocampal Neurogenesis Persists in Aged Adults and Alzheimer's Disease Patients. *Cell Stem Cell.* 2019; 24(6):974-982.e3. doi: 10.1016/j.stem.2019.05.003.
332. Toyofuku T, Yabuki M, Otsu K, Kuzuya T, Hori M, and Tada M. Direct association of the gap junction protein Cx-43 with ZO-1 cardiac myocytes. *J Biol Chem.* 1998; 273(2): 12725-31.
333. Trapp BD, Nishiyama A, Cheng D, and Macklin W. Differentiation and death of premyelinating oligodendrocytes in developing rodent brain. *J Cell Biol.* 1997; 137(2): 459–468.doi: 10.1083/jcb.137.2.459
334. Tress O, Maglione M, May D, Pivneva T, Richter N, Seyfarth J, Binder S, Zlomuzica A, Seifert G, Theis M, Dere E, Kettenmann H, and Willecke K. Panglial gap junctional communication is essential for maintenance of myelin in the CNS. *J. Neurosci.* 2012; 32(22): 7499-7518.
335. Tress O, Maglione M, Zlomuzica A, May D, Dicke N, Degen J, Dere E, Kettenmann H, Hartmann D, and Willecke K. Pathologic and Phenotypic Alterations in a Mouse Expressing a Connexin47 Missense Mutation That Causes Pelizaeus-Merzbacher–Like Disease in Humans. *PLOS Genetics.* 2011; https://doi.org/10.1371/journal.pgen.1002146.
336. Uhlenberg B, Schuelke M, Rüschendorf F, Ruf N, Kaindl AM, Henneke M, Theile H, Stoltenburg-Didinger S, Aksu F, Topaloglu H, Nürnberg P, Hüber C, Weschke B, and Gärtner J. Mutations in the Gene Encoding Gap Junction Protein a12 (Connexin 46.6) Cause Pelizaeus-Merzbacher–Like Disease. *Am J Hum Genet*. 2004;75:251-260. https://www.ncbi.nlm.nih.gov/pmc/articles/PMC1216059/pdf/AJHGv75p251.pdf.
337. Um S, Kim HY, Lee J, Song I, and Seo BM. TSG-6 secreted by mesenchymal stem cells suppresses immune reactions influenced by BMP-2 through p38 and MEK mitogen-activated protein kinase pathway. *Cell and Tissue Research.* 2017; 368: 551-561.
338. Van Der Voorn P, Tekstra J, Beelen RH, Tensen CP, Van Der Valk P, and De Groot CJ. Expression of MCP-1 by reactive astrocytes in demyelinating multiple sclerosis lesions. *Am J Pathol*. 1999;154:45-51.
339. Vanslyke JK, Naus CC, Musil LS. Conformational maturation and post-ER multisubunit assembly of gap junction proteins. *Molecular biology of the cell.* 2009;20(9):2451-2463.
340. Vavlitou N, Sargiannidou I, MarkoullisK, Kyriacou K, Scherer SS, and Kleopa KA. Axonal pathology precedes demyelination in a mouse model of X-linked demyelinating/type I Charcot-Marie-Tooth neuropathy. *J Neuropathol. Exp. Neurol.* 2010; 69: 945-958.
341. Voříšek I, Hájek M, Tintěra J, Nicolay K, Syková E. Water ADC, extracellular space

volume, and tortuosity in the rat cortex after traumatic injury. *Magn Reson Med*. 2002;48(6):994-1003. doi:10.1002/mrm.10305.
342. Wallraf A, Köhling R, Heinemann U, Theis M, Willecke K, and Steinhäuser C. The impact of astrocytic gap juncitonal coupling on potassium buffering in the hippocampus. *J Neurosci.* 2006; 26 (20): 5438-5447.
343. Wang G, Shi Y, Jiang X, Leak RK, Hu X, Wu Y, Pu H, Li W, Tang B, Wang Y, Gao Y, Zheng P, Bennett MVL, and Chen J. HDAC inhibition prevents white matter injury by modulating microglia/macrophage polarization through the GSK3β/PTEN/Akt axis. *PNAS.* 2015; 112 (9) 2853-2858. https://doi.org/10.1073/pnas.1501441112
344. Wang G, Zhang J, Hu X, Zhang L, Mao L, Jiang X. Liou AK, Leek RK, Gao Y, and Chen J. Microglia/macrophage polarization dynamics in white matter after traumatic brain injury. *J. Cereb. Blood Flow Metab.* 2013; 33, 1864–1874. 10.1038/jcbfm.2013.14
345. Wang J, Wang H, Wang Y, Chen T, Wu X, Jiang Y. Two novel gap junction protein alpha 12 gene mutations in two Chinese patients with Pelizaeus–Merzbacher-like disease. *Brain Dev*. 2010;32(3):236-243. doi:10.1016/j.braindev.2009.03.013.
346. Wang J, Zhang W, Zhang Y, Chen Y, Zou B, Jiang B, Pang R, Gu Q, Qiao L, Lan H, Kung HF, and Wong BC. c-Jun N-terminal kinase (JNK1) upregulates XIAP-associated factor 1 (XAF1) through interferon regulatory factor 1 (IRF-1) in gastrointestinal cancer. *Carcinogenesis.* 2009;30(2):222-9. doi: 10.1093/carcin/bgn271.
347. Wang Y, Cheng X, He Q, Zheng Y, Kim DH, Whittemore SR. et al. Astrocytes from the contused spinal cord inhibit oligodendrocyte differentiation of adult oligodendrocyte precursor cells by increasing the expression of bone morphogenetic proteins.. J. Neurosci. 2011; 31, 6053–6058. doi: 10.1523/JNEUROSCI.5524-09.2011
348. Wang Y, Cho C, Williams J, Smallwood PM, Zhang C, Junge HJ, and Nathans J. Interplay of the Norrin and Wnt7a/Wnt7b signaling systems in blood-brain barrier and blood-retina barrier development and maintenance. *Proc Natl Acad Sci U S A.* 2018;115(50):E11827-E11836. doi: 10.1073/pnas.1813217115.
349. Wasseff SK, Scherer SS. Cx32 and Cx47 mediate oligodendrocyte:astrocyte and oligodendrocyte:oligodendrocyte gap junction coupling. *Neurobiol Dis*. 2011;42(3):506-513. doi:10.1016/j.nbd.2011.03.003.
350. Watkins TA, Emery B, Mulinyawe S, and Barres BA. Distinct stages of myelination regulated by gamma-secretase and astrocytes in a rapidly myelinating CNS coculture system. *Neuron.* 2008; 60, 555–569. doi: 10.1016/j.neuron.2008.09.01
351. Wegener A, Deboux C, Bachelin C, Frah M, Kerninon C, Seilhean D, Weider M, Wegner M, and Nait-Oumesmar B. Gain of Olig2 function in oligodendrocyte progenitors promotes remyelination. *Brain.* 2015; 138(1): 120–135. doi: 10.1093/brain/awu375
352. Werheid F, Azzedine H, Zwerenz E, Boxkurt A, Moeller MJ, Lin L, Mull M, Häusler M, Schulz JB, Weis J, et al., Underestimated associated features in cmt neuropathies: Clinical indicators for the causative gene? *Brain Behav.* 2016: 6, e00451.
353. Wingard JC, Zhao H-B. Cellular and Deafness Mechanisms Underlying Connexin Mutation-Induced Hearing Loss - A Common Hereditary Deafness. *Front Cell Neurosci*. 2015;9:202. doi:10.3389/fncel.2015.00202.
354. Wolf NI, Cundall M, Rutland P, et al., Frameshift mutation in GJA12 leading to nystagmus, spastic ataxia and CNS dys-/demyelination. *Neurogenetics*. 2007;8(1):39-44. doi:10.1007/s10048-006-0062-0.

355. Wolswijk G, and Noble M. Cooperation between PDGF and FGF converts slowly dividing O-2Aadult progenitor cells to rapidly dividing cells with characteristics of O-2Aperinatal progenitor cells. *J Cell Biol.* 1992;118(4):889-900.
356. Yakolev PA, and Lecours IR. The myelogenetic cycles of regional maturation in the brain. *In: Regional development of the brain in early life.* 1967.
357. Yan X, Liu Z, and Chen Y. Regulation of TGF-β signaling by Smad7. *Acta Biochimica et Biophysica Sinica*. 2009; 41(4):v263–272, https://doi.org/10.1093/abbs/gmp018
358. Yamamoto T, Ochalski A, Hertzberg EL, and Nagy JI. LM and EM immunolocalization of the gap junctional protein connexin 43 in rat brain. *Brain Research.* 1990; 508: 313–319.
359. Ye F, Chen Y, Hoang T, Montgomery RL, Zhoa X, Bu H, Hu T, Taketo MM, van Es JH, Clevers H, Hsieh J, Bassel-Duby R, Olson EN, and Lu QR. HDAC1 and HDAC2 Regulate Oligodendrocyte Differentiation By Disrupting β-Catenin-TCF Interaction. *Nat Neurosci.* 2009; 12(7): 829–838. doi: 10.1038/nn.2333.
360. Ye P, Popken GJ, Kemper A, Mccarthy K, Popko B, and D'Ercole AJ. Astrocyte-specific overexpression of insulin-like growth factor-I promotes brain overgrowth and glial fibrillary acidic protein expression. *J. Neurosci. Res.* 2004; 78: 472–484. doi: 10.1002/jnr.20288
361. Yeager M, and Nicholson BJ. Structure of gap junction intercellular channels. *Current Opinion in Structural Biology*. 1996; 6(2):183-192.
362. Young KM, Psachoulia K, Tripathi RB, DunnSJ, Cosseell L, Atwell D, Tohyama K, and Richardson WD. Oligodendrocyte dynamics in healthy adult CNS: evidence for myelin remodeling. *Neuron*. 2013; 77: 873-885.
363. Yuen TJ, Silbereis JC, Griveau A, Chang SM, Daneman R, Fancy SPJ, Zahed H, Maltepe E, and Rowitch DH. Oligodendrocyte-encoded HIF function couples postnatal myelination and white matter angiogenesis. *Cell.* 2014; 158(2):383-396. doi: 10.1016/j.cell.2014.04.052
364. Zambelis T, Panas M, Kokotis P, Karadima G, Kararizou E, Karandreas N. Central motor and sensory pathway involvement in an X-linked Charcot-Marie-Tooth family. *Acta Neurol Belg*. 2008;108(2):44-47. http://www.ncbi.nlm.nih.gov/pubmed/18795595.
365. Zeger M, Popken G, Zhang J, Xuan S, Lu QR, Schwab MH, Nave KA, Rowitch D, D'ERcole AJ, and Ye P. Insulin-like growth factor type 1 receptor signaling in the cells of oligodendrocyte lineage is required for normal in vivo oligodendrocyte development and myelination. *Glia.* 2007; 55: 400–411. doi: 10.1002/glia.20469
366. Zeisel A, Muñoz-Manchado AB, Codeluppi S, Lönnerberg P, La Manno G, Juréus A, Marques S, Munguba H, He L, Betsholtz C, Rolny C, Castelo-Branco G, Hjerling-Leffler J, and Linnarsson S. Cell types in the mouse cortex and hippocampus revealed by single-cell RNA-seq. *Science.* 2015; 347(6226):1138-1142. Doi: 10.1126/science.aaa1934.
367. Zemke D, Majid A. The potential of minocycline for neuroprotection in human neurologic disease. *Clin Neuropharmacol.* 2004;27:293–298.
368. Zhang C, Zhang B, Wang H, Tao Q, Ge S, and Zhai Z. Tumor necrosis factor alpha-stimulated gene-6 (TSG-6) inhibits the inflammatory response by inhibiting the activation of P38 and JNK signaling pathway and decreases the restenosis of vein grafts in rats. *Heart and Vessels.* 2017; 32: 1536-1545.
369. Zhang K, Kaufman RJ. Protein Folding in the Endoplasmic Reticulum and the Unfolded

Protein Response. In: *Molecular Chaperones in Health and Disease*. Berlin/Heidelberg: Springer-Verlag; 2006:69-91. doi:10.1007/3-540-29717-0_3.
370. Zhang K, Kaufman RJ. The unfolded protein response: a stress signaling pathway critical for health and disease. *Neurology*. 2006;66(2 Suppl 1):S102-9. doi:10.1212/01.wnl.0000192306.98198.ec.
371. Zhang Y, Chen K, Sloan S, Bennett M, Scholze AR, O'Keefe S, Phatnani HP, Guarnieri P, Caneda C, Ruderisch N, Deng S, Liddelow S, Zhang C, Daneman R, Maniatis T, Barres B, Wu JQ. An RNA-Seq transcriptome and splicing database of glia, neurons, and vascular cells of the cerebral cortex. *J Neurosci.* 2014.
372. Zhao F, Hua Y, He Y, Keep RF, and Guohua X. Minocycline-Induced Attenuation of Iron Overload and Brain Injury After Experimental Intracerebral Hemorrhage. *Stroke*. 2011; 42:3587–3593.
373. Zhao Y, Yamasaki Rm Yamaguchi H, Nagata S, Une H, Cui Y, Masaki K, Nakamuta Y, Iinuma K, Watanabe M, Matsuchita T, Isobe N, and Kira J. Oligodendroglial connexin 47 regulates neuroinflammation upon autoimmune demyelination in a novel mouse model of multiple sclerosis. *PNAS*. 2020; 117 (4): 2160-2169. https://doi-org.proxy.cc.uic.edu/10.1073/pnas.1901294117
374. Zoidl G, Dermietzel R. Gap junctions in inherited human disease. *Pflügers Arch - Eur J Physiol*. 2010;460(2):451-466. doi:10.1007/s00424-010-0789-1.

APPENDIX 1

IMMUNOFLUORESENCE ANTIBODIES

IMMUNOCYTOCHEMISTRY ANTIBODIES

PRIMARY ANTIBODY	HOST	COMPANY	CATALOG #	DILUTION
O4	MS	Gift	-	Live Cell; 1:24
Pdgfrα-647	MS	Santa Cruz	sc-398206 AF647	1:200
GFAP	MS	Cell Signaling	3670	1:650
GFAP	Ch	Invitrogen	PA1-10004	1:400
Iba1	Rb	WAKO	019-19741	1:750
Ki67	Rb	Cell Signaling	D385	1:300
Sox10	Rb	Aviva Systems Biology	ARP33326	1:250

IMMUNOHISTOCHEMISTRY ANTIBODIES

PRIMARY ANTIBODY	HOST	COMPANY	CATALOG #	DILUTION
O4	MS	Gift	-	1:4
Iba1	Rb	WAKO	019-19741	1:500
ASPA	Rb	Genetex	GTX113389	1:200

IMMUNOFLUORESCENCE SECONDARY ANTIBODIES (1:600)

ALEXA FLUOR TAG	TARGET ANTIGEN	HOST	COMPANY	CATALOG #
488	MS	Goat	Invitrogen	A28175
546	MS	Goat	Molecular Probes	A11030
488	Rb	Goat	Invitrogen	A11034
594	Rb	Goat	Invitrogen	A11035
647	Rb	Goat	Invitrogen	A27040
546	Ch	Goat	Invitrogen	A11042

Table A1-A3. Immunofluorescence Antibodies. Primary antibodies and secondary antibodies are listed as stated. Abbreviations: O4 -; Pdgfrα – platelet derived growth factor receptor alpha; GFAP – glial fibrillary acidic protein; Iba1 – ionized calcium-binding adapter molecule 1; Ki67 – marker of proliferation; Sox10 – SRY-Box transcription factor 10; ASPA -aspartoacylase

APPENDIX 2

WESTERN BLOT ANTIBODIES

PRIMARY ANTIBODY	HOST	COMPANY	CATALOG #	DILUTION
iNOS	Rb	Protein Tech	18985-1-AP	1:750
nNOS	Rb	Cell Signaling	4231S	1:750

Table A4. Westernblot Antibodies. Primary antibodies and secondary antibodies are listed as stated. Abbreviations: iNOS – inducible nitric oxide synthase; nNOS – neuronal nitric oxide synthase

APPENDIX 3

qRT-PCR PRIMERS

IDT PRIMERS

Gene	Forward	Reverse
MOG	AGAGCAAGCACCTGAATACC	GTCTCTGAAGAAGCAGGTGTAG
GAPDH	ACCATCTTCCAGGAGCGAGA	ATGGTGGTGAAGACGCCAGT
β-actin	GACTCATCGTACTCCTGCTTG	GATTACTGCTCTGGCTCCTAG

Bio-Rad PrimePCR SYBR Green Assay Primers

Gene	Amplicon Context Sequence
Adamts4	1:171254023-171256255
Gjb1	X:101384589-101384695
Gjc2	11:59176802-59176914
Ndrg1	15:66929623-66929719

Table A5 & A6. qRT-PCR Primers. Primer sequences for qRT-PCR. All primer sets used in this experiment were designed against mouse genes. Integated DNA Technologies (IDT) primers abbreviations: MOG- myelin oligodendrocyte glycoprotein; GAPDH- glyceraldehyde 3-phosphate dehydrogenase; β-actin – beta-actin. PrimePCR SYBR Green Assay sets were commercially available and made by Bio-Rad. In accordance with the MIQE guidelines the amplicon context sequence is provided above. Primer abbreviations: a disintegrin and metallopeptidase with thrombospondin type 1 motif 4; Gjb1 – gap junction beta 1; Gjc2 – gap junction protein gamma 2; Ndrg1 – N-Myc downstream regulated 1

APPENDIX 4

qRT-PCR VALIDATION

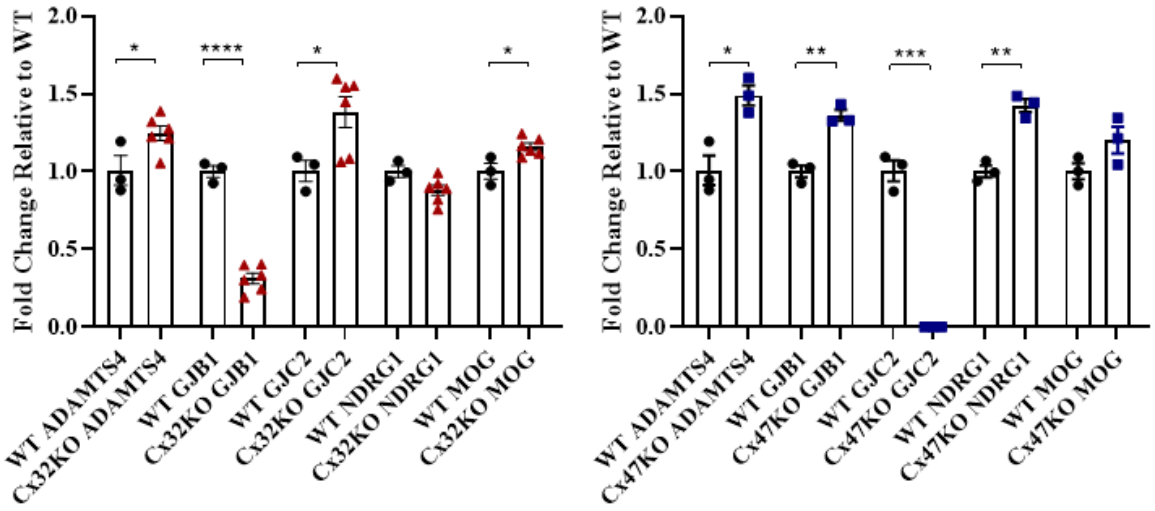

Figure 40. qRT-PCR Validation Based on RNA-seq results**.** Differentially expressed oligodendrocyte genes abbreviations: ADAMTS4-a disintegrin and metallopeptidase with thrombospondin tpe 1 motif 4; GJB1 – gap junction beta 1; GJC2 – gap junction protein gamma 2; Ndrg1 – N-Myc downstream regulated 1; MOG – myelin oligodendrocyte glycoprotein. A. qRT-PCR Validation for Cx32KO DEGs relative to WT. Significant increase in Adamts4, Gjc2, and MOG. Significant decrease in Gjb1. Decreased Ndrg1 but not significant by validation. B. qRT-PCR validation for Cx47KO DEGs relative to WT. Significant increase in Adamts4, Gjb1, and Ndrg1. Increase in MOG but not significant by validation. Significant decrease in Gjc2. Data represent mean ±SEM derived from n=3-6 in each group. *p<0.05, **p<0.01, ***p<0.001, ****p<0.0001.

APPENDIX 5

WT-PBS vs Cx32KO-PBS DEGs by Log Fold Change

Symbol	logFC	PValue	FDR
Gm43305	-5.98932	1.86E-114	5.74E-111
Gm49980	-4.06756	6.39E-104	1.69E-100
Gjb1	-3.50675	1.34E-152	6.19E-149
Mid1-ps1	-2.88009	1.38E-11	1.50E-08
AC149090.1	-2.61114	0	0
Gm42031	-2.56681	2.85E-07	0.000151
Soat2	-2.461	0.000447	0.076466
4930404N11Rik	-1.98738	6.15E-06	0.002704
Pisd-ps1	-1.85176	5.53E-142	2.05E-138
6330549D23Rik	-1.76278	5.62E-07	0.000273
Gm20628	-1.44251	1.67E-05	0.005924
Lrg1	-1.28245	0.000128	0.029903
Gm19040	-1.20829	0.000153	0.034013
F930015N05Rik	-1.20489	0.000591	0.095711
Cd59a	-1.18483	2.34E-30	4.32E-27
Dnajb13	-1.16551	0.000105	0.026953
Ctla2a	-1.16409	2.35E-05	0.008084
Hrct1	-1.10992	0.000601	0.096152
Plin4	-1.04336	2.67E-06	0.001233
Sspo	-1.03733	5.39E-05	0.016072
Tbx15	-0.99563	0.000103	0.026834
Cfap157	-0.95061	0.000229	0.044971
Fam166b	-0.91713	0.000271	0.052617
Car13	-0.91497	0.000283	0.053869
Alx4	-0.85989	1.52E-05	0.005506
Spag4	-0.85365	3.24E-09	2.49E-06
Hist2h2be	-0.82113	5.28E-11	4.88E-08
Ly6a	-0.80489	3.05E-05	0.01005
H2-K2	-0.74414	0.000471	0.07912
Chdh	-0.67377	2.83E-09	2.27E-06
2900097C17Rik	-0.63306	1.21E-59	2.79E-56
Dnah6	-0.6099	1.04E-05	0.00428
Serpina3n	-0.59931	7.20E-11	6.34E-08
5430405H02Rik	-0.59667	3.32E-05	0.01058
Emilin1	-0.59567	0.000309	0.057072

Fbln1	-0.58338	4.03E-08	2.66E-05
Tmem181b-ps	-0.55681	1.92E-31	3.94E-28
Itga10	-0.55242	0.000212	0.043107
2410022M11Rik	-0.55143	0.000629	0.097682
Gm14169	-0.44454	6.13E-07	0.00029
Neat1	-0.42658	8.00E-09	5.68E-06
Tgm2	-0.42214	0.000128	0.029903
Cfap100	-0.41843	0.000177	0.03795
Zfp697	-0.41211	3.69E-09	2.73E-06
Crlf1	-0.40574	0.000291	0.054959
Ly6c1	-0.38783	0.000138	0.031187
Ucp2	-0.37455	1.51E-10	1.27E-07
Fkbp5	-0.36508	0.00012	0.029903
Slc22a15	-0.34582	0.000106	0.026953
Cfap65	-0.32579	1.48E-05	0.005474
Rbm8a	-0.31517	2.17E-07	0.000127
Cep250	-0.3124	1.67E-11	1.72E-08
Tppp3	-0.28762	5.63E-06	0.002538
Podxl	-0.27644	0.000127	0.029903
Pnpla2	-0.25287	0.00047	0.07912
Uqcc1	-0.23683	2.36E-05	0.008084
Ndrg1	-0.22776	3.25E-05	0.010536
Nbl1	-0.22576	8.54E-05	0.023195
Col4a1	-0.22308	0.00043	0.074894
Rxra	-0.21861	0.000318	0.057534
Aar2	-0.21785	8.97E-05	0.024028
Ezr	-0.2136	0.000636	0.097913
Oplah	-0.20964	0.000305	0.056933
Slc27a1	-0.2023	2.28E-07	0.000127
Bckdha	-0.19238	0.000131	0.030311
Myh9	-0.15832	0.000363	0.06384
Map4k4	0.152055	0.000171	0.03717
Plekha1	0.162394	0.000185	0.039081
Csrnp3	0.165742	0.000559	0.091403
Sgtb	0.168565	0.000604	0.096152
Arhgap20	0.168937	0.00019	0.039352
Papss1	0.17385	0.000186	0.039081
1700020I14Rik	0.189636	4.52E-05	0.014161
Ttll7	0.191893	0.000165	0.036342
Trp53inp2	0.193331	6.67E-06	0.002824
Tent4b	0.198867	0.000194	0.039729
Cnp	0.203978	0.000281	0.053869

Gsn	0.209935	0.00051	0.084135
Wwp1	0.210104	9.53E-05	0.025163
Mtmr2	0.211668	1.41E-05	0.005413
Fut9	0.21402	0.000617	0.097494
Tulp4	0.218526	0.000219	0.044037
Ccp110	0.227599	5.59E-05	0.0164
Flrt2	0.23342	6.11E-05	0.01764
Cadm2	0.235044	0.00033	0.058622
Ano4	0.241219	0.000504	0.083976
Ptprd	0.242737	3.06E-07	0.000157
Gltp	0.257979	1.32E-05	0.00532
Mest	0.274653	0.000228	0.044971
Ncam2	0.28892	7.95E-05	0.021916
Adamts4	0.303188	5.22E-05	0.015926
Nup214	0.317014	4.42E-12	5.10E-09
Tspan2	0.330261	2.33E-07	0.000127
Il1rapl1	0.35901	0.000126	0.029903
Klhl4	0.365679	0.000316	0.057534
Pls1	0.379151	0.000321	0.057534
Adss	0.39115	2.61E-15	3.71E-12
Gprin3	0.40522	0.000629	0.097682
Nr4a2	0.411221	3.97E-07	0.000198
Wars2	0.492788	6.73E-06	0.002824
Ighm	0.524305	2.32E-07	0.000127
Atp10b	0.722954	1.35E-05	0.005322
Casq2	0.78577	2.48E-05	0.008323
Zfp804b	0.810712	0.000126	0.029903
Myh7b	0.850005	9.22E-21	1.55E-17
Gm10524	0.911105	2.03E-11	1.97E-08
2210011C24Rik	1.04153	0.000137	0.031187
Gm20633	1.066999	7.36E-05	0.020592
G530011O06Rik	1.30298	0.00044	0.075971
Gm5784	1.37596	2.22E-07	0.000127
Gm36356	1.496557	6.66E-05	0.018945
Gm43242	1.644408	1.76E-07	0.000112
Sla2	1.755644	3.41E-12	4.20E-09
Gm49769	1.870431	5.26E-05	0.015926
Phf20-ps	2.105976	2.64E-08	1.81E-05
Gm42743	2.377256	3.93E-13	5.19E-10
Slc5a1	3.671635	1.45E-05	0.005471
Gm7292	5.280687	1.45E-190	8.91E-187

Hist1h2al	5.435407	1.68E-19	2.58E-16
Gm15446	6.215316	1.40E-195	1.29E-191

APPENDIX 6

WT-PBS vs Cx47KO-PBS DEGs by Log Fold Change

Symbol	logFC	PValue	FDR
Olfr316	-6.70852	2.01E-11	1.44E-08
Slc6a4	-6.5521	1.10E-08	3.81E-06
Pou4f2	-3.46317	1.05E-07	3.21E-05
Pax5	-2.8631	1.02E-09	4.96E-07
Gjc2	-2.67321	4.08E-95	7.33E-91
Cnpy1	-2.39395	7.08E-06	0.001152
Fat2	-2.38749	4.29E-06	0.000756
Rln3	-2.3239	3.08E-05	0.00372
Gm48678	-2.31978	1.24E-07	3.67E-05
Dao	-2.26167	1.07E-08	3.81E-06
En1	-2.25754	0.000772	0.044164
Gm21887	-2.21197	2.03E-12	1.82E-09
Chrna6	-2.18561	1.07E-05	0.00161
2610507I01Rik	-2.15314	1.20E-22	4.32E-19
Mstn	-1.98259	0.000505	0.031916
Hsd17b2	-1.97488	0.001074	0.055616
Gm42756	-1.93658	5.64E-11	3.70E-08
Pitx3	-1.82873	0.000306	0.022929
Gm43242	-1.79592	0.001154	0.058212
Adgrg3	-1.79581	0.001619	0.073223
Th	-1.75338	1.02E-08	3.81E-06
Ucn	-1.69548	0.000207	0.017249
Barhl1	-1.6307	7.08E-09	2.77E-06
Slc18a2	-1.52547	0.000108	0.010568
Vwa7	-1.47107	6.53E-05	0.007075
Lif	-1.46427	0.00024	0.019004
C1ql4	-1.45812	8.47E-06	0.001336
Gm47283	-1.45702	5.76E-11	3.70E-08
Lyrm7	-1.44604	2.49E-24	1.12E-20
Nkx6-1	-1.41039	0.000384	0.026513
Gm10997	-1.3813	0.000911	0.049739
Tfap2b	-1.30529	5.00E-05	0.005684
Gata3	-1.22879	0.002196	0.087687
Tph2	-1.21317	0.001207	0.059399
Gm26644	-1.20619	0.000783	0.044691
2310058D17Rik	-1.19008	3.77E-06	0.000692

Sox14	-1.18496	0.000356	0.025263
Etaa1os	-1.1569	0.002023	0.083572
Derl3	-1.13134	1.74E-05	0.002312
Twist1	-1.12021	0.000381	0.026512
Gm45159	-1.11999	0.002644	0.099595
Slc26a7	-1.10394	0.000291	0.022279
Gucy2c	-1.10263	0.000306	0.022929
Mab21l2	-1.09094	0.000218	0.017728
Ebf3	-1.08205	8.35E-05	0.008621
Slc9a4	-1.0676	0.000188	0.0161
Trhr	-1.05522	0.001108	0.05641
1700056N10Rik	-1.01114	0.000852	0.047544
E030013I19Rik	-0.98628	0.001416	0.066599
Tal1	-0.90903	3.12E-05	0.003741
Ddc	-0.86685	2.23E-06	0.000435
Meig1	-0.84541	0.000883	0.048643
Csf2rb2	-0.84065	0.001672	0.074473
Fibcd1	-0.84019	2.63E-05	0.003196
Anxa1	-0.83389	0.001164	0.058212
Abca8a	-0.82649	7.94E-07	0.000181
Mrpl55	-0.82127	3.92E-12	3.20E-09
Cartpt	-0.79308	0.000131	0.012251
Slc47a1	-0.79152	0.000265	0.020616
Rxfp3	-0.75547	1.67E-05	0.002256
Slc26a4	-0.72793	0.000567	0.034985
Dcn	-0.71269	0.000506	0.031916
Ret	-0.7031	0.000295	0.02234
Spp1	-0.70184	2.43E-05	0.003001
Vgll3	-0.68677	0.00057	0.035087
Tspan18	-0.6618	0.001399	0.066599
Crym	-0.65559	9.41E-06	0.001446
Cecr2	-0.65213	1.05E-06	0.000224
Aloxe3	-0.64896	0.000876	0.048422
Nkd2	-0.64812	0.000188	0.0161
Cpne7	-0.62221	0.002012	0.083297
Sncg	-0.6202	8.40E-05	0.008621
Tnfaip8l3	-0.56915	0.000437	0.028575
Crlf1	-0.53266	0.000964	0.051864
Sertm1	-0.5272	2.08E-05	0.002651
Xaf1	-0.52587	0.001706	0.074929
Ccn3	-0.52128	1.08E-08	3.81E-06
Npy2r	-0.51234	0.000977	0.052016

Aldh1a1	-0.51193	3.81E-09	1.59E-06
Hist3h2a	-0.50948	0.001531	0.070656
C1ql2	-0.50071	0.00087	0.048396
Gm49284	-0.49067	0.002598	0.098676
Cys1	-0.48999	6.96E-05	0.007355
Rab27a	-0.48365	0.00163	0.073223
Tacr3	-0.45829	0.002167	0.087105
Fgf10	-0.4491	0.001121	0.056728
2010204K13Rik	-0.44607	0.000337	0.02431
Cpne6	-0.4392	0.000928	0.050511
Npas1	-0.4326	0.000142	0.012733
Itga4	-0.43104	0.001933	0.082105
Gm44562	-0.42969	0.00251	0.096569
Tnxb	-0.419	0.001415	0.066599
Kctd4	-0.4171	9.17E-05	0.009152
Trim17	-0.41587	0.002567	0.097868
Dgkg	-0.41519	0.001999	0.083297
Kcng2	-0.41268	0.001166	0.058212
Gm35339	-0.40443	0.000493	0.031538
Chrd	-0.39921	0.00012	0.011339
Il33	-0.39517	1.24E-05	0.001792
Syt17	-0.39185	0.000406	0.027302
Bhlhe22	-0.38819	4.15E-05	0.004812
Cldn5	-0.38672	7.76E-05	0.00807
Opalin	-0.37975	6.72E-05	0.007149
Egfl7	-0.37772	0.000738	0.042914
Ndnf	-0.37678	0.000422	0.028065
Fgf11	-0.37463	2.37E-06	0.000457
Ldb3	-0.37217	0.000978	0.052016
Foxo6	-0.36949	8.84E-05	0.008923
Col23a1	-0.36936	0.000946	0.051188
Kcng1	-0.36868	2.44E-05	0.003001
Ptpn14	-0.36768	0.00036	0.025487
Nrp1	-0.36702	0.0011	0.056152
Plekho2	-0.36111	0.0011	0.056152
Tafa1	-0.35153	0.000229	0.01847
Gria1	-0.34685	8.93E-06	0.001383
Arhgef28	-0.34265	0.000742	0.042984
Mas1	-0.3415	0.000169	0.014767
Kit	-0.34043	0.00052	0.032455
Wnt7b	-0.34034	0.001452	0.067941
Iqgap2	-0.33336	0.000216	0.017711

Ptpru	-0.32845	6.54E-05	0.007075
Ptpre	-0.31971	5.66E-05	0.006311
Kdm2b	-0.31779	0.000683	0.040088
Fezf2	-0.31183	0.001099	0.056152
Ak4	-0.30647	0.000638	0.037827
Mmd	-0.30017	4.45E-06	0.000776
Gabra5	-0.29215	0.001886	0.081006
Gabra2	-0.29193	0.000642	0.037926
Thbs3	-0.29072	0.001077	0.055616
Frmpd3	-0.2844	0.000137	0.012471
Crtac1	-0.28262	0.000834	0.046953
Galnt9	-0.27598	0.000328	0.023993
Jun	-0.27208	0.000251	0.019621
Zfpm2	-0.2719	0.002011	0.083297
mt-Nd6	-0.26735	0.000436	0.028575
Podxl	-0.26561	0.001307	0.062795
Kctd12	-0.26435	0.0005	0.031742
Clns1a	-0.25067	0.000121	0.011374
Nptx1	-0.25061	5.55E-05	0.006236
Chl1	-0.24338	0.001542	0.070671
Cbfa2t3	-0.23882	0.000941	0.051079
Cnot8	-0.23351	0.000485	0.031221
Sh3bp5	-0.23061	0.002353	0.092513
Snca	-0.22815	0.000294	0.02234
Rxra	-0.21414	0.002172	0.087105
Unc5a	-0.21073	0.002281	0.090457
Stim2	-0.20658	0.002434	0.094045
Pde1a	-0.2062	0.000215	0.017711
Gtf2a1	-0.20459	0.001984	0.082982
Pygm	-0.20447	0.0017	0.074921
Icam5	-0.19883	0.00046	0.029924
Lgi1	-0.18937	0.000603	0.036434
Tnks1bp1	-0.18796	0.000517	0.032455
Klhl3	-0.18703	0.001975	0.082982
mt-Rnr2	-0.18553	0.001951	0.082659
Thra	-0.17761	0.002571	0.097868
Mmd2	-0.17031	0.002376	0.092861
Nfasc	0.155648	0.002167	0.087105
Tbc1d9b	0.159735	0.00174	0.075752
Abca2	0.162433	0.002012	0.083297
Pacs2	0.162483	0.00141	0.066599
Ptpn11	0.164317	0.002532	0.096794

Dip2a	0.167638	0.001986	0.082982
Malat1	0.167932	0.002394	0.093328
Tpt1	0.171512	0.001178	0.058599
Ppp2r5d	0.177404	0.001181	0.058599
Atp1b3	0.181391	0.002532	0.096794
Kif1c	0.183766	0.001271	0.061409
Phldb1	0.18495	0.001678	0.074473
Asap1	0.187191	0.001984	0.082982
Extl3	0.18754	0.002517	0.096621
Tmem56	0.190032	0.001574	0.071615
Rpl31	0.191821	0.002617	0.099192
Ppp1r1a	0.193982	0.001268	0.061409
Dock10	0.194168	0.001065	0.05549
Gjc3	0.194462	0.001416	0.066599
Thsd7a	0.195296	0.001019	0.053542
Omg	0.196773	0.001777	0.077131
Ccdc136	0.198414	0.000599	0.036333
Scube1	0.202595	0.001628	0.073223
Zcchc24	0.203683	0.00015	0.013383
Anp32b	0.204609	0.002629	0.099329
Cdkl5	0.207968	0.001163	0.058212
Gpr37	0.208944	0.001834	0.079196
Map3k9	0.208999	0.002171	0.087105
Rap1gap	0.209394	0.002171	0.087105
Nacc2	0.209945	9.06E-05	0.009094
Pcdh10	0.210125	0.000195	0.01658
Shank3	0.210211	0.000237	0.018936
Npc1	0.210458	0.000575	0.035255
Kcnj10	0.211467	0.001247	0.06072
Slc44a1	0.2118	0.002074	0.085015
Ptpn4	0.213688	0.002086	0.0852
Cited2	0.21567	0.001054	0.055058
Trnp1	0.21763	0.000608	0.036434
Mtmr2	0.21779	0.001018	0.053542
Id4	0.219442	0.000134	0.012377
Sh3d19	0.219699	0.002313	0.091326
Nrep	0.225442	0.001286	0.06197
Tmem88b	0.227335	0.000394	0.026792
Slc2a1	0.227523	0.000435	0.028575
Polr3e	0.228267	0.002377	0.092861
Sorcs1	0.228483	0.002273	0.090344
Srebf1	0.229798	0.000156	0.013712

Shc3	0.230801	0.000585	0.035629
Cntn4	0.234865	0.002411	0.093358
Pkp4	0.235659	2.02E-05	0.002593
Pde4b	0.236874	1.94E-05	0.002509
Rnf152	0.240014	0.001917	0.081785
Zfpm1	0.240105	0.001514	0.070454
Errfi1	0.242451	0.000498	0.031699
Srgap1	0.243016	0.000738	0.042914
Ampd3	0.245139	0.00229	0.090613
Zfp281	0.245998	0.000118	0.011187
Ptgds	0.248171	0.000346	0.024896
Pogk	0.249301	7.53E-06	0.001208
Dgki	0.249356	0.000956	0.051576
Sertad2	0.249468	0.002094	0.0853
Serinc5	0.250675	0.000362	0.025489
Flrt2	0.25127	0.002179	0.087191
Rasgrp1	0.251333	0.000582	0.035562
Tnip1	0.253366	0.000303	0.022905
Kcnd2	0.254594	0.00039	0.026672
Myo1d	0.254621	0.000418	0.02792
Rims3	0.255475	7.12E-06	0.001152
Cux1	0.257128	0.001868	0.080473
Pdp1	0.260306	0.001116	0.056633
Kitl	0.260598	0.001244	0.06072
Cux2	0.267849	0.001546	0.070671
Syndig1	0.268579	0.00079	0.044913
Smad7	0.268955	0.000322	0.023713
Maob	0.269854	0.000351	0.025005
Kif5b	0.27011	3.58E-07	9.74E-05
Zfp804a	0.270234	0.000239	0.018992
Heg1	0.270464	4.88E-05	0.005582
Nr4a1	0.270469	0.001327	0.063594
Otud7b	0.274283	1.23E-06	0.000257
Gnb4	0.27442	0.000197	0.01658
Plcb4	0.274701	7.20E-05	0.007566
Egr1	0.274819	0.000655	0.038569
Kcns2	0.279407	0.001526	0.070656
Tcf7l2	0.279947	0.000903	0.049472
Fras1	0.280055	0.001212	0.059484
Atp11a	0.281294	4.99E-07	0.000123
Fgfr2	0.282949	1.90E-05	0.00248
Hcn2	0.284014	6.17E-07	0.000144

Scd1	0.28569	1.49E-05	0.002063
Ugt8a	0.286158	1.46E-06	0.000302
Bok	0.286263	0.000332	0.024182
Patj	0.286302	0.001623	0.073223
Gss	0.287188	0.002135	0.086794
Gabra4	0.287386	6.03E-05	0.00665
Adarb1	0.288498	5.84E-07	0.000138
Igsf11	0.294294	0.001683	0.074479
Kctd16	0.295137	0.001701	0.074921
Relt	0.297264	0.000769	0.044149
Lfng	0.297908	0.001188	0.058645
S100a1	0.304581	0.000322	0.023713
Eml1	0.309307	2.18E-05	0.002738
Trak2	0.311001	1.21E-07	3.61E-05
Kcnj12	0.31193	0.001679	0.074473
Olig2	0.313816	1.29E-05	0.001852
Nhlrc3	0.31447	0.002654	0.099767
Cacng4	0.314694	0.000313	0.02337
Myo1b	0.31687	0.002247	0.089532
Ptpn3	0.317622	1.73E-06	0.000345
Cit	0.317711	5.47E-07	0.000133
Zdhhc22	0.31773	8.65E-05	0.008778
Mag	0.320425	1.23E-06	0.000257
Strn	0.320491	0.000796	0.045109
Nudt4	0.32084	4.56E-07	0.000117
Cpne9	0.323175	0.000465	0.030168
Hapln2	0.324526	6.44E-07	0.000148
Enpp4	0.326993	1.34E-05	0.001898
Ldlrad3	0.327663	0.001967	0.082947
Stard10	0.329158	0.002369	0.092861
Tob2	0.329281	6.62E-06	0.001102
Qdpr	0.334181	1.73E-09	7.71E-07
Ephb1	0.336062	1.62E-06	0.000329
Pim3	0.337017	4.17E-07	0.000109
Kif13b	0.337757	4.74E-07	0.00012
Dusp1	0.339247	0.000524	0.032585
Fhdc1	0.339432	0.001741	0.075752
Hipk2	0.343564	1.75E-08	5.61E-06
Ntng1	0.345141	4.12E-06	0.000733
Lims2	0.350065	0.000288	0.022124
Tprn	0.350502	3.83E-06	0.000696
Tiparp	0.352742	0.001552	0.070776

Pitpnc1	0.353036	6.60E-09	2.64E-06
Wipf1	0.355336	0.000249	0.019516
Tgfa	0.355805	0.001963	0.082947
Spock3	0.355979	1.74E-05	0.002312
Gucy1a2	0.356752	0.000606	0.036434
Mobp	0.358407	4.43E-05	0.0051
Gsn	0.358524	1.41E-09	6.51E-07
A830036E02Rik	0.359934	0.000974	0.052016
Fmn1	0.360703	0.000874	0.048422
Rffl	0.364593	0.000142	0.012712
Rasgef1c	0.365039	0.002451	0.094487
Necab3	0.365346	0.000228	0.018416
Csrnp1	0.369501	0.001486	0.069338
Slc12a2	0.38324	3.79E-11	2.62E-08
Prr5l	0.391747	0.001408	0.066599
Gnal	0.392104	0.000196	0.01658
Aff1	0.396242	1.10E-05	0.001624
Samd4	0.39703	5.38E-10	2.68E-07
Chn2	0.399334	1.75E-07	5.06E-05
Gjb1	0.401975	0.000369	0.025868
Prkcq	0.40219	1.34E-05	0.001898
Osbpl3	0.405999	1.82E-06	0.000359
Myrf	0.409619	1.82E-13	2.04E-10
Gpr153	0.410773	3.19E-06	0.000609
Rgs4	0.41096	0.001229	0.060163
Cpne5	0.414439	0.000608	0.036434
Rassf3	0.421992	0.000245	0.019272
Pde8a	0.422015	4.11E-08	1.27E-05
Emilin2	0.423369	0.000635	0.037766
Fgf1	0.425449	5.32E-10	2.68E-07
Bc1	0.425614	1.85E-10	1.15E-07
Adra1b	0.426616	1.10E-05	0.001624
Oxsr1	0.431457	1.32E-12	1.25E-09
Adipor2	0.435008	6.99E-13	6.97E-10
Dbndd2	0.435777	2.79E-10	1.58E-07
Amotl1	0.436304	3.90E-07	0.000105
Apod	0.436499	1.63E-06	0.000329
Mtfr1	0.442058	0.001534	0.070656
Lrrc75a	0.442922	0.000136	0.012471
Phactr4	0.447814	1.79E-05	0.002342
Igfn1	0.449042	1.20E-05	0.00176
Plekhb1	0.449913	2.15E-12	1.84E-09

Plxnb3	0.451466	7.83E-14	1.04E-10
Pcp4l1	0.452307	0.000232	0.018596
Grm4	0.452492	3.56E-06	0.000661
Chdh	0.454066	5.08E-05	0.005743
Fbxo32	0.455331	6.65E-05	0.007149
Trpc3	0.459569	0.000111	0.010702
Syt9	0.463818	2.81E-09	1.20E-06
Arhgef5	0.466153	0.001721	0.075217
Foxp2	0.466879	3.15E-05	0.003752
Ankrd34c	0.470341	0.000205	0.017173
Meis2	0.47077	0.002077	0.085015
Hspbap1	0.475209	0.001623	0.073223
Rspo1	0.477752	0.001828	0.079132
Unc13c	0.481785	5.12E-12	4.00E-09
Lrrc55	0.484225	1.66E-08	5.42E-06
Fam222a	0.484429	1.35E-05	0.001899
Rora	0.485273	3.52E-10	1.92E-07
Slc38a2	0.487038	8.37E-14	1.04E-10
Rgs16	0.487907	1.22E-08	4.15E-06
Car2	0.490186	6.66E-14	9.97E-11
Cacng5	0.491646	5.28E-06	0.000903
Gabrd	0.492212	0.000968	0.051918
Ndrg1	0.494478	1.20E-16	2.16E-13
Rem2	0.494969	0.000481	0.031096
Pcp4	0.495668	7.11E-06	0.001152
Gpr83	0.49686	0.00073	0.042732
Adamts3	0.49878	0.000628	0.037511
Epn3	0.502183	9.72E-06	0.001479
Tnfaip6	0.505477	0.000137	0.012471
Plekhg1	0.509295	2.82E-10	1.58E-07
Pla2g3	0.517185	0.001428	0.066971
Arc	0.51969	1.76E-09	7.71E-07
Ddit4	0.51978	2.23E-07	6.25E-05
Rasd1	0.522054	1.56E-08	5.21E-06
Ramp3	0.526173	5.04E-06	0.00087
Prrg1	0.533887	0.000519	0.032455
Adcy5	0.536732	0.001921	0.081785
Arrdc2	0.540554	0.00241	0.093358
Kcnh4	0.54136	0.001161	0.058212
Prr18	0.547712	1.29E-20	3.32E-17
Pdyn	0.570111	0.002411	0.093358
Strip2	0.571707	8.54E-05	0.008717

Rab37	0.575532	5.33E-06	0.000903
Nfkbia	0.581159	3.31E-06	0.000627
Mctp2	0.589068	0.000887	0.048752
Cish	0.589321	2.50E-05	0.003062
Mbp	0.59168	4.24E-19	8.47E-16
Prkch	0.597246	0.000335	0.02427
2810021J22Rik	0.599419	9.92E-06	0.001498
Plekhf1	0.600897	0.000137	0.012471
Pgam2	0.604147	0.002062	0.084772
Pou6f2	0.608955	0.001639	0.073425
Pde7b	0.615794	1.77E-05	0.002333
Prkcd	0.620065	8.49E-07	0.000191
Zic1	0.624201	3.04E-21	9.11E-18
Shox2	0.628398	5.54E-09	2.26E-06
Ttf2	0.629191	0.001261	0.061222
Vash2	0.635146	7.77E-05	0.00807
Arl4d	0.645176	0.000197	0.01658
Adamts4	0.648235	8.68E-14	1.04E-10
Gprin3	0.649059	0.00191	0.081714
Ccdc187	0.661414	0.000215	0.017711
Slc25a13	0.671596	5.75E-05	0.006373
Kcnh5	0.672013	1.63E-05	0.002227
D7Ertd443e	0.673012	4.03E-07	0.000106
Fgd3	0.678232	7.80E-12	5.84E-09
A930017K11Rik	0.680657	0.001889	0.081006
Gbx2	0.681816	5.71E-06	0.000958
Atp10b	0.683656	0.000217	0.017728
Synpo2	0.685415	1.13E-09	5.34E-07
Gm43398	0.696917	4.49E-10	2.37E-07
Gm1821	0.700142	0.000541	0.033549
Tac2	0.709318	8.64E-06	0.00135
Gm19439	0.738955	8.95E-07	0.000196
Kcna5	0.75325	3.57E-06	0.000661
Cox6a2	0.760495	0.000275	0.021243
Scube3	0.780591	0.000349	0.025005
Trhr2	0.782643	0.000163	0.014293
Gm960	0.787399	0.000326	0.023923
Sgk1	0.797311	0.000764	0.044141
Slc45a3	0.80745	0.000181	0.015683
Slitrk6	0.856243	0.000109	0.010577
Sostdc1	0.861515	0.000767	0.044149
Gpr149	0.866879	0.001718	0.075217

Chrnb4	0.874321	3.98E-06	0.000715
Cckar	0.887779	0.00108	0.055616
Casq2	0.889621	1.64E-05	0.002227
Frem3	0.890064	2.02E-07	5.76E-05
Pde10a	0.900312	0.001646	0.07359
Grid2ip	0.90106	3.44E-16	5.62E-13
Nexn	0.918057	8.76E-07	0.000194
Scd3	0.923642	4.88E-07	0.000122
Zfp804b	0.932345	6.70E-05	0.007149
Abhd12b	0.979956	9.30E-05	0.009227
Wnt3	0.981017	2.32E-10	1.39E-07
Slc35d3	1.022219	0.00205	0.08447
Six3os1	1.024192	0.001041	0.054559
Ngfr	1.029268	0.000405	0.027302
Six3	1.063565	0.000133	0.012377
Epha1	1.081329	0.000847	0.047394
Pex11g	1.088312	0.001184	0.058609
Gpr151	1.098282	1.10E-08	3.81E-06
Tmem252	1.123378	0.000994	0.052677
Cftr	1.137092	3.30E-05	0.003901
4833415N18Rik	1.184044	0.000388	0.026599
Penk	1.231511	2.30E-05	0.002873
Ppp1r1b	1.233601	0.000268	0.020719
Syndig1l	1.23525	0.000375	0.026229
Bcas1	1.268048	1.71E-78	1.54E-74
Zfp960	1.276701	0.00108	0.055616
Isl1	1.298764	0.000139	0.012558
Drd1	1.310367	0.000386	0.026581
Syt15	1.314118	1.39E-05	0.00194
Igkc	1.380205	0.002153	0.087105
Rgs9	1.458522	0.000186	0.0161
Slc5a7	1.459104	0.000108	0.010558
Gpr88	1.47564	0.000109	0.010577
Obscn	1.492561	5.82E-07	0.000138
Pkd2l1	1.512127	3.95E-13	4.18E-10
Gm42727	1.568108	0.002631	0.099329
Dsg1c	1.607031	0.001541	0.070671
Gm5741	1.625698	3.17E-07	8.75E-05
Depp1	1.634456	0.000383	0.026513
Gm16425	1.700964	0.001524	0.070656
Bcas1os1	1.70214	0.000836	0.046953
Slc18a3	1.723083	4.03E-05	0.004708

Ptprv	1.803375	0.000402	0.027284
Gm15446	1.832156	0.001341	0.064105
Gpr6	1.839498	6.47E-05	0.007075
Ido1	1.90853	0.000492	0.031538
Sh3rf2	1.962717	0.000153	0.013502
Adora2a	1.982253	1.00E-04	0.009871
Gm14239	2.066723	0.000411	0.02757
Abcc2	2.077633	0.001015	0.053542
Cd4	2.153949	0.002332	0.09189
Snx31	2.211711	7.38E-09	2.82E-06
Chat	2.249166	8.36E-06	0.001329
Gbx1	2.32056	0.000831	0.046953
Impg1	2.624928	0.000432	0.028568
Gm19587	2.659574	2.72E-08	8.57E-06
Lhx8	2.794554	0.000426	0.028246
Gm36737	3.197401	3.95E-05	0.004641
AC127331.2	3.686432	2.02E-34	1.21E-30
Gm39043	4.367252	0.000315	0.023385
Gm18860	4.455281	5.38E-20	1.21E-16
Prl	4.909913	0.000114	0.010913
Gh	5.131947	2.16E-05	0.002735
Cga	7.009524	1.04E-06	0.000224

APPENDIX 7

WT-PBS vs WT-LPS DEGs by Log Fold Change

Symbol	logFC	PValue	FDR
Gm9946	-4.1788	3.11E-09	1.28E-07
Gm45552	-3.35925	4.37E-21	7.21E-19
Gpr34	-2.82849	1.71E-25	4.18E-23
Gkn3	-2.72251	5.85E-09	2.31E-07
Dipk2b	-2.71337	9.80E-16	9.13E-14
Ssu2	-2.61507	9.73E-05	0.001625
Cd180	-2.47496	2.65E-09	1.10E-07
Myct1	-2.37743	5.84E-06	0.000131
Slco1a4	-2.32877	1.06E-23	2.18E-21
Alox12	-2.28958	1.24E-06	3.19E-05
Sox18	-2.28423	1.22E-37	6.69E-35
Olfr464	-2.25558	8.84E-07	2.35E-05
Abcc6	-2.17544	3.86E-08	1.33E-06
Degs2	-2.1737	3.01E-16	3.02E-14
Srms	-2.16666	2.07E-07	6.20E-06
S1pr4	-2.13523	1.31E-07	4.03E-06
Tek	-2.12238	6.46E-36	3.09E-33
Fendrr	-2.0852	2.33E-11	1.26E-09
Sox17	-2.07174	4.75E-38	2.76E-35
Gm45650	-2.00728	0.000298	0.004352
AU021092	-1.94866	7.43E-08	2.42E-06
Pkn3	-1.92156	4.60E-08	1.56E-06
Slc40a1	-1.91009	2.43E-27	7.80E-25
Gm29260	-1.86172	0.00166	0.018448
Slc38a5	-1.81806	2.51E-14	1.96E-12
Gm43143	-1.78662	0.009637	0.077347
Susd3	-1.78408	9.58E-08	3.04E-06
Gm10790	-1.77714	2.19E-06	5.39E-05
Notum	-1.76526	8.79E-10	3.89E-08
Slc47a1	-1.75716	7.99E-09	3.14E-07
Zfp366	-1.72802	8.67E-15	7.25E-13
Ushbp1	-1.72749	3.54E-21	5.95E-19
P2ry12	-1.72445	4.08E-15	3.54E-13
Slco1b2	-1.72217	0.003265	0.032179
Hmcn1	-1.7103	3.47E-07	9.87E-06
Tmem51os1	-1.6963	0.00209	0.022365
Myo1f	-1.68709	5.04E-12	3.01E-10
Flvcr2	-1.68343	6.26E-10	2.82E-08

Nlrp1b	-1.68231	9.27E-06	0.000196
Slc2a5	-1.6389	3.23E-15	2.84E-13
Has2	-1.63132	0.000137	0.002218
Rab38	-1.63031	2.17E-05	0.000422
Gm4524	-1.62977	0.001272	0.014826
Abcb1a	-1.60508	2.78E-36	1.36E-33
Fzd10	-1.60409	8.38E-09	3.27E-07
Gm44317	-1.59599	0.003196	0.031656
Gm43231	-1.56834	0.000309	0.004479
Inmt	-1.56527	0.00013	0.002112
Insc	-1.54362	2.91E-19	3.85E-17
Kcne2	-1.53034	5.28E-05	0.000949
Thegl	-1.52418	0.006862	0.058704
Ptprb	-1.52075	1.86E-14	1.49E-12
Gm33858	-1.51603	0.000393	0.005546
Nkx2-9	-1.50795	0.002116	0.022527
Depdc7	-1.50376	1.11E-06	2.90E-05
1110035H17Rik	-1.49455	4.80E-05	0.000871
Aplnr	-1.49321	0.001295	0.015067
Tie1	-1.48807	1.29E-35	6.03E-33
Slc52a3	-1.48366	1.12E-10	5.66E-09
Magix	-1.47936	0.000778	0.009891
Kdr	-1.47893	1.14E-41	7.61E-39
Slc26a7	-1.474	6.89E-07	1.86E-05
Slc22a8	-1.47157	8.88E-14	6.57E-12
Cass4	-1.47002	0.001758	0.019368
Spp2	-1.46687	0.01232	0.093267
Tbx1	-1.45948	9.81E-05	0.001636
Gm45426	-1.45016	4.54E-06	0.000104
Prdm6	-1.43801	0.00434	0.04075
F2rl1	-1.43644	0.001103	0.013186
Mmp28	-1.43564	2.60E-14	2.03E-12
Serpinb1a	-1.43035	6.65E-16	6.32E-14
Clec14a	-1.42185	3.53E-09	1.44E-07
Gm10863	-1.42041	1.07E-05	0.000224
Gm43242	-1.41676	0.001338	0.015474
Vwf	-1.41365	3.05E-21	5.22E-19
Edn3	-1.38958	3.86E-06	9.06E-05
Fli1	-1.36764	1.56E-16	1.61E-14
Gm16046	-1.36655	0.000664	0.008581
Gm8189	-1.35871	0.000919	0.011307
Gm5086	-1.34839	0.000884	0.010979

Gm30655	-1.33886	0.00276	0.028031
Gm18859	-1.3353	0.008551	0.070298
Irf6	-1.33366	0.0016	0.017893
Gm48655	-1.32776	0.009409	0.075914
Olfml2a	-1.30917	1.89E-10	9.25E-09
Rad54b	-1.30784	1.22E-05	0.000253
Itpr3	-1.30241	2.48E-18	2.90E-16
Lyl1	-1.29655	6.61E-07	1.79E-05
Aoc3	-1.29243	2.07E-05	0.000406
Hk3	-1.28845	5.90E-06	0.000132
Slco1c1	-1.26775	1.34E-34	5.81E-32
Crabp2	-1.26072	1.10E-07	3.44E-06
Wfdc1	-1.25319	3.40E-10	1.61E-08
Slc22a2	-1.23745	0.000854	0.0107
Zfp979	-1.23545	0.001002	0.012174
Trp63	-1.23354	0.000248	0.003729
Foxc2	-1.22538	5.65E-07	1.55E-05
Gsx1	-1.22257	0.000165	0.002594
Dnase1l1	-1.22014	9.23E-07	2.44E-05
Rassf9	-1.21914	3.98E-06	9.28E-05
Slc22a6	-1.21819	0.000192	0.002958
Hes5	-1.21702	1.39E-15	1.28E-13
Hspa12b	-1.21403	1.82E-18	2.18E-16
Lpar4	-1.21294	4.02E-07	1.13E-05
Slc19a3	-1.21137	7.74E-07	2.08E-05
Mypopos	-1.20042	0.002477	0.025708
Gm14573	-1.19974	0.012007	0.091478
Gipc3	-1.19371	1.78E-08	6.55E-07
Rasgrp3	-1.19327	3.17E-18	3.67E-16
Dennd2c	-1.19269	0.005234	0.04728
2010001K21Rik	-1.19249	0.000525	0.007055
Gm43333	-1.19245	0.009647	0.077362
Cfap157	-1.18766	7.17E-05	0.001243
5830444B04Rik	-1.18731	0.011816	0.090316
Slc16a4	-1.18151	5.98E-06	0.000133
Foxl2os	-1.18119	0.010047	0.07968
Clec10a	-1.17817	0.008882	0.072536
Wnt6	-1.17408	0.002555	0.026313
Itm2a	-1.1738	1.11E-17	1.22E-15
Prr32	-1.16631	0.002813	0.028441
Tbxa2r	-1.16543	2.16E-05	0.00042
Msx1	-1.16148	1.61E-05	0.000324

Cldn5	-1.15687	3.44E-20	5.34E-18
1700024G13Rik	-1.15481	0.011619	0.089151
Gm30075	-1.14911	0.006152	0.054033
Trim59	-1.14151	5.42E-13	3.62E-11
1700063D05Rik	-1.13905	0.000104	0.001731
Zfp474	-1.13282	0.003585	0.034851
Gm6089	-1.13165	0.00136	0.015686
Gm29683	-1.12892	1.08E-05	0.000226
Gm2629	-1.12789	5.08E-05	0.00092
Cx3cr1	-1.12265	7.23E-13	4.75E-11
Ajuba	-1.11323	4.60E-09	1.83E-07
Folr2	-1.11215	0.012412	0.093657
BB187690	-1.10881	0.008698	0.071191
Foxl2	-1.10414	0.001845	0.020133
Ly6g6d	-1.10362	0.006779	0.058079
Car9	-1.10116	0.000451	0.006195
Tgm6	-1.09912	0.006684	0.057458
Sox13	-1.08665	1.42E-24	3.14E-22
Pgm5	-1.08401	4.40E-10	2.05E-08
Pax3	-1.07604	0.009172	0.074255
Chdh	-1.07009	1.54E-06	3.91E-05
Gm34934	-1.06865	0.001745	0.019245
H2-Q1	-1.06397	0.00791	0.065986
Asgr1	-1.06388	0.00103	0.01243
Sigirr	-1.06378	0.00061	0.008001
Thsd1	-1.06365	2.35E-11	1.27E-09
Tcf7	-1.06067	2.41E-06	5.90E-05
Adgre5	-1.05922	6.45E-20	9.61E-18
Tcea3	-1.05877	0.00313	0.031112
Mrgprf	-1.05399	0.002116	0.022527
Morn3	-1.05286	0.012014	0.091478
Hist1h3d	-1.05178	0.01146	0.08815
Akr1c14	-1.04767	0.001398	0.016046
Anpep	-1.04643	3.44E-11	1.84E-09
B230206H07Rik	-1.04386	1.21E-09	5.19E-08
Mir219a-2	-1.04355	0.001216	0.014308
Cysltr1	-1.03737	0.002997	0.029945
Gm49335	-1.03709	0.000321	0.004638
Tbxas1	-1.03535	1.90E-05	0.000376
Mir132	-1.03422	0.006897	0.058879
Fcgrt	-1.02716	1.05E-14	8.64E-13
Kcp	-1.02628	2.48E-06	6.05E-05

Inhba	-1.02334	2.68E-10	1.29E-08
Fam166b	-1.0214	0.003177	0.031525
AI467606	-1.01644	0.000899	0.011127
Cxcl12	-1.0138	4.59E-20	6.95E-18
Gm42495	-1.01182	0.003851	0.036956
Atp10a	-1.00999	9.56E-14	7.04E-12
Mstn	-1.00842	0.010893	0.084908
Adgra2	-1.00584	4.55E-21	7.44E-19
Hpgds	-1.00391	1.10E-06	2.86E-05
Bmx	-0.99734	0.002158	0.022884
Alkal2	-0.99364	0.00026	0.003885
Clec1a	-0.99275	0.006515	0.056265
Gm5089	-0.99083	2.71E-05	0.000517
Sned1	-0.99008	8.58E-28	2.86E-25
Mrc2	-0.98688	1.69E-11	9.37E-10
Sox21	-0.97757	1.95E-10	9.54E-09
Acvrl1	-0.97382	5.01E-18	5.69E-16
Gas1	-0.97272	2.47E-14	1.94E-12
AC121821.3	-0.96826	0.012402	0.093631
Slc23a3	-0.95964	0.001884	0.020459
Foxq1	-0.9585	7.26E-12	4.25E-10
Ptpn18	-0.95731	0.001382	0.015903
Gm20515	-0.957	9.37E-05	0.001579
A230009B12Rik	-0.9568	0.004833	0.044652
Foxd2	-0.9525	0.008533	0.070182
Fzd6	-0.95019	1.55E-06	3.92E-05
Slc8b1	-0.94666	3.26E-10	1.56E-08
Gng11	-0.94347	2.25E-11	1.23E-09
Pltp	-0.93891	8.66E-20	1.22E-17
Slc38a11	-0.93659	2.79E-05	0.000531
C1qtnf2	-0.93538	0.001414	0.016195
Aif1l	-0.93442	3.33E-10	1.59E-08
Sema3g	-0.93376	8.17E-10	3.63E-08
C030005K06Rik	-0.93113	0.000419	0.005845
Grap	-0.92437	8.02E-08	2.59E-06
Ccdc180	-0.92393	0.011908	0.090846
Crocc2	-0.92155	0.003575	0.034772
A330076C08Rik	-0.91952	6.72E-05	0.001172
3110045C21Rik	-0.91901	0.00625	0.054643
Gm49417	-0.91851	0.001037	0.012481
Celsr1	-0.91717	3.43E-12	2.12E-10
Gstt3	-0.91585	4.63E-05	0.000845

Dnah6	-0.91564	6.00E-05	0.00106
Pld4	-0.91564	4.07E-05	0.000752
Angptl2	-0.91479	2.65E-05	0.000507
Bnc2	-0.91289	0.00568	0.050737
Gm37415	-0.91262	0.009294	0.07508
Ccm2l	-0.91026	3.31E-10	1.58E-08
Ranbp3l	-0.90979	1.22E-08	4.58E-07
C030018K13Rik	-0.90948	0.00077	0.009817
Sall1	-0.90688	3.22E-19	4.19E-17
Rasgrp4	-0.90301	0.001883	0.020459
Abcc3	-0.90246	0.001236	0.014489
Pthlh	-0.90212	5.66E-08	1.90E-06
Aox3	-0.90172	0.000622	0.008135
A930005G22Rik	-0.89802	0.012707	0.095181
Adamts12	-0.89549	0.003667	0.035449
Mecom	-0.89349	0.000281	0.004159
Ninj2	-0.89164	0.000606	0.007959
Mob3b	-0.88965	3.83E-09	1.55E-07
Smad6	-0.88907	1.75E-06	4.39E-05
Trim36	-0.88893	3.88E-11	2.07E-09
Lhcgr	-0.88431	0.008069	0.067033
Wdr63	-0.88295	0.000825	0.010386
Six5	-0.87735	3.59E-06	8.50E-05
Olfml3	-0.87694	5.11E-16	4.91E-14
Smtn	-0.87398	1.56E-13	1.10E-11
Nkx2-2	-0.87391	1.07E-09	4.64E-08
Sp7	-0.87326	0.003555	0.034633
Ptgis	-0.8705	8.40E-05	0.001432
Daw1	-0.8703	0.0127	0.095181
Aspa	-0.87028	1.36E-11	7.53E-10
Bdnf	-0.8693	2.47E-14	1.94E-12
Vamp5	-0.86484	8.24E-05	0.00141
AC163221.1	-0.86478	0.000402	0.005646
Serpinb6b	-0.86103	0.000788	0.009988
Ephb4	-0.85796	5.32E-11	2.80E-09
Cped1	-0.85236	2.29E-05	0.000444
Gm26735	-0.84773	0.007723	0.064687
Morn5	-0.84469	0.010146	0.080225
Siglech	-0.84338	4.04E-07	1.14E-05
Sox2ot	-0.84214	4.75E-18	5.43E-16
Gm44758	-0.83827	0.002283	0.023994
Nipal4	-0.83347	1.09E-07	3.43E-06

AC124108.1	-0.83035	2.83E-06	6.79E-05
Dnaaf1	-0.82677	0.010293	0.081112
BC028528	-0.82574	0.000384	0.005439
Adamtsl3	-0.82327	0.000846	0.010647
Gldc	-0.82283	2.40E-16	2.43E-14
Plscr4	-0.81649	1.25E-06	3.21E-05
D030068K23Rik	-0.81406	0.011766	0.090055
Cxcr4	-0.80845	0.000608	0.007984
Smagp	-0.80714	0.003671	0.035449
Eva1b	-0.80603	0.000429	0.005943
Ccnb2	-0.79694	0.003496	0.034114
Aldh1a3	-0.79591	0.006663	0.057329
Ccdc146	-0.79478	0.001261	0.014734
Abca9	-0.79397	5.35E-05	0.000959
Rdh5	-0.79359	0.001556	0.017506
Gna15	-0.79074	0.000559	0.007444
Heyl	-0.79016	2.23E-05	0.000433
Wnt7a	-0.79009	2.90E-08	1.02E-06
Aspn	-0.7895	0.009721	0.077846
Foxd1	-0.78607	0.004779	0.044243
She	-0.78589	0.000132	0.002147
Kank2	-0.78498	1.32E-13	9.41E-12
Dock6	-0.78339	7.51E-24	1.56E-21
Hacd4	-0.77923	0.003061	0.03051
A930033H14Rik	-0.77822	7.74E-05	0.001331
Hic1	-0.77483	0.010577	0.083031
Lmod1	-0.77472	0.000178	0.002773
Meig1	-0.77311	0.000239	0.003602
Mycn	-0.77229	9.77E-09	3.76E-07
Eya2	-0.77143	0.000848	0.01066
P2ry13	-0.77027	3.04E-06	7.28E-05
Dnajb13	-0.76858	0.005476	0.049228
Phf21b	-0.76746	3.39E-08	1.18E-06
Kif26a	-0.76529	2.98E-07	8.65E-06
Ogn	-0.76474	6.10E-05	0.001076
Cd248	-0.76274	8.86E-08	2.84E-06
C230072F16Rik	-0.76053	0.009239	0.074736
Npas4	-0.75953	0.004788	0.044294
Hcar1	-0.75828	0.012735	0.095281
Sox2	-0.75821	3.28E-23	6.48E-21
Ctsh	-0.75677	4.17E-09	1.68E-07
Dock8	-0.75559	1.01E-05	0.000212

Tbx3	-0.75538	4.46E-05	0.000816
Gm34256	-0.75435	0.00138	0.015891
Prrx1	-0.75371	3.75E-07	1.06E-05
C230021G24Rik	-0.75208	0.000927	0.011373
Gm3693	-0.75201	0.006066	0.053431
Sspo	-0.75169	0.009811	0.07834
Lrrk1	-0.75074	5.26E-06	0.000119
Cracr2b	-0.74839	0.000317	0.004588
Fgd5	-0.74741	1.44E-10	7.21E-09
Erbb3	-0.74147	3.23E-06	7.70E-05
Myoc	-0.73934	7.54E-10	3.38E-08
Gli3	-0.7392	8.95E-08	2.85E-06
H2-Aa	-0.73919	0.005767	0.051373
Rab11fip1	-0.73407	3.92E-06	9.18E-05
Bmp6	-0.73387	7.44E-08	2.42E-06
Slc6a13	-0.73377	0.000878	0.010932
Nat8	-0.73372	0.00951	0.076461
Bdh2	-0.73215	0.00409	0.038734
Lamc3	-0.73051	1.29E-07	4.00E-06
Col1a1	-0.72983	8.98E-07	2.38E-05
Gjc2	-0.72907	5.72E-13	3.81E-11
Lsr	-0.72872	1.19E-05	0.000246
A930017K11Rik	-0.72846	0.007704	0.064631
Gm9917	-0.72779	0.004407	0.041231
Wnt9a	-0.72363	3.55E-10	1.67E-08
2010007H06Rik	-0.72197	0.00265	0.027068
Tent5c	-0.71759	0.002526	0.026098
Lair1	-0.715	1.69E-07	5.11E-06
Fmod	-0.71393	0.000351	0.005007
Mcam	-0.71369	3.54E-14	2.74E-12
Cavin2	-0.71251	3.75E-09	1.52E-07
Fgfr2	-0.71239	1.47E-24	3.22E-22
Tnc	-0.71085	5.97E-07	1.63E-05
Cav1	-0.70988	9.49E-12	5.42E-10
Plau	-0.70944	0.005382	0.048429
Nr4a3	-0.70934	5.45E-06	0.000123
Map3k19	-0.70931	1.81E-05	0.00036
Txlnb	-0.70885	0.00079	0.010008
Myh11	-0.70848	2.57E-09	1.07E-07
Sox10	-0.70383	2.57E-21	4.43E-19
Cdc42ep1	-0.70371	1.90E-19	2.57E-17
Ecm2	-0.70291	2.00E-05	0.000393

Tec	-0.70139	0.001226	0.014401
Rep15	-0.70003	0.011229	0.086977
Rad51ap2	-0.6988	0.011258	0.087099
Cavin1	-0.69618	4.62E-14	3.50E-12
Eogt	-0.69325	1.95E-19	2.62E-17
Cbfa2t3	-0.69285	2.17E-09	9.04E-08
Jcad	-0.69239	1.26E-18	1.56E-16
Dock2	-0.69228	0.000187	0.002898
Clec3b	-0.69133	0.003589	0.034876
Exoc3l4	-0.69097	0.00031	0.004479
Gm266	-0.69067	0.005545	0.049756
Gjb1	-0.68727	6.92E-12	4.08E-10
Gm3764	-0.68646	1.94E-32	7.86E-30
Arhgef19	-0.68593	3.72E-12	2.27E-10
Cckbr	-0.68513	5.02E-12	3.01E-10
Eln	-0.6842	3.33E-15	2.91E-13
Myof	-0.68138	1.33E-06	3.40E-05
Aebp1	-0.68069	3.22E-19	4.19E-17
Caskin2	-0.67971	2.23E-13	1.55E-11
Abcg2	-0.67388	1.22E-13	8.84E-12
Lama1	-0.67281	7.13E-05	0.001237
Pln	-0.67045	0.003532	0.03445
Gm37940	-0.66893	0.011447	0.088104
Ascl1	-0.66829	5.95E-05	0.001053
Lrmp	-0.66756	0.003378	0.033188
Myom3	-0.66643	0.004616	0.042949
Serpinb1b	-0.6658	0.013531	0.099675
Sh3tc1	-0.66489	0.001417	0.01622
1110002E22Rik	-0.66457	3.53E-05	0.000659
Car2	-0.66436	4.80E-30	1.69E-27
Sypl2	-0.66386	0.002196	0.023192
Wdfy4	-0.66304	0.001578	0.017689
AC115119.1	-0.66256	0.006357	0.055312
Gm49130	-0.66173	0.009448	0.076073
Hydin	-0.6616	0.000424	0.005889
Enpp1	-0.66036	1.77E-05	0.000354
Plekho2	-0.65793	6.72E-06	0.000148
Car14	-0.65647	4.02E-10	1.88E-08
Col4a6	-0.65141	0.001353	0.015621
Bcam	-0.64997	5.34E-18	6.04E-16
Baiap2l2	-0.64854	0.002154	0.022856
Zfhx2os	-0.64801	8.18E-05	0.001401

Tgfbi	-0.64792	3.10E-06	7.41E-05
Gli1	-0.64747	8.61E-05	0.001462
Acta2	-0.64715	8.09E-09	3.17E-07
Ankub1	-0.64682	0.000616	0.008072
Ndnf	-0.64627	1.82E-06	4.54E-05
2810459M11Rik	-0.64516	0.000108	0.001791
Fgd2	-0.64428	0.000607	0.007971
Gask1b	-0.64294	0.000527	0.007077
Egfl7	-0.6411	6.34E-11	3.29E-09
Evi2a	-0.63709	4.93E-08	1.66E-06
Sfn	-0.63666	0.000717	0.009219
Gm42656	-0.63547	0.006992	0.059569
Tead2	-0.6334	0.001933	0.020894
Acacb	-0.63215	0.000909	0.011227
Gulp1	-0.63179	0.000761	0.009712
Gab1	-0.63053	1.62E-14	1.31E-12
Mfng	-0.62842	0.000192	0.002963
Rhobtb1	-0.62706	0.003568	0.034727
Bmp4	-0.62475	0.00124	0.014528
Tnfaip6	-0.62195	4.46E-06	0.000103
Tmem119	-0.62053	2.06E-08	7.39E-07
Kcnk13	-0.62045	7.67E-06	0.000167
Efs	-0.61821	5.79E-10	2.61E-08
Emp3	-0.61593	0.0051	0.046504
Pantr2	-0.61526	0.001926	0.02084
Gask1a	-0.61224	0.001035	0.012459
Dpp4	-0.61211	0.000275	0.004073
Alpl	-0.61073	5.64E-07	1.55E-05
Col26a1	-0.6103	7.01E-07	1.89E-05
Adcy8	-0.60872	4.49E-06	0.000103
Cartpt	-0.60754	0.004169	0.039388
Arap3	-0.60513	4.57E-08	1.56E-06
Atp13a5	-0.60422	2.80E-06	6.76E-05
9330188P03Rik	-0.60352	0.007514	0.063308
Slc13a4	-0.60052	1.47E-05	0.0003
Dlx6os1	-0.59875	3.69E-06	8.73E-05
Fmnl3	-0.59771	6.78E-10	3.05E-08
Aif1	-0.59733	0.000773	0.009837
Klf10	-0.59616	5.93E-08	1.99E-06
Ptch1	-0.59493	9.96E-13	6.47E-11
Sox1	-0.59406	0.000126	0.00205
Bmp3	-0.59264	1.46E-07	4.46E-06

Slc7a5	-0.59001	2.84E-15	2.53E-13
Tmem204	-0.58765	0.000522	0.007026
Cmtm7	-0.58588	0.012756	0.095357
Egflam	-0.58575	0.0002	0.003086
Il17rd	-0.5854	2.87E-05	0.000544
Mtss2	-0.58298	5.04E-16	4.87E-14
Klf4	-0.58252	0.001772	0.01951
Tnfrsf19	-0.58204	6.20E-23	1.19E-20
Csf3r	-0.58192	0.004398	0.04117
Col1a2	-0.58187	8.71E-07	2.32E-05
Padi2	-0.5809	5.97E-15	5.06E-13
Opalin	-0.57899	0.000231	0.003488
9130019O22Rik	-0.57492	0.002121	0.022561
Zfp114	-0.57457	0.01053	0.082697
Gm26606	-0.57128	0.009066	0.073651
Kcng1	-0.56472	0.000492	0.006686
Slc9a3r2	-0.56227	3.36E-16	3.33E-14
Def6	-0.5619	0.000753	0.009628
Hspg2	-0.56019	2.45E-11	1.32E-09
Trpc6	-0.55907	0.000174	0.002733
Ccdc8	-0.55831	0.000994	0.012089
Osr1	-0.55744	0.00982	0.07836
2900052L18Rik	-0.55683	0.000289	0.004246
Rxfp3	-0.55377	0.004674	0.04342
Kctd12b	-0.55351	0.001012	0.012288
Abcc4	-0.54931	8.87E-07	2.35E-05
Clic5	-0.54899	5.82E-05	0.001036
Tnfsf12	-0.54603	0.000627	0.008188
Ptpn14	-0.54479	0.000895	0.011088
Dock5	-0.54461	1.96E-08	7.10E-07
Rfx2	-0.54387	0.000284	0.004169
Zfp773	-0.54097	0.002604	0.026735
Atp2a3	-0.53938	1.51E-05	0.000306
Ocln	-0.53886	4.69E-05	0.000853
Vsir	-0.53794	0.000753	0.009632
Derl3	-0.53652	0.004693	0.043535
C030029H02Rik	-0.53362	0.009632	0.077344
Sdf2l1	-0.53314	0.002849	0.02869
Gpr37	-0.53234	1.49E-15	1.36E-13
Sh3tc2	-0.53079	0.007537	0.063419
Otx1	-0.52851	6.68E-05	0.001167
Trem2	-0.52799	0.000675	0.0087

Rnf43	-0.52778	0.005931	0.052575
Rasl12	-0.52683	0.001017	0.012325
Mas1	-0.52602	1.06E-07	3.35E-06
Nr2e1	-0.52448	8.15E-06	0.000176
Ets1	-0.52345	7.89E-06	0.000171
Kcnv1	-0.5231	1.98E-08	7.15E-07
Mmp2	-0.52161	0.008058	0.067013
Srpk3	-0.52158	0.000298	0.004352
Gm39326	-0.52146	0.000987	0.01201
Gm973	-0.51906	7.95E-05	0.001364
Crtap	-0.51795	0.000412	0.005761
Prkg2	-0.51609	0.000216	0.003304
Crybb1	-0.51353	0.006921	0.059058
Apbb1ip	-0.51196	0.001074	0.012878
Opn3	-0.51081	0.013387	0.098909
Fjx1	-0.50957	1.98E-11	1.08E-09
Slc13a3	-0.50932	0.000504	0.006843
Ldlrad3	-0.50908	1.64E-06	4.13E-05
Pik3c2b	-0.50895	3.97E-14	3.03E-12
Hrh1	-0.50837	1.15E-06	2.99E-05
Ramp2	-0.50752	0.000156	0.002475
Mxra8	-0.50643	6.48E-05	0.001135
Bfsp2	-0.50536	0.002096	0.022396
Prdm16os	-0.50458	3.27E-06	7.80E-05
Acad12	-0.5045	0.008989	0.073164
1700007K13Rik	-0.50442	0.007053	0.059943
Cxxc5	-0.5044	2.26E-13	1.57E-11
Gstt2	-0.50413	0.006696	0.057483
Emcn	-0.50336	0.000274	0.00407
Gm15721	-0.50322	0.01181	0.090313
Hist2h2be	-0.50255	0.000672	0.008669
Foxf2	-0.50253	0.001921	0.020806
Nat8f4	-0.50131	0.001458	0.01659
Frem2	-0.50124	0.010095	0.079926
Pllp	-0.49802	3.95E-06	9.23E-05
Car12	-0.49772	0.007096	0.060246
Pcdhac1	-0.4977	0.004153	0.039292
Ccdc171	-0.49721	0.00156	0.017523
AW047730	-0.49699	2.55E-06	6.22E-05
2810410L24Rik	-0.49613	0.001164	0.013787
Megf6	-0.49559	0.001217	0.014311
Dynlt1a	-0.49507	0.005766	0.051373

Ltbp4	-0.49464	3.88E-12	2.36E-10
Rfx4	-0.49278	8.70E-06	0.000187
Nos3	-0.49187	2.46E-05	0.000473
Gm29514	-0.49117	0.005877	0.052157
St8sia4	-0.4899	0.000153	0.002444
Adcyap1	-0.48951	0.004018	0.038203
Lmo2	-0.48944	4.26E-05	0.000783
Zfp710	-0.48932	4.74E-10	2.19E-08
Bche	-0.48913	0.006754	0.057899
Paqr6	-0.48766	7.89E-05	0.001353
C2cd4c	-0.48736	9.69E-05	0.001619
Scarf2	-0.48637	0.000464	0.006351
Prelp	-0.48406	4.83E-07	1.34E-05
Cdc42ep2	-0.48109	0.000283	0.004161
Mill2	-0.48047	0.005977	0.052867
Traf4	-0.4803	9.89E-06	0.000209
Chst3	-0.47719	0.002159	0.022884
Gcnt4	-0.47577	0.000282	0.004161
Csrp2	-0.47516	0.002244	0.023636
Tmem74b	-0.47445	0.007622	0.063989
Rspo2	-0.47359	0.002804	0.028389
Vwa1	-0.47333	1.31E-06	3.34E-05
Lppos	-0.47292	0.002238	0.023601
Rnd3	-0.4723	0.001388	0.015961
Dok5	-0.4705	1.59E-06	4.00E-05
Ermn	-0.46982	1.36E-05	0.00028
Bmp7	-0.46888	0.000272	0.00404
Ap5b1	-0.46826	0.001219	0.014319
Slitrk2	-0.4675	2.53E-06	6.17E-05
Myl9	-0.46743	7.21E-06	0.000158
Sox12	-0.46628	9.43E-10	4.16E-08
Pecam1	-0.46573	0.000112	0.001854
Glis2	-0.46536	1.07E-06	2.81E-05
Garem2	-0.46465	1.95E-07	5.85E-06
Adamts15	-0.46392	8.96E-06	0.000191
Fhod1	-0.46285	0.000349	0.004984
Zbtb46	-0.46284	0.000428	0.005929
Slco2b1	-0.46178	0.002692	0.027369
Stox1	-0.46011	0.007952	0.066278
Gatm	-0.45997	9.95E-16	9.22E-14
Maml3	-0.45744	0.000181	0.00283
Sstr2	-0.45676	8.49E-06	0.000182

Ddr2	-0.45574	0.000458	0.006282
Tmem74	-0.45292	0.001935	0.020894
Ttc7	-0.45243	9.19E-06	0.000195
Nptx2	-0.45173	0.000164	0.002587
Lims2	-0.45121	0.000191	0.002956
Nrp1	-0.45103	0.004959	0.045503
Homer1	-0.44782	2.80E-09	1.16E-07
Tprkb	-0.44743	3.54E-08	1.22E-06
Dlx1as	-0.44733	0.004979	0.045641
Lamb2	-0.44601	1.86E-13	1.30E-11
Cnn2	-0.44592	0.001112	0.013259
Dusp4	-0.44423	5.68E-06	0.000127
AC109619.1	-0.44422	0.002334	0.024462
Tgfb1	-0.4436	0.000336	0.004831
Cecr2	-0.44262	0.000164	0.002588
Foxo6	-0.44118	2.30E-05	0.000445
Pde8a	-0.43796	5.10E-05	0.000923
Lef1	-0.437	0.000787	0.009988
Islr	-0.435	0.003407	0.033458
Ephb3	-0.43457	1.29E-07	4.00E-06
Phldb1	-0.43455	1.03E-12	6.67E-11
Emp2	-0.43448	3.28E-06	7.81E-05
Tagln	-0.43437	0.007417	0.062632
Htra3	-0.43385	0.006099	0.053664
Sstr3	-0.43271	3.41E-07	9.71E-06
Colec12	-0.43123	0.00082	0.010344
Cdh11	-0.43086	1.16E-07	3.63E-06
Cdyl2	-0.4304	0.001158	0.013724
Capn3	-0.42852	0.004943	0.04543
Zfp467	-0.42836	8.12E-10	3.62E-08
Ugt8a	-0.42834	2.89E-07	8.39E-06
Usp43	-0.42661	0.00896	0.073017
Fam53b	-0.4257	2.25E-06	5.53E-05
Acads	-0.4242	0.005619	0.050246
Vwa3b	-0.42407	0.009885	0.078706
Tmem98	-0.42353	0.001198	0.014127
Rlbp1	-0.42299	0.000378	0.005359
Gna12	-0.41973	1.94E-16	1.97E-14
Gm2115	-0.41972	8.00E-05	0.00137
Nkd1	-0.41967	0.002355	0.024671
Frmd8	-0.41897	6.98E-07	1.88E-05
Arhgap29	-0.41654	9.19E-06	0.000195

Kif21b	-0.416	1.08E-20	1.74E-18
Fam163a	-0.41522	7.36E-05	0.001273
Lasp1	-0.41327	7.39E-12	4.30E-10
Sema6d	-0.40667	1.10E-09	4.75E-08
Tmem200a	-0.40376	0.000211	0.003239
Kifc3	-0.4036	6.79E-08	2.26E-06
Ak4	-0.4016	0.009953	0.07912
Stk10	-0.40159	0.000944	0.011565
C630043F03Rik	-0.4013	0.007304	0.061818
Zfp36l2	-0.40101	7.93E-08	2.56E-06
Neurod6	-0.40096	0.00028	0.004151
Tmem109	-0.40081	8.88E-08	2.84E-06
Plxnb3	-0.39838	2.12E-08	7.58E-07
Tbc1d8b	-0.39743	0.002432	0.025347
Rps6ka1	-0.39699	1.75E-05	0.000349
Bcar3	-0.39695	0.013102	0.097397
Slc38a3	-0.39642	1.41E-09	5.99E-08
Mid1ip1	-0.3958	4.88E-14	3.68E-12
Zfp395	-0.3952	2.82E-05	0.000536
Mpzl1	-0.39457	9.64E-05	0.001613
Hist1h1c	-0.39348	0.010074	0.07979
Sall3	-0.39303	0.001803	0.019802
Nr3c1	-0.39273	4.59E-09	1.83E-07
Fnbp1	-0.39235	1.47E-18	1.78E-16
Cbln2	-0.391	3.74E-07	1.06E-05
Klhdc8b	-0.39096	2.82E-07	8.20E-06
Wls	-0.39002	2.03E-09	8.56E-08
Gm6145	-0.38875	1.11E-05	0.00023
Vgf	-0.3879	2.15E-08	7.66E-07
Flrt1	-0.38787	2.50E-08	8.87E-07
Plekho1	-0.38778	0.000104	0.001729
Zic2	-0.38764	0.000347	0.00497
Apcdd1	-0.38671	0.000645	0.008385
Mtss1	-0.38606	2.01E-06	4.97E-05
Ppp1r35	-0.38581	0.001392	0.015989
Pcsk1	-0.38504	0.000122	0.002001
Appl2	-0.38491	3.24E-12	2.00E-10
Adrb1	-0.38462	1.69E-05	0.000339
Crybg3	-0.38422	0.0006	0.007893
Hdac5	-0.38389	3.17E-08	1.11E-06
Tmc7	-0.38325	0.000176	0.002753
Tyro3	-0.38134	6.86E-08	2.27E-06

Cpne2	-0.37963	0.001541	0.017367
Egr3	-0.37896	1.02E-06	2.69E-05
Fat4	-0.3786	0.001059	0.012723
Trib2	-0.37846	0.000119	0.001957
Csgalnact1	-0.37809	0.000227	0.003443
Abca7	-0.37788	1.11E-06	2.90E-05
Ppp1r14a	-0.37734	0.000913	0.011252
Slain1	-0.37654	1.62E-08	6.02E-07
Nwd1	-0.37596	7.18E-08	2.34E-06
Adam19	-0.37401	0.000282	0.004161
Card10	-0.37391	0.003228	0.031865
Itpripl2	-0.37388	0.00424	0.039993
Vtn	-0.3734	4.58E-09	1.83E-07
Dhrs3	-0.373	2.12E-05	0.000414
Kank3	-0.37205	1.08E-05	0.000226
Map6d1	-0.37133	1.09E-08	4.18E-07
Rtn4rl2	-0.37124	1.12E-08	4.23E-07
Slc30a10	-0.37068	0.000355	0.00506
Unc5b	-0.37003	6.57E-07	1.78E-05
Rassf3	-0.36994	0.001635	0.018224
Lama5	-0.36979	5.18E-05	0.000936
Gm26794	-0.3688	0.012556	0.094434
Hdac9	-0.36854	3.50E-08	1.21E-06
Gjc3	-0.36801	7.65E-06	0.000167
Smo	-0.36705	0.000337	0.004835
Bgn	-0.36703	8.76E-06	0.000187
Ccnd1	-0.36695	2.99E-05	0.000565
Sh3d19	-0.3658	0.000239	0.003602
Amotl2	-0.36577	5.86E-05	0.00104
Synj2	-0.36524	1.09E-07	3.44E-06
Inpp5d	-0.36401	0.000853	0.0107
Spred3	-0.36365	6.91E-08	2.27E-06
Myorg	-0.36196	0.000326	0.004694
Cemip	-0.36077	0.005061	0.046233
Wdr78	-0.36024	0.001616	0.018033
Vav3	-0.36005	0.013278	0.09832
Fam234a	-0.35924	4.53E-07	1.26E-05
Bcorl1	-0.35914	0.000189	0.002921
Yes1	-0.3589	0.000297	0.00435
Mmp15	-0.35872	2.79E-07	8.15E-06
Tom1l1	-0.35848	0.00025	0.003747
Fam222a	-0.35817	0.012336	0.093267

Pls1	-0.35721	0.00025	0.003751
Prag1	-0.35712	0.000441	0.006071
Tmem88b	-0.35712	6.67E-06	0.000147
Xylt1	-0.35693	2.45E-07	7.22E-06
Pcdh18	-0.35693	0.006432	0.055808
Nrep	-0.35509	0.000145	0.002321
Shroom3	-0.3549	0.006236	0.05459
C1ql1	-0.35452	0.002221	0.023437
Nog	-0.35432	0.002678	0.027261
Ltbp1	-0.35349	0.006248	0.054643
Rftn1	-0.3526	0.005464	0.049148
Etv5	-0.35104	1.90E-08	6.91E-07
Axin2	-0.35076	3.33E-07	9.54E-06
Kcnk3	-0.35047	1.38E-07	4.25E-06
Nat8f1	-0.35032	0.007042	0.059874
Mex3b	-0.34995	0.001021	0.012345
Pcdh8	-0.34985	0.00143	0.016305
Tst	-0.34862	0.002645	0.027036
Gm11611	-0.34697	0.001538	0.017344
Sgms1	-0.34575	3.44E-06	8.17E-05
Elovl7	-0.34538	0.002376	0.024836
Rasgef1b	-0.34509	0.000116	0.001912
Prkd3	-0.34388	0.000151	0.002407
Rarg	-0.34329	0.000386	0.00546
Cyren	-0.34284	0.010652	0.083544
Phlda1	-0.34208	0.002953	0.029586
Dact2	-0.34137	2.23E-05	0.000433
2310022B05Rik	-0.34119	7.68E-05	0.001321
Eml1	-0.34041	1.55E-06	3.91E-05
P4ha1	-0.33969	0.002503	0.025932
Folh1	-0.33873	0.001914	0.020747
Cttnbp2	-0.33848	4.46E-05	0.000816
Mapk7	-0.33833	1.19E-05	0.000248
Marveld1	-0.33742	0.005241	0.047322
Lpar1	-0.33619	2.64E-05	0.000506
Gpc6	-0.33605	0.005887	0.052222
Itgb5	-0.33529	0.004737	0.043901
Maf	-0.33507	2.30E-05	0.000445
Cobll1	-0.33439	0.000882	0.010972
Gm11175	-0.33434	0.006047	0.053333
Gdf11	-0.33403	0.000235	0.003546
Zeb2	-0.33402	3.76E-06	8.87E-05

Bahcc1	-0.33387	1.05E-06	2.76E-05
Prr18	-0.33372	3.80E-06	8.92E-05
Kif13a	-0.33195	2.04E-07	6.11E-06
P2rx7	-0.33164	0.005183	0.046946
Pak6	-0.3315	5.80E-06	0.00013
Lrrtm1	-0.33109	4.98E-06	0.000113
Cdk2ap1	-0.33028	0.002672	0.027211
Crhr1	-0.32964	5.59E-05	0.000999
Pdia6	-0.32933	0.002126	0.022586
Lrp5	-0.32925	0.000227	0.003443
Ston2	-0.32784	0.00052	0.006996
Elk3	-0.32527	0.010875	0.084805
Plekhh3	-0.32525	0.000266	0.003963
Plekhh2	-0.32333	0.010405	0.081821
1700086L19Rik	-0.32332	0.003854	0.036967
Als2cl	-0.32326	4.43E-05	0.000812
Tmem28	-0.32257	0.001429	0.016305
Map3k20	-0.32255	0.002824	0.0285
Pcsk6	-0.32233	0.000143	0.002296
Dusp14	-0.32216	0.000147	0.002344
Dock1	-0.32192	2.35E-06	5.76E-05
Paqr7	-0.32148	1.05E-07	3.34E-06
Pdzrn3	-0.32133	9.50E-05	0.001596
Ctbp2	-0.32095	0.006215	0.054483
Jag2	-0.32019	3.87E-09	1.56E-07
Nr2f1	-0.31995	1.93E-08	7.02E-07
Dsel	-0.31981	0.000654	0.008476
Ankrd34a	-0.31828	1.28E-06	3.29E-05
Kcna4	-0.31825	0.00044	0.006071
Nectin3	-0.3172	0.000299	0.004353
Sall2	-0.31718	4.90E-07	1.36E-05
Klf16	-0.31656	7.62E-07	2.05E-05
Plxdc2	-0.31596	4.16E-05	0.000767
Map3k1	-0.31532	0.00087	0.01086
Wnt7b	-0.31519	0.009391	0.075796
Pamr1	-0.3138	0.012053	0.091684
Olig2	-0.31374	2.68E-06	6.48E-05
Nwd2	-0.31209	5.27E-06	0.000119
Hexim1	-0.31191	6.07E-06	0.000135
Pld2	-0.31156	7.38E-06	0.000161
Tafa1	-0.31063	0.000942	0.011551
Snx7	-0.31034	0.002266	0.023842

St8sia5	-0.30923	4.51E-06	0.000104
Vgll4	-0.30896	0.000508	0.006873
Gm26917	-0.3079	0.005186	0.046946
Slc6a6	-0.3063	5.80E-05	0.001035
Tmem121b	-0.30592	3.25E-08	1.13E-06
Nol4l	-0.30494	9.49E-09	3.66E-07
Gm9954	-0.30489	0.002651	0.027068
Fmnl1	-0.30481	4.00E-06	9.31E-05
Fgf11	-0.30371	0.007432	0.062734
Gdpd2	-0.3035	0.002009	0.021585
Ttll3	-0.30344	0.002836	0.028582
Rasa2	-0.30306	0.000465	0.006364
Jup	-0.30295	0.000544	0.007282
Kctd12	-0.30143	0.000211	0.003233
Lhfpl2	-0.30057	0.003317	0.032642
Adra1d	-0.30034	0.005497	0.049393
Qk	-0.30032	7.37E-09	2.90E-07
Tmem64	-0.30023	0.001207	0.014218
Otud1	-0.29858	0.00194	0.020923
Rhoq	-0.29817	2.41E-05	0.000465
Acaa2	-0.29728	0.009876	0.07869
Metrn	-0.29672	5.84E-06	0.000131
Igdcc4	-0.29588	0.000397	0.005592
Kcna6	-0.29346	6.46E-08	2.16E-06
Lingo1	-0.29316	3.05E-07	8.80E-06
Gprc5b	-0.29271	4.70E-12	2.83E-10
Bcor	-0.29189	2.37E-05	0.000457
Sowahb	-0.29153	0.008221	0.068099
Ubtd2	-0.29129	0.005256	0.047409
Bsg	-0.2907	2.32E-11	1.26E-09
Xpo1	-0.29062	4.06E-06	9.41E-05
Diras2	-0.29057	4.38E-06	0.000101
Cdh9	-0.29052	0.001649	0.018352
Hist1h2bc	-0.29045	0.006225	0.05454
Tgfb2	-0.29034	0.013029	0.097012
Nr3c2	-0.29025	0.002479	0.025708
Fgd6	-0.2898	0.003048	0.030413
Nfia	-0.28879	4.76E-06	0.000109
Tmem200c	-0.28858	0.004681	0.043447
Sfpq	-0.28848	0.000584	0.007743
Afap1	-0.28837	1.71E-05	0.000343
Shc3	-0.28829	0.005023	0.045957

Bach2	-0.28794	0.002952	0.029586
Pou3f3	-0.28785	6.90E-06	0.000152
Entpd1	-0.28739	0.00665	0.057249
Tmeff2	-0.28636	1.67E-05	0.000336
Ablim1	-0.28629	6.74E-08	2.24E-06
Gpr12	-0.28628	0.001268	0.014789
Stard9	-0.28537	5.01E-05	0.000909
Cryab	-0.28384	0.000501	0.006799
Gprin1	-0.28375	2.09E-05	0.000409
Hapln1	-0.28316	0.007769	0.064988
Gal3st1	-0.28095	0.007174	0.060801
Numb	-0.28093	5.28E-05	0.000949
Pcsk5	-0.28091	0.013331	0.098634
Vstm2b	-0.28068	0.000381	0.005398
Eya1	-0.28006	0.011006	0.085606
Utrn	-0.27916	2.75E-05	0.000523
Fam13c	-0.27888	0.001668	0.018518
Dok4	-0.27829	0.002566	0.026412
Phkg1	-0.27797	0.00014	0.002249
Tmem63a	-0.27745	0.000854	0.0107
Acvr1	-0.27707	8.99E-05	0.001522
Skida1	-0.27694	0.009953	0.07912
Plpp3	-0.27686	2.17E-07	6.49E-06
Fam43b	-0.27549	0.002399	0.025063
Mylip	-0.27527	0.00181	0.019838
Shisal1	-0.27474	0.002538	0.02618
D16Ertd472e	-0.27464	0.002914	0.02926
Spats2l	-0.27389	0.000203	0.003117
Slc22a23	-0.27302	7.31E-06	0.00016
Sox6	-0.2729	0.000406	0.005687
Kctd15	-0.27287	0.007211	0.061089
Hcn3	-0.2724	0.005037	0.046041
Lrp4	-0.27202	6.11E-05	0.001077
Ccp110	-0.27168	4.01E-06	9.32E-05
Mical2	-0.27161	4.58E-06	0.000105
Cmtm5	-0.27142	6.32E-05	0.001109
Fam20c	-0.27086	0.000689	0.008866
Tpcn1	-0.27082	1.12E-06	2.91E-05
Cacng3	-0.27061	3.03E-06	7.26E-05
Vegfa	-0.27035	0.000587	0.007779
Tmem144	-0.26921	0.008484	0.069903
Sema3c	-0.26916	0.005864	0.05207

Fgd1	-0.26867	0.001146	0.013613
Fam174b	-0.26811	0.002107	0.02248
Pyurf	-0.2681	0.009822	0.07836
R3hdm1	-0.268	3.37E-07	9.62E-06
Emx1	-0.26754	0.01227	0.092994
Nanos1	-0.26601	0.000367	0.00522
Ppp2r5a	-0.2653	1.08E-05	0.000226
Shisa6	-0.26529	0.010588	0.083089
Tmem150a	-0.26493	0.011552	0.088745
Heatr5a	-0.26487	0.006381	0.055494
Amd1	-0.26335	0.006422	0.055742
Raver2	-0.26316	0.009265	0.074909
Inppl1	-0.26165	0.003197	0.031656
Raph1	-0.26159	0.001571	0.017631
Calr	-0.26089	0.00264	0.027013
Trim8	-0.26012	6.53E-07	1.78E-05
Golim4	-0.25979	0.000359	0.00511
Fkbp4	-0.2596	7.11E-05	0.001233
Hivep1	-0.25901	3.65E-05	0.00068
Wscd1	-0.25867	5.24E-05	0.000945
Dtx4	-0.25802	0.002689	0.02736
Kirrel	-0.25682	0.01257	0.094503
Rasa1	-0.25663	0.003283	0.03232
Ypel2	-0.25647	0.000416	0.005806
Ehbp1l1	-0.25487	0.000878	0.010932
Dtx1	-0.25467	6.02E-06	0.000134
Grasp	-0.25405	0.000425	0.00589
Bcl9l	-0.25394	3.09E-05	0.000582
Mdga1	-0.25345	0.003722	0.035899
Nr2f6	-0.25326	0.000157	0.00249
Usp31	-0.25301	9.57E-05	0.001605
Tnrc18	-0.25266	8.17E-08	2.63E-06
Hexa	-0.25262	1.94E-05	0.000382
Afap1l2	-0.25255	0.004369	0.040941
Tada1	-0.25173	0.003949	0.037699
Taf4	-0.251	0.000351	0.005007
Josd2	-0.25062	0.000293	0.004298
Prdm16	-0.25056	0.008008	0.066624
Elovl6	-0.25007	0.009886	0.078706
Pdgfb	-0.24999	6.72E-05	0.001172
Myadm	-0.24994	0.000599	0.007881
Lactb	-0.24972	0.011203	0.086811

Hsp90b1	-0.2497	0.00143	0.016305
Phgdh	-0.24959	0.001266	0.014775
Ubtf	-0.24906	1.22E-06	3.14E-05
2510009E07Rik	-0.24888	0.000119	0.001954
Tmem229a	-0.24829	0.000167	0.002627
Tle4	-0.24807	0.00048	0.006528
Lgi4	-0.24771	1.75E-05	0.000349
Ttl	-0.2477	0.001167	0.013815
Lgr4	-0.24768	0.001565	0.017566
Map3k5	-0.24736	0.000901	0.011144
Ankrd6	-0.24728	0.000855	0.010705
Ttyh2	-0.24692	0.012438	0.093774
Tcf3	-0.2467	5.27E-05	0.000948
Pcdh1	-0.24663	8.82E-06	0.000189
Fam171a2	-0.24547	0.000143	0.002296
Pou2f1	-0.24544	0.000406	0.005687
Cd276	-0.24507	0.010139	0.080225
Prmt2	-0.24472	0.00387	0.037092
Plin3	-0.24451	0.010861	0.084797
Sgsm1	-0.24442	0.005119	0.04658
Grm3	-0.24377	0.002095	0.022396
Ccdc167	-0.24362	0.006781	0.058079
Usp28	-0.24167	0.003753	0.036151
Phlpp1	-0.24137	3.61E-06	8.54E-05
Ankrd50	-0.24011	4.81E-05	0.000872
Stx2	-0.23985	0.007981	0.066466
4931428F04Rik	-0.2389	0.001302	0.015118
Mpp6	-0.23878	0.000637	0.008304
Kcnip3	-0.23845	3.11E-05	0.000585
Jam2	-0.23828	0.000922	0.011323
Usp21	-0.23816	0.001425	0.016279
Slit2	-0.23813	0.004971	0.045589
Mpdz	-0.23799	0.001209	0.014236
Micall1	-0.23789	4.86E-06	0.00011
Rtn4r	-0.23727	0.008298	0.068581
Laptm5	-0.2364	0.000919	0.011307
Hcfc2	-0.23635	0.000224	0.003409
Nim1k	-0.23485	0.01169	0.089622
3110039I08Rik	-0.23398	0.009109	0.073942
Arhgap33	-0.23304	1.66E-05	0.000334
Spred2	-0.23278	0.000402	0.005646
Acsf2	-0.23226	0.009666	0.077485

Pou2f2	-0.23222	0.008388	0.069266
Plekhh1	-0.23145	0.002326	0.024411
Vldlr	-0.23144	0.000154	0.002449
Nectin1	-0.23108	0.008074	0.067033
Fa2h	-0.23104	0.00087	0.01086
Tmem44	-0.2298	7.48E-05	0.001289
Fam135b	-0.22976	0.007449	0.062849
Myl6b	-0.22941	0.006695	0.057483
Tdrp	-0.22882	0.007706	0.064631
Akt2	-0.22847	0.000134	0.002179
Kcnj16	-0.2275	0.00417	0.039388
Dip2a	-0.22737	8.35E-07	2.23E-05
Lrrc7	-0.22721	0.002611	0.026781
Mex3d	-0.22711	0.00846	0.069766
Lrrc73	-0.22647	0.00368	0.035516
Cdk19	-0.2264	0.010501	0.082506
Nlk	-0.22601	0.002452	0.025512
Ick	-0.22599	0.00366	0.035449
Adgra3	-0.22503	0.001896	0.020567
Bcl7c	-0.22503	0.00513	0.046664
Hmg20b	-0.22482	0.008236	0.068173
Rgs10	-0.22446	0.013084	0.097301
Nbeal2	-0.22394	0.001274	0.01484
Slc35d1	-0.22357	0.012936	0.096484
Sipa1l2	-0.2224	0.001067	0.012792
Trps1	-0.22238	0.005017	0.045923
Bicd2	-0.22213	0.002528	0.026103
Cdh20	-0.2211	0.005327	0.047964
Nfix	-0.22075	0.001616	0.018033
Pkn1	-0.2207	8.37E-05	0.001428
Slc25a18	-0.2206	0.00022	0.003344
Plekha7	-0.22052	0.000879	0.010932
Dynll1	-0.22042	0.000877	0.010932
Arhgap5	-0.2204	0.00037	0.005254
Pak7	-0.22034	0.000735	0.009435
Setbp1	-0.2203	0.004243	0.040001
Col11a2	-0.22023	0.000821	0.010351
Hsph1	-0.22002	0.002641	0.027013
Plaat3	-0.21908	0.001811	0.019838
Epas1	-0.21881	1.92E-05	0.000379
Psd2	-0.21874	0.000196	0.003017
Mpp3	-0.21844	0.006326	0.05513

Foxg1	-0.2183	0.002814	0.028441
Osbpl8	-0.21687	5.28E-05	0.000949
Daglb	-0.21659	0.001132	0.013491
Hunk	-0.21618	0.008332	0.068831
Gpr27	-0.21426	0.006251	0.054643
Grip2	-0.21415	0.003665	0.035449
Celf3	-0.21324	3.78E-05	0.0007
Nkain1	-0.21272	0.002868	0.028835
Tet1	-0.21263	0.009866	0.078681
Adcy3	-0.21195	0.001716	0.018977
Foxo4	-0.21149	0.004775	0.04423
P3h3	-0.21094	0.004104	0.03885
Rhobtb2	-0.21074	0.001503	0.01701
Syt4	-0.21068	0.001451	0.016525
Plekhg5	-0.20978	0.013083	0.097301
Bahd1	-0.20862	0.00074	0.0095
Lmo4	-0.20841	5.41E-05	0.000968
Camk1	-0.20839	5.94E-05	0.001053
Zfp61	-0.20824	0.01197	0.091241
Smad7	-0.20779	0.008616	0.070727
6330403L08Rik	-0.20762	0.000891	0.011067
Fyco1	-0.20761	0.007906	0.065986
Ggcx	-0.20719	0.005745	0.051254
Cald1	-0.20714	0.01127	0.087119
Pdia3	-0.20707	0.003628	0.035194
Wwc1	-0.20598	0.001014	0.012301
Itgb8	-0.20559	0.005933	0.052575
Rimklb	-0.20553	0.009727	0.077846
Zfc3h1	-0.20438	0.005083	0.0464
Cpd	-0.20399	0.001792	0.019706
Mylk	-0.20375	0.008115	0.067309
Nacad	-0.2034	0.000386	0.00546
Srpk1	-0.20288	0.000535	0.007175
Ankrd28	-0.20272	0.000593	0.007824
Lrp8	-0.20232	0.001738	0.019188
Kcnb2	-0.20163	0.00489	0.045003
Tanc2	-0.20159	0.000163	0.002569
Mfge8	-0.20091	0.003668	0.035449
Dnajb2	-0.20019	0.000213	0.003256
Man1c1	-0.19947	0.008075	0.067033
Lrfn3	-0.19849	0.002579	0.026511
D130017N08Rik	-0.19817	0.012194	0.09253

Btbd3	-0.19816	0.001178	0.013913
B4galt3	-0.19802	0.004395	0.04116
Dock10	-0.19776	0.001559	0.017523
Nrn1	-0.19676	0.000166	0.002608
Pacsin1	-0.19636	9.64E-05	0.001613
Tmeff1	-0.19615	0.000566	0.007523
Cactin	-0.19562	0.000853	0.0107
Pacsin3	-0.19544	0.009082	0.073753
D630045J12Rik	-0.19522	0.001285	0.014956
Unc13a	-0.19518	2.42E-05	0.000466
Slc7a10	-0.19477	0.00166	0.018448
Soga3	-0.19454	0.008131	0.067408
Vps13a	-0.19442	0.010303	0.081154
Crocc	-0.19399	0.005699	0.050869
Sec11c	-0.19333	0.001524	0.017215
Kif13b	-0.19314	0.004839	0.044687
Hyou1	-0.19296	0.010219	0.080631
Gramd4	-0.19198	0.004252	0.040014
Ptar1	-0.19192	0.006012	0.053151
Dnajb5	-0.19141	0.006314	0.055066
Pex5	-0.19116	0.001376	0.015845
Wasf1	-0.19025	0.000437	0.006035
Atp2c1	-0.1896	5.68E-05	0.001014
Cspg5	-0.1885	6.07E-05	0.001072
Chst10	-0.18705	0.003762	0.036212
Strip1	-0.18623	0.006086	0.053574
Scrib	-0.18617	0.000944	0.011565
Fbxl19	-0.18607	0.00092	0.01131
Spcs3	-0.18571	0.001483	0.01682
Rgma	-0.18516	0.000467	0.006377
Inpp5f	-0.18513	0.001668	0.018518
Srsf9	-0.18503	0.005963	0.052792
Pnpla6	-0.18486	0.001336	0.015455
Zfp608	-0.18442	0.012712	0.095181
Arhgef2	-0.18402	0.002079	0.022253
Nfic	-0.18393	0.002994	0.029934
Fam193b	-0.18335	0.001027	0.012414
Qdpr	-0.1825	0.002462	0.0256
Dact3	-0.18219	0.000149	0.00238
Pcdhac2	-0.18167	0.011411	0.087914
Mapk4	-0.18141	0.003223	0.031837
Lrfn4	-0.18131	0.009327	0.075317

Plod1	-0.18115	0.007297	0.06179
Zdhhc2	-0.18082	0.010258	0.080868
Mafg	-0.1808	0.003621	0.03515
Fmn2	-0.18053	0.00042	0.005852
Vash1	-0.18037	0.010751	0.084153
Gm37494	-0.18006	0.01102	0.085679
Ppfia2	-0.17981	0.003781	0.036375
Ifnar1	-0.17955	0.002945	0.029537
Myo9b	-0.17948	0.00044	0.006071
Numa1	-0.17948	0.002624	0.026901
Jph4	-0.17892	0.001534	0.017307
Bcl9	-0.17879	0.002491	0.025823
Klhl5	-0.1787	0.012072	0.09179
Map4k2	-0.17793	0.00026	0.003885
Sash1	-0.1778	0.005108	0.046527
4930402H24Rik	-0.17758	0.000267	0.003974
Mpp2	-0.17707	0.000756	0.009663
Fam149a	-0.17694	0.005791	0.051566
Myo10	-0.17634	0.004671	0.04342
Tmem198	-0.1761	0.00408	0.038674
Dpy19l3	-0.17583	0.00303	0.030243
Slc6a9	-0.17578	0.001964	0.021163
Arpp21	-0.17473	0.011373	0.087659
Ryk	-0.17467	0.01249	0.094091
Map3k11	-0.17373	0.004253	0.040014
Ankrd52	-0.17352	0.002971	0.029736
Msi1	-0.17276	0.002875	0.028881
Rps6kc1	-0.17256	0.006231	0.054571
Lrfn1	-0.17232	0.002863	0.028795
Dpy19l1	-0.17186	0.003159	0.031366
Ampd2	-0.17144	0.002258	0.023776
Zdhhc8	-0.17067	0.006596	0.056872
R3hdm2	-0.16977	0.001951	0.021028
Prr12	-0.16949	0.004249	0.040014
Tmem47	-0.16921	0.005173	0.04689
Clip2	-0.16869	0.000624	0.008155
Pla2g7	-0.16853	0.000394	0.005551
Srrm4	-0.16764	0.008291	0.068556
Kmt2a	-0.16763	0.007525	0.063344
Tmem151b	-0.16725	0.012778	0.095485
Coro1a	-0.16685	0.004729	0.043852
Lpcat1	-0.16615	0.007383	0.062377

Enho	-0.16596	0.007029	0.059815
Shank1	-0.16591	0.002863	0.028795
Apc2	-0.16575	0.000389	0.005495
Ugp2	-0.16552	0.008604	0.07067
Stip1	-0.1653	0.011241	0.087039
6-Sep	-0.16521	0.003089	0.03077
Elavl3	-0.16518	0.001176	0.013897
Sorbs2	-0.16506	0.002798	0.028355
Mmd2	-0.16498	0.006669	0.057353
Smap2	-0.16494	0.000554	0.007389
Dusp7	-0.16445	0.004011	0.038161
Igf1r	-0.16419	0.003919	0.037492
Gpr26	-0.16333	0.001189	0.014033
Flii	-0.16311	0.010059	0.079712
Dnmt3a	-0.16285	0.001821	0.019915
Fads2	-0.16241	0.000787	0.009988
Asrgl1	-0.16142	0.00059	0.007796
Llgl1	-0.16115	0.005549	0.049771
Dscaml1	-0.16071	0.013263	0.09828
Phyhipl	-0.16067	0.001552	0.017466
Rdx	-0.16055	0.004468	0.041743
Cpsf6	-0.16036	0.009199	0.074439
Fam102a	-0.16026	0.000976	0.011884
Sh2b1	-0.15976	0.001934	0.020894
Atp1a2	-0.15883	0.000254	0.003804
Ccdc85c	-0.15864	0.006553	0.056541
Cacnb1	-0.15836	0.000674	0.008688
Cdk5r1	-0.15816	0.004354	0.040849
Trim46	-0.15775	0.00337	0.033126
Slc20a1	-0.15759	0.00606	0.053397
Bsn	-0.15701	0.001319	0.015286
Sirpa	-0.15697	0.000796	0.010074
Rgmb	-0.15617	0.009973	0.079228
Hip1r	-0.15595	0.008105	0.067255
Car10	-0.15579	0.00319	0.031625
Jpt1	-0.15578	0.009468	0.076163
Rai1	-0.15573	0.001482	0.01682
Sel1l	-0.15564	0.006015	0.053156
Tspan13	-0.15555	0.00499	0.04572
Cnnm1	-0.1554	0.000948	0.011603
Rimbp2	-0.15384	0.003568	0.034727
Nin	-0.15266	0.006348	0.055258

Zbtb18	-0.15234	0.012948	0.096523
Gga3	-0.1516	0.002109	0.022487
Mn1	-0.15141	0.012141	0.092168
Rcc2	-0.15114	0.003415	0.033519
Nova1	-0.15065	0.003146	0.031256
Ube2ql1	-0.15036	0.002124	0.022586
Nptxr	-0.14972	0.010818	0.084507
Insyn1	-0.14956	0.006044	0.053333
Rph3a	-0.1491	0.012924	0.096484
Chpf	-0.14903	0.003645	0.035348
Tex2	-0.14809	0.006852	0.058659
Dmd	-0.14728	0.011113	0.086242
Pygb	-0.14662	0.00206	0.022066
Spock2	-0.14643	0.000772	0.009837
Celf5	-0.14635	0.005976	0.052867
Clasrp	-0.1463	0.010155	0.080225
Nefm	-0.14624	0.008498	0.069988
Macf1	-0.14609	0.002415	0.025189
Sltm	-0.14537	0.007487	0.063134
Ptma	-0.14514	0.00487	0.044861
Pacs2	-0.14506	0.002463	0.025604
Map4k4	-0.14473	0.002405	0.025111
Tmcc2	-0.14469	0.003933	0.037593
Ahdc1	-0.14449	0.003983	0.037967
Efnb3	-0.14433	0.01156	0.088768
Bin1	-0.14377	0.003994	0.038056
Palm	-0.14306	0.006894	0.058879
Zbtb7a	-0.14303	0.00495	0.045441
Map6	-0.14281	0.003664	0.035449
Ptov1	-0.14261	0.003121	0.031042
Mllt6	-0.14257	0.002322	0.024383
Phc1	-0.14249	0.012082	0.091833
Plcg1	-0.14185	0.004846	0.044735
Tet3	-0.14163	0.005592	0.050085
Suds3	-0.14097	0.00557	0.049936
Caskin1	-0.14087	0.006495	0.056225
Rusc1	-0.14087	0.005162	0.046879
Arhgap23	-0.14026	0.007331	0.062023
Daam1	-0.13988	0.012331	0.093267
Rnpepl1	-0.13983	0.013548	0.099724
Dmtn	-0.13909	0.001033	0.012459
Sybu	-0.13851	0.011168	0.086616

Mast2	-0.13805	0.007498	0.063204
Sccpdh	-0.1376	0.012426	0.093722
Tppp	-0.13751	0.000923	0.011328
Sgsm2	-0.13679	0.002362	0.024719
Myo6	-0.13612	0.009773	0.078139
Khdrbs3	-0.13603	0.0109	0.084928
Ncan	-0.1351	0.005247	0.047355
Drp2	-0.13336	0.011421	0.087959
Sobp	-0.13244	0.013153	0.097664
Slc38a1	-0.13219	0.004032	0.038303
Lrrtm2	-0.13106	0.012342	0.093275
Srebf2	-0.12971	0.003061	0.03051
Anp32a	-0.12964	0.004215	0.039772
Cep170b	-0.12956	0.002029	0.021761
Lrrc4b	-0.12895	0.012747	0.095333
Gnaq	-0.1267	0.003203	0.031681
Usp46	-0.12558	0.009955	0.07912
Dusp3	-0.12557	0.013354	0.098725
Bace1	-0.12518	0.012336	0.093267
Fez1	-0.12186	0.005157	0.046865
Hspa4	-0.12051	0.00995	0.07912
Rock2	-0.11928	0.013445	0.099158
Srcin1	-0.11534	0.008894	0.07258
Ap3d1	-0.11202	0.006421	0.055742
Madd	-0.10918	0.011108	0.086242
Cbarp	-0.10695	0.007916	0.066007
Sptbn1	-0.10593	0.009728	0.077846
Acot7	-0.10539	0.012717	0.095181
Cap1	-0.10411	0.008478	0.069882
Arhgdia	-0.09827	0.012382	0.093538
Tbc1d9b	0.117502	0.009145	0.074119
Sub1	0.118633	0.011731	0.089862
Mrtfb	0.124159	0.012511	0.094169
Plk2	0.12553	0.004865	0.044843
Add2	0.127918	0.003917	0.037492
Rogdi	0.128328	0.009469	0.076163
Acox1	0.129923	0.00468	0.043447
Gng12	0.130914	0.012928	0.096484
Map1lc3b	0.132147	0.006508	0.05626
Med13l	0.133091	0.00452	0.042183
Mkln1	0.133151	0.008917	0.072733
Ncl	0.134373	0.002166	0.022939

Etf1	0.135993	0.009429	0.075972
Fbxo21	0.137761	0.004862	0.044834
Isca1	0.138354	0.009127	0.074053
Klhl2	0.138354	0.011667	0.089481
Sod2	0.138694	0.004815	0.044508
Csrnp3	0.139248	0.013426	0.09906
Ostm1	0.141568	0.01255	0.094424
Fth1	0.143389	0.007037	0.059861
Ilf2	0.143829	0.00735	0.062123
Phf20	0.144673	0.00457	0.042606
Mecp2	0.14687	0.002162	0.022909
Capza2	0.147399	0.001745	0.019245
Zfp365	0.148499	0.010047	0.07968
Sbf2	0.149508	0.007335	0.062025
Exoc6b	0.150037	0.006597	0.056872
Nf2	0.15107	0.003999	0.038082
Ubr3	0.152946	0.008276	0.068463
Cdk5	0.153682	0.009449	0.076073
Timm29	0.154425	0.010315	0.081215
Insr	0.154447	0.008238	0.068173
Impa1	0.156003	0.010691	0.083787
Chka	0.156397	0.007524	0.063344
Arl6ip1	0.156798	0.002112	0.022501
Pitpnm2	0.157419	0.001577	0.017684
Slc35c2	0.157507	0.006185	0.054293
Agpat5	0.15871	0.011333	0.087426
Zfyve27	0.158745	0.001053	0.012656
Tpm3	0.160282	0.006141	0.053989
Rasgrf2	0.161311	0.002847	0.028678
Vmp1	0.161933	0.008854	0.07234
Atp6v1g1	0.162948	0.009583	0.077016
Jade2	0.163227	0.001856	0.020225
Sulf2	0.163726	0.001076	0.012885
Galnt11	0.164912	0.006106	0.053701
Tnik	0.164959	0.008595	0.070628
Pnrc2	0.165659	0.008511	0.070063
Syt16	0.165795	0.009705	0.077759
Ubxn7	0.167016	0.009023	0.0734
Psma6	0.167259	0.004662	0.043352
Trio	0.168231	0.000589	0.007779
Anapc16	0.168242	0.005084	0.0464
Tollip	0.168624	0.001229	0.014413

Rapgef2	0.169414	0.000895	0.011088
Zfp281	0.169477	0.011328	0.087417
Rgl1	0.170655	0.012937	0.096484
Atp11a	0.170666	0.001599	0.017885
Slc25a17	0.170771	0.006982	0.059557
Ackr1	0.172465	0.013107	0.097397
Nmt1	0.173764	0.000319	0.004615
Apbb2	0.174533	0.010183	0.080419
Hmgn3	0.174649	0.006503	0.056239
Asic2	0.174943	0.003964	0.037832
Peli1	0.176341	0.004051	0.038437
Nprl3	0.176888	0.007741	0.064785
Slc9a1	0.177092	0.000281	0.004157
Stmn4	0.177813	0.012284	0.093063
Farsa	0.177891	0.005632	0.050345
Cetn3	0.178201	0.012709	0.095181
Aldh6a1	0.178503	0.004949	0.045441
Ypel5	0.178509	0.002512	0.025969
Bclaf1	0.178523	0.000869	0.01086
Rpl11	0.179349	0.007887	0.065857
Tef	0.179803	2.81E-05	0.000534
Rab8b	0.182107	0.012331	0.093267
Ncbp1	0.18294	0.000953	0.011651
Plxna2	0.184224	0.000266	0.003966
Ranbp9	0.184614	0.002133	0.022646
Eif2b2	0.184802	0.005766	0.051373
Prickle2	0.185173	0.000213	0.003256
D430019H16Rik	0.185279	0.004447	0.041565
Ets2	0.185538	0.001357	0.015658
Pnpt1	0.18577	0.012138	0.092168
Naaa	0.185837	0.007731	0.064726
Sphkap	0.186405	0.000129	0.002105
Acap2	0.186701	0.000282	0.004161
Pkia	0.186897	0.001021	0.012345
Usp24	0.187097	0.007613	0.063943
Acvr1b	0.187145	0.000112	0.00185
Ssh2	0.187203	0.001516	0.017139
Fbh1	0.187663	0.001258	0.014712
Epb41l4b	0.188405	0.002659	0.02712
Lamp2	0.189019	0.002271	0.023882
Tmem19	0.190695	0.003482	0.034084
Chst11	0.191056	0.000292	0.004283

Gpt2	0.191117	0.009983	0.079272
Pdk2	0.191205	0.000174	0.002732
Tns1	0.191577	0.000549	0.007334
Sh3gl1	0.192431	0.006693	0.057483
Ube2g2	0.192433	0.001932	0.020894
Sec22b	0.192584	0.000973	0.011863
Rchy1	0.192985	0.012957	0.096553
Slc6a1	0.193422	2.67E-06	6.47E-05
Sowaha	0.19366	0.001142	0.013577
Arhgap26	0.193979	3.58E-05	0.000667
Armh3	0.194139	0.002963	0.029673
Anxa7	0.19498	0.008895	0.07258
Senp1	0.195062	0.013347	0.09871
Mdm2	0.195065	0.000622	0.008134
Ercc5	0.195509	0.007714	0.064676
Cdh22	0.196152	0.005589	0.050082
Stx17	0.196632	0.013204	0.09796
Arpc2	0.196937	8.94E-05	0.001516
Adipor2	0.198546	0.00023	0.003482
Trub1	0.199147	0.0096	0.077118
Fbxo10	0.199733	0.006449	0.055931
Nampt	0.200504	0.006478	0.056106
Cdc37l1	0.200863	9.89E-05	0.001649
Phka2	0.201454	0.011887	0.09076
Klf13	0.201491	9.52E-05	0.001598
Mmab	0.202105	0.002184	0.023085
mt-Nd1	0.203909	0.003116	0.031004
Srxn1	0.204748	0.003453	0.033831
Lgi3	0.204928	0.006392	0.055564
Mpi	0.205298	0.000164	0.002588
H3f3b	0.205306	0.008522	0.070121
Cpped1	0.205381	0.004326	0.040638
Gpam	0.205566	0.001973	0.021246
Usp40	0.205895	0.00135	0.015599
Tppp3	0.208224	0.000913	0.011252
Cbs	0.209074	0.001611	0.018003
Cacnb2	0.209293	0.002834	0.02858
Ell	0.209672	0.008975	0.073105
Hsd17b7	0.209788	0.00375	0.036135
Kcnab3	0.210167	0.005952	0.052722
Slc3a2	0.210498	5.52E-05	0.000987
Ogfr	0.211887	0.001487	0.016843

Paxx	0.212814	0.004245	0.040001
Crkl	0.213257	0.002196	0.023192
Extl2	0.213885	0.000161	0.002547
Pxn	0.213896	0.001919	0.020793
Exosc2	0.213962	0.011192	0.086767
Tbc1d22a	0.214315	0.000437	0.006035
Slc35f3	0.214405	0.001062	0.012746
Emc8	0.214586	0.006896	0.058879
Irf2	0.215186	0.001014	0.012301
Chst2	0.215208	6.42E-06	0.000142
Rnf2	0.215282	0.006152	0.054033
Flnb	0.215529	0.000235	0.003546
Cd164	0.215635	0.000298	0.004352
Uvrag	0.216451	0.000569	0.007555
Fbxo31	0.216475	1.86E-05	0.000369
Nedd4l	0.216816	9.00E-05	0.001522
Ctsl	0.217324	0.000598	0.007881
Mbd1	0.217846	0.000102	0.001698
Arhgap20	0.218649	8.33E-05	0.001424
Ybx3	0.218822	0.003795	0.036473
Tbc1d23	0.21943	0.0013	0.015106
Prex2	0.220062	0.000354	0.005053
Crnkl1	0.221436	0.005234	0.04728
Fam117b	0.221993	0.000187	0.002907
Zfp260	0.222139	0.000417	0.005817
Zfp941	0.222368	0.001981	0.021306
Foxo3	0.22287	0.000421	0.005857
Adam9	0.223524	0.000333	0.004788
Eif1a	0.223804	0.003658	0.035449
Il6st	0.224037	0.01006	0.079712
Kdm6b	0.224275	0.006476	0.056106
Fam110b	0.224341	0.003198	0.031656
Mknk1	0.224505	0.001939	0.020921
Elk1	0.224703	0.000648	0.00841
Rcan2	0.22554	0.012588	0.094596
Ssr3	0.225916	4.51E-06	0.000104
Trappc1	0.227008	0.01352	0.099636
Bnip3	0.227729	9.32E-05	0.001573
Selenom	0.228943	0.000158	0.00251
Itpr2	0.229529	0.001191	0.014045
Crcp	0.229836	0.001707	0.018893
Zfp276	0.230713	0.004942	0.04543

Rapgef6	0.231075	0.003432	0.03366
Tiam2	0.231773	0.013234	0.098148
Bcat1	0.232041	3.56E-06	8.45E-05
Per3	0.232067	0.000283	0.004161
Psmb2	0.234019	1.07E-05	0.000225
Amer3	0.236136	0.001886	0.020471
Bach1	0.236137	0.006623	0.057038
Inpp5j	0.237682	0.000479	0.006525
Pdgfra	0.238088	0.000274	0.00407
Ptpn11	0.23827	3.74E-05	0.000694
Limd2	0.239983	0.000741	0.009502
Gpsm1	0.241138	0.000811	0.010252
Btg1	0.241248	0.003833	0.036802
Sppl2a	0.241948	0.001173	0.013875
Gsto1	0.242524	0.005829	0.05183
Psme1	0.243554	0.010734	0.08409
Rnf115	0.245056	0.000136	0.002203
Tnip2	0.245747	0.003487	0.034092
Bak1	0.245808	0.001782	0.019609
Cast	0.246696	0.013307	0.098489
Sntb2	0.247034	0.001593	0.017842
Hipk1	0.247228	1.74E-08	6.42E-07
Ptgfrn	0.247985	0.002821	0.028499
Mrps22	0.248312	0.005275	0.047564
Ern1	0.248429	0.008457	0.069766
Itpk1	0.248505	0.003492	0.034093
Atp6v0e	0.248919	0.00381	0.036598
Crebrf	0.249349	0.002533	0.026135
Ociad2	0.249447	0.00175	0.019291
Fbxl4	0.249524	0.006265	0.054741
Adra2a	0.249668	0.011905	0.090846
Slc2a1	0.249784	0.00148	0.01682
R3hcc1l	0.25056	0.007823	0.06538
Plat	0.250675	0.000458	0.006282
Dpysl4	0.250831	0.000188	0.002921
Efr3b	0.251332	1.56E-06	3.94E-05
Fgfr1	0.251332	0.001152	0.013663
Plpp1	0.2516	0.001396	0.01603
Ankrd45	0.251973	0.000588	0.007779
Ksr1	0.253743	0.001805	0.019802
Dapk1	0.253864	1.41E-07	4.33E-06
Gjb6	0.254793	1.79E-05	0.000357

Polr3c	0.254812	0.001374	0.015839
Zfp1	0.254948	0.004004	0.038108
Pdrg1	0.255014	0.001525	0.017215
Cep83os	0.255751	0.001818	0.01991
Mtmr2	0.256489	4.64E-05	0.000845
Rapgef3	0.257135	0.011345	0.087481
Erlin2	0.257154	1.60E-05	0.000323
Itprid2	0.258268	0.001076	0.012885
Cd200	0.258619	8.72E-05	0.001481
Lgals8	0.2589	0.000968	0.011803
Gpx1	0.259783	0.001033	0.012459
Rnaseh1	0.259927	0.013259	0.09828
Ddx21	0.262862	0.010757	0.084162
B3galnt2	0.26344	0.009065	0.073651
C1qa	0.265704	0.004614	0.042949
Ttc39c	0.265801	6.87E-05	0.001195
Cdh19	0.265933	0.00894	0.072886
Hapln2	0.265961	1.61E-05	0.000324
Cpne8	0.266096	0.006327	0.05513
Sra1	0.266168	0.000114	0.001879
Ubr7	0.266431	0.002769	0.028087
Esyt1	0.266822	0.008794	0.071887
Vcan	0.267615	0.000662	0.008567
Napepld	0.268602	0.00272	0.027644
2410131K14Rik	0.268907	3.89E-05	0.00072
2410006H16Rik	0.269144	0.006993	0.059569
Oprl1	0.270002	1.31E-05	0.000269
Ptpn1	0.270307	0.000213	0.003255
Tmem176b	0.271795	0.001997	0.021468
Hmgcll1	0.271987	0.006293	0.054932
Herpud1	0.272245	9.06E-06	0.000193
Tet2	0.272553	0.000894	0.011088
Irf2bp2	0.272876	0.000518	0.00698
Psme4	0.273169	0.000658	0.008526
1600014C10Rik	0.273567	0.000185	0.002885
Ccnl1	0.274001	2.14E-05	0.000417
Wasf2	0.274189	1.39E-05	0.000284
Snx1	0.274939	0.000118	0.001936
Ctss	0.274966	0.003926	0.037546
Rcc1	0.275809	0.00975	0.077985
Ifrd1	0.27615	0.001142	0.013577
E130308A19Rik	0.276377	0.001839	0.020075

Ppp1r2	0.278354	0.000345	0.00494
Rtkn	0.278557	0.000557	0.007429
Zc3h6	0.279111	0.010976	0.085444
Zfp423	0.280074	4.48E-05	0.000819
Mrtfa	0.28128	4.01E-06	9.31E-05
Rwdd2a	0.281438	0.003749	0.036135
Jmjd1c	0.281555	2.85E-05	0.00054
Resf1	0.283015	0.003107	0.03093
Orc6	0.283835	0.000424	0.005889
Tmem87b	0.28722	8.04E-06	0.000174
Pdxk	0.287608	1.90E-07	5.73E-06
Fdft1	0.288087	9.71E-06	0.000205
Rassf1	0.288307	0.011865	0.090628
Ly6c1	0.28843	0.007565	0.063568
Ankrd35	0.289536	0.004599	0.042838
Sec24d	0.290944	0.011278	0.08714
Pik3r1	0.293746	3.10E-07	8.93E-06
Nkapd1	0.295135	0.002021	0.021679
Ccng1	0.296295	0.000171	0.002693
Nek6	0.29658	0.004585	0.042726
Agfg2	0.296895	1.15E-06	2.98E-05
Sun2	0.297009	0.0043	0.040436
Prkab2	0.297694	1.22E-05	0.000252
Htr2a	0.299037	0.0028	0.028359
Tyrobp	0.299689	0.013182	0.097836
Mbd2	0.299852	5.99E-05	0.001059
Armcx5	0.302179	0.004916	0.045226
Kcnt1	0.303198	7.44E-05	0.001285
Slc41a1	0.30334	1.91E-08	6.93E-07
Lgalsl	0.303345	1.06E-05	0.000223
Nhsl2	0.304166	2.00E-05	0.000394
Sat1	0.305428	0.009131	0.074053
Lyst	0.306427	1.10E-08	4.20E-07
Ppp1r15a	0.30899	0.004028	0.038281
Adamts2	0.310001	0.006865	0.058704
Zfp788	0.310062	9.48E-05	0.001595
Mat2a	0.310976	1.05E-08	4.04E-07
Dbndd2	0.311022	2.71E-05	0.000517
Mthfd1l	0.311182	0.002479	0.025708
Aldh1l1	0.312119	3.49E-05	0.000652
Cd302	0.313141	0.012975	0.096649
Zfp46	0.313185	0.000206	0.003163

Bag3	0.314432	0.012016	0.091478
Prelid3a	0.315883	0.010747	0.084153
Epha10	0.316528	9.68E-08	3.07E-06
Rbms1	0.31682	0.000184	0.002858
Rcan1	0.31726	7.40E-06	0.000161
Dysf	0.317307	0.006289	0.054921
Nek7	0.31771	4.50E-05	0.000821
Slc24a4	0.319336	0.000896	0.01109
Shisa5	0.319989	1.38E-05	0.000283
Arfgap3	0.320702	0.000107	0.001768
Cab39l	0.323171	4.37E-05	0.000803
Ilk	0.323476	1.86E-08	6.80E-07
Rpain	0.323938	0.001824	0.019937
Camkk1	0.324101	9.17E-07	2.43E-05
Shc1	0.325272	0.000548	0.007332
Zfp617	0.325473	0.002766	0.028075
Trafd1	0.326256	2.15E-07	6.43E-06
Tnip1	0.328397	2.80E-06	6.76E-05
Apbb3	0.328648	1.81E-05	0.00036
Tmem229b	0.328837	2.04E-06	5.04E-05
Arhgef3	0.329136	8.46E-09	3.29E-07
Susd6	0.330001	0.000239	0.003602
Nsun4	0.331851	0.003918	0.037492
Arhgap18	0.332369	0.001684	0.018683
Bc1	0.333612	0.000506	0.006856
Bcl6	0.334226	0.000631	0.008236
Slc25a33	0.33441	0.003216	0.031797
Ino80c	0.3349	0.002361	0.024716
Dlg5	0.335709	0.000797	0.010087
Esam	0.335799	3.97E-05	0.000734
Ip6k2	0.336165	8.14E-10	3.62E-08
Rbm3	0.336401	0.002433	0.025347
Zgrf1	0.336455	0.008679	0.071102
Pdzd2	0.338548	0.000513	0.006934
Id2	0.339132	0.000588	0.007779
Mad1l1	0.339346	0.000779	0.009891
Fam189a2	0.341684	0.003544	0.034542
Fbf1	0.343317	6.87E-08	2.27E-06
Wipf3	0.343592	2.81E-06	6.78E-05
Lamc2	0.343593	0.000345	0.00494
H2-T22	0.343735	0.006213	0.054483
Lrig1	0.34548	0.012497	0.094107

Cdc42ep4	0.345757	1.17E-06	3.04E-05
Slc19a2	0.346418	0.000139	0.002237
Birc2	0.34683	0.00019	0.002937
Mphosph6	0.347242	0.000724	0.009301
Greb1l	0.347852	0.002636	0.026994
Wdhd1	0.349164	0.005157	0.046865
Strn	0.349194	1.73E-06	4.33E-05
Nrip2	0.3503	0.000454	0.006236
4930451G09Rik	0.350955	0.010154	0.080225
Mapkapk2	0.35145	0.000618	0.008098
Rell1	0.353132	2.27E-05	0.00044
Tsc22d4	0.353241	7.04E-08	2.30E-06
Nde1	0.353971	7.67E-05	0.001321
Daam2	0.354373	1.98E-08	7.15E-07
Dph2	0.355002	0.001018	0.012333
Eci2	0.355624	1.77E-06	4.43E-05
Fmnl2	0.355725	0.001419	0.016231
Scrg1	0.356091	0.000113	0.001861
Oplah	0.356175	4.41E-07	1.23E-05
Bcl2l1	0.356707	2.28E-12	1.44E-10
Plekhg2	0.358162	0.000384	0.005439
Mterf2	0.359316	0.000251	0.003756
Rnd1	0.360263	0.001802	0.019802
Psme2	0.360834	0.004309	0.040494
Litaf	0.361533	0.001819	0.019911
Tns2	0.361748	2.48E-08	8.81E-07
Mospd1	0.361849	0.007977	0.066462
Tmem243	0.362187	0.010208	0.080575
Htra1	0.362397	1.53E-10	7.62E-09
Zfas1	0.367303	0.000467	0.006382
Etv6	0.367777	0.008662	0.071026
Scrt2	0.368482	6.21E-05	0.00109
Map3k14	0.368491	0.01145	0.088104
Zfp410	0.368714	4.63E-07	1.29E-05
Erich1	0.369804	0.011497	0.088398
Dgat2	0.370407	0.000178	0.002775
Rab40c	0.371618	1.30E-08	4.86E-07
Flt4	0.371733	0.002656	0.027107
Sik1	0.372553	8.21E-06	0.000177
Olfml2b	0.373063	0.000507	0.006866
Arid5b	0.374957	1.57E-05	0.000318
Nsmce1	0.377717	0.003267	0.032185

Snhg1	0.380508	0.012613	0.094742
Bmpr1b	0.380943	0.002505	0.025933
Kndc1	0.382273	1.44E-07	4.40E-06
Fam107a	0.382523	1.03E-14	8.54E-13
Mettl27	0.382597	0.005171	0.04689
Tm6sf1	0.385819	0.002823	0.028499
Flnc	0.386992	0.01182	0.090316
Relt	0.387942	0.000136	0.0022
Il17ra	0.388399	0.002243	0.023636
Fam43a	0.389157	8.26E-06	0.000178
Map2k3	0.390466	0.000117	0.001928
Smox	0.390914	1.10E-08	4.20E-07
Gpsm2	0.391409	0.001734	0.019155
Col5a3	0.392298	0.002511	0.025969
C2cd2	0.39272	0.001484	0.01682
Cplx3	0.397434	0.001139	0.013553
Traip	0.39781	0.000142	0.002284
D7Ertd443e	0.398103	0.00281	0.028429
Dcbld2	0.399334	6.79E-07	1.84E-05
Sav1	0.399766	4.22E-05	0.000776
Per1	0.401969	6.53E-07	1.78E-05
Tmem123	0.402347	0.000244	0.003667
Msrb1	0.402912	1.37E-05	0.000282
AA986860	0.4035	0.007166	0.060786
Wdr76	0.404502	0.009151	0.074119
Gm15624	0.406102	0.006199	0.05439
Cited2	0.406244	8.44E-06	0.000181
Azin1	0.406804	2.22E-13	1.55E-11
Vwa5a	0.406984	0.006722	0.057653
1110008L16Rik	0.409322	0.011755	0.090011
Ranbp17	0.410508	0.009792	0.078232
Cflar	0.412112	5.41E-05	0.000968
Plcd4	0.412336	9.47E-08	3.01E-06
Rela	0.412664	2.64E-05	0.000507
Slc39a1	0.412675	0.000512	0.006921
Mipol1	0.413446	0.010243	0.080788
Slc41a3	0.414731	0.003243	0.031999
Irs2	0.415328	1.23E-08	4.63E-07
Atp10d	0.416369	0.006309	0.055044
Plin2	0.416807	0.003974	0.037905
Ptpdc1	0.417959	5.97E-11	3.12E-09
Endod1	0.418519	2.21E-07	6.59E-06

Cish	0.419145	0.001266	0.014775
Ripk2	0.419634	0.005294	0.047709
Tnfrsf11a	0.419858	0.003433	0.03366
Usp54	0.423157	7.68E-12	4.44E-10
Klhdc7a	0.423752	4.78E-08	1.62E-06
B3galt5	0.424363	8.65E-08	2.78E-06
Zbtb7b	0.424531	1.48E-06	3.77E-05
Fhad1	0.424975	0.003337	0.03282
Gm17322	0.427686	0.006053	0.05336
Cd24a	0.427706	0.003223	0.031837
Vstm5	0.427956	0.002605	0.026735
Slc25a30	0.428811	0.000405	0.005677
Ppp1r3g	0.43042	0.00019	0.002942
Rnf39	0.43043	0.013065	0.097243
Fes	0.431936	0.000448	0.006158
Zfp811	0.435253	0.000305	0.004428
Thrsp	0.436027	1.95E-05	0.000383
Ifngr1	0.436811	1.71E-06	4.28E-05
Gm45869	0.436841	0.000598	0.007881
Lfng	0.437892	2.80E-07	8.16E-06
Armc5	0.438307	2.00E-08	7.18E-07
Lurap1l	0.438353	0.000132	0.002139
Lyrm1	0.439096	1.19E-05	0.000248
Pttg1ip	0.439121	6.08E-13	4.00E-11
Dhx33	0.439548	1.48E-06	3.77E-05
Gpd1	0.439707	4.94E-11	2.61E-09
Epb41l4aos	0.440384	0.012617	0.094742
Icosl	0.44172	0.001859	0.020246
Pld1	0.442187	1.26E-06	3.23E-05
Spata13	0.443063	0.000175	0.002743
Tle3	0.443894	2.90E-09	1.19E-07
Ppp1r18	0.445537	0.001299	0.015097
Pik3c2a	0.448503	1.84E-08	6.74E-07
Suox	0.448715	3.95E-06	9.23E-05
Apaf1	0.449112	0.003264	0.032179
Mcl1	0.45421	5.21E-07	1.44E-05
Gadd45a	0.454821	0.000505	0.006851
Gata2	0.454863	9.11E-05	0.001539
Brca2	0.455061	0.001425	0.016279
Cdkl4	0.45628	0.000157	0.0025
Kyat3	0.456391	0.004075	0.038653
Islr2	0.45707	1.83E-06	4.57E-05

Slc35e4	0.458151	2.80E-07	8.16E-06
Hcls1	0.461051	0.003944	0.037678
Fam214a	0.461639	2.87E-12	1.80E-10
Nppc	0.461982	0.004789	0.044294
C1qb	0.462145	1.26E-07	3.91E-06
Phactr3	0.463757	8.74E-12	5.03E-10
Clcn1	0.464323	0.007559	0.063568
Ciart	0.464925	0.000816	0.010299
Vcam1	0.467935	0.000152	0.002423
Klf6	0.468083	6.90E-08	2.27E-06
Myo1h	0.470283	0.008069	0.067033
Pde4b	0.47158	1.30E-09	5.56E-08
Mrps18c	0.472413	0.001835	0.020042
Rnf169	0.472419	4.66E-08	1.58E-06
Klf9	0.47262	9.42E-10	4.16E-08
Plek	0.472846	0.008697	0.071191
Zfp52	0.474561	0.002102	0.022437
Ppp2r3a	0.474778	3.52E-10	1.66E-08
Dusp1	0.474967	0.000817	0.010315
Pros1	0.475248	3.86E-06	9.06E-05
Pcolce2	0.476172	0.001693	0.01877
Eef2k	0.47627	3.96E-12	2.39E-10
Sh3pxd2b	0.477075	0.004876	0.044896
Gm11549	0.479648	6.17E-05	0.001085
Ezh2	0.480343	0.00091	0.011227
Hacd2	0.480509	7.77E-11	4.01E-09
Sesn1	0.481175	4.38E-08	1.49E-06
Lamc1	0.481217	3.08E-15	2.72E-13
Fam78a	0.484633	0.002174	0.023004
Col4a2	0.484665	2.71E-17	2.97E-15
Gpr4	0.486474	0.000469	0.0064
Syn3	0.487437	5.27E-06	0.000119
Klhl25	0.489774	0.005015	0.045923
Mchr1	0.489814	9.97E-10	4.37E-08
Klf2	0.490907	0.000105	0.001745
Ezr	0.4914	1.46E-08	5.46E-07
Rassf4	0.491466	0.001544	0.017387
Tcf19	0.49165	0.011265	0.087117
Map4k1	0.491807	0.007061	0.059976
Usp53	0.492223	0.000135	0.002188
Jak3	0.492606	7.70E-06	0.000167
Gmnn	0.492751	0.010341	0.081385

Lrrc8c	0.495436	4.25E-09	1.70E-07
Mfsd2b	0.500021	0.013268	0.098281
Plk4	0.502759	0.002672	0.027211
Tgfbr2	0.504598	1.88E-10	9.24E-09
Wbp1l	0.504981	1.01E-16	1.07E-14
Smad1	0.505611	1.00E-10	5.09E-09
Tmem268	0.506006	5.49E-06	0.000123
Cep152	0.506968	0.00013	0.002112
Dll4	0.507366	0.001332	0.015431
Cdk6	0.509149	0.000687	0.008842
Lrrc58	0.511735	2.38E-20	3.73E-18
F8	0.511835	0.005611	0.050228
Serpinb8	0.512774	1.09E-05	0.000228
Adssl1	0.512838	4.36E-08	1.49E-06
Cbr3	0.514435	0.001133	0.013491
Ankrd13a	0.517729	1.55E-13	1.10E-11
Itgb2	0.517899	6.88E-05	0.001196
Nt5c3	0.519066	1.46E-13	1.04E-11
Clic1	0.523708	0.000339	0.004861
Mro	0.524959	1.37E-09	5.85E-08
Dab2	0.527952	0.000102	0.001701
Cdc42ep3	0.53123	1.03E-05	0.000217
AI506816	0.531458	0.008671	0.071067
Ptgs2	0.531476	0.000326	0.004694
Dyrk3	0.532198	4.48E-07	1.25E-05
Arpc1b	0.535092	6.30E-05	0.001105
Sh3d21	0.535361	0.011297	0.087256
Lacc1	0.536031	0.007811	0.065305
Pycr1	0.541356	0.011115	0.086242
Gpr182	0.541656	0.005824	0.051811
Klhl36	0.542388	2.04E-05	0.0004
Dmrtc1a	0.54506	0.002406	0.025111
Filip1l	0.545828	6.97E-05	0.00121
Rhob	0.545999	6.97E-25	1.62E-22
Pm20d2	0.546009	0.004039	0.038346
Slc14a1	0.546718	0.002446	0.025467
Wnk4	0.546911	1.27E-05	0.000263
Asap3	0.54752	0.007996	0.066557
Cenpj	0.54754	0.001699	0.018818
Cemip2	0.548651	1.28E-07	3.98E-06
Pvr	0.549184	6.66E-05	0.001164
Irak2	0.549239	1.62E-05	0.000325

Rhbdf1	0.549852	3.07E-05	0.000579
Endou	0.549892	0.010871	0.084805
Tob2	0.552791	4.79E-16	4.65E-14
Zbtb7c	0.554236	0.000633	0.008256
Fstl1	0.554333	0.000812	0.010263
Slc16a10	0.55456	0.001977	0.02127
Hhatl	0.555474	0.000775	0.009857
Nfe2l2	0.560856	0.000207	0.003175
Myc	0.56179	0.006018	0.053158
Zfp975	0.562254	0.002333	0.024462
Snx24	0.564028	3.24E-07	9.31E-06
Frmpd1	0.56535	4.59E-10	2.13E-08
Dusp5	0.566806	6.78E-05	0.001181
Gm27000	0.569897	0.012404	0.093631
Igdcc3	0.570339	0.000368	0.005224
Pim3	0.571123	9.06E-17	9.59E-15
Polr3e	0.574408	1.02E-11	5.76E-10
Mxd4	0.575608	4.51E-16	4.43E-14
Mitd1	0.576955	0.000118	0.00194
Rrp8	0.577445	1.70E-09	7.19E-08
Gcnt2	0.578998	1.64E-10	8.11E-09
Arhgef37	0.579004	3.25E-05	0.000611
Gpx3	0.581389	0.000586	0.007771
Gm13091	0.581684	0.008754	0.071618
Lrrc8a	0.582244	1.13E-11	6.36E-10
4931415C17Rik	0.584761	0.013419	0.099047
Mocs1	0.586737	6.05E-06	0.000134
Kirrel2	0.586931	0.000125	0.002035
Bambi	0.587967	0.000286	0.004206
Casp7	0.589298	0.000645	0.008385
Pdlim4	0.58938	0.010974	0.085444
Igfbp3	0.590908	3.77E-06	8.87E-05
Abca1	0.592471	9.40E-12	5.39E-10
Rgcc	0.59497	3.53E-10	1.66E-08
Tm4sf1	0.595183	0.000183	0.002849
Ucp3	0.596713	0.002777	0.02816
Cbx2	0.601603	0.000302	0.004401
Tpm4	0.602021	5.39E-08	1.82E-06
Arrdc3	0.602374	8.30E-19	1.05E-16
Zfp541	0.603961	0.012653	0.094919
Mid1	0.60621	0.00188	0.02044
Trim16	0.606412	0.010804	0.084463

Igsf10	0.608775	0.000569	0.007555
Gcnt1	0.608945	0.000546	0.007302
Il12rb1	0.612234	0.001632	0.018197
Ism1	0.612714	3.02E-06	7.26E-05
Rai14	0.615307	1.02E-09	4.44E-08
Atp6ap1l	0.615526	0.000245	0.003687
Spag6	0.615964	0.003871	0.037092
Hk2	0.616526	0.00042	0.005848
Pik3r6	0.620165	0.00131	0.015203
Cmpk2	0.620814	1.20E-09	5.18E-08
Cpt2	0.621848	1.84E-06	4.58E-05
Ripk1	0.622147	0.001079	0.012911
Carhsp1	0.625672	5.38E-13	3.61E-11
Zbtb16	0.6259	5.01E-10	2.29E-08
Tfcp2l1	0.626473	0.000749	0.009589
F3	0.626853	5.65E-17	6.12E-15
Ovol2	0.632776	0.002364	0.024722
Hspb6	0.635168	1.49E-05	0.000304
Vash2	0.636153	0.00106	0.012723
Rin2	0.636953	1.47E-08	5.46E-07
Mfsd2a	0.63784	1.22E-11	6.82E-10
Gm42047	0.641255	0.003789	0.036437
Phyhd1	0.642918	3.37E-05	0.000631
Gm4876	0.64327	0.002543	0.026218
K230015D01Rik	0.644761	0.00899	0.073164
Rac2	0.645461	0.01339	0.098909
Nupr1	0.646107	0.004509	0.042105
Rab31	0.646558	3.08E-16	3.07E-14
Msn	0.649354	4.19E-07	1.17E-05
Adgrg2	0.649759	0.000748	0.009585
Tapbp	0.653081	3.76E-06	8.87E-05
Sdc4	0.65384	7.03E-09	2.78E-07
Samhd1	0.654173	1.03E-10	5.21E-09
Trim56	0.654905	0.000298	0.004352
Tsc22d3	0.655315	1.58E-31	5.90E-29
Stc1	0.656634	3.14E-07	9.04E-06
Lipe	0.657438	5.05E-10	2.31E-08
Igfbpl1	0.658307	0.005112	0.046543
Fam83d	0.658479	0.001399	0.016046
Gpr146	0.661973	5.42E-11	2.85E-09
Ppp1r3c	0.665114	4.60E-10	2.13E-08
Tes	0.672686	0.00486	0.044834

Scd3	0.67348	0.000255	0.003805
Gm15743	0.676275	0.004357	0.040849
Gm44090	0.676746	0.008618	0.070727
Pla2g4e	0.689487	0.005187	0.046946
Csf1	0.690873	1.28E-06	3.29E-05
Btg2	0.691781	6.14E-05	0.001081
Tlr13	0.693405	0.000657	0.008516
Cdca8	0.696377	0.011246	0.087041
Alpk1	0.697189	1.06E-05	0.000223
Sh3bp2	0.698112	4.95E-06	0.000112
Apobec1	0.698213	0.006867	0.058704
Klhl40	0.698253	0.000402	0.005646
Eif4ebp1	0.698397	0.000275	0.00408
Cd93	0.698459	0.0021	0.022432
Arid5a	0.699008	2.75E-06	6.66E-05
Gldn	0.699072	0.012037	0.091599
Tmem106a	0.700278	0.003599	0.034954
Zfp459	0.704166	0.008624	0.070741
Pik3ap1	0.704684	0.004084	0.038691
Plce1	0.705122	9.46E-05	0.001593
Gtse1	0.705496	0.012874	0.096168
Cd109	0.707462	0.004167	0.039388
Trim12c	0.709375	0.011716	0.089781
Stat2	0.709432	3.30E-07	9.49E-06
Ecscr	0.710595	0.001865	0.020304
Gnmt	0.711343	0.007017	0.059745
Plin5	0.712851	0.009292	0.07508
Fyb2	0.715362	0.000505	0.006844
Pemt	0.716232	0.003487	0.034092
Clic4	0.719123	2.10E-09	8.81E-08
Shcbp1l	0.719268	9.40E-06	0.000199
Spp1	0.720583	0.01037	0.081582
Trim72	0.721649	0.011792	0.090214
Pml	0.722006	9.74E-11	4.96E-09
Vav1	0.722862	1.38E-05	0.000283
Trib1	0.724219	4.33E-05	0.000795
Clec2d	0.726319	6.00E-05	0.00106
Sap30	0.731773	2.17E-06	5.35E-05
Net1	0.736213	1.16E-08	4.41E-07
Gm960	0.736979	0.00065	0.00843
Zfp189	0.737009	2.07E-09	8.72E-08
Timeless	0.740081	1.49E-07	4.55E-06

Tnfrsf1b	0.741238	2.83E-06	6.79E-05
Pdpn	0.74434	0.000301	0.004388
Fcgr1	0.74478	0.006619	0.057032
Gm11627	0.746029	0.00095	0.01162
Stom	0.747301	1.58E-15	1.42E-13
Gpr179	0.748197	5.85E-05	0.00104
9630013A20Rik	0.750286	0.000246	0.003696
Cmtm3	0.752529	9.65E-11	4.93E-09
Sult1a1	0.753275	5.23E-09	2.08E-07
H6pd	0.754168	3.21E-08	1.12E-06
Spi1	0.75474	0.002594	0.026654
Gm5805	0.75572	0.00551	0.049485
Mall	0.756989	0.012647	0.094919
B2m	0.757337	2.33E-13	1.61E-11
Serping1	0.75819	0.000274	0.00407
Elmsan1	0.758234	8.83E-25	2.01E-22
Ltbr	0.758891	3.27E-05	0.000613
Tead1	0.761628	4.56E-11	2.42E-09
Rhou	0.76544	1.33E-26	3.64E-24
Ankdd1a	0.768637	0.000642	0.008352
Synm	0.769792	4.54E-20	6.93E-18
Fzd2	0.775331	6.06E-20	9.11E-18
Myd88	0.776216	5.89E-06	0.000131
Lcp1	0.777936	2.57E-06	6.24E-05
Spry1	0.778659	3.19E-14	2.48E-12
Stat5a	0.778757	0.000863	0.010799
H2-Bl	0.780353	0.007171	0.060801
Rab32	0.782085	0.00077	0.009817
Igfbp7	0.782406	7.72E-06	0.000168
St6galnac2	0.782978	0.005682	0.050737
Dclre1b	0.783475	3.73E-10	1.75E-08
H2-T23	0.784894	5.15E-15	4.40E-13
Klf15	0.785824	2.17E-18	2.56E-16
Phactr4	0.787104	3.41E-17	3.71E-15
Mvp	0.79179	9.25E-09	3.59E-07
Csrnp1	0.793296	6.91E-08	2.27E-06
Rnf207	0.795614	2.47E-09	1.03E-07
Parp3	0.796252	1.94E-05	0.000382
Itprip	0.797216	0.001111	0.013259
Psd4	0.797428	0.002626	0.026907
Pnp	0.801462	7.20E-06	0.000158
Cd33	0.805065	2.99E-07	8.66E-06

Gm48393	0.807734	0.006402	0.055625
Stat1	0.808826	4.07E-06	9.41E-05
Pgf	0.809013	1.52E-05	0.000308
4930523C07Rik	0.809243	2.96E-05	0.000559
Epsti1	0.811939	0.005102	0.046504
Pfkfb3	0.813002	8.07E-11	4.15E-09
Fcrlb	0.81473	0.006501	0.056239
Zc3hav1	0.815697	9.00E-06	0.000192
Cd52	0.815706	0.011101	0.086238
Gfpt2	0.815883	9.33E-07	2.46E-05
Lbp	0.816453	3.22E-05	0.000605
Mthfd2	0.817028	3.99E-14	3.03E-12
Mamstr	0.818678	2.65E-06	6.44E-05
Rps18-ps3	0.820616	0.010804	0.084463
Pex11g	0.82438	0.009422	0.075972
Epha2	0.82829	3.37E-05	0.000631
Sh2d4b	0.830764	0.000186	0.002889
Apod	0.830856	5.16E-27	1.55E-24
Trp53inp1	0.832054	2.57E-07	7.56E-06
Emilin2	0.832703	5.61E-12	3.34E-10
Adamtsl2	0.832809	1.08E-07	3.39E-06
Col4a1	0.833318	2.26E-29	7.67E-27
Hspb1	0.836351	0.001431	0.016306
Spsb1	0.842238	5.27E-25	1.24E-22
Smco3	0.843754	8.20E-14	6.11E-12
Slc39a14	0.844036	1.17E-08	4.43E-07
Gm8399	0.845184	0.009042	0.073521
Lrp8os2	0.84585	0.012452	0.093837
Lrrc32	0.847187	5.16E-06	0.000117
Trim12a	0.847571	0.000554	0.007389
Bmf	0.8516	3.96E-06	9.23E-05
Rhoc	0.851766	7.02E-11	3.63E-09
Spns2	0.852601	3.56E-27	1.09E-24
Cd53	0.853061	1.62E-07	4.91E-06
Ikbke	0.855367	0.00031	0.004479
C3ar1	0.866095	0.006459	0.055988
Plekha4	0.875308	0.000217	0.003306
Rtkn2	0.875941	3.33E-07	9.54E-06
C4b	0.876165	9.43E-09	3.65E-07
Rhbdf2	0.876267	0.000398	0.0056
Gfap	0.878435	4.76E-06	0.000109
Lyn	0.878487	7.16E-06	0.000157

Ackr2	0.880116	0.00878	0.071804
Tspan4	0.88304	1.22E-13	8.84E-12
Ncaph	0.884707	0.000965	0.011782
Tspo	0.886274	4.06E-05	0.00075
Acer2	0.886934	5.46E-07	1.50E-05
Acat3	0.887549	0.001699	0.018818
Hmox1	0.888674	1.04E-06	2.73E-05
Colec11	0.891131	0.010819	0.084507
Gm7785	0.893254	0.012201	0.092544
Ampd3	0.894211	1.73E-14	1.39E-12
Znfx1	0.895979	3.30E-23	6.48E-21
6330415G19Rik	0.902123	0.000479	0.006528
Hvcn1	0.905546	0.001407	0.016125
Obscn	0.912596	3.67E-05	0.000681
Mtfr2	0.91345	0.013148	0.097664
Vmn2r1	0.9135	0.011321	0.087405
Cebpa	0.91432	1.61E-08	5.99E-07
Trim14	0.916337	0.012656	0.094919
H2-D1	0.918297	1.66E-09	7.06E-08
Ucp2	0.91842	5.90E-13	3.90E-11
Csf2rb2	0.919435	1.89E-05	0.000374
4933408B17Rik	0.922054	0.000306	0.004437
3110009E18Rik	0.923491	0.006988	0.059569
Ptges	0.926266	0.000983	0.011972
Gm37669	0.928585	0.011614	0.08915
Fcer1g	0.928689	2.84E-08	1.00E-06
Dio2	0.935141	8.56E-19	1.08E-16
Edn1	0.936992	5.56E-06	0.000125
Nod2	0.938308	0.000544	0.007282
Spint1	0.940641	0.000222	0.003373
4833411C07Rik	0.941171	0.001257	0.014706
2700046A07Rik	0.942912	0.00039	0.005497
Nrap	0.946054	0.002036	0.021824
Mfsd7a	0.94952	3.78E-05	0.0007
Gm6548	0.951082	3.57E-05	0.000665
Stat3	0.955869	7.15E-12	4.21E-10
Tmem140	0.959774	7.46E-05	0.001287
Irf9	0.959852	3.56E-07	1.01E-05
Gm7908	0.960914	0.000418	0.005838
Tgif1	0.962069	0.000283	0.004161
Wnt3	0.964369	1.57E-06	3.96E-05
Nuak2	0.96863	1.15E-06	2.97E-05

Hgf	0.968821	1.06E-07	3.34E-06
Il13ra1	0.969377	8.40E-06	0.000181
Elf4	0.972807	2.53E-06	6.18E-05
Tnfaip3	0.975456	1.22E-05	0.000252
Plekhf1	0.975457	1.29E-13	9.25E-12
Dtx3l	0.976488	1.51E-05	0.000306
Myh4	0.977077	0.00257	0.026434
Herc6	0.977548	2.91E-10	1.40E-08
Dennd3	0.978217	8.79E-14	6.53E-12
Gadd45g	0.979702	1.36E-16	1.41E-14
Gm4593	0.980618	0.012233	0.092751
Ncf1	0.981018	4.47E-15	3.86E-13
Itpripl1	0.981037	6.02E-08	2.02E-06
4933427G23Rik	0.981529	0.007146	0.060646
Nlrp3	0.986415	0.006022	0.053165
Asb4	0.987324	0.003491	0.034093
Serpine1	0.988021	0.000226	0.003425
Gm33940	0.996405	0.001422	0.016259
Tnfrsf10b	1.001407	0.001034	0.012459
Serpina3g	1.003121	0.000359	0.00511
Adora3	1.00455	0.001151	0.013663
Naip2	1.006483	0.000129	0.002102
Psme2b	1.008364	0.001482	0.01682
Gm45187	1.010087	3.35E-05	0.000628
Stxbp3	1.010214	3.02E-27	9.38E-25
Hs3st3b1	1.013452	4.96E-06	0.000112
Cd44	1.014334	0.007721	0.064687
Gm42922	1.01657	0.009643	0.077362
Gm44421	1.018605	8.01E-10	3.58E-08
Tor3a	1.020828	8.39E-07	2.24E-05
Xaf1	1.02446	1.05E-09	4.59E-08
Gm47108	1.027219	0.000638	0.008308
Fyb	1.027453	3.23E-08	1.13E-06
Il20rb	1.031102	0.000305	0.004435
Fzd4	1.031335	8.48E-22	1.53E-19
Itgb7	1.034814	0.000664	0.008581
Mindy4b-ps	1.037368	0.000206	0.003163
Sapcd1	1.041165	0.009875	0.07869
Siglec1	1.042658	3.31E-05	0.000621
Ackr3	1.043613	8.40E-27	2.41E-24
Parp12	1.044455	3.45E-12	2.12E-10
Trim25	1.051395	1.81E-07	5.45E-06

Muc2	1.054521	0.001109	0.013246
Samsn1	1.064967	0.003488	0.034092
Rasd1	1.066095	2.74E-16	2.76E-14
Tead3	1.068546	2.91E-05	0.000551
Tifa	1.069379	1.30E-06	3.32E-05
Spns3	1.070849	0.005616	0.050246
Casp12	1.071083	0.00046	0.006303
Rbm47	1.080874	0.000135	0.002194
5033406O09Rik	1.084672	0.000561	0.00747
S100a11	1.085626	8.41E-06	0.000181
Pglyrp1	1.086755	2.99E-09	1.23E-07
Gabrr2	1.087753	1.32E-07	4.07E-06
Gm46136	1.096389	0.000856	0.010711
Ly6a	1.103129	7.64E-08	2.47E-06
Gm42727	1.10626	0.011946	0.091094
A730020M07Rik	1.106634	2.14E-05	0.000417
Zfand4	1.107249	8.92E-19	1.12E-16
Hif3a	1.110715	3.78E-14	2.90E-12
Otoa	1.11847	0.001867	0.020318
Robo4	1.120415	1.22E-16	1.27E-14
Greb1	1.128651	5.24E-07	1.44E-05
Gm34425	1.129133	0.005798	0.051604
Rasip1	1.129939	5.61E-16	5.36E-14
Ifi203	1.130162	7.61E-08	2.47E-06
Arhgap8	1.131525	0.011001	0.085606
Nrros	1.137089	1.48E-26	3.94E-24
Pilra	1.138706	0.013547	0.099724
Cldn14	1.140927	2.83E-10	1.36E-08
Slc4a11	1.147777	2.18E-07	6.49E-06
Aff1	1.154678	5.02E-43	3.60E-40
Mc4r	1.15916	3.37E-09	1.38E-07
Adamts14	1.165956	8.62E-07	2.30E-05
Pnpla2	1.167006	1.92E-30	6.90E-28
Cenpp	1.168234	0.006513	0.056265
Trim34a	1.168252	5.20E-05	0.000938
Cebpb	1.174195	3.07E-12	1.91E-10
Ier3	1.175824	2.78E-13	1.91E-11
Ip6k3	1.182277	0.002318	0.024353
Lpin3	1.183116	1.62E-07	4.91E-06
Sap30bpos	1.18475	0.002555	0.026313
Tap2	1.191162	6.55E-07	1.78E-05
Lgals3bp	1.191252	9.58E-16	8.97E-14

Cysltr2	1.196133	0.01	0.079377
Ifi203-ps	1.197741	0.001335	0.015448
Ebi3	1.200582	0.001493	0.016903
Hes3	1.209674	0.013496	0.099492
Ube2l6	1.209901	1.69E-12	1.08E-10
Ripk4	1.213552	0.000243	0.003655
Gm3696	1.216196	0.005167	0.046879
Cdh5	1.218459	2.17E-23	4.39E-21
Nfkb2	1.22074	0.000159	0.002517
Treml2	1.223347	0.000432	0.005973
Sbno2	1.225256	6.18E-19	8.00E-17
Fgf2	1.229319	5.15E-07	1.42E-05
Mafk	1.238517	8.89E-31	3.25E-28
Smim3	1.240139	6.55E-20	9.69E-18
Phf11c	1.242477	1.38E-05	0.000283
Alox12b	1.242793	6.81E-34	2.89E-31
Ptprv	1.242977	0.006535	0.056411
Trat1	1.245362	0.001249	0.014618
Cyp1b1	1.249132	1.93E-06	4.79E-05
Sh2b2	1.251118	7.76E-33	3.21E-30
Gm19439	1.254035	1.75E-25	4.24E-23
Plscr1	1.256669	8.41E-05	0.001432
Rab20	1.257689	0.000517	0.006976
Sla	1.25818	3.89E-21	6.47E-19
Tead4	1.259827	5.82E-05	0.001036
Plscr2	1.2605	2.26E-07	6.73E-06
Slc25a13	1.261671	1.95E-18	2.31E-16
Ggta1	1.263043	1.25E-07	3.88E-06
Rgs9bp	1.270048	0.000671	0.008663
Uba7	1.272111	3.86E-12	2.35E-10
Myhas	1.272521	0.009151	0.074119
Eif2ak2	1.274645	1.42E-09	6.04E-08
Tiparp	1.276488	1.29E-20	2.06E-18
Chil1	1.281144	1.55E-05	0.000313
9930111J21Rik1	1.294966	0.001111	0.013259
Bst1	1.295729	0.004437	0.041496
Gem	1.298747	2.57E-07	7.56E-06
Nt5e	1.301038	3.76E-08	1.29E-06
Il1r1	1.305729	1.69E-26	4.43E-24
Nfkbiz	1.311483	7.12E-15	5.98E-13
H2-K1	1.313516	2.20E-08	7.83E-07
4732419C18Rik	1.314049	0.000532	0.007146

Itk	1.322042	0.001598	0.017885
Slc18a3	1.322674	0.010655	0.083544
Kcna5	1.328419	2.15E-14	1.70E-12
Irf1	1.329792	2.24E-10	1.09E-08
Gm37120	1.33168	0.000849	0.010669
2310074N15Rik	1.332629	0.004356	0.040849
B4galt1	1.338174	3.16E-24	6.70E-22
Il6ra	1.339664	2.34E-37	1.25E-34
Pdk4	1.346394	2.41E-39	1.50E-36
BC018473	1.347149	0.00293	0.029409
Mt1	1.347233	1.84E-21	3.21E-19
Adm	1.349186	2.05E-11	1.12E-09
Fut7	1.351616	0.00454	0.042351
Fcgr3	1.352062	1.24E-21	2.23E-19
Gm45091	1.354021	0.005534	0.049685
Gm11827	1.357843	0.00033	0.004753
Sdcbp2	1.359868	2.83E-05	0.000537
Gimap6	1.364593	3.86E-09	1.56E-07
4833403J16Rik	1.366859	0.012127	0.09214
Scara5	1.369634	7.03E-08	2.30E-06
Abhd15	1.371211	2.78E-07	8.15E-06
Ncf4	1.371697	0.000146	0.002343
Mc5r	1.377423	1.87E-05	0.00037
Tagap	1.377716	8.99E-05	0.001522
Il2rg	1.379703	1.88E-05	0.000372
Pik3r5	1.384989	1.74E-13	1.22E-11
9930111J21Rik2	1.385381	8.22E-07	2.20E-05
Parp10	1.385503	9.81E-10	4.31E-08
Ddit4	1.389853	3.29E-68	5.11E-65
Fcgr2b	1.390874	0.000294	0.004309
Trim29	1.399653	0.003029	0.030243
Muc1	1.40825	1.87E-12	1.19E-10
Nlrp6	1.408384	3.81E-10	1.78E-08
Ifit2	1.412681	1.02E-09	4.44E-08
Crybg1	1.417277	5.55E-10	2.52E-08
Clec4a1	1.417965	0.00185	0.020174
Tnfsf10	1.421619	1.20E-08	4.52E-07
Errfi1	1.422795	3.53E-54	3.29E-51
Slc25a34	1.424758	8.91E-23	1.68E-20
Tlr7	1.425652	9.11E-16	8.57E-14
Tekt4	1.428738	5.73E-14	4.30E-12
Ccn1	1.430363	1.05E-14	8.64E-13

Samd9l	1.43049	1.70E-10	8.40E-09
Tnfrsf1a	1.431084	4.66E-13	3.15E-11
Gm37285	1.432184	0.00844	0.069664
Gm8995	1.43437	3.01E-09	1.24E-07
Vwce	1.437189	1.75E-09	7.38E-08
Wfikkn1	1.440745	0.000153	0.002442
Itgad	1.443079	3.53E-07	1.00E-05
Snx31	1.443542	0.001317	0.015273
Cftr	1.445716	1.11E-05	0.000232
Trim21	1.456324	8.34E-06	0.00018
Gm38297	1.458543	0.00367	0.035449
AB124611	1.46142	0.007881	0.065834
Stra6	1.465536	8.78E-11	4.51E-09
Ido1	1.475553	0.005034	0.046034
Sp100	1.479227	4.51E-16	4.43E-14
B3gnt3	1.479409	9.44E-07	2.49E-05
Emp1	1.481291	4.20E-11	2.23E-09
Jaml	1.483024	7.88E-05	0.001353
St14	1.485553	3.53E-07	1.00E-05
Ifih1	1.495923	7.30E-12	4.27E-10
Itga5	1.498652	1.58E-15	1.42E-13
Fkbp5	1.499442	1.29E-191	1.20E-187
Hck	1.504128	3.71E-09	1.51E-07
Setdb2	1.5208	1.29E-18	1.58E-16
Ehf	1.523343	0.002663	0.027149
Srgn	1.525446	1.51E-10	7.53E-09
Cd86	1.53659	1.04E-13	7.60E-12
Tlr1	1.537311	0.002972	0.029736
Gm31323	1.541018	0.006709	0.057566
Gimap9	1.551455	0.000481	0.006537
Glipr2	1.552974	1.82E-08	6.68E-07
Apobec3	1.555444	1.46E-14	1.18E-12
Gm16464	1.563824	0.01106	0.085961
Helz2	1.568541	5.29E-32	2.10E-29
Txnip	1.572821	5.62E-67	6.98E-64
Klrg2	1.573968	7.45E-05	0.001286
Il18rap	1.574311	0.003186	0.031596
Cxcl5	1.57707	0.013396	0.098916
Cd40	1.577381	0.0001	0.001666
Gm4070	1.581058	0.005103	0.046504
Cybb	1.585159	1.29E-05	0.000266

Gprc5a	1.585288	0.005832	0.051833
Rpl7a-ps5	1.599132	0.000403	0.005646
Gm47870	1.607079	0.010152	0.080225
C1ra	1.611711	2.86E-08	1.01E-06
Gm32815	1.615448	0.005165	0.046879
Arl4d	1.618254	9.92E-44	7.39E-41
Olfr920	1.619976	0.005844	0.051912
Tuba1c	1.621189	6.95E-08	2.28E-06
Ifi27l2a	1.62376	0.000519	0.006996
Atp2c2	1.635127	3.63E-12	2.23E-10
AC138228.3	1.63714	6.51E-06	0.000144
Tgm2	1.641752	1.47E-26	3.94E-24
Psmb9	1.64295	1.87E-07	5.63E-06
Runx1	1.643824	8.72E-16	8.25E-14
Aspg	1.647432	1.06E-13	7.72E-12
Dhx58	1.654992	1.73E-11	9.55E-10
Pla1a	1.662054	1.04E-08	4.00E-07
9330121J05Rik	1.668479	1.38E-19	1.88E-17
Grrp1	1.670902	7.29E-27	2.12E-24
Arrdc2	1.673126	2.34E-25	5.60E-23
Tma16	1.675852	2.04E-81	5.43E-78
Rhoj	1.680466	7.88E-13	5.15E-11
Cyyr1	1.68392	4.64E-64	5.08E-61
Csf2rb	1.688475	1.12E-11	6.32E-10
Ccl22	1.690032	0.008171	0.067711
Sp110	1.693875	1.30E-08	4.86E-07
Galnt15	1.704914	2.03E-27	6.65E-25
Gm27252	1.705555	6.54E-08	2.18E-06
Cp	1.706767	1.31E-11	7.29E-10
Gvin1	1.707264	0.001726	0.019082
Cxcl16	1.71405	9.17E-05	0.001547
Sgk1	1.718614	4.36E-20	6.71E-18
Gm45188	1.728095	0.000106	0.001748
Zc3h12a	1.735146	3.90E-11	2.08E-09
Lrg1	1.735692	6.50E-08	2.17E-06
Plet1	1.736605	2.23E-05	0.000433
Sgk3	1.745785	3.10E-79	7.22E-76
Gm44799	1.748648	0.010868	0.084805
Upp1	1.751965	2.67E-07	7.85E-06
S100a9	1.7609	6.54E-05	0.001145
Bst2	1.765794	4.07E-10	1.90E-08
Fas	1.773306	2.71E-12	1.70E-10

Foxo6os	1.774641	5.84E-05	0.001039
Mt2	1.784353	2.65E-27	8.37E-25
Tmem154	1.801015	2.28E-07	6.76E-06
Scn10a	1.802548	5.18E-07	1.43E-05
Slc15a3	1.805102	9.94E-12	5.67E-10
Lilrb4a	1.807273	0.001228	0.014407
Nfkbia	1.811562	5.34E-87	1.66E-83
Plin4	1.816307	1.42E-29	4.90E-27
Gm20559	1.817395	2.57E-08	9.10E-07
E230013L22Rik	1.821017	0.000966	0.011791
Il4ra	1.82245	2.50E-54	2.45E-51
Prg4	1.82536	5.14E-07	1.42E-05
Ddx58	1.826816	6.55E-19	8.42E-17
Pkd1l2	1.826903	8.71E-06	0.000187
P2ry2	1.833455	1.12E-10	5.65E-09
Tcim	1.834721	6.02E-18	6.76E-16
Il1r2	1.841162	1.53E-05	0.00031
Pla2g3	1.845683	7.15E-35	3.25E-32
Ifitm2	1.845721	3.25E-18	3.73E-16
Lrrc25	1.8472	0.000219	0.003344
Ly6c2	1.848906	0.009426	0.075972
Serpina3n	1.858335	1.08E-08	4.12E-07
Gimap4	1.868167	0.000871	0.01086
Gm12115	1.874894	0.010461	0.082227
Fcgr4	1.878729	1.97E-06	4.88E-05
Sp140	1.88152	0.000333	0.004786
Lox	1.887909	5.57E-07	1.53E-05
Ccl17	1.888145	0.000437	0.006035
Ltf	1.891715	0.009793	0.078232
Ifitm1	1.89178	1.88E-08	6.84E-07
Slc43a3	1.893379	1.64E-10	8.12E-09
Ifi35	1.902101	7.43E-19	9.48E-17
Siglece	1.912401	2.42E-19	3.22E-17
Map3k8	1.914762	1.11E-24	2.49E-22
Gm43808	1.92335	0.000906	0.011192
Ccl9	1.928428	1.19E-07	3.71E-06
A730049H05Rik	1.943673	0.000226	0.003428
Xdh	1.944376	6.09E-95	2.84E-91
C5ar1	1.953131	5.96E-15	5.06E-13
Akap12	1.954262	2.16E-90	8.06E-87
Gm45356	1.961692	0.002019	0.021673
Slfn5	1.978499	3.83E-48	2.97E-45

Pirb	1.986699	2.13E-09	8.90E-08
3930402G23Rik	1.990024	6.41E-07	1.75E-05
Abcc2	2.015081	0.000538	0.007217
Gm45774	2.016953	8.20E-13	5.34E-11
Serpinf2	2.031445	4.84E-06	0.00011
Birc3	2.032054	5.73E-10	2.59E-08
Irgm2	2.033524	3.91E-12	2.37E-10
Rnf213	2.037675	5.94E-17	6.39E-15
Parp9	2.051996	3.39E-13	2.31E-11
Gimap5	2.065161	4.60E-06	0.000105
Rtp4	2.07429	8.34E-12	4.81E-10
Irak3	2.074968	1.14E-14	9.26E-13
Kif2c	2.091935	2.00E-06	4.94E-05
Adamts9	2.108816	1.67E-53	1.42E-50
Crispld2	2.109312	1.89E-14	1.51E-12
Adamts1	2.113543	7.70E-23	1.46E-20
C3	2.114381	2.60E-06	6.32E-05
Phf11b	2.125553	6.41E-06	0.000142
Milr1	2.134214	0.001805	0.019802
Lgals9	2.134708	5.89E-38	3.32E-35
Psmb8	2.137469	5.12E-15	4.40E-13
Chil3	2.139127	0.007564	0.063568
Ctla2a	2.143303	3.12E-21	5.28E-19
Gbp7	2.143728	1.99E-12	1.26E-10
Insl6	2.157236	1.16E-05	0.000241
Gm26676	2.165992	2.38E-07	7.03E-06
Marco	2.166095	0.005305	0.047783
Gm807	2.16675	1.54E-07	4.68E-06
Ifitm3	2.170941	2.92E-12	1.82E-10
A2m	2.171392	5.61E-09	2.23E-07
Cd101	2.173157	1.52E-06	3.85E-05
Ngp	2.17528	0.000422	0.005861
Lao1	2.183394	2.17E-10	1.06E-08
Ms4a4a	2.18379	4.85E-10	2.23E-08
Oas1g	2.207942	0.000144	0.002319
H2-Q7	2.21348	1.57E-07	4.79E-06
Apol9a	2.214994	0.000309	0.004479
Tmem82	2.221877	7.27E-20	1.05E-17
Gpr84	2.222623	8.55E-05	0.001456
Mx2	2.222713	2.96E-12	1.84E-10
Plac8	2.226129	2.46E-06	6.02E-05
Zfp36	2.228443	2.77E-63	2.87E-60

S100a8	2.239708	3.41E-07	9.71E-06
Cd274	2.253534	1.29E-13	9.25E-12
Tnf	2.256975	0.000122	0.001998
Slfn3	2.266492	9.20E-11	4.71E-09
BB123696	2.271851	0.001478	0.016809
Tnfaip2	2.272766	1.83E-05	0.000363
Trim30b	2.278205	1.38E-06	3.52E-05
9330175E14Rik	2.298463	0.001029	0.01243
Ly6d	2.300707	3.45E-08	1.19E-06
Ccl12	2.301612	0.001162	0.013772
Stx11	2.310977	1.29E-08	4.84E-07
Map3k6	2.31985	1.36E-108	8.44E-105
Dmrta1	2.321575	4.89E-13	3.29E-11
Atf3	2.322527	1.49E-05	0.000304
Bcl2a1a	2.326489	0.004176	0.039423
Tktl2	2.330688	1.57E-05	0.000318
Slfn8	2.333838	3.38E-10	1.61E-08
Gm12185	2.337681	1.72E-08	6.37E-07
Irgm1	2.339495	6.12E-14	4.58E-12
Cdkn1a	2.344043	3.49E-76	7.23E-73
Ms4a6b	2.344943	1.30E-19	1.78E-17
Trim30d	2.346597	3.98E-13	2.70E-11
Pmaip1	2.350652	2.59E-24	5.54E-22
Ifi207	2.352973	4.18E-07	1.17E-05
Igtp	2.366839	1.36E-12	8.73E-11
Dnah2os	2.375444	0.001639	0.018261
Cebpd	2.377195	7.93E-26	1.97E-23
Oas1b	2.381454	3.70E-15	3.22E-13
Apold1	2.381469	8.18E-72	1.39E-68
Ms4a6c	2.388905	7.20E-25	1.66E-22
Ada	2.415699	1.20E-34	5.34E-32
Gm10309	2.419995	9.46E-09	3.66E-07
Ddx60	2.444265	6.08E-12	3.61E-10
Batf2	2.458704	1.62E-06	4.07E-05
Piwil4	2.488637	0.002506	0.025933
Apol9b	2.496373	0.000146	0.002343
Slfn9	2.506137	2.36E-07	6.98E-06
Rnf125	2.513354	5.30E-27	1.57E-24
Gbp9	2.514283	1.50E-21	2.66E-19
Gm5431	2.529138	2.76E-08	9.74E-07
Oas2	2.569862	1.01E-11	5.76E-10

Cst7	2.573132	0.003481	0.034084
Apol10b	2.580208	3.74E-13	2.55E-11
Fpr1	2.594295	1.41E-05	0.000287
Tap1	2.597299	1.79E-16	1.83E-14
Clcnka	2.605018	0.000158	0.00251
Madcam1	2.616593	0.001512	0.017099
Ifi211	2.620795	0.000752	0.009627
Igsf6	2.630133	2.30E-07	6.80E-06
Parp14	2.650092	1.09E-19	1.52E-17
Oasl2	2.654539	2.45E-15	2.19E-13
Ifit3b	2.66074	1.14E-11	6.43E-10
Batf	2.669685	4.09E-06	9.45E-05
Ccl4	2.67534	0.002473	0.025686
Gm4951	2.752371	3.67E-08	1.27E-06
Angptl4	2.792702	6.29E-54	5.58E-51
Cd244a	2.80447	5.16E-10	2.35E-08
Ms4a6d	2.813808	1.08E-09	4.69E-08
Osmr	2.818196	1.84E-21	3.21E-19
H19	2.818449	2.68E-05	0.000512
Slfn1	2.838687	0.000173	0.002715
Socs3	2.843938	3.89E-42	2.68E-39
AW112010	2.847974	7.16E-17	7.62E-15
Hp	2.851252	2.36E-10	1.14E-08
Angpt2	2.877293	4.15E-68	5.53E-65
Maff	2.881724	1.11E-16	1.16E-14
Icam1	2.885155	1.84E-12	1.17E-10
Slfn2	2.891008	5.64E-32	2.19E-29
Glycam1	2.893262	8.87E-06	0.000189
Msr1	2.897386	8.39E-08	2.69E-06
Phf11d	2.901783	1.75E-11	9.64E-10
Tlr2	2.911045	2.63E-08	9.28E-07
Aire	2.933493	1.30E-20	2.06E-18
H2-Q4	2.964692	3.62E-14	2.79E-12
Trim30a	2.982608	1.92E-36	9.67E-34
Serpina3h	2.986131	1.12E-06	2.91E-05
Cnr2	2.991597	8.90E-08	2.84E-06
Sell	3.009192	2.88E-07	8.37E-06
Bhlha15	3.018421	0.011505	0.088421
Oas3	3.074148	4.55E-08	1.55E-06
Oas1a	3.080458	4.55E-16	4.44E-14
Serpina3i	3.109817	0.000326	0.004694
Tubb6	3.136789	8.64E-21	1.40E-18

Gbp3	3.156987	2.70E-23	5.40E-21
Cd14	3.160823	3.59E-22	6.63E-20
Mlkl	3.163928	1.13E-12	7.31E-11
Pilrb2	3.172568	4.37E-06	0.000101
Ifi44	3.178551	8.49E-18	9.42E-16
Ifit3	3.184977	6.70E-12	3.96E-10
Gm4841	3.216068	8.57E-05	0.001457
Clec4d	3.231922	1.01E-05	0.000213
Gbp4	3.236936	6.87E-20	1.01E-17
Ifi205	3.239135	0.000175	0.002743
Ifit1	3.246755	8.35E-18	9.32E-16
H2-Q6	3.263159	1.17E-10	5.86E-09
Isg15	3.268789	2.97E-15	2.63E-13
F730311O21Rik	3.278714	0.001649	0.018352
Hcar2	3.301152	2.38E-05	0.000458
Ccl3	3.327466	3.41E-08	1.18E-06
Slfn10-ps	3.34854	3.79E-06	8.91E-05
Tgtp2	3.350892	1.01E-13	7.42E-12
Nlrc5	3.364217	1.74E-18	2.09E-16
Usp18	3.369508	7.86E-20	1.12E-17
Ifi209	3.383131	1.77E-08	6.51E-07
F830016B08Rik	3.385276	7.01E-08	2.30E-06
Ms4a4c	3.390686	3.83E-07	1.08E-05
Klk2-ps	3.395935	0.000212	0.003239
Slamf8	3.454092	5.20E-05	0.000938
Ptx3	3.459448	0.000443	0.006095
Fgf21	3.481037	0.000913	0.011252
H2-Q5	3.495837	7.11E-06	0.000157
Irf7	3.500252	7.31E-20	1.05E-17
Ifi204	3.510545	1.56E-15	1.41E-13
F10	3.521941	7.75E-07	2.08E-05
Tfpi2	3.523838	0.002176	0.023014
Trim30c	3.540029	0.000146	0.002344
Ifi206	3.557417	8.03E-09	3.15E-07
Bcl3	3.564618	6.26E-15	5.28E-13
Ifi213	3.575174	3.12E-18	3.64E-16
Mmp13	3.611853	0.006331	0.055137
Acod1	3.615649	1.19E-09	5.13E-08
Il19	3.62838	0.000441	0.006073
Mcoln2	3.638238	1.83E-06	4.57E-05
Sele	3.665224	2.37E-10	1.15E-08
Lcn2	3.701438	0.000594	0.007832

Cd300lf	3.709914	3.15E-26	8.04E-24
Isg20	3.729927	1.81E-24	3.92E-22
Lbx1	3.741249	2.36E-05	0.000456
Plaur	3.741984	6.06E-51	4.91E-48
Gm12250	3.768105	1.33E-11	7.42E-10
Ifi47	3.830254	1.05E-26	2.95E-24
Fgr	3.891408	5.56E-11	2.91E-09
Casp4	3.905016	3.91E-23	7.60E-21
Ccl7	3.930256	9.57E-05	0.001605
Ccl11	3.962797	1.53E-07	4.68E-06
Gbp6	4.090161	3.37E-13	2.31E-11
Cxcl11	4.109621	1.14E-07	3.56E-06
Oasl1	4.121593	1.15E-19	1.59E-17
Slc5a1	4.139464	7.28E-06	0.000159
Gbp5	4.162225	6.82E-26	1.72E-23
Tgtp1	4.169167	1.15E-18	1.43E-16
Trem1	4.196767	4.89E-06	0.000111
Tgm1	4.200535	5.09E-10	2.32E-08
Timp1	4.228296	2.08E-09	8.74E-08
Gbp2	4.239393	9.52E-20	1.33E-17
Mx1	4.429857	1.01E-15	9.32E-14
Rsad2	4.447162	6.40E-37	3.31E-34
BC023105	4.448628	1.04E-06	2.73E-05
Gm32568	4.45036	6.16E-11	3.21E-09
Phox2a	4.470264	0.005228	0.047274
Loxl4	4.603901	7.63E-08	2.47E-06
Iigp1	4.627814	1.26E-38	7.60E-36
Depp1	4.656581	1.26E-66	1.47E-63
Slfn4	4.657375	6.27E-24	1.31E-21
Saa2	4.675042	2.03E-08	7.28E-07
Cxcl2	4.679188	4.24E-08	1.45E-06
Gpr65	4.741334	2.64E-26	6.82E-24
Tnfsf8	4.839955	2.98E-11	1.60E-09
Bcl2a1d	4.871181	0.000566	0.007523
Slc10a6	4.881005	1.40E-18	1.70E-16
Ch25h	4.896354	1.52E-72	2.83E-69
Saa1	4.907106	4.92E-10	2.26E-08
Selp	5.008485	7.08E-20	1.03E-17
Olfr56	5.152114	1.07E-14	8.76E-13
Zbp1	5.153514	1.12E-31	4.24E-29
Tnfsf11	5.189573	4.79E-05	0.000871
Steap4	5.255967	9.14E-15	7.60E-13

Sct	5.31143	2.60E-05	0.000499
Serpina3m	5.380379	1.68E-05	0.000337
Tmem252	5.429456	3.07E-302	5.71E-298
Pomc	5.738744	0.00522	0.047227
Spib	5.774792	4.34E-07	1.21E-05
Ccl2	5.780119	1.18E-10	5.89E-09
Ccl5	6.150105	4.18E-09	1.68E-07
Il1rn	6.55981	7.61E-12	4.42E-10
Clec4e	6.665192	8.23E-09	3.21E-07
Cxcl9	6.775043	4.35E-22	7.94E-20
Mmp12	6.824386	0.000106	0.00176
Saa3	6.85251	2.03E-22	3.77E-20
Gbp10	7.149079	5.74E-13	3.81E-11
Serpina3f	7.203051	3.67E-68	5.26E-65
Cxcl10	7.354627	6.51E-17	6.97E-15
Mmp3	7.567852	4.46E-05	0.000816
Cxcl1	7.727218	1.22E-26	3.39E-24
Csf3	10.27255	1.58E-40	1.02E-37

APPENDIX 8

Comparative DEGs WTPBS-WTLPS and WTPBS-Cx32KOPBS

DEGs in Both WTPBS-WTLPS & WTPBS-Cx32KOPBS			
Downregulated WTP-L & WTP-Cx32KOP	Upregulated WTP-L & WTP-Cx32KOP	Upregulated WTP-L, Downregulated WTP-Cx32KOP	Downregulated WTP-L, Upregulated WTP-Cx32KOP
Cfap157	Arhgap20	Col4a1	Ccp110
Chdh	Csrnp3	Ctla2a	Gm43242
Dnah6	Ezr	Fkbp5	**Pls1**
Dnajb13	**Map4k4**	Lrg1	
Fam166b	**Mtmr2**	Ly6a	
Gjb1	Oplah	Ly6c1	
Hist2h2be	Slc5a1	Plin4	
Sspo		Pnpla2	
		Serpina3n	
		Tgm2	
		Tppp3	
		Ucp2	

Table A7. Differentially Expressed Gene Comparison. DEGs shared in both the WTPBS-WTLPS and WTPBS-Cx32KOPBS comparisons. These DEGs were compared as an assessment of inflammatory expression in Cx32KO tissue. Bolded genes were discussed throughout the document, with particular focus on microglial genes Tgm2, Ucp2 and Pls1 in Chapter 4 discussion. Column A are genes that were downregulated after LPS treatment and after Cx32 KO. Column B are genes that are upregulated after treatment and Cx32KO. Column C and D represent differentially expressed genes after treatment compared to Cx32KO as stated.

APPENDIX 9

Comparative DEGs WTPBS-WTLPS and WTPBS-Cx47KOPBS

DEGs in Both WTPBS-WTLPS & WTPBS-Cx47KOPBS				
Downregulated WTP-L & WTP-Cx47KOP	**Upregulated WTP-L & WTP-Cx47KOP**		**Upregulated WTP-L, Downregulated WTP-Cx47KOP**	**Downregulated WTP-L, Upregulated WTP-Cx47KOP**
Ak4	Abcc2	Obscn	Csf2rb2	A930017K11Rik
Cartpt	Adipor2	Pacs2	**Mmd2**	Car2
Cbfa2t3	Aff1	Pde4b	Spp1	Chdh
Cecr2	Ampd3	Pex11g	**Xaf1**	Dip2a
Cldn5	Apod	Phactr4		Dock10
Derl3	Arl4d	Pim3		Eml1
Egfl7	Arrdc2	Pla2g3		Fam222a
Fgf11	Atp11a	Plekhf1		**Fgfr2**
Foxo6	Bc1	Polr3e		**Gjb1**
Gjc2	Cftr	Ptpn11		**Gjc3**
Gm43242	Cish	Ptprv		**Gpr37**
Kcng1	Cited2	Rasd1		Kif13b
Kctd12	Csrnp1	Relt		Ldlrad3
Mas1	D7Ertd443e	Scd3		Lims2
Meig1	Dbndd2	Sgk1		**Nrep**
Mstn	Ddit4	Slc18a3		**Olig2**
Ndnf	Depp1	Slc25a13		Pde8a
Nrp1	**Dusp1**	Slc2a1		Phldb1
Opalin	Emilin2	Snx31		Plxnb3
Plekho2	Errfi1	Strn		Prr18
Ptpn14	Gm19439	Tbc1d9b		Qdpr
Rxfp3	Gm42727	Tiparp		Rassf3
Slc26a7	Gm960	Tmem252		Sh3d19
Slc47a1	Hapln2	Tnip1		Shc3
Tafa1	Ido1	Tob2		**Smad7**
Wnt7b	Kcna5	Vash2		Tmem88b
	Lfng	**Wnt3**		**Tnfaip6**
	Mtmr2	Zfp281		Ugt8a
	Nfkbia			

Table A8. Differentially Expressed Gene Comparison. DEGs shared in both the WTPBS-WTLPS and WTPBS-Cx47KOPBS comparisons. These DEGs were compared as an assessment of inflammatory expression in Cx47KO tissue. Bolded genes were discussed throughout the document but specifically in Chapter 4 RNA-seq discussion. Column comparisons as listed.

VITA

NAME:	SAMANTHA ANN KEIL
EDUCATION:	B.A., Biology, Neuroscience, Pre-Medicine, Augustana College, Rock Island, Illinois, 2012
	Ph.D., Neuroscience, University of Illinois at Chicago, Chicago, IL, 2020
TEACHING:	Graduate Neuroscience Program, Department of Biology, University of Illinois at Chicago EXPERIENCE: Seminar in Neurobiology 386, Undergraduate Lecture, Spring Lecture 2017-2020
	Graduate Neuroscience Program, Department of Biology, University of Illinois at Chicago EXPERIENCE: BIOS 101: Population and Community, Undergraduate Lab and Discussion, Spring Lecture 2015
HONORS:	Graduate Student Council Travel Award, 2019 Student Presenter Travel Award, Graduate College, 2019 Graduate Student Council Travel Award, 2018 Student Presenter Travel Award, Graduate College, 2018 Chancellor's Student Service Award,2018 Graduate Student Council Travel Award, 2017 Student Presenter Travel Award, 2017 Graduate Student Council Travel Award, 2016 Student Presenter Travel Award, 2016
PROFESSIONAL MEMBERSHIP:	Society for Neuroscience, Member Graduate Women in Science, Eta Chapter Executive Board Science Policy Outreach Taskforce, Vice President and Founder Professional Women's Nexus, Member
PRESENTATIONS: *Oral Presentations*	**Keil, S.A.** "Glial response to connexin knockout in the murine central nervous system," Science Talks. *Graduate Women in Science – Chicago.* Northwestern University, October 2019 **Keil, S.A.** "Proliferation and inflammation: The effects of Cx32 deficiency on the CNS," Data blitz series. *Laboratory of Integrative Neuroscience Spring Symposium.* UIC, April 2019

Keil, S.A. "Proliferation and inflammation: The effects of Cx32 deficiency on the CNS," Data blitz series. *Laboratory of Integrative Neuroscience Spring Symposium.* UIC, April 2019

Keil, S.A. "The effects of Cx32 deficiency within the central nervous system," *Neuroscience Graduate Research Symposium*. UIC, Feb 2019

Keil, S.A. "Direct vascular channels connect skull bone marrow and the brain surface enabling myeloid cell migration." *Graduate Program in Neuroscience Journal Club.* UIC, Sept 2018

Keil, S.A. "Determination of the effect of connexin knockout within oligodendrocytes of the CNS." *Laboratory of Integrative Neuroscience Spring Symposium.* UIC, April 2018

Keil, S.A. "Single-cell methylomes identify neuronal subtypes and regulatory elements in mammalian cortex." *Graduate Program in Neuroscience Journal Club.* UIC, Sept 2017

Keil, S.A. "Comparison of the effects of human dental pulp stem cells and human bone marrow-derived mesenchymal stem cells on ischemic human astrocytes in vitro." *Graduate Program in Neuroscience Journal Club.* UIC, Feb 2016

Keil, S.A. "Effects of postconditioning on neurogenesis and angiogenesis during the recovery phase after focal cerebral ischemia." *Graduate Program in Neuroscience Journal Club.* UIC, Nov 2015

Poster Presentations

Keil, S.A., Freidin, M.M., Abrams, C.A Myelinating glial connexin deficiency within the central nervous system results in an increased inflammatory response and decreased oligodendrocyte development. *Society for Neuroscience*, Chicago, IL, October 2019

Keil, S.A., Freidin, M.M., Abrams, C.A. Glial activation alters development in murine models of oligodendrocytic connexin deficiency. *Great Lakes Glia Meeting 2019,* Traverse City, MI, Sept 2019

Keil, S.A., Freidin, M.M., Abrams, C.A. The effects of myelinating glial connexin deficiency within the central nervous system. *Chicago Chapter Society for Neuroscience Meeting*, Northwestern University, Chicago, IL Feb 2019

Keil, S.A., Freidin, M.M., Abrams, C.A. Cortical cell-type differences at baseline in the presence of connexin deficiency. *Society for Neuroscience*, San Diego, CA, Nov 2018

Keil, S.A., Freidin, M.M., Abrams, C.A. Cortical cell-type proliferation changes in the presence of connexin deficiency. *Annual Neuroscience Research Day*, Chicago, IL, Oct 2018

Keil, S.A., Freidin, M.M., Abrams, Apoptosis and proliferation in mixed glial culture from connexin knockout mice. *Society for Neuroscience*, Washington, D.C. Nov 2017

Keil, S.A., Freidin, M.M., Abrams, C.A. Apoptosis and proliferation in mixed glial cultures from oligodendrocytic connexin knockout mice. *Annual Neuroscience Research Day,* Chicago, IL, Oct 2017

Keil, S.A., Mathew, B., Torres, L., Roth, S. Mechanisms of ischemic post-conditioning in the retina. *Society for Neuroscience,* San Diego, CA, Nov 2016

Keil, S.A., Rafferty, M., Corcos, D., Madhavan, S. Effect of aerobic exercise intensity dose on corticomotor excitability, intracortical inhibition and intracortical facilitation. *Society for Neuroscience*, Chicago, IL, Oct 2015

Childs, E., **Keil, S.A.**, Lutz, J. Development of a reward learning task using virtual environments. *Annual Psychiatry Poster Extravaganza*, University of Illinois at Chicago, Chicago, IL, Oct 2015

Keil, S.A., Larson, J.R., Impaired olfactory discrimination learning in Fragile X knockout mice. *Society for Neuroscience*, Washington, D.C. Nov 2014

Keil, S.A., Larson, J.R., Impaired olfactory discrimination learning in Fragile X knockout mice. *Annual Psychiatry Research Forum*, University of Illinois at Chicago, Sept 2014